
THE UNIVERSITY
*of* EDINBURGH

# Future Cellular Systems: Fundamentals and the Role of Large Antenna Arrays

Sudip Biswas


A thesis submitted for the degree of Doctor of Philosophy.
The University of Edinburgh.
December, 2016.

As my Father always says...

"যদি তোর ডাক শুনে কেউ না আসে
তবে একলা চলো রে"

*-Rabindranath Tagore*

# Abstract

In this thesis, we analyze the performance of three promising technologies being considered for future fifth generation (5G) and beyond wireless communication systems, with primary goals to: i) render 10-100 times higher user data rate, ii) serve 10-100 times more users simultaneously, iii) 1000 times more data volume per unit area, iv) improve energy efficiency on the order of 100 times, and iv) provide higher bandwidths. Accordingly, we focus on massive multiple-input multiple-output (MIMO) systems and other future wireless technologies, namely millimeter wave (mmWave) and full-duplex (FD) systems that are being considered to fulfill the above requirements.

We begin by focusing on fundamental performance limits of massive MIMO systems under practical constraints such as low complexity processing, array size and limited physical space. First, we analyze the performance of a massive MIMO base station (BS) serving spatially distributed multi-antenna users within a fixed coverage area. Stochastic geometry is used to characterize the spatially distributed users while large dimensional random matrix theory is used to achieve deterministic approximations of the sum rate of the system. We then examine the deployment of a massive MIMO BS and the resulting energy efficiency (EE) by considering a more realistic set-up of a rectangular array with increasing antenna elements within a fixed physical space. The effects of mutual coupling and correlation among the BS antennas are incorporated by deriving a practical mutual coupling matrix which considers coupling among all antenna elements within the BS. Accordingly, the optimum number of antennas that can be deployed for a particular antenna spacing when EE is considered as a design criteria is derived. Also, it is found that mutual coupling effect reduces the EE of the massive system by around 40-45% depending on the precoder/receiver used and the physical space available for antenna deployment.

After establishing the constraints of antenna spacing on massive MIMO systems for the current microwave spectrum, we shift our focus to mmWave frequencies (more than 100GHz available bandwidth), where the wavelength is very small and as a result more antennas can be rigged within a constrained space. Accordingly, we integrate the massive MIMO technology with mmWave networks. In particular, we analyze the performance of a mmWave network consisting of spatially distributed BS equipped with very large uniform circular arrays (UCA) serving spatially distributed users within a fixed coverage area. The use of UCA is due to its capability of scanning through both the azimuth as well as elevation dimensions. We show that using such 3D massive MIMO techniques in mmWave systems yield significant performance gains. Further, we show the effect of blockages and path loss on mmWave networks. Since blockages are found to be quite detrimental to mmWave networks, we create alternative propagation paths with the aid of relays. In particular, we consider the deployment of relays in outdoor mmWave networks and then derive expressions for the coverage probability and transmission capacity from sources to a destination for such relay aided mmWave networks using stochastic geometric tools. Overall, relay aided mmWave transmission is seen to improve the signal to noise ratio at the destination by around 5-10dB with respect to specific coverage probabilities.

Finally, due to the fact that the current half duplex (HD) mode transmission only utilizes half the spectrum at the same time in the same frequency, we consider a multiuser MIMO cellular system, where a FD BS serves multiple HD users simultaneously. However, since FD systems are plagued by severe self-interference (SI), we focus on the design of robust transceivers, which can cancel the residual SI left after antenna and analog cancellations. In particular, we address the sum mean-squared-errors (MSE) minimization problem by transforming it into an equivalent semidefinite programming (SDP) problem. We propose iterative alternating algorithms to design the transceiver matrices jointly and accordingly show the gains of FD over HD systems. We show that with proper SI cancellation, it is possible to achieve gains on sum rate of up to 70-80% over HD systems.

# Lay Summary

The advent of internet, smartphones, social media, online video streaming, online gaming, etc., has heralded an explosive growth in the amount of data being created. This explosive growth of mobile data traffic has led to an ever-growing demand for much higher capacity, lower latency, and energy efficiency (EE) in wireless networks, which has culminated in the development of the fifth generation (5G) and beyond wireless communication systems. In particular, 5G is expected to be deployed by the year 2020, with key goals of data rates in the range of Gbps, billions of connected devices, lower latency, improved coverage and reliability, and low-cost, energy efficient, and environment friendly operation. Accordingly, future 5G and beyond wireless systems have to comply with three primary requirements: i) rendering very high capacity (10-100× more than 4G) and increasing energy efficiency (on the order of 100×), ii) serving a large number of users simultaneously (10-100× more than 4G), iii) providing an increase in area capacity of 1000× from 4G and iv) providing higher bandwidths.

Several promising technologies such as millimeter wave (mmWave) networks, massive multiple-input multiple-output (MIMO), full duplex (FD), non-orthogonal multiple access (NOMA), etc., are being considered for 5G systems. In particular, mmWave bands with significant amounts of unused or moderately used bandwidths can provide a significant boost to the spectral efficiency/bandwidth requirements. However, due to the very high frequencies used in mmWave, the path-loss increases with the frequencies for omni-directional antennas. To overcome the dependency of frequency on path-loss, large antenna aperture can be used, which can be achieved by using very large antenna arrays, also known as massive MIMO arrays. In fact, massive MIMO technology on its own can provide considerable improvement in both capacity and energy efficiency. In this approach, a base station (BS) with very large antenna array serving tens of users in the same time-frequency resource is used to eliminate inter-cell interference through highly directional beamforming. Another technology that has gained considerable attention in recent years is full duplex (FD) MIMO, which has the potential to double the spectral efficiency of current half duplex systems. The combination of FD communication with massive MIMO technology can provide bi-directional wireless communication at very high spectral and energy efficiency.

Accordingly, in this thesis, we provide a hollistic study of these three technologies and discuss the importance of using very large antenna arrays in future wireless communications systems. We provide several advantages and corresponding trade-offs of these technologies with respect to several real-life implementation constraints, such as physical space for massive MIMO, blockages for mmWave, and self-interference for FD. Overall, we show that these three technologies will indeed be the ones to fulfil the objectives of 5G, and will shape the way we communicate in the near and far future.

# Declaration of Ingenuity

I hereby declare that the work presented in this thesis is my exclusive work excepting wherever mentioned. This report has never been presented to any other university for any purpose including examination or degree.

**Sudip Biswas**

# Acknowledgements

First and foremost, I would like to express my gratitude to my supervisor, Prof. Tharmalingam Ratnarajah for giving me the opportunity to pursue my aspirations. Whilst others didn't, he believed in me and gave me this wonderful opportunity to do research. I will always be indebted to him for this. I also appreciate his continuous support and valuable guidance throughout my PhD period.

I would also like to acknowledge the financial support of the Seventh Framework Programme for Research of the European Commission under grant number HARP-318489 and ADEL-619647.

I would further like to thank all my colleagues at the Institute for Digital Communications, where I had the chance to meet many people with great minds. In particular, I would like to thank Ali Cirik, Jiang Xue and Satyanarayana Vuppala for their assistance during my PhD.

I also thank my friends in Edinburgh, specially Amr Hani, Oleksander Boiko, Paula Aquilina, Yuki Wong, Danai Kore, Sarthak Jain, Callum Egan and Tarek Al Abbas for making my Edinburgh journey memorable. I also would like to thank my guardian in Edinburgh, Beth Egan. I can't express how lucky I am to be staying at your place. Your care for me throughout the course of my PhD has been nothing short of what my own mother would do.

I also take this opportunity to show my gratitude towards my fiancée Ayanima Maity and my friends Aniruddha Ganguly, Juglul Pasha and Priya Krithivasan, who continuously supported me throughout my PhD and aided me with means that words cannot describe.

Last but not least, I would like to extend my deepest gratitude to my beloved parents, Dr. Suresh Biswas and Mayna Biswas, and my brother Dr. Sandip Biswas, for their constant love and unconditional support throughout the long path of my academic journey. Finally, a special note to my father, Dr. Suresh Biswas. I want to thank you for being such a great father. You have given your sweat and blood to see me and my brother where we are today. I owe to you and mother all I have ever accomplished.

# Contents

# List of Figures

# List of Tables

# List of Abbreviations

| | |
|---|---|
| 5G | Fifth Generation |
| 4G | Fourth Generation |
| BS | Base Station |
| CCI | Co Channel Interference |
| CDF | Cumulative Distribution Function |
| CR | Cognitive Radio |
| CSI | Channel State Information |
| CSI | Channel State Information |
| DOA | Direction of Arrival |
| DOD | Direction of Departure |
| DL | Downlink |
| EE | Energy Efficiency |
| ESD | Empirical Spectral Density |
| EMF | Electromotive Force |
| FD | Full Duplex |
| FDD | Frequency Division Duplex |
| GHz | Giga Hertz |
| Gbps | Giga Bits per Second |
| HD | Half Duplex |
| HCPP | Hard Core Point Process |
| LOS | Line of Sight |
| LSD | Limiting Spectral Density |
| LTE | Long Term Evolution |
| LMI | Linear Matrix Inequality |
| MIMO | Multiple Input Multiple Output |
| mmWave | Millimeter Wave |
| MRC | Maximum Ratio Combining |
| MRT | Maximum Ratio Transmission |
| MSE | Mean Squared Error |
| MHCPP | Matérn Hard Core Point Process |
| NLOS | Non Line of Sight |
| OBI | Other Base Station Interference |
| PDF | Probability Density Function |
| PPP | Poisson Point Process |
| PU | Primary User |

| | |
|---|---|
| QoS | Quality of Service |
| RF | Radio Frequency |
| RMT | Random Matrix Theory |
| SDP | Semi Definite Programming |
| SOCP | Second Order Cone Programming |
| SE | Spectral Efficiency |
| SI | Self Interference |
| SINR | Signal to Interference plus Noise Ratio |
| SISO | Single Input Single Output |
| SNR | Signal to Noise Ratio |
| SU | Secondary User |
| TDD | Time Division Duplex |
| UE | User Equipment |
| UL | Uplink |
| Wi-Fi | Wireless Fidelity |
| ZMCSCG | Zero Mean Circular Symmetric Complex Gaussian |
| ZF | Zero Forcing |

# Notation

| | |
|---|---|
| $\mathbf{A}$ | A matrix notation |
| $\mathbf{a}$ | A vector notation |
| $\lvert \cdot \rvert$ | Absolute Value of a number |
| $\mathcal{CN}(\mu, \sigma^2)$ | Circular symmetric complex Gaussian distribution with mean $\mu$ and variance $\sigma^2$ |
| $\mathcal{N}(\mu, \sigma^2)$ | Circular symmetric real Gaussian distribution with mean $\mu$ and variance $\sigma^2$ |
| $\det(\mathbf{A})$ | Determinant of matrix $\mathbf{A}$ |
| $h(\cdot)$ | Differential entropy operator |
| $\mathrm{diag}\{\bullet\}$ | Diagonal operator |
| $e$ | Euler's number |
| $\mathbb{E}(\cdot)$ | Expectation Operator |
| $\mathbf{A}^H$ | Hermitian of matrix $\mathbf{A}$ |
| $\mathbf{A}^{-1}$ | Inverse of matrix $\mathbf{A}$ |
| $\log_2(a)$ | Logarithm of $a$ to the base 2 |
| $\max(f(\cdot))$ | Maximize a function $f(\cdot)$ |
| $\min(f(\cdot))$ | Minimize a function $f(\cdot)$ |
| $\mathbb{P}(\cdot)$ | Probability |
| $\prod$ | Product operator |
| $\mathbb{C}$ | Set of complex numbers |
| $\mathbb{Z}$ | Set of integers |
| $\mathbb{N}$ | Set of natural numbers |
| $\mathbb{R}$ | Set of real numbers |
| $\sum$ | Summation Operator |
| $\mathrm{tr}(\mathbf{A})$ | Trace of matrix $\mathbf{A}$ |
| $\mathbf{A}^T$ | Transpose of matrix $\mathbf{A}$ |
| $\mathrm{vec}\{\bullet\}$ | Vector operator |

# Chapter 1

# Introduction

## 1.1 Background

Communication technologies have gone through numerous innovations over the past century. Among all the communication technologies, wireless communication, by all measure, has been the fastest growing segment of the communications industry. Perhaps, it is fair to say that mobile and cellular communications, which directly impact our daily lives have seen the most astonishing advancements of wireless communications. This has become more prominent with the shift in paradigm of communication from voice centric to data centric. The surge in internet usage, mobile applications usage, social media and online video streaming through mobile devices (mobile phones, tablets, laptops, etc.) [Fig. 1.1] [1] has heralded an explosive growth in the amount of data being requested. Accordingly, Fig. 1.2 [2] shows the overall projected growth in mobile data traffic from 2015 to 2020, revealing an 8-fold growth of up to 30.6 exabytes per month (the equivalent of 7,641 million DVDs each month).

This growth has continually resulted in an ever-growing demand for much higher capacity, lower latency and energy efficiency in wireless networks. Furthermore, as the electromagnetic spectrum with favourable communication properties below 20 GHz is almost completely expended, it is evident that the future demand for mobile data traffic will not be met. As a result, research has been directed towards developing alternative technologies and utilizing alternative spectrum regions. These have culminated in the development of the fifth generation (5G) and beyond wireless communication systems, expected to be deployed by the year 2020, with key goals of data rates in the range of Gbps, billions of connected devices, lower latency, improved coverage and reliability,

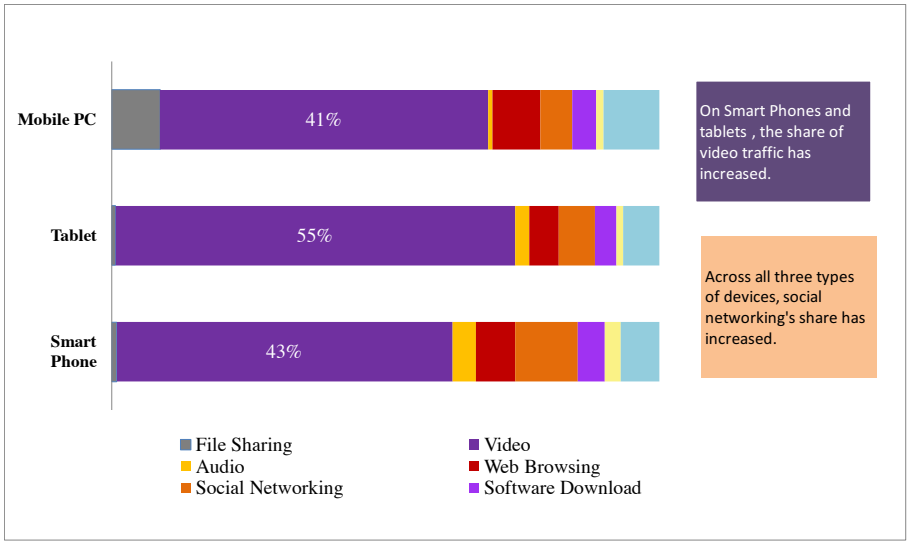


***Figure 1.1:*** *Mobile data traffic volumes by application and device type currently.*

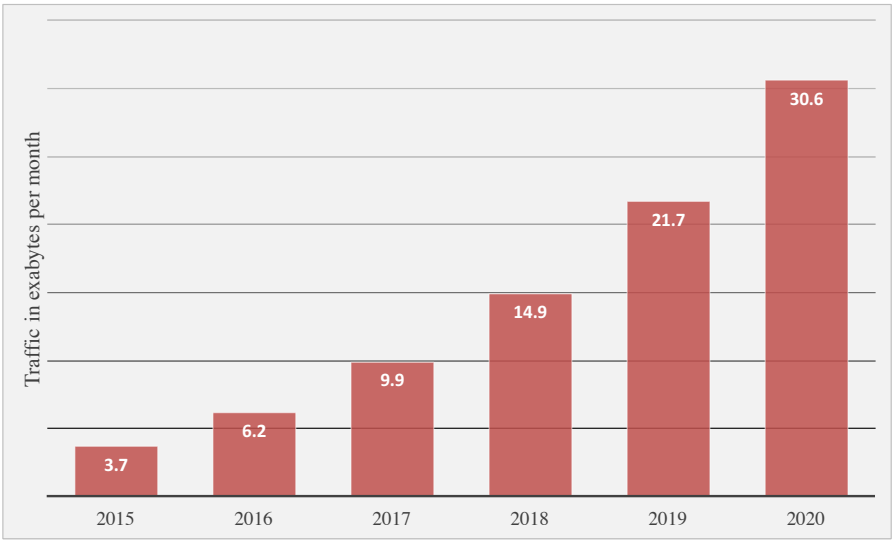


***Figure 1.2:*** *Projected global mobile data traffic from 2015 to 2020 (in exabytes per month).*

and low-cost, energy efficient and environment-friendly operation. To further signify the eminence of 5G, Fig. 1.3 shows the evolution of mobile technologies since the emergence of 1G. However, a question that has often been asked by many is: "What will 5G be?". To seek the answer to this question, we refer to [4, 5, 6], where it has been mentioned that the next generation wireless communication technology, also termed as 5G will be achieved through gains in the following categories:

1. Increasing the spectral efficiency through advances in multiple-input multiple-

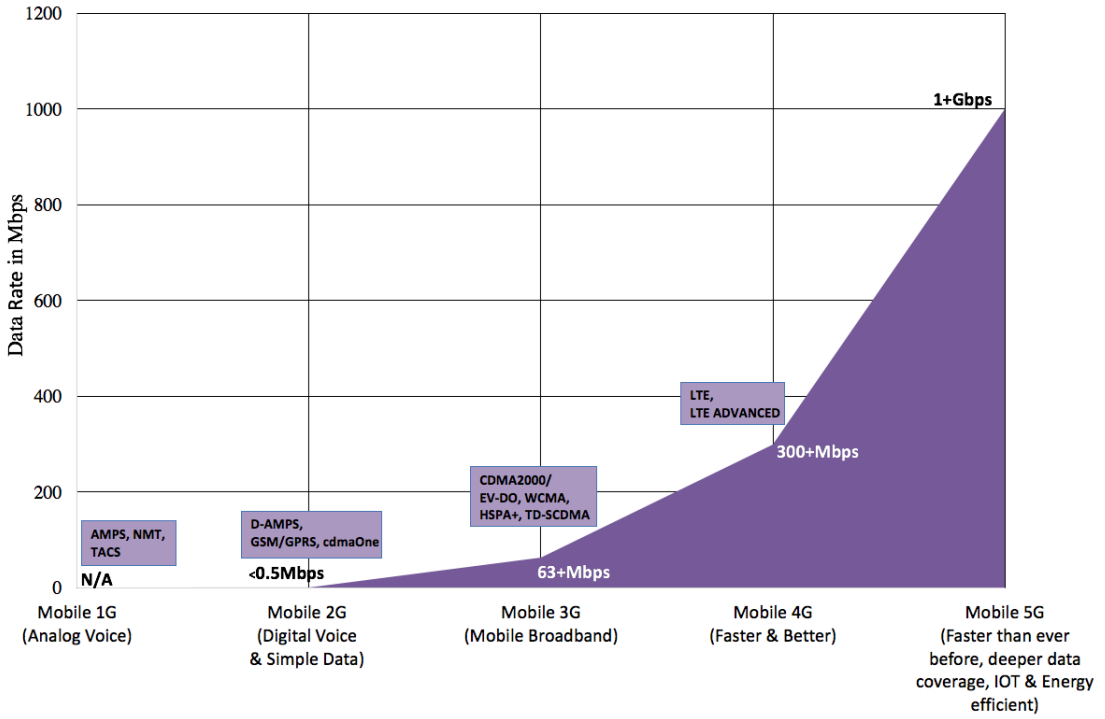


***Figure 1.3:*** *Evolving mobile technologies [3]. While 1G established seamless mobile connectivity by introducing mobile voice services, 2G increased voice capacity and delivered data to masses through mobile. 3G introduced mobile broadband services for faster and better connectivity and 4G LTE delivers more capacity for faster and better mobile broadband experience. 5G promises to improve on the existing LTE and LTE advanced technology. Enhanced mobile broadband with faster and more reliable user experience, varied low cost internet of things (IOT) with a wide range of coverage, lower latency and higher reliability are a few of the design goals of 5G.*

output (MIMO) to support more bits/s/Hz per node.

2. Increasing the energy efficiency of wireless networks to improve the battery life of user devices and reduce the transmitted power at the base stations.

3. Increasing bandwidth by shifting towards the millimeter wave (mmWave) spectrum.

4. Increasing the area spectral efficiency through densification of networks by implementing more active nodes per unit area.

Accordingly in this thesis, we will try to address these requirements by taking into account three promising technologies: 1) Massive multiple input multiple output, 2) full duplex, and 3) mmWave. In particular, we will study the performance of mas-

sive MIMO and full duplex to address the first and second requirement and mmWave systems to address the third. The fourth requirement can be addressed through the realization of heterogenous networks involving new 5G standards such as at mmWave frequencies and existing 4G LTE and 3G networks. However, this is beyond the scope of discussion of this thesis and will only be mentioned for the readers' better understanding.

## 1.2 Summary of Specific Contributions

In this thesis, we provide a hollistic study of the above mentioned three technologies and the importance of using very large antenna arrays in future wireless communications systems. In particular, massive MIMO antenna arrays can help overcome the dependency of frequency on path-loss in mmWave systems and cancel self interference in full duplex (FD) systems. Nonetheless, massive MIMO may require major architectural changes, particularly in the design of macro base stations, which will lead to new types of deployments. Consequently, in this thesis, we focus on the fundamental performance limit analysis of these technologies and provide several advantages and corresponding trade-offs with respect to several real life implementation constraints, such as physical space for massive MIMO, blockages for mmWave and self-interference for full duplex. Overall, we show that these three technologies will indeed be the ones to fulfill the objectives of 5G, that will shape the way we communicate in the near and far future. The most important contributions along with related publications are summarized as follows:

- We begin by presenting approximations of the sum-rate of an uplink single-cell multi-user MIMO system consisting of large number of antennas at the BS and multiple antennas at user equipments (UEs) in Chapter 3, while adhering to the consideration that the users follow a Poisson point process (PPP) within the cell. We consider correlated Rayleigh fading and uniformly distributed UEs within the cell and power-law path loss, where the path loss exponent determines the large scale fading of the users. We then provide high and low SNR approximations of the sum-rate of the system, which can be considered as good low complexity approximations of the analytical capacity. We also provide the approximate sum rate for the $k$th ordered user. Further, we also touch on the analysis of the energy efficiency (EE) of the whole system considering a realistic power consumption model which includes the circuit power consumption of the system.

*Publications related to this chapter:*

1. S. Biswas, J. Xue, F Khan, T. Ratnarajah, "Performance Analysis of Correlated Massive MIMO Systems with Spatially Distributed Users," in press, *IEEE Systems Journal*, 2016.
2. S. Biswas, J. Xue, F. Khan and T. Ratnarajah, "On the Capacity of Correlated Massive MIMO Systems using Stochastic Geometry," in Proc. *IEEE International Symposium on Information Theory (ISIT)*, Hong Kong, June 14-19, 2015.

- In Chapter 4, we consider realistic setups of massive MIMO and analyze how large MIMO systems bounded by fixed physical spaces fare to the demands of increasing EE while contributing towards high spectral efficiencies (SE). We re-examine the question- "How many antennas do we need?" [7] by means of EE under a) realistic antenna deployments in fixed physical spaces, and b) thorough and pragmatic power consumption models. We reflect on both the uplink and downlink of a multi-user MIMO system which models antenna correlation and coupling at the BS. We calculate the SE and transmitted power for both uplink and downlink and also the EE of this system with the help of a power consumption model similar to Chapter 3, but with additional parameters like power consumed by amplifiers and other digital circuits. We then provide an analytical expression for EE of this system by considering zero forcing (ZF) receiver/precoder and simulation results for both maximum ratio combining (MRC)/maximum ratio transmission (MRT) and ZF.

  *Publications related to this chapter:*

  1. S. Biswas, C. Masouros and T. Ratnarajah, "Performance Analysis of Large Multiuser MIMO Systems With Space-Constrained 2-D Antenna Arrays," *IEEE Transactions on Wireless Communications*, vol. 15, no. 5, pp. 3492-3505, May 2016.
  2. S. Biswas, C. Masouros and T. Ratnarajah, "On the Energy Efficiency of Massive MIMO with Space-Constrained 2D Antenna Arrays", In Proc. *IEEE International Conference on Communications (ICC)*, Kuala Lumpur, Malaysia, May 23-27, 2016.

- In Chapter 5, we analyze the performance of a mmWave network aided by relays. In particular, we present a relay modeling technique in mmWave networks

considering blockages, in which we compute the density of active relays that aid the transmission. A closed form expression for end-to-end signal-to-noise-ratio (SNR) is provided and the best random relay path in a mmWave network using order statistics is calculated. To investigate the asymptotic increase in the number of transmission paths, extreme value theory is used and accordingly the maximum end-to-end SNR of random relay paths is found to approach the Gumbel distribution. Finally, we provide an analysis on the coverage probability and the transmission capacity of relay aided mmWave networks.

*Publications related to this chapter:*

1. S. Biswas, S. Vuppala, J. Xue and T. Ratnarajah, "On the Performance of Relay Aided Millimeter Wave Networks," *IEEE Journal on Selected Topics in Signal Processing (Special Issue on mmWave)*, vol. 10, no. 3, pp. 576-588, April 2016.
2. S. Biswas, S. Vuppala, J. Xue, and T. Ratnarajah, "An Analysis on Relay Assisted Millimeter Wave Networks," in proc, *IEEE International Conference on Communications (ICC)*, Kuala Lumpur, Malaysia, May 23-27, 2016.

- In Chapter 6, we provide an analytical framework for a mmWave system with massive 3D circular antenna arrays at the BSs. In particular, by considering a 3D propagation model, we take both the azimuth and elevation dimensions into account. Accordingly, we find the optimal beamformer to achieve the maximum signal-to-interference-plus-noise ratio (SINR) that can be provided to a user. We then derive a closed-form expression for the first negative moment of the SINR. To model the blockages, we carry out our analysis by incorporating the exponential blockage model. Accordingly, we derive the coverage probability of the system. We also extend our analysis to a multiple BS scenario, where a user may be associated with the nearest BS. In order to analyze the performance of our model, we begin by calculating the average rate of the system. With the help of this rate and a certain outage probability, we analyze the transmission capacity of the network. Via numerical results, we provide a detailed analysis on the effect of the number of BS antennas, blockage density, path loss coefficient, node density, and SINR threshold on a mmWave network, where BSs are equipped with very large antenna arrays.

  *Publications related to this chapter:*

  1. S. Biswas, S. Vuppala and T. Ratnarajah, "An Analysis on mmWave Sys-

tems Equipped with Large 3D Antenna Arrays," under revision in *IEEE Journal*, 2016.

- In Chapter 7, we consider a cognitive radio scenario, where a secondary BS operating in full duplex (FD) mode communicates with uplink (UL) and downlink (DL) secondary users (SUs) operating in HD mode simultaneously within the service range of multiple primary users (PUs). In addition to self-interference, co-channel interference (CCI) is also taken into account to design the optimum robust beamformers under a norm-bounded-error model. We study the sum mean squared error (sum-MSE) as the objective function to minimize, subject to power constraints at the UL SUs and secondary BS, and interfering power constraints at the PUs and propose two robust iterative algorithms. We then show with simulation results that the proposed robust designs can significantly increase robustness to the channel state information (CSI) errors and can provide an improvement in performance over the non-robust design. Moreover, it is shown that the proposed FD system can achieve a significant improvement of throughput over half duplex (HD) system.

  *Publications related to this chapter:*

  1. A. C. Cirik, S. Biswas, and T. Ratnarajah, "Robust transceiver design in full-duplex MIMO cognitive radios," under revision, *IEEE Transactions on Vehicular Technology*, 2016.
  2. A. C. Cirik, S. Biswas, S. Vuppala, and T. Ratnarajah, "Robust transceiver design for full-duplex multi-user MIMO systems," *IEEE Wireless Communications Letters*, vol. 5, no. 3, pp. 172-175, May 2016.
  3. A. C. Cirik, S. Biswas, O. Taghizadeh, A. Liu, and T. Ratnarajah, "Robust transceiver design in full-duplex MIMO cognitive radios," in proc, *IEEE International Conference on Communications (ICC)*, Kuala Lumpur, Malaysia, May 23-27, 2016.

**Other Related Papers Not Included in the Thesis:**

The works mentioned below were undertaken during the PhD period but are not included in the thesis either because they do not fit within the main objective of the thesis, or they are earlier versions of the journal publications included in the thesis.

- S. Biswas, S.Vuppala, and T. Ratnarajah, "On the Performance of mmWave

Networks aided by Wirelessly Powered Relays," *IEEE Journal of Selected Topics in Signal Processing (Special Issue on Exploiting Interference towards Energy Efficient and Secure Wireless Communications)*, vol. 10, no 8, pp 1522-1537, Dec, 2016.

- A. C. Cirik, S. Biswas, S. Vuppala and T. Ratnarajah, "Beamforming design for full-duplex MIMO interference channels-QoS and energy efficiency considerations," *IEEE Transactions on Communications*, vol 64, no 11, pp. 4635-4651, Nov 2016.

- S. Vuppala, S. Biswas, T. Ratnarajah "An Analysis on Secure Communication in Millimeter/Micro-Wave Hybrid Networks," *IEEE Transactions on Communications*, vol. 64, no. 8, pp. 3507-3519, Aug, 2016.

- A. C. Cirik, S. Biswas, S. Vuppala, and T. Ratnarajah, "Energy efficient beamforming design for full-duplex MIMO interference channels," in proc *IEEE International Conference on Communications (ICC)*, Paris, France, May 21-25, 2017.

- A. C. Cirik, J. Xue, S. Biswas, T. Ratnarajah and M. Sellathurai, "Transceiver design of optimum wirelessly powered full-duplex MIMO interference channel," In Proc *IEEE 17th International Workshop on Signal Processing Advances in Wireless Communications (SPAWC)*, Edinburgh, UK, July 3-6, 2016.

- S. Vuppala, S. Biswas, J. Xue, and T. Ratnarajah, "On the Security Region of Best Source Indices in Random Wireless Networks," in proc, *IEEE International Conference on Communications (ICC)*, Kuala Lumpur, Malaysia, May 23-27, 2016.

- S. Vuppala, S. Biswas, T. Ratnarajah, "Analysis of secure communication in millimetre wave networks: are blockages beneficial?," *IEEE International Conference on Acoustics, Speech and Signal Processing (ICASSP)*, Shanghai, China, March 20-25, 2016.

- S. Biswas, C. Masouros and T. Ratnarajah, "On the effect of antenna correlation and coupling on energy-efficiency of massive MIMO systems," in proc, *IEEE Personal, Indoor, and Mobile Radio Communication (PIMRC)*, Washington D.C., USA, Sep 02-5, 2014.

## 1.3 Thesis Layout

The thesis is organized as follows:

Chapter 1 provides the motivation of research in this thesis as well as a brief overview of research and structure of the thesis.

Chapter 2 provides an overview of wireless communications and in particular MIMO communication techniques.

In Chapter 3, we consider the performance analysis of a correlated massive MIMO system with spatially distributed users. In particular, we provide a deterministic sum rate of this system with respect to different number of antennas at the BS as well as the intensity of the users within the coverage area of the cell.

In Chapter 4, we address the issue of mutual coupling in massive MIMO antennas arrays. In particular, we consider a realistic planar array bounded by a fixed physical space with an area of about $1m^2$ and analytically account for the full mutual coupling model of the array. Accordingly, we derive the optimum number of antennas that can be accommodated when EE is considered as a design criteria.

In Chapter 5, we analyze the performance of mmWave networks in the presence of blockages. In particular, we investigate the potential benefits of deploying relays in outdoor mmWave networks. We present a relay modeling technique for mmWave networks considering blockages and compute the density of active relays that aid the transmission. We study the coverage probability from sources to a destination for such systems aided by the active relays.

In Chapter 6, we look into the implementation aspect of massive MIMO antenna arrays in mmWave systems. We take into consideration a 3D propagation scenario where both the azimuth and the elevation angles of the array are considered. Using stochastic geometric tools, the coverage probability and transmission capacity of this system is analysed by taking blockages into consideration.

In Chapter 7, we investigate the potential benefits of a multiuser MIMO FD system over a HD system. However, since FD systems are plagued by severe self-interference (SI), we focus on the design of robust transceivers, which can cancel the SI. Furthermore, we also discuss schemes, where the excess antennas of massive MIMO systems can be utilized to eradicate the SI.

Finally in Chapter 8, we provide conclusions of this thesis and suggest future possible research extensions and directions based on the current work.

# Chapter 2

# An Overview of MIMO Wireless Communications

## 2.1 Introduction

In this chapter, we reflect on some of the basic concepts of multiple-input multiple-output (MIMO) wireless communications along with the evolution of smart antenna technology from single-user MIMO to multi-user MIMO. First, we consider the point-to-point communications followed by multi-user MIMO communications. Further, since the spectrum crunch is one of the major issues that has plagued network providers over the past decade, we discuss possible technologies that can be used to address this issue. In particular, we introduce massive MIMO and discuss how it can significantly boost the spectrum efficiency. We then place our focus on millimeter wave (mmWave) frequencies, which offer vast unused spectrum beyond 20GHz and full duplex (FD) communications, which can potentially double the spectrum efficiency by transmitting and receiving data at the same time and within the same frequency. Finally, we discuss some important mathematical preliminaries and tools, that will be used in this thesis to develop tractable models to analyze the performance of the systems under consideration.

## 2.2 MIMO Communications

MIMO is an antenna technology for wireless communications, in which multiple antennas are used at both the transmitter and the receiver. In particular, MIMO is one

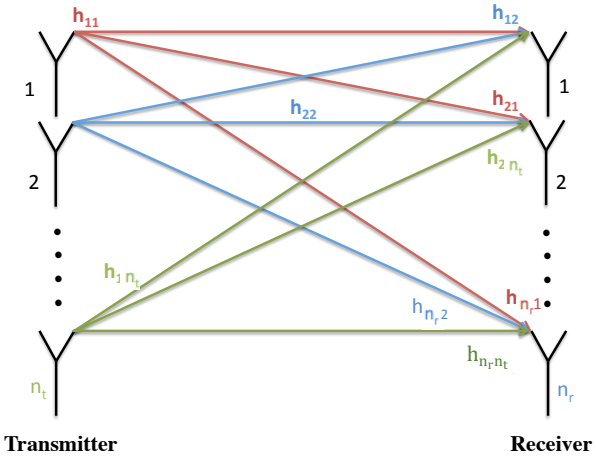


***Figure 2.1:*** *An illustration of a $n_r \times n_t$ MIMO system.*

of several forms of smart antenna technology, where the antennas at each end of the communications system are combined to minimize errors and optimize data rate. In conventional wireless communications, a single antenna is used at the transmitter, and another single antenna is used at the receiver, also known as single-input single-output (SISO) system. In some cases, this gives rise to problems with multipath effects. With multipath, transmitted signal bounces off buildings, trees, walls, ceilings, and other objects, reaching the receiving antenna multiple times via different angles and at slightly different times. Affected by the surrounding environment, the transmitted signal may undergo a change in amplitude, phase and frequency and the received multipath components may add up destructively, which results in severe degradation of quality of the transmitted signal at the receiver. The amplitude variations of the received signals are also known as fading [8] in wireless communications, which can cause a reduction in data rate and an increase in the number of erroneous symbols.

### 2.2.1 Point-to-point MIMO

MIMO technology, unlike SISO takes advantage of the multipath behavior by using multiple, smart transmitters and receivers with an added spatial dimension [8]. In particular, MIMO increases receiver's signal-capturing power by enabling antennas to combine data streams arriving from different paths and at different times. Smart antennas use spatial diversity technology, which puts surplus antennas to good use.

When antennas outnumber spatial streams, the antennas can add receiver diversity and increase performance and range. Fig. 2.1 illustrates a MIMO system with $n_t$ transmit and $n_r$ receive antennas[1]. Accordingly, the received signal for this system can be given as

$$\mathbf{y} = \mathbf{H}\mathbf{x} + \mathbf{n}, \tag{2.1}$$

where $\mathbf{x} = [x_1, x_2, \ldots, x_{n_t}]^T$ is the vector of signals, simultaneously transmitted by $n_t$ antennas and $\mathbf{y} = [y_1, y_2, \ldots, y_{n_r}]^T$ is the vector of signals simultaneously received by $n_r$ antennas. $\mathbf{H}$ is the $n_r \times n_t$ channel matrix between the transmitters and receivers and $\mathbf{n}$ is a $n_r \times 1$ vector of additive white gaussian noise defined as $\mathcal{CN}(0, \sigma^2\mathbf{I}_{n_r})$. Further, the channel matrix $\mathbf{H}$ can be elaborately written as

$$\begin{bmatrix} h_{11} & h_{12} & \ldots & h_{1n_t} \\ h_{21} & h_{22} & \ldots & h_{2n_t} \\ \vdots & \vdots & \ddots & \vdots \\ h_{n_r1} & h_{n_r2} & \ldots & h_{n_rn_t} \end{bmatrix}, \tag{2.2}$$

where $h_{ji} = [\mathbf{H}]_{ji}$ is the channel coefficient between the $j$th receive antenna and the $i$th transmit antenna. The channel gain $|h_{ji}|$ is usually Rayleigh distributed in a rich scattering environment with no line of sight (LOS) components. For such a Rayleigh fading model, $h_{ji} = [\mathbf{H}]_{ji}$ can be defined as

$$h_{ji} = \mathcal{N}\left(0, \frac{1}{2}\right) + \sqrt{-1}\,\mathcal{N}\left(0, \frac{1}{2}\right). \tag{2.3}$$

In particular, if $\mathbf{H}$ has i.i.d. elements chosen from a continuous distribution (like Rayleigh), the system capacity can be increased by a factor of $N = \min\{n_t, n_r\}$ without using additional transmit power or spectral bandwidth.

### 2.2.2 MIMO channel capacity

Considering the MIMO system in Fig. 2.1, the received signal can be given as in (2.1). In the following, we will derive the deterministic and ergodic capacity of such a system.

[1]The notations $n_t$ and $n_r$ used in this chapter for transmit and receive antennas, respectively are only for point to point communications. Other notations wherever used hereinafter, will be exclusively defined.

#### 2.2.2.1 Deterministic capacity

For a random MIMO channel, the capacity can be defined as the maximum mutual information that can be achieved by varying the probability density function (PDF) of the transmit signal vector and is expressed as [8]

$$C = \max_{\mathrm{tr}(\mathbf{\Phi}_{xx}) \leq P_t} I(\mathbf{x};\mathbf{y}) \text{ bits/channel use}, \tag{2.4}$$

where $I(\mathbf{x};\mathbf{y})$ is the mutual information of random vectors $\mathbf{x}$ and $\mathbf{y}$ and $P_t$ is the maximum transmit power constraint. Now, the mutual information of two continuous random vectors $\mathbf{x}$ and $\mathbf{y}$ can be given as

$$\begin{aligned} I(\mathbf{x};\mathbf{y}) &= h(\mathbf{y}) - h(\mathbf{y}|\mathbf{x}) \\ &= h(\mathbf{y}) - h(\mathbf{H}\mathbf{x} + \mathbf{n}|\mathbf{x}) \\ &= h(\mathbf{y}) - h(\mathbf{n}) \end{aligned} \tag{2.5}$$

The differential entropy of $\mathbf{y}$ is maximized if $\mathbf{y}$ is zero-mean circular symmetric complex Gaussian (ZMCSCG), which accordingly also requires $\mathbf{x}$ to be ZMCSCG. Now, the differential entropy of $\mathbf{y}$ and $\mathbf{n}$ are respectively given as

$$h(\mathbf{y}) = \log_2\{\det(\pi e \mathbf{\Phi}_{yy})\}, \tag{2.6}$$

$$h(\mathbf{n}) = \log_2\{\det(\pi e \sigma^2 \mathbf{I}_{n_r})\}, \tag{2.7}$$

where $e = 2.71828$ is the Euler's number and $\Phi_{yy}$ is the covariance matrix of the received signal $\mathbf{y}$ given as

$$\begin{aligned} \Phi_{yy} &= \mathbb{E}\left\{\mathbf{y}\mathbf{y}^H\right\} \\ &= \mathbb{E}_H\left\{(\sqrt{\rho}\mathbf{H}\mathbf{x} + \mathbf{n})(\sqrt{\rho}\mathbf{H}\mathbf{x} + \mathbf{n})^H\right\} \\ &= \mathbb{E}\left\{(\sqrt{\rho}\mathbf{H}\mathbf{x}\mathbf{x}^H\mathbf{H}^H) + (\mathbf{n}\mathbf{n}^H)\right\} \\ &= \rho\mathbb{E}\left\{(\mathbf{H}\mathbf{x}\mathbf{x}^H\mathbf{H}^H)\right\} + \mathbb{E}\left\{\mathbf{n}\mathbf{n}^H\right\} \\ &= \rho\mathbf{H}(\mathbb{E}\left\{\mathbf{x}\mathbf{x}^H\right\}\mathbf{H}^H + \sigma^2\mathbf{I}_{n_r} \\ &= \rho\mathbf{H}\mathbf{\Phi}_{xx}\mathbf{H}^H + \sigma^2\mathbf{I}_{n_r}, \end{aligned} \tag{2.8}$$

where $\Phi_{xx}$ is the covariance matrix of transmitted signal $\mathbf{x}$. Now using (2.5) - (2.8), the mutual information can be given as

$$I(\mathbf{x};\mathbf{y}) = \log_2\{\det(\pi e \mathbf{\Phi}_{yy})\} - \log_2\{\det(\pi e \sigma^2 \mathbf{I}_{n_r})\}$$

$$= \log_2 \det \left( \mathbf{I}_{n_r} + \frac{1}{\sigma^2} \mathbf{H} \mathbf{\Phi}_{xx} \mathbf{H}^H \right). \tag{2.9}$$

Therefore, for a deterministic MIMO channel, the capacity can be given as

$$C = \max_{\mathrm{tr}(\mathbf{\Phi}_{xx}) \leq P_t} \left\{ \log_2 [\det(\mathbf{I}_{n_r} + \frac{1}{\sigma^2} \mathbf{H} \mathbf{\Phi}_{xx} \mathbf{H}^H)] \right\} \text{ bits per transmission.} \tag{2.10}$$

It is to be noted that the above optimization of the channel capacity depends on the knowledge of the channel matrix $\mathbf{H}$. If full CSI is available at the transmitter side, an optimal transmission scheme can be obtained by allocating more power to the sub-channels with more gains using the water-filling algorithm [8]. However, when the transmitter side has no knowledge about the CSI, the optimal transmission scheme is obtained by allocating equal power among all transmit antennas. The capacity of the MIMO channel is then given as

$$C = \log_2 \det \left( \mathbf{I}_{n_r} + \frac{\mathrm{SNR}}{n_t} \mathbf{H} \mathbf{H}^H \right) \text{ bits per transmission,} \tag{2.11}$$

with $\mathrm{SNR} = \frac{P_t}{\sigma^2}$ being the nominal SNR of the system.

#### 2.2.2.2 Ergodic capacity

In Section 2.2.2.1, we assumed that MIMO channels are deterministic. In general, however, MIMO channels change randomly due to the effects of channel fading. Consequently, $\mathbf{H}$ is time-variant and becomes a random matrix. Accordingly, the MIMO channel capacity can be given by averaging over all channel realizations as

$$C_{\mathrm{Erg}} = \max_{\mathrm{tr}(\mathbf{\Phi}_{xx}) \leq P_t} \mathbb{E}_H \left\{ \log_2 [\det(\mathbf{I}_{n_r} + \frac{1}{\sigma^2} \mathbf{H} \mathbf{\Phi}_{xx} \mathbf{H}^H)] \right\} \text{ bits per transmission.} \tag{2.12}$$

For the case of i.i.d. Rayleigh faded channel model, optimal transmission scheme can be obtained by equally allocating power among all transmit antennas. Accordingly, $\mathbf{\Phi}_{xx} = \frac{P_t}{n_t} \mathbf{I}$. The resulting capacity is then given as

$$\begin{aligned} C_{\mathrm{Erg}} &= \mathbb{E}_H \left\{ \log_2 \det \left( \mathbf{I}_{n_r} + \frac{\mathrm{SNR}}{n_t} \mathbf{H} \mathbf{H}^H \right) \right\} \\ &= \mathbb{E} \left\{ \log_2 \prod_i^N (1 + \frac{\mathrm{SNR}}{n_t} \lambda_i) \right\} \end{aligned}$$

$$= \sum_{i}^{N} \mathbb{E}\left\{\log_2(1+\frac{\text{SNR}}{n_t}\lambda_i)\right\} \quad \text{bits per transmission,} \tag{2.13}$$

where $N = \min(n_t, n_r)$ is total number of channel eigenmodes or spatial sub-channels (i.e., non-vanishing singular values of the channel matrix) and $\lambda_1, \ldots, \lambda_N$ are the eigenvalues of $\mathbf{H}\mathbf{H}^H$. Further, by considering i.i.d. Gaussian input signaling, the achievable sum rate of the system can be similarly given as

$$R \approx \sum_{i}^{N} \mathbb{E}\left\{\log_2(1+\gamma_i)\right\} \quad \text{bits per transmission,} \tag{2.14}$$

where $\gamma_i$ can be considered to be the received SNR per spatial sub-channel. It is worthwhile to note that $\gamma_i$ for any wireless communication system depends on several factors, such as channel statistics, employed communication techniques, number of antennas used, correlation among antennas, etc. Accordingly, $\gamma_i$ and hence sum rate will be considered as one of the important metrics to evaluate the system performance in the forthcoming chapters.

### 2.2.3 Multi-user MIMO

Initially, MIMO came along as an optional technology with the 802.11n wireless standard in 2007. It enabled multiple streams of data to be simultaneously transmitted or received between two Wi-Fi devices (a WiFi router and a user device) using multiple antennas and beamforming technology, which helped increase the rate at which data passes between the devices. However, the most obvious downside to point-to-point/single-user MIMO is that the multiple streams of data must be sent or received between just one device at a time. Furthermore, single-user MIMO requires both the transmitting and receiving Wi-Fi radios to support the MIMO technology, along with having multiple antennas. While having multiple antennas at the WiFi router is feasible, the multiple antennas at the user devices add cost, weight, and size to the devices and the processing of the MIMO signals requires more resources as well. These became even more evident with the proliferation of smaller devices, such as smartphones and tablets.

Multi-user MIMO (MU-MIMO) on the other hand is a set of MIMO technologies for wireless communication, in which a set of users or wireless terminals, each with one or more antennas, communicate with each other. In contrast, single-user MIMO considers a single multi-antenna transmitter communicating with a single multi-antenna receiver.

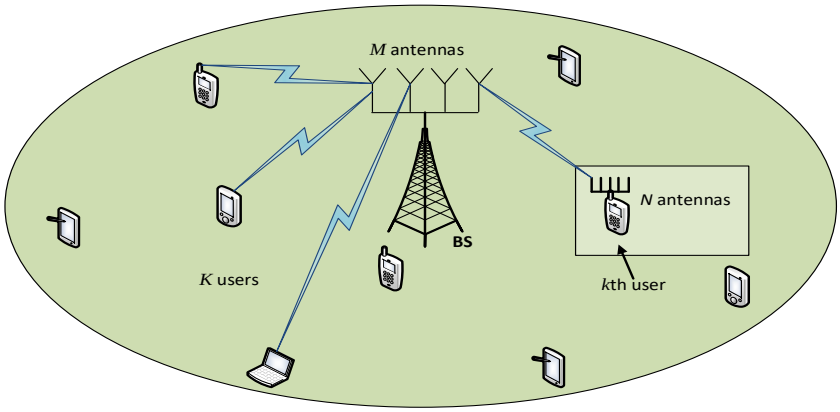


***Figure 2.2:*** *An illustration of a multi-user MIMO communications system.*

In particular, in a similar way that OFDMA adds multiple access (multi-user) capabilities to OFDM, MU-MIMO adds multiple access (multi-user) capabilities to MIMO. MU-MIMO has been investigated since the beginning of research into multi-antenna communication, including work by authors in [9, 10] on the capacity of the MU-MIMO links. Furthermore, multi-user MIMO offers big advantages over conventional point-to-point MIMO: it works with cheap single-antenna terminals, a rich scattering environment is not required, and resource allocation is simplified because every active terminal utilizes all of the time-frequency bins. Such systems are currently being implemented in various wireless communication technologies such as LTE-Advanced [11] and 802.11n [12] to name a few. In the multi-user MIMO system, downlink and uplink channels are referred to as broadcast channel (BC) and multiple access channel (MAC), respectively. Fig. 2.2 illustrates a multi-user MIMO communications system, where a base station (BS) equipped with $M$ antennas communicates with $K$ independent users, each equipped with $N$ antennas. The $K$ users form a virtual set of $K \times N$ antennas and the end-to-end configuration between the BS and the users can be considered as a $(KN) \times M$ MIMO system for downlink, or $M \times (KN)$ MIMO system for uplink. Alternatively when $N = 1$, the end-to-end configuration between the BS and the users can be considered as a $K \times M$ or $M \times K$ MIMO in the downlink or uplink respectively.

#### 2.2.3.1 MIMO BC

Let $\mathbf{x} = [x_1, x_2, \ldots, x_M]^T$ be the downlink transmitted signal from the BS to the $K$ users. Then the $N \times 1$ received signal at the $k$ user, with $k = 1, 2, \ldots, K$ can be given

as

$$\mathbf{y}_k \;=\; \mathbf{H}_k^{DL}\mathbf{x} + \mathbf{n}. \tag{2.15}$$

Here, $\mathbf{H}_k^{DL}$, with $k = 1, 2, \ldots, K$ is the $N \times M$ downlink channel between the $k$th user and the BS and $\mathbf{n}$ is the $N \times 1$ noise vector. Further, the overall received downlink signals can be represented in a vector form as

$$\underbrace{\begin{bmatrix}\mathbf{y}_1\\ \mathbf{y}_2\\ \vdots\\ \mathbf{y}_K\end{bmatrix}}_{\mathbf{y}_{\mathrm{BC}}} = \underbrace{\begin{bmatrix}\mathbf{H}_1^{DL}\\ \mathbf{H}_2^{DL}\\ \vdots\\ \mathbf{H}_K^{DL}\end{bmatrix}}_{\mathbf{H}^{DL}} \mathbf{x} + \underbrace{\begin{bmatrix}\mathbf{n}_1\\ \mathbf{n}_2\\ \vdots\\ \mathbf{n}_K\end{bmatrix}}_{\mathbf{n}}. \tag{2.16}$$

#### 2.2.3.2 MIMO MAC

Let $\mathbf{x}_k = [x_1, x_2, \ldots, x_N]^T$ be the uplink transmitted signal to the BS from the $k$th user, where $k = 1, 2, \ldots, K$. Then the $M \times 1$ received signal at the BS from $K$ users can be given as

$$\begin{aligned}\mathbf{y}_{\mathrm{MAC}} &= \mathbf{H}_1^{UL}\mathbf{x}_1 + \mathbf{H}_2^{UL}\mathbf{x}_2 + \cdots + \mathbf{H}_K^{UL}\mathbf{x}_K + \mathbf{n}\\ &= [\mathbf{H}_1^{UL}, \mathbf{H}_2^{UL}, \ldots, \mathbf{H}_K^{UL}] \begin{bmatrix}\mathbf{x}_1\\ \mathbf{x}_2\\ \vdots\\ \mathbf{x}_K\end{bmatrix} + \mathbf{n}.\end{aligned} \tag{2.17}$$

Here, $\mathbf{H}_k^{UL}$, with $k = 1, 2, \ldots, K$ is the $M \times N$ uplink channel between the BS and the $k$th user and $\mathbf{n}$ is the $M \times 1$ noise vector.

Unlike a single user MIMO system, where the user device is required to have multiple antennas, in a multi-user MIMO, the $K$ users can also be equipped with a single antenna, i.e., $N = 1$. The concept of MIMO still holds and the system is now equivalent to a $K \times M$ in the downlink and $M \times K$ in the uplink. Furthermore, the nice thing about single antenna users is that they are inexpensive, simple and energy efficient and each user still gets typically high throughput. Also, the assumption that users have single antennas can be considered as a special case of users having multiple antennas when the extra antennas are treated as additional autonomous users [13]. To ascertain this, we consider two cases for a MIMO MAC channel: 1) a multi-user MIMO system

with one BS and two single antenna users (i.e., $K = 2, N = 1$), each transmitting with power $P_t$ and 2) a multi-user MIMO system with one BS and one dual antenna users (i.e., $K = 1, N = 2$) with a power constraint of $2P_t$. For the first case, the sum rate for the two users can be given as [8]

$$R_1 = \log_2\left(1 + \frac{P_t||\mathbf{h}_1^{UL}||^2}{\sigma^2}\right) + \log_2\left(1 + \frac{P_t||\mathbf{h}_2^{UL}||^2}{\sigma^2}\right). \tag{2.18}$$

Further, the sum rate for the second case can be given as

$$R_2 = \log_2\left(\det\left(\mathbf{I} + \frac{1}{\sigma^2}[\mathbf{h}_1\mathbf{h}_2]\begin{bmatrix} P_t & 0 \\ 0 & P_t \end{bmatrix}\begin{bmatrix} \mathbf{h}_1^H \\ \mathbf{h}_2^H \end{bmatrix}\right)\right). \tag{2.19}$$

In the above, $\mathbf{h}_k$ with $k = 1, 2$ is the channel vector between the $k$th user (or $k$th antenna of the multi-antenna user) and the BS and $\sigma^2$ is the noise power. Further, (2.18) and (2.19) are equal and hence, $K$ multiple users having single antennas is equivalent to having one $K$-antenna user.

In this thesis, we will focus mostly on multi-user MIMO systems, where users are either equipped with single or multiple antennas depending on the system model considered.

## 2.3 Massive MIMO

Multi-user MIMO, as originally envisioned, with roughly equal numbers of service antennas and terminals and frequency-division duplex operation, is not a scalable technology. On the contrary, massive MIMO is an emerging technology that scales up MIMO by possibly orders of magnitude compared to the current state-of-the-art. As illustrated in Fig. 2.3, massive MIMO systems use antenna arrays with a few hundred antennas to eliminate inter-cell interference through highly directional beamforming. The escalation of the antenna number makes the random channel deterministic and orthogonal, which in turn eliminates the effects of uncorrelated noise and small-scale fading. Furthermore, the large antenna arrays lead to the use of simpler linear signal processing techniques, such as matched filter precoding/detection and the required transmit energy per bit goes to zero as the number of antennas approach to infinity [7]. In such a system, while less power will be used by the UEs for uplink transmission thus saving their battery, the BS will emit less RF power for downlink transmission, which will help in reducing the electricity consumed by associated circuits, amplifiers,

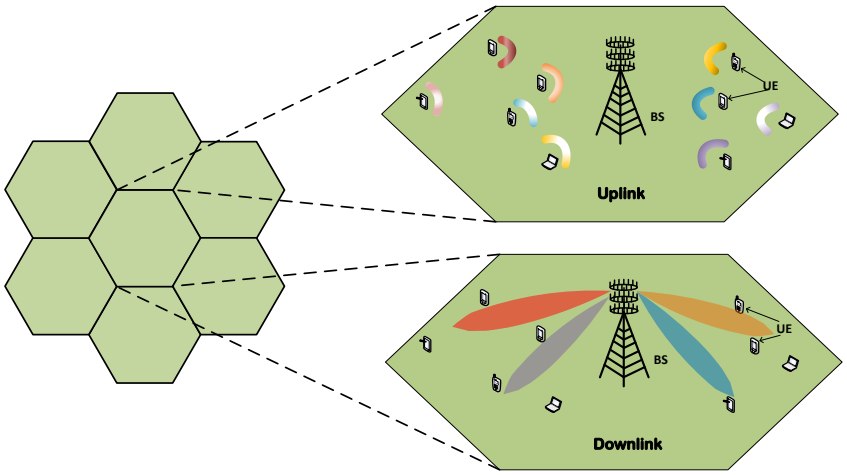


***Figure 2.3:*** *An illustration of a massive MIMO setup. Let $M$ be the number of BS antennas and $K$ be the number of UEs in a particular cell. Then, $\frac{M}{K} >> 1$.*

etc. It was shown in [14, 13] that every single-antenna user in a massive MIMO system can scale down its transmit power proportional to the number of antennas at the BS with perfect CSI, while the transmit power scales down proportional to the square root of the number of BS antennas with imperfect CSI, to get the same performance as a corresponding SISO system. This results in significant improvements in energy efficiency (EE) for future wireless networks [5, 15]. On the other hand, massive MIMO systems can significantly extend the range of operation compared to a single antenna system if adequate transmit power is available.

The basic idea behind massive MIMO is to reap all the benefits of standard MIMO, but on a much larger scale. Overall, massive MIMO is an enabler for the development of future broadband (fixed and mobile) networks, which will be energy-efficient, secure, and robust, and will boost the spectrum efficiency of the current state-of-the-art MIMO systems. As such, it is an enabler for the future digital society infrastructure that will connect the internet of people and internet of things with clouds and other network infrastructure. Accordingly, in this thesis, Chapters 3, 4 and 6 will particularly deal with the performance analysis of massive MIMO systems.

## 2.4 Other Future Cellular Systems

While Massive MIMO alone can provide significant boost to the efficiency of the spectrum, in order to meet the goals of data rates in the range of Gbps, billions of connected

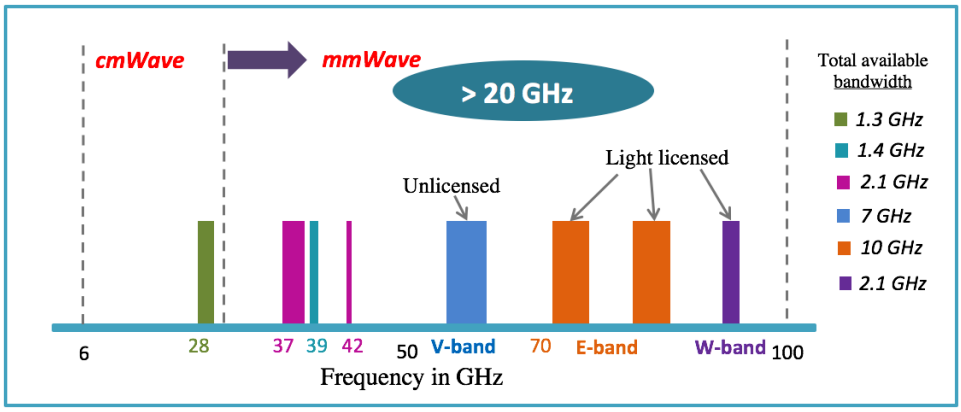


***Figure 2.4:*** *Available bandwidth in the mmWave spectrum. More than 20 GHz bandwidth is available.*

devices, lower latency, improved coverage, reliability, and low-cost, it is imperative to look for alternate spectrums or techniques that can further alleviate the spectrum crunch. In this regard, two new technologies, mmWave and FD are considered. Furthermore, both technologies can take advantage of the large antenna arrays used in massive MIMO technology to alleviate some of their respective design constraints.

### 2.4.1 Millimeter wave

MmWave bands with significant amounts of unused or moderately used bandwidths are being considered as a suitable alternative to the current microwave spectrum. As shown in Fig. 2.4 [16], the availability of bands in the range of 20-100 GHz makes mmWave a lucrative prospect in the design of 5G networks. The authors in [16] explore the available mmWave frequency bands to design a 5G enhanced local area network. While [17] proposes a general framework to analyze the coverage and rate performance of mmWave networks, [18] proposes a tractable mmWave cellular network model and analyzes the coverage rate.

However, one must remember that mmWave cellular communication is heavily dependent on the propagation environment. MmWave signals are affected by several environmental factors such as $O_2$ absorption and atmospheric conditions and cannot penetrate through obstacles like buildings, concrete walls, vehicles, trees, etc. Further, because of the high frequencies used in mmWave, the path-loss with omni-directional antennas increases with frequency. Due to these limitations, such bands were not considered suitable for cellular transmission for a long time. The authors in [19] analyze

the performance of mmWave cellular systems using real time propagation channel measurements. Blockage effects and angle spreads were also incorporated in [20] to analyze such systems. Generally in a communication system, path losses are computed for both line of sight (LOS) and non line of sight (NLOS) measurements. It was stated in [21] that blockages cause substantial differences in the LOS and NLOS propagation characteristics. Hence, it is very important to appropriately model the LOS and NLOS links in mmWave networks. Furthermore, the measurements for path loss were carried out for 73 GHz frequency in [22] and [23].

Recent studies and measurements have revealed that the natural way to combat omnidirectional path loss is by proportionally increasing the antenna aperture. This can be achieved in practice by using massive MIMO antenna arrays. The resulting array gain overcomes the frequency dependency on the path-loss and allows mmWave systems to provide reasonable link margin. Hence, massive MIMO technology can be considered to be an integral setup in the implementation of mmWave networks. Accordingly, in this thesis, the performance of mmWave systems will be evaluated in Chapter 5 and 6.

### 2.4.2 Full duplex

Currently, the downlink (DL) and uplink (UL) of MU-MIMO cellular systems operate in half duplex (HD) mode, where transmission happens either in separate time slots (Time Division Duplex, TDD) or in separate frequencies (Frequency Division Duplex, FDD). Hence, systems are operating only at half the spectrum efficiency and losing either on time or frequency resources. Among the emerging technologies for next-generation wireless networks, that is believed to potentially double the spectral efficiency (compared to conventional HD systems) is FD wireless communication. In this approach, data is transmitted and received at the same time and within the same frequency band as shown in Fig. 2.5. However, the benefits promised by FD can be limited by the so-called self-interference (SI), which is a fundamental challenge in implementing a full-duplex radio.

In particular, the SI refers to the transmitted signals that are directly received at the terminal's receive chain (in addition to the signals received from other transmitters). At the receiver, the SI is generally around 110dB larger than the signal of interest. Many feasible solutions including antenna, analog and digital cancellation have been demonstrated experimentally to mitigate the overwhelming self-interference [24]-[25].

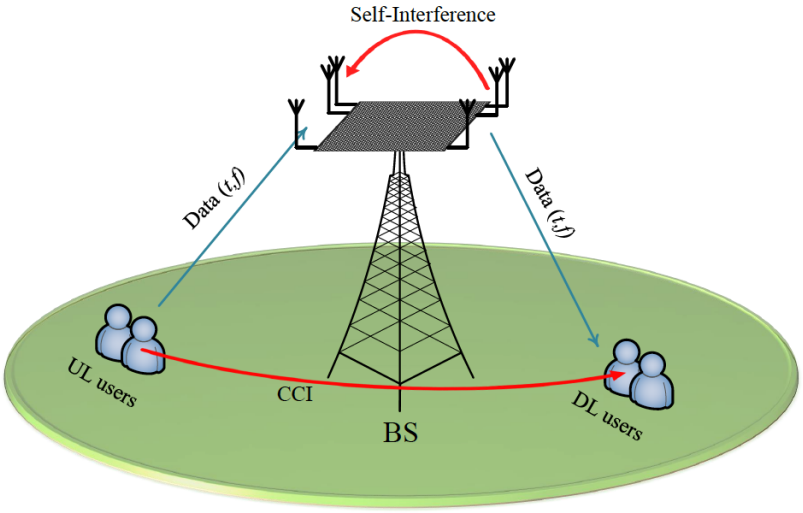


***Figure 2.5:*** *An illustration of FD communication. Data is transmitted between the UL users and the BS and the BS and the DL users in the same time and frequency.*

While antenna cancellation alleviates around 20dB SI, analog cancellation leads to a further reduction of 50dB SI. However, the combination of both cancellations is still less than the required 110dB SI cancellation. Accordingly, the performance is limited by around 30-40dB residual self-interference, which is induced by the imperfection of the transmit and receive front-end chains [26]-[27]. Depending on the strength of the residual self-interference, optimal transmit strategies for HD systems can be far from optimal for FD systems.

In addition to self-interference, co-channel interference (CCI) from UL users to DL users is another challenge in FD networks that needs to be overcome before the multi-access nature of the wireless medium in conjunction with full-duplex systems can be fully exploited. To optimize system performance, self-interference and CCI in FD systems should be addressed jointly through digital beamforming [28, 29, 30, 31]. Additionally, in order to solve the fundamental issue of self interference, a massive antenna array may be deployed at the BS that can exploit the excess antennas to eliminate the self-interference. Massive MIMO has the potential to achieve all-digital full-duplex, which will alleviate the need for new expensive analog cancellation techniques by going all digital through the aid of simple linear precoders/recievers [32, 33]. Accordingly, in this thesis, Chapter 7 will particularly deal with the performance evaluation of a FD system.

## 2.5 Preliminaries and Tools

In this section, we discuss some preliminaries related to MIMO channel capacity and some important mathematical tools that will be considered in the subsequent chapters to evaluate the system performance.

### 2.5.1 MSE and its relationship with sum rate

In the downlink of a cellular system, since BSs can have access to partial or perfect CSI, it is appropriate to shift the bulk of signal processing to the transmitter side to keep the circuitry of UEs simple and cheap. Accordingly, the transmitted signal can be pre-processed by passing it through matrix $\mathbf{B}$ in the transmitter side which is countered at the receiver side by post-processing it through another matrix $\mathbf{A}^H$.

Let $\mathbf{s} \in \mathbb{C}^{n_t \times 1}$ be the transmitted vector such that, $\mathbf{s} = \mathbf{Bx}$, where $\mathbf{B}$ is the precoder and $\mathbf{x} \in \mathbb{C}^{L \times 1}$ is the vector of $L$ transmitted symbols. After the received signal is processed through an equalizer, the $L \times 1$ estimated received vector is given by $\hat{\mathbf{x}} = \mathbf{A}^H\mathbf{y}$, where $\mathbf{A} \in \mathbb{C}^{n_r \times L}$ is the receiver matrix. The mean squared error (MSE) matrix can now be defined as the covariance matrix of the error vector of the transmitted and received vector and given as

$$\begin{aligned} \mathbf{MSE} &\triangleq \mathbb{E}\left\{(\hat{\mathbf{x}} - \mathbf{x})(\hat{\mathbf{x}} - \mathbf{x})^H\right\} \\ &= \mathbb{E}\left\{\hat{\mathbf{x}}\hat{\mathbf{x}}^H\right\} - \mathbb{E}\left\{\hat{\mathbf{x}}\mathbf{x}^H\right\} - \mathbb{E}\left\{\mathbf{x}\hat{\mathbf{x}}^H\right\} + \mathbb{E}\left\{\mathbf{x}\mathbf{x}^H\right\}. \end{aligned} \tag{2.20}$$

Now,

$$\begin{aligned} \mathbb{E}\left\{\hat{\mathbf{x}}\hat{\mathbf{x}}^H\right\} &= \mathbf{A}^H\mathbb{E}\left\{(\mathbf{Hs} + \mathbf{n})(\mathbf{Hs} + \mathbf{n})^H\right\}\mathbf{A} \\ &= \mathbf{A}^H\mathbb{E}\left\{(\mathbf{HBs} + \mathbf{n})(\mathbf{HBx} + \mathbf{n})^H\right\}\mathbf{A} \\ &\overset{(a)}{=} \mathbf{A}^H\left[\mathbf{HBB}^H\mathbf{H}^H + \mathbf{R}_n\right]\mathbf{A}, \\ \mathbb{E}\left\{\hat{\mathbf{x}}\mathbf{x}^H\right\} &= \mathbb{E}\left\{(\mathbf{A}^H(\mathbf{Hs} + \mathbf{n})\mathbf{x}^H)\right\} \\ &= \mathbf{A}^H\mathbf{HB}\mathbb{E}\left\{\mathbf{x}\mathbf{x}^H\right\} + \mathbf{A}^H\mathbb{E}\left\{\mathbf{n}\mathbf{x}^H\right\} \\ &\overset{(b)}{=} \mathbf{A}^H\mathbf{HB}, \end{aligned} \tag{2.21}$$

where $\mathbf{R}_n = \sigma^2\mathbf{I}_{n_r}$, $(a)$ is obtained due to the fact that the transmitted signal and noise vectors are independent of each other and $(b)$ is obtained due to $\mathbb{E}\left\{\mathbf{x}\mathbf{x}^H\right\} = \mathbf{I}$. Similarly, it can be shown that $\mathbb{E}\left\{\mathbf{x}\hat{\mathbf{x}}^H\right\} = \mathbf{B}^H\mathbf{H}^H\mathbf{A}$. Hence, the MSE can now be

given as

$$\mathbf{MSE} = \mathbf{A}^H \left[\mathbf{HBB}^H\mathbf{H}^H + \mathbf{R}_n\right] \mathbf{A} - \mathbf{A}^H\mathbf{HB} - \mathbf{B}^H\mathbf{H}^H\mathbf{A} + \mathbf{I}. \tag{2.22}$$

It is imperative to minimize the MSE in order to reach the capacity limits of the MIMO system. Two step optimization techniques to iteratively optimize $\mathbf{B}$ and $\mathbf{A}$ has been extensively studied in literature [29, 34]. Considering a minimum mean squared error (MMSE) receiver [35], we have

$$\mathbf{A}^{\text{opt}} = (\mathbf{HBB}^H\mathbf{H}^H + \mathbf{R}_n)^{-1}\mathbf{HB}. \tag{2.23}$$

Now, applying this receiver, the MSE can be given as

$$\begin{aligned} \mathbf{MSE} &= \mathbf{I} - \mathbf{B}^H\mathbf{H}^H \left(\mathbf{HBB}^H\mathbf{H}^H + \mathbf{R}_n\right)^{-1} \mathbf{HB} \\ &\overset{(a)}{=} (\mathbf{I} + \mathbf{B}^H\mathbf{H}^H\mathbf{R}_n^{-1}\mathbf{HB})^{-1}, \end{aligned} \tag{2.24}$$

where $(a)$ is obtained using the Woodbury identity [36]. Now defining the interference plus noise covariance matrix for the $i$th stream as $\mathbf{R}_i \triangleq (\mathbf{HBB}^H\mathbf{H}^H + \mathbf{R}_n - \mathbf{Hb}_i\mathbf{b}_i^H\mathbf{H}^H)$, the signal to interference plus noise ratio (SINR) for the $i$th data stream can be given as

$$\begin{aligned} \text{SINR}_i &\triangleq \frac{|\mathbf{a}_i^H\mathbf{Hb}_i|^2}{\mathbf{a}_i^H\mathbf{R}_i\mathbf{a}_i} \\ &\leq \mathbf{b}_i^H\mathbf{H}^H(\mathbf{R}_i)^{-1}\mathbf{Hb}_i, \end{aligned} \tag{2.25}$$

where the inequality comes from Cauchy-Schwarz's inequality [37]. Further, the MSE for the $i$th stream is the $i$th diagonal element of $\mathbf{MSE}$ and can be given as

$$\begin{aligned} \text{MSE}_i &= \left[(\mathbf{I} + \mathbf{B}^H\mathbf{H}^H\mathbf{R}_n^{-1}\mathbf{HB})^{-1}\right]_{ii} \\ &= \frac{1}{1 + \mathbf{b}_i^H\mathbf{H}^H(\mathbf{HBB}^H\mathbf{H}^H + \mathbf{R}_n - \mathbf{Hb}_i\mathbf{b}_i^H\mathbf{H}^H)^{-1}\mathbf{Hb}_i}. \end{aligned} \tag{2.26}$$

Hence, from the above the MSE can be linked to SINR as

$$\text{MSE}_i = \frac{1}{1 + \text{SINR}_i}. \tag{2.27}$$

This allows us to establish the fact that when an MMSE receiver is used, then the

achievable rate can be given as

$$R = \log\det(\mathbf{MSE}^{-1}) \text{ bits per transmission.} \tag{2.28}$$

Hence, it can be seen that maximizing the rate is equivalent to minimizing the MSE. Accordingly, a sum MSE minimization problem for a MIMO FD system will be studied in Chapter 7 of this thesis.

### 2.5.2 Mutual information and Stieltjes transform

Let $\mathbf{W} \triangleq \mathbf{H}\mathbf{H}^H$. As previously discussed, the mutual information of a MIMO channel can be associated with the eigenvalues of the matrix $\mathbf{W}$. Further, according to random matrix theory (RMT), the empirical spectral distribution (ESD) of the eigenvalues of $\mathbf{W}$, can be given as

$$\mu_{\mathbf{W}}(\lambda) = \frac{1}{n_r}[\text{number of eigenvalues of}\,\mathbf{W} \leq \lambda]. \tag{2.29}$$

While it has been a constant endeavor of researchers to study the limit of the empirical distribution, also known as limiting spectral density (LSD) $\mu$ of $\mathbf{W}$, [38] and [39] does that with the help of Stieltjes transform of $\mu_{\mathbf{W}}$ defined as

$$\begin{aligned} S_{\mathbf{W}}(z) &\triangleq \left[\int_{\mathbb{R}^+} \frac{1}{\lambda - z} \mathrm{d}\mu_{\mathbf{W}}(\lambda)\right]_{\forall z \in \mathbb{R}^+} \\ &= \frac{1}{n_r}\mathrm{tr}(\mathbf{W} - z\mathbf{I}_{n_r})^{-1}. \end{aligned} \tag{2.30}$$

The Stieltjes transform provides a direct way to identify the LSD of large-dimensional random matrices. According to [40], to show that the difference between $\mu_{\mathbf{A}}$ and $\mu$ converges vaguely to zero, it is equivalent to show that

$$S_{\mathbf{W}}(z) - S(z) \xrightarrow{a.s.} 0, \tag{2.31}$$

where $S(z)$ is the Stieltjes transform of $\mu$.

Now, with respect to a MIMO channel, the mutual information as given in (2.11) can be expressed as functionals of the Stieltjes transform of $\mathbf{W}$ i.e., $\frac{1}{n_r}\mathrm{tr}(\mathbf{W} + \rho\mathbf{I}_{n_r})^{-1}$, with $\rho$ denoting the effective signal to noise ratio (SNR) as [41, 42]

$$\frac{\partial C_{\mathbf{W}}}{\partial \rho} = \frac{1}{n_r}\mathbb{E}\left[\mathrm{tr}(\mathbf{W} + \rho\mathbf{I}_{n_r})^{-1}\right] - \frac{1}{\rho} \tag{2.32}$$

Now with the help of Fubini's theorem, the above derivative can be expressed as

$$C_{\mathbf{W}}(\rho) = \int_{\rho}^{\infty} \left( \frac{1}{\omega} - \frac{1}{n_r} \mathrm{tr}(\mathbf{W} + \omega \mathbf{I}_{n_r})^{-1} \right) \mathrm{d}\omega. \tag{2.33}$$

In [41] it was shown that when the number of antennas grow asymptotically, there exists a matrix valued function $\mathbf{T}(z)$ such that

$$\frac{1}{n_r} \mathrm{tr}(\mathbf{W} - z\mathbf{I}_{n_r})^{-1} - \frac{1}{n_r} \mathrm{tr}(\mathbf{T}(z)) \to 0. \tag{2.34}$$

Accordingly, $C_{\mathbf{W}}(\rho)$ in (2.33) was approximated as

$$\bar{C}_{\mathbf{W}}(\rho) = \int_{\rho}^{\infty} \left( \frac{1}{\omega} - \frac{1}{n_r} \mathrm{tr}(\mathbf{T}(-\omega))^{-1} \right) \mathrm{d}\omega. \tag{2.35}$$

In other words, when the number of antennas grow asymptotically,

$$C_{\mathbf{W}}(\rho) - \bar{C}_{\mathbf{W}}(\rho) \to 0. \tag{2.36}$$

A closed form expression for $\bar{C}_{\mathbf{W}}(\rho)$ was also given in [41] as

$$\begin{aligned} \bar{C}_{\mathbf{W}}(\rho) &= \frac{1}{n_r} \log\det \left[ \frac{\mathbf{\Psi}(-\rho)^{-1}}{\rho} + \tilde{\mathbf{\Psi}}(-\rho) \right] + \frac{1}{n_r} \log\det \frac{\tilde{\mathbf{\Psi}}(-\rho)^{-1}}{\rho} \\ &\quad - \frac{\rho}{n_t n_r} \sum_{i,j} \sigma_{ij}^2 \mathbf{T}_{ii}(-\rho) \tilde{\mathbf{T}}_{jj}(-\rho), \end{aligned} \tag{2.37}$$

where

$$\mathbf{T}(\rho) = \left( \mathbf{\Psi}^{-1}(\rho) - \rho \tilde{\mathbf{\Psi}}(\rho) \right)^{-1}, \tag{2.38}$$

$$\tilde{\mathbf{T}}(\rho) = \left( \tilde{\mathbf{\Psi}}^{-1}(\rho) - \rho \mathbf{\Psi}(\rho) \right)^{-1}, \tag{2.39}$$

$$\mathbf{\Psi}(\rho) = \mathrm{diag}(\mathbf{\Psi}_1(\rho), \ldots, \mathbf{\Psi}_{n_t}(\rho)), \tag{2.40}$$

$$\tilde{\mathbf{\Psi}}(\rho) = \mathrm{diag}(\tilde{\mathbf{\Psi}}_1(\rho), \ldots, \tilde{\mathbf{\Psi}}_{n_r}(\rho)), \tag{2.41}$$

$$\mathbf{\Psi}_i(\rho) = \frac{-1}{\rho \left( 1 + \frac{1}{n} \mathrm{tr}(\tilde{\mathbf{D}}_i) \tilde{\mathbf{T}}(\rho) \right)}, \ \forall 1 \le i \le n_r, \tag{2.42}$$

$$\tilde{\mathbf{\Psi}}_i(\rho) = \frac{-1}{\rho \left( 1 + \frac{1}{n} \mathrm{tr}(\mathbf{D}_j) \mathbf{T}(\rho) \right)}, \ \forall 1 \le j \le n_t, \tag{2.43}$$

$$\mathbf{D}_j = \mathrm{diag}(\sigma_{ij}^2, \ 1 \le i \le n_t), \tag{2.44}$$

$$\tilde{\mathbf{D}}_i = \mathrm{diag}(\sigma_{ij}^2, \ 1 \le j \le n_r). \tag{2.45}$$

It is to be noted that it is much easier to compute $\mathrm{tr}(\mathbf{T}(z))$ than $\mathrm{tr}(\mathbf{W} - z\mathbf{I}_{n_r})^{-1}$. Accordingly, using the above closed-form expressions, in Chapter 3 we will evaluate the deterministic equivalent of the ergodic capacity of the uplink of a massive MIMO system when the users are spatially distributed.

### 2.5.3 Stochastic geometry

Stochastic geometry approach has recently gained significant attention to develop tractable models to analyze the performance of wireless networks. In this approach, the wireless network is abstracted to a convenient point process that is used to capture the wireless network properties. For example, various stochastic geometric techniques have been used in [43, 44] to study connectivity and signal power in wireless networks, where the transmitters and receivers are modeled according to a certain distribution. The following text is a brief discussion on a few fundamentals of stochastic geometry.

#### 2.5.3.1 Borel $\sigma$-algebra

In a 2-dimensional topological space, a Borel set $\mathcal{B}^2$ is any set that can be formed by taking the complement, countable unions and intersections of closed, open or half-open sets. The Borel $\mathcal{B}^2$-algebra is formed by the collection of all Borel sets. In a 2 dimensional space, if there exists a point $x \in \mathbb{R}^2$ and value $r \in \mathbb{R}$, so that a ball centered at $x$ with radius $r$ has $A \subset b(x, r)$, then the set $A \subset \mathbb{R}^2$ is said to be bounded.

#### 2.5.3.2 Poisson point process

A point process $\Phi$ can be defined as a countable random collection of points that reside in some measurable space, usually the 2 dimensional Euclidian space [43]. Poisson point process (PPP) is the most popular and tractable point process to model the locations of users and BSs in wireless networks. A PPP assumes that the locations of the nodes are totally independent of each other. If a Poisson process has the same intensity $\lambda$ all over the Euclidean plane, it is called a homogeneous PPP, which will have the following properties:

- For any compact set $A$, $\Phi(A)$ has a Poisson distribution with a mean value of $\lambda|A|$, where $|\cdot|$ denotes the Lebesgue measure.

- Let $A_1, \ldots, A_n$ be disjoint bounded sets, then $\Phi(A_1), \ldots, \Phi(A_n)$ are independent random variables.

#### 2.5.3.3 Campbell's theorem

Campbell's theorem relates the expectation of a function summed over a point process to an integral involving the intensity measure of the point process. Let $f : \mathbb{R}^2 \to [0, \infty)$ denote a measurable function and $\Phi$ a point process, then Campbell's theorem can be expressed as [45]

$$\mathbb{E}\left[\sum_{x \in \Phi} f(x)\right] = \int_{\mathbb{R}^2} f(x)\Lambda(\mathrm{d}x), \tag{2.46}$$

where $\Lambda(\cdot)$ denotes the intensity measure of the set $A \subset \mathcal{B}^2$, which is the expected number of points falling in the set $A$ and can be expressed as $\Lambda(A) = \mathbb{E}[\Phi(A)]$.

Inspired by the stochastic geometry approach to analyze the performance of wireless networks, in Chapters 3, 5 and 6 of this thesis, we will use this approach to characterize the spatially distributed users as well as the BSs in the network.

# Chapter 3

# Massive MIMO Systems with Spatially Distributed Users

## 3.1 Introduction

The presence of large number of antennas in a massive-multiple input multiple-output (MIMO) system makes it increasingly difficult to carry out the exact performance analysis of such a system due to the complexity of the resulting analytical expressions. In this chapter, we analyze the performance of an uplink large scale MIMO system with a single base station (BS) serving spatially distributed multi-antenna users within a fixed coverage area of a densely built up urban environment. In such an environment, it is quite hard to find dominant propagation of the signals along the line of sight (LOS). Hence, it is quite reasonable to consider a Rayleigh faded channel in such a scenario. Stochastic geometry is used to characterize the spatially distributed users, while large dimensional random matrix theory is used to achieve deterministic approximations of the sum rate of the system. In particular, the users in the vicinity of the BS are considered to follow a Poisson point process (PPP) within the fixed coverage area. The sum rate of this system is analyzed by varying the number of antennas at the BS as well as the intensity of the users within the coverage area of the cell. Closed-form approximations for the deterministic rate at low and high SINR regimes are derived, which have very low computational complexity. Further, the deterministic rate for a general $k$th ordered user is also derived. It is shown that the deterministic approximations offer a reliable estimate of the ergodic sum-rate obtained by Monte-

Carlo simulations. At this point we would like to note that our results complement the contribution of [39]. However, we consider the more general and realistic case in which the stochastic nature of the users and their individual path losses are considered.

Furthermore, we briefly analyze the energy efficiency (EE) of such systems, which is currently one of the primary design goals of any wireless communication system. EE of a communication link is usually defined as the total energy required for transmission in order to achieve a specific spectral efficiency (SE) [46], [13]. The significance of the total power consumption in MIMO systems has been emphasized in [47] with respect to EE. MIMO systems have been stated to offer improved EE on account of array gains and diversity effects [8]. A common practice in determining EE is to consider the total transmitted energy to be a constant quantity [13] which aids in reducing the complexity of calculations. Hence, the definition of EE can be quite delusive at times especially when a massive MIMO scenario is considered with the number of antennas increasing asymptotically leading towards unbounded EE, which is quite improbable for practical scenarios. The effect of number of BS antennas on EE has been discussed in [12] and [48], while [49] discusses designing optimal EE for the uplink massive MIMO systems considering both radio frequency (RF) and circuit power consumptions. A trade-off between the EE and SE was also given in [49]. In our analysis, we take into consideration the circuit power consumption of both the BS and the user equipments (UEs) and accordingly form an EE expression which varies with the number of BS antennas and the users.

The main contributions of this chapter can be summarized in the following points:

- We have presented approximations of the sum-rate of a single-cell multi-user MIMO system with large number of antennas at BS and multiple antennas at UEs. This is adhering to the consideration that the users follow a PPP within the cell.

- We have considered correlated Rayleigh fading and uniformly distributed UEs within the cell and power-law path loss. The path loss exponent determines the large scale fading of the users.

- We have provided high and low signal to noise ratio (SNR) approximations of the sum-rate of the system which can be considered as good low complexity approximations of the analytical capacity.

- We have also provided the approximate sum rate for the $k$th ordered user.

- We also touch on the EE analysis of the system considering a realistic power consumption model which includes the circuit power consumption of the system.

## 3.2 System Model

In this chapter, we consider the uplink of a single-cell multi-user MIMO Multiple Access Channel (MAC) system consisting of a typical BS located at the origin of the cell. We use a homogeneous PPP, $\mathbf{\Phi}(\mathbf{u}) \subset \mathbb{R}^2$ with intensity $\kappa$ to model the locations of the users on the plane. Let, $\mathcal{U}$ be the set of all users in $\mathbf{\Phi}(\mathbf{u})$, which are connected to the BS at the same time. Also, let the cardinality of $\mathcal{U}$ be $K$. The number of users connected at a particular time is given as $K = \min(U_{max}, N)$, where $U_{max}$ is the maximum number of users that can be scheduled[1] in a time slot and $N$ is the total number of users connected to the BS. The BS with $M$ antennas, receive signals from $K$ users, each equipped with $n_1, \ldots, n_K$ antennas respectively. The number of users, $K$ is a function of $\kappa$. A schematic illustration[2] of the system under consideration is given in Fig. 3.1. Considering a separable correlation model for analytical tractability, we model the $M \times n_k$ channel, $\mathbf{W}_k$ between the BS and the $k$th user as

$$\mathbf{W}_k = \mathbf{H}_k ||\mathbf{u}_k||^{-\frac{\alpha}{2}}, \tag{3.1}$$

with

$$\mathbf{H}_k = \mathbf{R}_k^{\frac{1}{2}} \mathbf{G}_k \mathbf{T}_k^{\frac{1}{2}}, \tag{3.2}$$

where $\mathbf{R}_k^{\frac{1}{2}}$ and $\mathbf{T}_k^{\frac{1}{2}}$ are $M \times M$ and $n_k \times n_k$ deterministic receive and transmit correlation matrices respectively. Here, $\mathbf{G}_k \in \mathbb{C}^{M \times n_k}$ consists of complex random identically independently distributed (i.i.d) variables with zero mean and unit variance which models independent fast fading. We assume that the users do not have any line of sight with the BS and hence, $\mathbf{G}_k$ is Rayleigh-faded. The separable model allows us to keep the correlation between any two transmitting antennas to be fixed irrespective of the receiving antenna and vice versa. Moreover, $\mathbf{u}_k \in \mathbb{R}^2$ denotes the physical location

[1] More sophisticated algorithms on decisions on how many and which users to schedule in a resource block may be considered. However, for the sake of tractability, we ignore this aspect here.

[2] We consider a circular cell of radius $r$ in $\mathbb{R}^2$ with an area of $\pi r^2$. A hexagonal cell in $\mathbb{R}^2$ can also be considered. The radius of the cell, $r$ can then be considered from the center to the vertex and the area (considering a regular hexagon with side $b$) is given as $3b\sqrt{r - \frac{b^2}{4}}$.

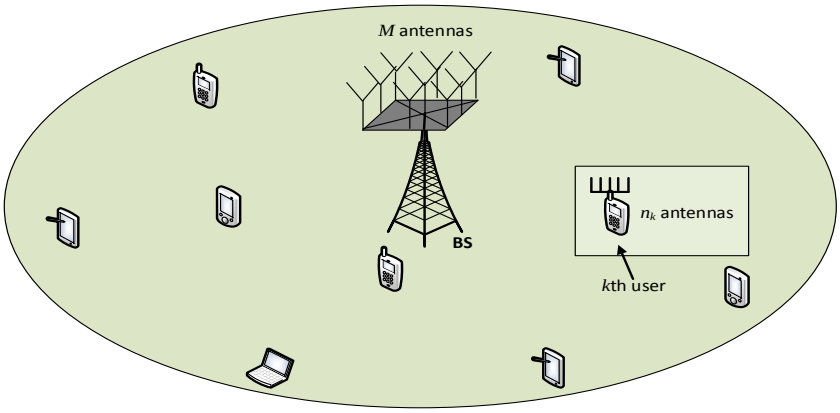


***Figure 3.1:*** *An illustration of a multi-user MIMO setup with multiple antennas both at the BS and users.*

(distance between the UE and the centre of the cell) of the $k$th user in meters and it is computed with respect to the BS. The large-scale fading at a specific user location is described by the function $\mathcal{F}(\cdot) : \mathbb{R}^2 \to \mathbb{R}$. Thus the average channel attenuation due to path loss and shadowing[3] at user location $\mathbf{u}_k$ can be represented by $\mathcal{F}(\mathbf{u}_k)$. The large scale fading is assumed to be independent over $M$ and also constant over many coherence time intervals. This assumption is quite reasonable due to the fact that the distances between the users and the BS are much larger than the distance between the antennas at the BS. Also, $\alpha$ in (3.1) denotes the path loss exponent varying from 2 to 4, with 2 denoting a free space propagation and 4 a relatively lossy environment.

Let $r$ denote the radius of the circular cell and $u = ||\mathbf{u}||$. The user locations can be described by the probability density function (PDF) as

$$f(\mathbf{u}) = \begin{cases} \frac{2u}{r^2} & 0 \leq u \leq r \\ 0 & \text{otherwise.} \end{cases} \tag{3.3}$$

Furthermore, we model the large scale fading as

$$\mathcal{F}(\mathbf{u}) = u^{-\frac{\alpha}{2}}, \tag{3.4}$$

[3]The results in this chapter are produced with the assumption that large-scale fading is dominated by path-loss. However, these results are also applicable for more complicated fading models including shadowing effects. For example, adding log-normal shadowing to the corresponding results is straightforward and can be done by modifying (1) as $\mathbf{W}_k = \mathbf{H}_k \beta_k / \|\mathbf{x}_k\|^{\frac{\alpha}{2}}$, where $\beta_k$ is a log-normal random variable with standard deviation $\sigma_{shadow}$.

which is then put together with the fast fading as given in (3.1). $\mathcal{F}(\mathbf{u}_k)$ is a key requisite in all our subsequent discussions throughout the chapter. Assuming the average transmitted power of each user to be equal, the $M \times 1$ received vector at the BS can now be expressed as

$$\mathbf{y} = \sqrt{p} \sum_{k \in \mathbf{\Phi}(\mathbf{u})} \mathbf{W}_k \mathbf{x}_k + \mathbf{z}, \tag{3.5}$$

where $\sqrt{p}\mathbf{x}_k$ is the $n_k \times 1$ vector of symbols transmitted by the $k$th user, with $p = \frac{P}{K}$ denoting the average transmitted power of each user and $\mathbf{z}$ a vector of additive white Gaussian noise with zero mean and co-variance matrix $\sigma^2\mathbf{I}_M$. $P$ is the total transmitted power of all the users and is considered to be fixed.

### Assumptions and Preliminaries

A few necessary assumptions which will be used throughout the chapter are stated below.

1. Perfect Channel State Information : Throughout the chapter we assume that the channel matrices $\{\mathbf{W}_k\}_{\forall k}$ are perfectly known at the BS.

2. Signal-to-Noise Ratio : We assume for each transmission link $G_{k_{ji}}$, $\mathbb{E}\{|G_{k_{ji}}|^2\} = 1$. When only transmit antenna $i$ is active, the instantaneous received SNR at the receiving antenna $j$ is $\frac{p|G_{k_{ji}}|^2}{\sigma^2}$, with $p$ being the transmit power. Thus the effective transmit SNR for the communication link can be given as $\rho = \frac{p}{\sigma^2}$. For analytical convenience, we set the same noise level ($\sigma^2$) at all the antennas, though this is not mandatory. The performance analyses performed in the later sections of this chapter will mostly be as a function of $\rho$.

3. $\mathbf{R}_k$ and $\mathbf{T}_k$ are deterministic and non-negative definite and are normalised as

$$\begin{aligned} \mathrm{tr}(\mathbf{R}_k) &= M, \\ \mathrm{tr}(\mathbf{T}_k) &= n_k. \end{aligned} \tag{3.6}$$

## 3.3 Sum Rate Analysis

For very large MIMO systems, when both $M, K \to \infty$, it becomes increasingly difficult to analyze the performance of the system based on exact analytical expressions, as

they are often too complicated to evaluate. Even computer simulations can be quite demanding for systems with such large dimensions. In such cases, large RMT can help to develop approximate analytical expressions, which substantially reduce the computational complexity. Accordingly, in this section, we formulate the approximate ergodic sum rate of the system under consideration.

## Deterministic sum rate

Let $\mathbf{\Xi}_k$ be the covariance matrix of the transmitted vectors, $\mathbf{x}_k$ of the $k$th user such that

$$\mathbb{E}\{\mathbf{x}_k\mathbf{x}_l^*\} = \begin{cases} \mathbf{\Xi}_k & if \;\; l = k \\ 0 & \text{otherwise,} \end{cases} \tag{3.7}$$

and

$$\mathbf{T}_k = \mathbf{T}_k^{\frac{1}{2}}\mathbf{\Xi}_k\mathbf{T}_k^{\frac{1}{2}}. \tag{3.8}$$

$\mathbf{\Xi}_k$ can be easily optimized for the case of Rayleigh i.i.d channel as $\mathbf{I}_{n_k}$. This is due to the consideration that $\mathbf{u}_k$ are independent and have the same transmit power. Further, let

$$\mathbf{A}_M \triangleq \sum_{k\in\mathbf{\Phi}(\mathbf{u})} \mathbf{W}_k\mathbf{W}_k^H. \tag{3.9}$$

Without loss of generality, the mutual information of a MIMO channel can be associated with the eigenvalues of the matrix $\mathbf{A}_M$ as was discussed in Section 2.5.3. The ergodic sum rate[4] of such a MIMO MAC can be given as[5] [9, 50]

$$\mathcal{R}_{\mathbf{A}_M}(\rho) \equiv \frac{1}{M}\mathbb{E}_{\mathbf{H}}\left\{\log\det\left(\mathbf{I}_M + \rho\mathbf{A}_M\right)\right\}, \tag{3.10}$$

where $\rho = \frac{p}{\sigma^2}$ is the transmit SNR of the system as described earlier and $\mathbf{A}_M$ is as discussed in the previous section. Considering the properties of a PPP, $\sum_{k\in\mathbf{\Phi}(\mathbf{u})} n_k \to \infty$ for some specific probability. Furthermore, we focus on a single BS receiver with

[4]When the channel is a time-varying channel, the capacity of the channel can have multiple definitions depending on the channel state information (CSI) at the transmitter and/or receiver. These definitions have different operational meanings. In particular, when the instantaneous channel gains, also known as the CSI, are known perfectly at both transmitter and receiver, the transmitter can adapt its transmission strategy (power and/or rate) relative to the instantaneous channel state. In this case the ergodic capacity is the maximum mutual information averaged over all channel states.

[5]For simplicity, in this chapter we assume a maximum likelihood sequence estimator at the BS to separate different data streams.

multiple antennas such that $M \to \infty$, which receives signals from multiple users. At this point, we stress that while the original massive MIMO definition in [7] assumed that $\frac{M}{K} \gg 1$, we consider the more general definition from [51], where $\frac{M}{K}$ can also be a small constant.

Before we proceed any further, it is worth mentioning the contribution of [38] and [39]. A deterministic equivalent of the ergodic mutual information for Rician faded Kronecker MIMO channel was found by Zhang et al. in [39] using the Shanon transform. This is further elucidated as Lemma 3.2 in Appendix 3.A. Let $\mu_{\mathbf{A}_M}(\lambda)$ and $\mu_M$ be the Empirical Spectral Density (ESD) and Limiting Spectral Density (LSD) of $\mathbf{A}_M$. While it has been a constant endeavour of researchers to study the limit of the empirical distribution of $\mathbf{A}_M$, [38] and [39] do that with the help of Stieltjes transform when $M \to \infty$ as

$$S_{\mathbf{A}_M}(\lambda) - S_M(\lambda) \xrightarrow{a.s.} 0, \tag{3.11}$$

where $S_{\mathbf{A}_M}(\lambda)$ and $S_M(\lambda)$ are the Stieltjes transform of $\mu_{\mathbf{A}_M}(\lambda)$ and $\mu_M$ respectively, which was discussed in Section 2.5.3. This was then used to find a deterministic equivalent of the ergodic mutual information and show that

$$\mathcal{R}_{\mathbf{A}_M} - \mathcal{R}_M \xrightarrow{a.s.} 0, \tag{3.12}$$

where $\mathcal{R}_M$ is the deterministic equivalent of the sum rate. Accordingly, we also aim to achieve the same by deriving $\mathcal{R}_M$ analytically. Further, $\mathcal{R}_{\mathbf{A}_M}$ is computed through simulations and the convergence between $\mathcal{R}_M$ and $\mathcal{R}_{\mathbf{A}_M}$ is validated in the numerical results section of this chapter.

**Lemma 3.1.** *For a single-cell massive MIMO system following a PPP in $\mathbb{R}^2$, the general probability of finding $K$ users within the coverage area of the cell can be given as [52]*

$$\mathbb{P}[K \textit{users in the cell}] = \exp\{-\kappa\mu(A)\}\frac{(\kappa\mu(A))^K}{K!}, \tag{3.13}$$

*where $\kappa$ is the intensity and $\mu(A)$ is the standard Lebesgue measure of a bounded Borel $A \subset \mathbb{R}^2$, which is formed by the topological space of the cell.*

Now, leveraging the results of [19, Sec III.A] and making use of (2.37)-(2.45), for the system model in consideration, the capacity of the system can be approximated as in the following theorem.

**Proposition 3.1.** *The ergodic sum rate of a single-cell massive MIMO system with users following a PPP, based on the LSD of* $\mathbf{A}_M$ *can be approximated as*

$$\begin{aligned}\mathcal{R}_M(\rho) &= \frac{1}{M}\log\det\left(\mathbf{I}_M+\sum_{k=0}^{\infty}\tilde{\epsilon}_k(\rho)\mathbf{R}_k\ \mathbb{P}(k)\right) \\ &+ \frac{2}{\alpha M\ln 10}\sum_{k=0}^{\infty}\sum_{i=1}^{n_k}G_{3,3}^{2,2}\left(\frac{r^{\alpha}}{\psi_k\lambda_{ki}}\middle|\begin{matrix}1-\frac{2}{\alpha},0,\ 1\\ 0,\quad 0,-\frac{2}{\alpha}\end{matrix}\right)\mathbb{P}(k)-\sum_{k=0}^{\infty}\epsilon_k(\rho)\tilde{\epsilon}_k(\rho)\ \mathbb{P}(k),\end{aligned} \tag{3.14}$$

*where*

$$\epsilon_k(\rho) = \frac{1}{M}\mathrm{tr}\left(\rho\mathbf{R}_k\left[\mathbf{I}_M+\sum_{k=0}^{\infty}\tilde{\epsilon}_k(\rho)\mathbf{R}_k\ \mathbb{P}(k)\right]^{-1}\right), \tag{3.15}$$

$$\tilde{\epsilon}_k(\rho) = \frac{1}{n_k}\mathrm{tr}\left(\rho\mathbf{T}_k\left\langle\mathrm{diag}\left[\mathbf{I}_{n_k}+\frac{M\epsilon_k(\rho)\mathbf{T}_k}{n_k}\right]^{-1}_{\forall k\in\mathbf{\Phi}(\mathbf{u})}\right\rangle\right). \tag{3.16}$$

*Further,* $G_{p,q}^{m,n}\{\cdot\}$ *is the hyper-geometric function also known as Meijer G-function [[53], eq. (9.301)] and* $\lambda_{ki} = eig(\mathbf{T}_k)$*. There is a unique solution to* (3.15) *and* (3.16) *for* $\rho\in\mathbb{R}^+$*, where* $\epsilon_k(\rho)\in\mathbb{S}(\mathbb{R}^+)$ *and* $\tilde{\epsilon_k}(\rho)\in\mathbb{S}(\mathbb{R}^+)$ *for* $k\in\mathbf{\Phi}(\mathbf{u})$*. Furthermore,* $\mathbb{S}(\mathbb{R}^+)$ *can be interpreted as the class of all Stieltjes transforms of finite positive measures carried over* $\mathbb{R}^+$ *and* $\mathbb{P}(k)$ *is obtained from Lemma 3.1.*

*Proof.* It is to be noted that the number of users is calculated based on a PPP with respect to the probability given by Lemma 3.1 and the intensity of the users, $\kappa$. Our aim now is to derive the closed form expression of the deterministic ergodic sum rate as given in (3.14) and also to show that there is a unique solution to (3.15) and (3.16). For better understanding, we divide the proofs into two parts. The detailed derivation of (3.14) is given in Appendix 3.B, while the proof of uniqueness of (3.15) and (3.16) is given in Appendix 3.C. □

## 3.4 High and Low SNR Approximations

In this section, we provide the high and low SNR approximations of the derived sum rate in (3.14).

### 3.4.1 High SNR regime

Fast fading channels have the same properties at high SNR as time-invariant channels, irrespective of the knowledge of channel state information at the transmitter. In this sub-section, we analyse the capacity in the high SNR regime i.e., $\rho \to \infty$.

**Corollary 3.1.** *Let $\psi_k = \frac{M}{n_k}\epsilon_k(\rho)$. Then at relatively high SNR ($\rho \to \infty$) regime for correlated massive MIMO channels, $\mathcal{R}_{\mathcal{M}}$ approaches the exact sum rate and can be given as*

$$\mathcal{R}_{\mathcal{M}\rho\to\infty}(\rho) = \frac{1}{M}\sum_{k=0}^{\infty}\log(\mathrm{tr}(\tilde{\epsilon}_k(\rho)\mathbf{R}_k))\mathbb{P}(k) \tag{3.17}$$
$$+ \quad \frac{1}{2}\sum_{k=0}^{\infty}\sum_{i=1}^{n_k}\left[2\log(\psi_k\lambda_{ki}) + \left(2\log(r^{-\alpha}) + \alpha\right)\right]\mathbb{P}(k) - \sum_{k=0}^{\infty}\epsilon_k(\rho)\tilde{\epsilon}_k(\rho)\ \mathbb{P}(k).$$

*Proof.* Considering $\rho$ to be large, (3.42) can be approximated as

$$\mathcal{R}_{\mathcal{M}\rho\to\infty}(\rho) \approx \frac{1}{M}\log\det\left(\sum_{k=0}^{\infty}\tilde{\epsilon}_k(\rho)\mathbf{R}_k\right)\mathbb{P}(k) \tag{3.18}$$
$$+ \quad \frac{2}{r^2}\sum_{k=0}^{\infty}\left(\sum_{i=1}^{n_k}\int_0^r \log(\psi_k\lambda_{ki}u^{-\alpha})u\mathrm{d}u\right)\mathbb{P}(k) - \sum_{k=0}^{\infty}\epsilon_k(\rho)\tilde{\epsilon}_k(\rho)\ \mathbb{P}(k).$$

Using integration by parts and substituting the limits of the integral in the above we obtain the proof. □

### 3.4.2 Low SNR regime

When the SNR of the system is relatively low, the multiplexing gains of the system are lost. In such a scenario when $\rho \to 0$, the sum rate can be approximated by the following corollary.

**Corollary 3.2.** *Similar to the high SNR case, at low SNR the sum rate can be approximated as*

$$\mathcal{R}_{\mathcal{M}\rho\to 0} = \sum_{k=0}^{\infty}\left[\frac{1}{M}\frac{\mathrm{tr}(\tilde{\epsilon}_k(\rho)\mathbf{R}_k)}{\log 10} + \frac{2r^{1-\alpha}\mathrm{tr}(\psi_k\mathbf{T}_k)}{(2-\alpha)M\log 10}\right]\mathbb{P}(k) \tag{3.19}$$

*Proof.* This can be easily proved by using the approximation $\log_2(1+a) \approx a/\log 2$ for small $a$ in (3.14). □

### 3.4.3 Complexity analysis

In this subsection, we analyze the complexity of both the high and low SNR approximations with respect to (3.14). We focus on the complexity of calculation and running time for common mathematical operations that are used in our algorithms. Complexity in this analysis refers to the time complexity of performing computations with respect to a reference Turing machine [54].

We consider the upper bound of the operation time such that for a sufficiently large number $n$, the limiting behavior of a function $f(n)$ is denoted by $O\left(g(n)\right)$, where the function $f$ is bounded above by the function $g$. Let the complexity of $\epsilon_k$ and $\tilde{\epsilon}_k$ be denoted by $O(\phi_1)$ and $O(\phi_2)$. Then, following the complexity of some basic mathematical calculations as given in [55], for a single iteration under $\mathbf{\Phi}(\mathbf{u})$, the complexity of the approximation in Proposition 3.1, Corollary 3.1 and Corollary 3.2 can be approximated as $O(n^3 \log n + n^2(\log n)^2 + \phi_1\phi_2)$, $O(n^2 \log n + \log n + \phi_1\phi_2)$ and $O(n^2)$ respectively. Hence, it can be stated that the high and low SNR approximations have low computational complexities when compared to the sum rate approximation given in Proposition 3.1. Later, in the numerical section of this chapter we show that these two approximations are quite tight and can be used appropriately in the respective regimes.

## 3.5 $k$th User Capacity

We have so far focused our discussion based on the total number of users, $K$ within the coverage area of the BS. We now order the users based on their distances from the BS as $||\mathbf{u}_1|| < ||\mathbf{u}_2|| < ||\mathbf{u}_3|| < \cdots < ||\mathbf{u}_k|| < \cdots < ||\mathbf{u}_K||$. In this section, we discuss the capacity of the $k$th order user selected from the Poisson point process based on the probability and intensity of the users.

**Proposition 3.2.** *Considering the order of the users as described, the distribution of the location of the $k$th ordered user with respect to the BS can be given as [52]*

$$f(||\mathbf{u}_k||) = \exp(-\kappa\pi r^2)\frac{2(\kappa\pi r^2)^k}{r\Gamma(k)} \tag{3.20}$$

*The ergodic rate for this user can now be approximated as*

$$\begin{aligned}\mathcal{R}_M^k(\rho) &= \frac{1}{M}\log\det\left(\mathbf{I}_M+\tilde{\epsilon}_k(\rho)\mathbf{R}_k\right)+\sum_{n=0}^{\infty}\frac{2(-1)^n(\sqrt{\kappa\pi})^{(2n+k)}r^{(2(n+k)+1)}}{\alpha n!\Gamma(k)}\\ &\times \sum_{i=1}^{n_k}G_{3,3}^{2,2}\left(\frac{r^\alpha}{\psi_k\lambda_{ki}}\middle|\begin{matrix}1-\frac{2(n+k)+1}{\alpha},0,\ 1\\ 0,\quad 0,-\frac{2(n+k)+1}{\alpha}\end{matrix}\right)-\epsilon_k(\rho)\tilde{\epsilon}_k(\rho),\end{aligned} \tag{3.21}$$

*where $G_{p,q}^{m,n}\{\cdot\}$ is the hyper-geometric function and $n\in\mathbb{R}$ with $0\leq n\leq\infty$. All other parameters are as previously defined.*

*Proof.* To prove this, we build on our previous proof of (3.14) and consider a random user. The detailed derivation is given in Appendix 3.D. □

**Corollary 3.3.** *Considering the order of the users as described in this section, the distribution of the first user in the order can be given as*

$$f(||\mathbf{u}_1||)=2\exp(-\kappa\pi r^2)\kappa\pi r. \tag{3.22}$$

*Accordingly, the rate for this user can be approximated as*

$$\begin{aligned}\mathcal{R}_M^1(\rho) &= \frac{1}{M}\log\det\left(\mathbf{I}_M+\tilde{\epsilon}_1(\rho)\mathbf{R}_1\right)+\sum_{n=0}^{\infty}\frac{2(-1)^n(\sqrt{\kappa\pi})^{(2n+1)}r^{(2(n+1))}}{\alpha n!}\\ &\times \sum_{i=1}^{n_k}G_{3,3}^{2,2}\left(\frac{r^\alpha}{\psi_1\lambda_{1i}}\middle|\begin{matrix}1-\frac{2(n+1)}{\alpha},0,\ 1\\ 0,\quad 0,-\frac{2(n+2)}{\alpha}\end{matrix}\right)-\epsilon_1(\rho)\tilde{\epsilon}_1(\rho).\end{aligned} \tag{3.23}$$

## 3.6 Energy Efficiency

The energy efficiency of a communication link is the ratio of the achievable sum rate to the total power consumed and is given in bits/joule [14], [46]. The corresponding energy efficiency as studied in many existing works is thus given as [56, 14, 57]

$$\xi=\frac{\mathcal{R}_M}{p^{PA}+p^{RF}}, \tag{3.24}$$

where $p^{PA}$ is the power consumed by the power amplifiers and $p^{RF}$ is the power consumed by the RF components of both BS and UEs.

### 3.6.1 Power amplifiers

The average power in watt consumed by the power amplifiers during uplink can be approximated as [9, 57]

$$p^{PA} = P(\alpha + 1), \tag{3.25}$$

where $\alpha = \frac{\zeta}{\eta} - 1$ with $\zeta$ being the modulation-dependent peak to average power ratios (PAPR) for uplink while $\eta$ is the power amplifier efficiency and $P$ is the total transmitted power of all users as described earlier.

### 3.6.2 RF chains

The average power in watt consumed in the RF chains for a typical MIMO transmitter-receiver set can be given as [46]

$$p^{RF} = Mp^{BS} + Kp^{UE}, \tag{3.26}$$

where $p^{BS}$ is the power required at the BS to run the circuit components and $p^{UE}$ is the power associated with the user equipments. They are further defined as follows

$$p^{BS} = p^{BS}_{mix} + p^{BS}_{filt} + p^{BS}_{ADC} + p^{BS}_{DAC} + p^{BS}_{OSC}, \tag{3.27}$$

$$p^{UE} = p^{UE}_{mix} + p^{UE}_{filt} + p^{UE}_{ADC} + p^{UE}_{DAC} + p^{UE}_{OSC}, \tag{3.28}$$

where $p_{mix}$, $p_{filt}$, $p_{ADC}$, $p_{DAC}$ and $p_{OSC}$ denote the power consumed by the mixers, filters, analog-to-digital converters, digital-to-analog converters and local oscillator respectively[6].

Most existing works consider the total power consumed in the RF cicuits of the system to be fixed. This consideration can be very detrimental in the analysis of a large scale MIMO system, like ours, where both $M$, $K \to \infty$, which eventually leads to unbounded EE. This outcome is the consequence of disregarding the fact that dedicated circuit components with non-zero power consumption are required for each antenna at the BS. As a matter of fact, EE does not always increase with $M$ or $K$.

[6]The components considered in this chapter may vary from set-ups used in practical scenarios. Any other components used can easily be included in the expressions of $p^{BS}$ and $p^{UE}$ while the ones that are not used may be removed.

Furthermore, we have previously assumed the average fixed power transmitted by all the users to be equal. However, the optimization of power to attain better energy efficiency is of paramount importance. While in this chapter we give an appropriate model for $p^{RF}$ and validate our assumptions with simulations, the optimization of the power and the number of antennas at the BS to attain a energy efficient system is dealt with in Chapter 4.

## 3.7 Numerical Results

This section validates the system model and also verifies our result in Proposition 3.1 and the resulting corollaries by making comparisons between the ergodic sum rate and the approximate sum rate. We analyze the behavior of the system model under consideration with respect to increasing SNR while varying other significant system parameters. In general, the computation of the ergodic sum rate is done through Monte Carlo simulations (1000 realizations) which is then used to validate the simulation of the analytical results. Unless stated otherwise, most of the values of the parameters used are inspired from literature mentioned in references [13, 58]. For the system guidelines, we consider a circular cell as stated earlier with a radius of $r = 1000$ meters. The users are uniformly distributed within the coverage area of the cell and their numbers are governed by Poisson distribution with intensity $\kappa$ and probability given by (3.13) in Lemma 3.1. Hereinafter, we consider all the users in the system to be equipped with two antennas and examine the validity of our approximations with respect to simulations. While Fig. 3.2 shows the uplink sum rate versus SNR for various antenna configurations at the BS, Fig. 3.3 shows the uplink sum rate versus SNR for different user intensities, $\kappa$ inside the coverage area of the cell. Specifically, these two figures attempt at validating Proposition 3.1. In other words, we intend to see how well $\mathcal{R}_M(\rho)$ in (3.14) approximates to $\mathcal{R}_{\mathbf{A}_M(\rho)}$ in (3.10). Here, we choose the path loss exponent, $\alpha = 2.2$ and the intensity of the users, $\kappa = 0.01$. In Fig. 3.2, understandably, the sum rate increases as we increase the average SNR. But what is notable is that, as we increase the number of antennas from 8 to 150, the analytic curve tends to converge tightly towards the simulation. This implies that $\mathcal{R}_M(\rho) - \mathcal{R}_{\mathbf{A}_M(\rho)} \to 0$ which proves the validity of our approximation for large MIMO systems. Nevertheless, it is also important to see how the analytical approximation fares when the system dimension is not so large. In this regard, we see that the approximation also holds true for fewer number of antennas as can be seen for the cases of $M = 8, 12, 20, 50$ but with

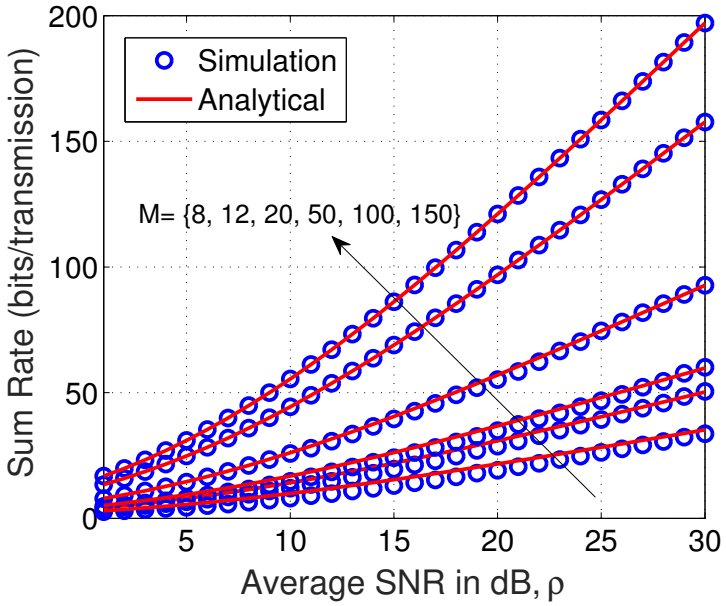


***Figure 3.2:*** *Simulation and analytical sum rate versus SNR for different number of antennas, $M$ at the BS. $\kappa = 0.01$, $\alpha = 2.2$.*

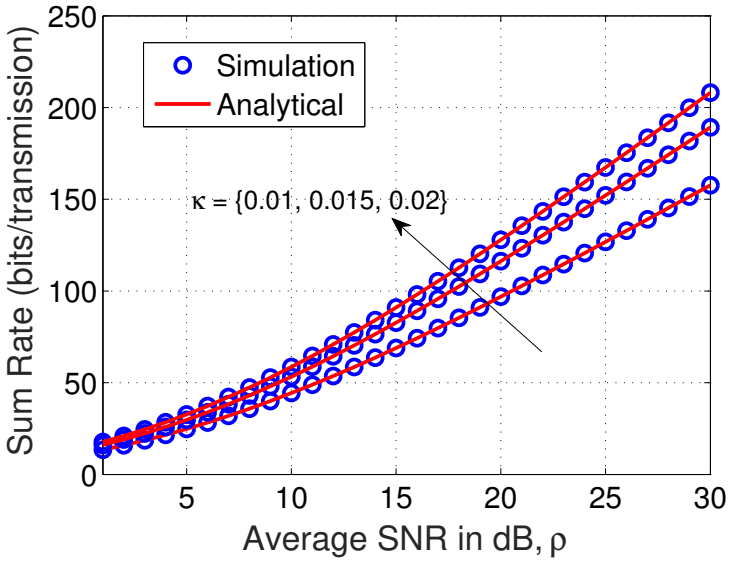


***Figure 3.3:*** *Simulation and analytical sum rate versus SNR for different intensities, $\kappa$ of the users within the cell. $M = 100$, $\alpha = 2.2$.*

error of a few bits. Hence, it is crucial to investigate the scenarios when the number of antennas is not a very large number, which we concentrate on in our subsequent analyses. In addition, as we increase $M$, the ergodic sum rate also increases. For the case of Fig. 3.3, we choose $M = 100$ and $\alpha = 2.2$. We vary $\kappa$ from 0.01 to 0.02 in

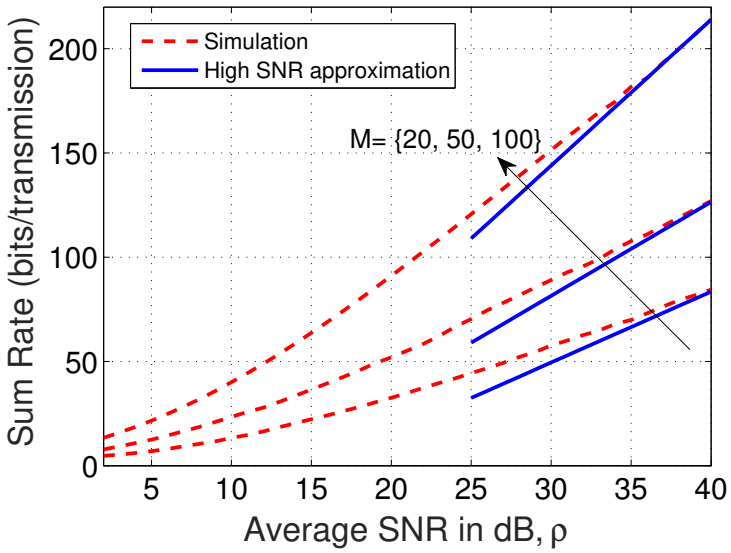


***Figure 3.4:*** *High SNR approximation of sum rate versus SNR for different number of antennas, $M$ at the BS. $\kappa = 0.01$, $\alpha = 2.2$.*

steps of 0.005. Our approximation holds good for all the three cases and hence, we can assert the convergence of our analytic approximation for a massive MIMO scenario. Furthermore, the sum rate of the system increases owing to the increase in $\kappa$ which in turn increases $K$, thus increasing the transmit antennas. The increase in sum rate follows a similar pattern as Fig. 3.2 with the scaling more pronounced when increasing from $\kappa = 0.01$ to 0.015 than 0.015 to 0.02.

In Fig. 3.4, we plot the approximate sum rate for the high SNR regime from Corollary 3.1 versus the average SNR for different combinations of $M$. $M$ is varied while $\kappa$ is kept at 0.01 and $\alpha$ at 2.2. It is quite evident from the figure that at high SNR regime the path loss fluctuations are negated due to high transmit power of the users, thus producing very high sum rates. Also it can be seen that the simulations and approximations converge at relatively high SNR which validates our analysis. As can be expected, $M = 100$ yields the maximum sum rate followed by other combinations. Furthermore, the slopes of the curves become steeper with the increase in $M$ and the approximations converge with the simulations at very high SNR, thus validating our result.

In Fig. 3.5 we show the sum rate approximation in the low SNR regime from Corollary 3.2. We consider similar settings as in Fig. 3.4 with the exception of the SNR range. Both simulations and analytic expression considering various $M$ are plotted. The approximations effectively converge with the simulations for very low SNR while

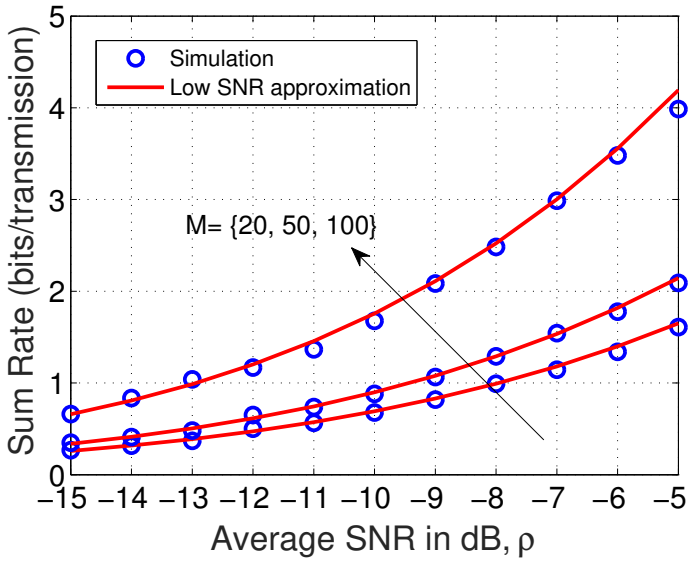


***Figure 3.5:*** *Low SNR approximation of sum rate versus SNR for different number of antennas, $M$ at the BS. $\kappa = 0.01$, $\alpha = 2.2$.*

they diverge from the simulations in the moderately low SNR region. Moreover, it can be seen that the gap in performance when the number of antennas are increased is quite minimal. This is due to the fact that the multiplexing gains are lost in the low SNR regime.

At this point it is worth mentioning the fact that the high and low SNR approximations are quite tight and considerably reduce the computation complexity of the sum rate of the system. From a system design point of view, they can be quite easy for engineers to implement in terms of computation time and complexity.

Next we analyze the EE of our system model with respect to a reference EE. We define this EE as relative EE. First we calculate the EE of a reference system model and then simulate the EE of our system by normalizing it with the reference system model. We start by considering a single input single output (SISO) system with the single user equipped with a single antenna transmitting to the BS equipped with one antenna only. We consider $P^{BS} = 1W$ and $p^{UE} = 0.1W$ and $p = 10dB$ [13]. Thus, from (3.24) we have

$$\xi_{ref} = \frac{\mathcal{R}_{Mref}}{p_{ref} + Mp^{BS} + Kp^{UE}}. \tag{3.29}$$

Numerically we calculate $\mathcal{R}_{Mref} = 0.6$ bits/ transmission for $M = 1$ and $K = 1$. Hence, from (3.29) we get $\xi_{ref} = 0.054$ bits/Joule. The following EE discussion will be

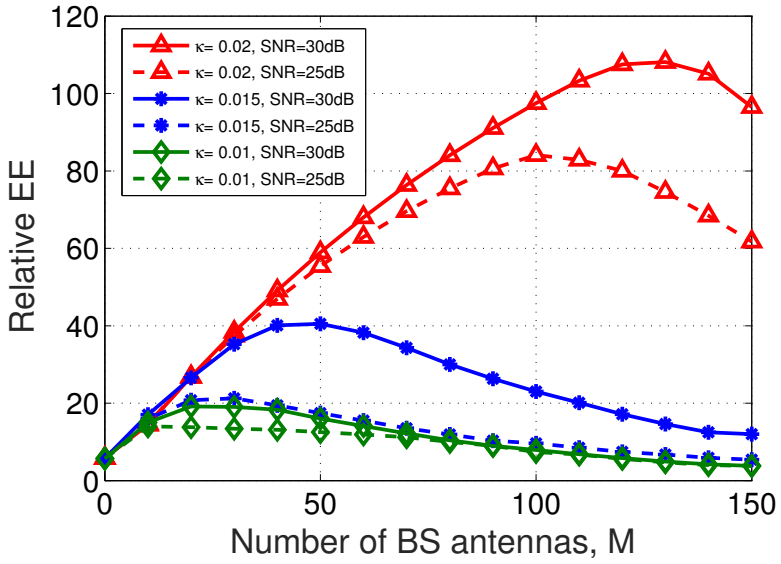


***Figure 3.6:*** *Relative energy efficiency versus number of BS antennas, $M$ with respect to a reference system ($M = 1$, $K = 1$, $n_k = 1$), for different SNR and user intensities. Here, $\alpha = 2.2$.*

based on relative EE, defined as $\frac{\xi}{\xi_{ref}} = \frac{\xi}{0.054}$. Since it is a ratio, it is dimensionless. Fig. 3.6 illustrates the relative EE of the system with respect to $M$ for different user intensities and transmit powers. For a particular transmit SNR, as we increase the number of antennas at the BS, the EE increases for a while, attains a local maximum and then starts descending. This is an expected result as we consider a power consumption model, which is a function of $M$ and $K$ with respect to the circuit power consumption. Moreover, for a particular user intensity, with varying transmit power, the EE also increases in the beginning, attains a local maximum and then starts decreasing. For example, for the case of $\kappa = 0.02$, the EE curves for SNR 25 and 30 dBs start falling between 100 and 150 antennas. This implies that a certain level of maximized EE can be achieved in such systems by increasing the number of BS antennas but with the important discrepancy of not requiring to increase the transmit power. In a nutshell, the EE curve is a quasi-concave function of $M$ which doesn't always increase with $M$ in large MIMO systems.

## 3.8 Summary

The uplink performance of a massive MIMO system was analyzed. We use stochastic geometry to characterise the spatially distributed users while large dimensional RMT was used to achieve deterministic approximations of the sum rate of the system. We analysed the sum rate of such a system both by means of simulations and analyti-

cal expressions. In particular, the BS along with the users were considered to follow a PPP. Approximations for the analytical sum rate were provided along with closed-form expressions at the low and high SNR regimes. The approximations were further validated with Monte-Carlo simulations. The performance was evaluated with respect to the number of antennas at the BS and the intensity of the users. Analytical approximation for the rate of the general $k$th ordered user based on a PPP was derived. We also provided an analysis of the energy efficiency of the system by taking into consideration the circuit power consumption, which was shown to be a function of the number of antennas and the users. The relative energy efficiency of the system was plotted with respect to varying BS antennas for different SNR range. It was shown that the energy efficiency is a quasi-concave function of the number of base station antennas and does not always increase linearly with it.

Unlike the sum rate, EE doesn't monotonically increase with the number of BS antennas and hence it is important to find the optimum number of antennas. Accordingly, in the following chapter, we derive the optimum number of antennas that can be rigged in a space constrained massive MIMO system when EE is considered as a design criteria.

# Appendix 3.A Useful Lemmas

**Lemma 3.2.** *Let* $\Upsilon_k = \frac{M}{n_k}$ *and* $M, n_k \to \infty$*, such that* $0 < \min_k \liminf_M \Upsilon_k < \max_k \limsup_M \Upsilon_k < \infty$*. Then, the deterministic equivalent of the uplink ergodic sum rate for a large antenna MIMO system consisting of* $M$ *antennas and* $K$ *users based on the Stieltjes and Shannon transform can be given as [39]*

$$\begin{aligned}\bar{\mathcal{R}}_M(\rho) =& \frac{1}{M}\log\det\left(\frac{\mathbf{\Gamma^{-1}}(\rho)}{\rho}\right) + \frac{1}{M}\sum_{k=1}^{K}\log\det\left(\frac{\mathbf{\tilde{\Delta}^{-1}}(\rho)}{\rho}\right) \\ &- \rho\sum_{k=1}^{K}\varepsilon_k(\rho)\tilde{\varepsilon}_k(\rho),\end{aligned} \tag{3.30}$$

*where*

$$\mathbf{\Gamma}(\rho) = \left(\mathbf{\Delta}(\rho)^{-1} - \rho\tilde{\mathbf{H}}\tilde{\mathbf{\Delta}}(\rho)\tilde{\mathbf{H}}^H\right)^{-1}, \tag{3.31}$$

$$\tilde{\mathbf{\Gamma}}(\rho) = \left(\tilde{\mathbf{\Delta}}(\rho)^{-1} - \rho\tilde{\mathbf{H}}\mathbf{\Delta}(\rho)\tilde{\mathbf{H}}^H\right)^{-1}, \tag{3.32}$$

$$\mathbf{\Delta}(\rho) = \frac{1}{\rho}\left(\mathbf{I}_M + \sum_{k=1}^{K} \tilde{\varepsilon}_k(\rho)\mathbf{R}_k\right), \tag{3.33}$$

$$\tilde{\mathbf{\Delta}}(\rho) = \frac{1}{\rho}\text{diag}\left(\mathbf{I}_{n_k} + \Upsilon_k \varepsilon_k(\rho)\mathbf{T}_k\right)_{\forall k}, \tag{3.34}$$

$$\varepsilon_k(\rho) = \frac{1}{M}\text{tr}(\mathbf{R}_k\mathbf{\Gamma}(\rho))_{\forall k}, \tag{3.35}$$

$$\tilde{\varepsilon}_k(\rho) = \frac{1}{n_k}\text{tr}(\mathbf{T_k}\langle\tilde{\mathbf{\Gamma}}(\rho)\rangle_k)_{\forall k}, \tag{3.36}$$

*with* $\tilde{\mathbf{H}}_k$ *being the LOS channel between the BS and the user* $k$ *and* $\rho$ *the total SNR of the system. All other parameters are as previously defined.*

**Lemma 3.3.** *[59] A continuous function* $f(a)$ *converges if it is a contraction. Moreover, the continuous function* $f(a)$ *is a contraction if the absolute value of its first order derivative is always less than* 1*.*

# Appendix 3.B Proof of Proposition 3.1

*Proof.* For the case of Rayleigh faded channels with no line of sight, Lemma 3.2 can be modified as

$$\begin{aligned}\hat{\mathcal{R}}_M(\rho) =& \frac{1}{M}\log\det\left(\frac{\mathbf{\Lambda^{-1}}(\rho)}{\rho}\right) + \frac{1}{M}\sum_{k=1}^{K}\log\det\left(\frac{\tilde{\mathbf{\Lambda}}^{\mathbf{-1}}(\rho)}{\rho}\right) \\ & - \rho\sum_{k=1}^{K}\epsilon_k(\rho)\tilde{\epsilon}_k(\rho),\end{aligned} \tag{3.37}$$

where

$$\mathbf{\Lambda}(\rho) = \frac{1}{\rho}\left(\mathbf{I}_M + \sum_{k=1}^{K}\tilde{\varepsilon}_k(\rho)\mathbf{R}_k\right), \tag{3.38}$$

$$\tilde{\mathbf{\Lambda}}(\rho) = \frac{1}{\rho}\text{diag}\left(\mathbf{I}_{n_k} + \frac{M}{n_k}\varepsilon_k(\rho)\mathbf{T}_k\right)_{\forall k}, \tag{3.39}$$

$$\epsilon_k(\rho) = \frac{1}{M}\text{tr}(\mathbf{R}_k\mathbf{\Lambda}(\rho))_{\forall k}, \tag{3.40}$$

$$\tilde{\epsilon}_k(\rho) = \frac{1}{n_k}\text{tr}(\mathbf{T_k}\langle\tilde{\mathbf{\Lambda}}(\rho)\rangle_k)_{\forall k}. \tag{3.41}$$

Therefore, simplifying (3.37)-(3.41) and incorporating the path losses for the users, which follow a PPP within the cell, the sum rate of a MIMO system can be approxi-

mated as

$$\begin{aligned}\mathcal{R}_M(\rho) &= \frac{1}{M}\log\det\left(\mathbf{I}_M+\sum_{k\in\mathbf{\Phi}(\mathbf{u})}\tilde{\epsilon}_k(\rho)\mathbf{R}_k\right) \\ &+ \mathbb{E}_{\mathbf{u}}\left\{\frac{1}{M}\sum_{k\in\mathbf{\Phi}(\mathbf{u})}\log\det\left(\mathbf{I}_{n_k}+\frac{M}{n_k}\mathcal{F}(\mathbf{u})\epsilon_k(\rho)\mathbf{T}_k\right)\right\}-\rho\sum_{k\in\mathbf{\Phi}(\mathbf{u})}\epsilon_k(\rho)\tilde{\epsilon}_k(\rho),\end{aligned} \tag{3.42}$$

where $\epsilon_k(\rho)$and $\tilde{\epsilon}_k(\rho)$ are as described in (3.15) and (3.16) and $\mathcal{F}$ denotes the large scale fading as described before. Our aim now is to derive a closed form expression for the second term on the right hand side of (3.42).

Let $\psi_k=\frac{M}{n_k}\epsilon_k(\rho)$. Then

$$\begin{aligned}&\mathbb{E}_{\mathbf{u}}\left\{\log\det(\mathbf{I}_{n_k}+\mathcal{F}(\mathbf{u})\psi_k\mathbf{T}_k)\right\} \\ =\;& \frac{2}{r^2}\int_0^r\log\det(\mathbf{I}_{n_k}+\psi_k\mathbf{T}_k u^{-\alpha})u\mathrm{d}u \qquad (3.43)\\ =\;& \frac{2}{r^2}\int_0^r\log\prod_{i=1}^{n_k}(1+\psi_k\lambda_{ki}u^{-\alpha})u\mathrm{d}x \\ =\;& \frac{2}{r^2}\int_0^r\sum_{i=1}^{n_k}\log(1+\psi_k\lambda_{ki}u^{-\alpha})u\mathrm{d}u \\ =\;& \frac{2}{r^2\ln 10}\sum_{i=1}^{n_k}\int_0^r\ln(1+\psi_k\lambda_{ki}u^{-\alpha})u\mathrm{d}u \\ \overset{(a)}{=}\;& \frac{2}{r^2\ln 10}\sum_{i=1}^{n_k}\int_0^r G_{2,2}^{1,2}\left(\psi_k\lambda_{ki}\,u^{-\alpha}\middle|\begin{smallmatrix}1,1\\1,0\end{smallmatrix}\right)u\mathrm{d}u \\ \overset{(b)}{=}\;& \frac{2}{r^2\ln 10}\sum_{i=1}^{n_k}\int_0^r G_{2,2}^{2,1}\left(\frac{1}{\psi_k\lambda_{ki}}u^{\alpha}\middle|\begin{smallmatrix}0,1\\0,0\end{smallmatrix}\right)u\mathrm{d}u. \qquad (3.44)\end{aligned}$$

Here, $(a)$ is obtained using the identity [60]

$$\log(1+\beta z)=\frac{\ln(1+\beta z)}{\ln 10}=\frac{1}{\ln 10}G_{2,2}^{1,2}\left(\beta z\mid\begin{smallmatrix}1,1\\1,0\end{smallmatrix}\right), \tag{3.45}$$

and $(b)$ is obtained from [[53], eq. (7.811)]. Substituting $y$ with $u^{\alpha}$ and changing the limits of integration, (3.44) becomes,

$$\frac{2}{r^2\ln 10}\sum_{i=1}^{n_k}\int_0^{r^{\alpha}}G_{2,2}^{2,1}\left(\frac{1}{\psi_k\lambda_{ki}}y\middle|\begin{smallmatrix}0,1\\0,0\end{smallmatrix}\right)\frac{1}{\alpha}y^{(\frac{2}{\alpha}-1)}\mathrm{d}y. \tag{3.46}$$

Again, substituting $\frac{y}{r^\alpha}$ with $z$ and changing the corresponding limits of integration we have

$$\begin{aligned}
& \mathbb{E}_{\mathbf{u}}\left\{\log\det(\mathbf{I}_{n_k}+\mathcal{F}(\mathbf{u})\psi_k\mathbf{T}_k)\right\} \\
= & \frac{2}{r^2\ln 10}\sum_{i=1}^{n_k}\int_0^1 G_{2,2}^{2,1}\left(\frac{r^\alpha}{\psi_k\lambda_{ki}}z\middle|\begin{matrix}0,1\\0,0\end{matrix}\right)\times\frac{1}{\alpha}\left(zr^\alpha\right)^{(\frac{2}{\alpha}-1)}r^\alpha\mathrm{d}z \\
= & \frac{2}{\alpha\ln 10}\sum_{i=1}^{n_k}\int_0^1 G_{2,2}^{2,1}\left(\frac{(r)^\alpha}{\psi_k\lambda_{ki}}z\middle|\begin{matrix}0,1\\0,0\end{matrix}\right)z^{(\frac{1}{\alpha}-1)}\mathrm{d}z \\
= & \frac{2}{\alpha\ln 10}\sum_{i=1}^{n_k}\Gamma(1)G_{3,3}^{2,2}\left(\frac{(r)^\alpha}{\psi_k\lambda_{ki}}\middle|\begin{matrix}1-\frac{2}{\alpha},0,\ 1\\0,\quad 0,-\frac{2}{\alpha}\end{matrix}\right), \qquad (3.47)
\end{aligned}$$

where (3.47) is obtained using [[53], eq. (7.813)]. Now, plugging (3.47) in (3.42) and summing for $k$ users (using Lemma 3.1), (3.14) is obtained. □

# Appendix 3.C Proof of uniqueness of eq. (3.15) and eq. (3.16)

In order to prove that $\epsilon_k(\rho)$ and $\tilde{\epsilon}_k(\rho)$ in (3.15) and (3.16) have unique solutions, it is sufficient to show that after a single update or an iteration, $\epsilon_k(\rho)$ and $\tilde{\epsilon}_k(\rho)$ converge. In particular, we will use the Contraction principle [59] to show that $\epsilon_k^{t+1}(\rho)-\epsilon_k^t(\rho)\to 0$ and $\tilde{\epsilon}_k^{t+1}(\rho)-\tilde{\epsilon}_k^t(\rho)\longrightarrow 0$, where $t$ is any instant. Now, at instant $t+1$, eq. (3.15) and eq. (3.16) can be given as

$$\epsilon_k^{t+1}(\rho) = \frac{1}{M}\mathrm{tr}\left(\rho\mathbf{R}_k\left[\mathbf{I}_M+\sum_{k=0}^{\infty}\tilde{\epsilon}_k^t(\rho)\mathbf{R}_k\,\mathbb{P}(k)\right]^{-1}\right),\mathrm{diag} \qquad (3.48)$$

$$\tilde{\epsilon}_k^{t+1}(\rho) = \frac{1}{n_k}\mathrm{tr}\left(\rho\mathbf{T}_k\left\langle\mathrm{diag}\left[\mathbf{I}_{n_k}+\frac{M\epsilon_k^t(\rho)\mathbf{T}_k}{n_k}\right]^{-1}_{\forall k\in\mathbf{\Phi}(\mathbf{u})}\right\rangle\right). \qquad (3.49)$$

We assume that $\lambda_i(\mathbf{A})$ is the $i$th eigenvalue of the matrix $\mathbf{A}$. Without loss of generality, the $\lambda_i(\mathbf{A})$s are sorted in non-increasing order as $\lambda_1(\mathbf{A})\geq\lambda_2(\mathbf{A})\geq\lambda_3(\mathbf{A})\geq\cdots\geq\lambda_K(\mathbf{A})$. Herein, (3.48) and (3.49) are equivalent to [61]

$$\epsilon_k^{t+1}(\rho)=\frac{1}{M}\sum_{i=1}^{M}\frac{\lambda_i(\rho\mathbf{R}_k)}{1+\lambda_i\left(\sum_{k=0}^{\infty}\tilde{\epsilon}_k^t(\rho)\mathbf{R}_k\right)\mathbb{P}(k)}, \qquad (3.50)$$

$$\tilde{\epsilon}_k^{t+1}(\rho) = \frac{1}{n_k} \sum_{i=1}^{n_k} \frac{\lambda_i(\rho \mathbf{T}_k)}{1 + \lambda_i \left( \frac{M \epsilon_k^t(\rho)}{n_k} \mathbf{T}_k \right)}. \tag{3.51}$$

It should be noted that in our model, we assume the correlation matrices at the BS, $\mathbf{R}_k$s to be all the same and hence without loss of generality, we write $\mathbf{R}_k = \mathbf{R}$. Furthermore, let

$$\Psi_k^t = \frac{1}{n_k} \left( 1 + \frac{n_k}{M \epsilon_k^t(\rho)} \sum_{i=1}^{n_k} \frac{1}{\lambda_i(\mathbf{T}_k)} \right). \tag{3.52}$$

Then, the eigenvalues of matrix $\mathbf{T}_k$ is given by

$$\lambda_i(\mathbf{T}_k) = \left( \Psi_k^t \lambda_i(\mathbf{T}_k) - \frac{n_k}{M} \left( \epsilon_k^t(\rho) \right)^{-1} \right)_+, \tag{3.53}$$

where $(\mathbf{A})_+$ is the element-wise positive part of matrix $(\mathbf{A})$, while for scalar $(x)_+ \triangleq \max\{0, x\}$. With the help of (3.52) and (3.53), $\tilde{\epsilon}_k^{t+1}(\rho)$ can now be rewritten as

$$\begin{aligned} \tilde{\epsilon}_k^{t+1}(\rho) =& \frac{\rho}{n_k} \sum_{i=1}^{n_k} \frac{\Psi_k^t \lambda_i(\mathbf{T}_k) - \frac{n_k}{M} \left( \epsilon_k^t(\rho) \right)^{-1}}{\frac{M}{n_k} \epsilon_k^t(\rho) \Psi_k^t \lambda_i(\mathbf{T}_k)} \\ =& \frac{\rho}{\epsilon_k^t(\rho) \Psi_k^t M} \\ =& \frac{\rho \frac{n_k}{M}}{\epsilon_k^t(\rho) + \frac{n_k}{M} \sum_{i=1}^{n_k} \frac{1}{\lambda_i(\mathbf{T}_k)}}. \end{aligned} \tag{3.54}$$

Letting $v_k^t = \ln\left(\tilde{\epsilon}_k^t(\rho)\right)$, the convergence problem of $\epsilon_k^{t+1}(\rho)$ and $\tilde{\epsilon}_k^{t+1}(\rho)$ is equivalent to the convergence problem of the following function

$$v_k^{t+1} = f(v_k^{t-1}), \tag{3.55}$$

where $f(v_k^{t-1})$ can be written as

$$\begin{aligned} f(v_k^{t-1}) =& \ln\left(\frac{\rho n_k}{M}\right) - \ln\left( \frac{1}{M} \sum_{i=1}^{M} \frac{\lambda_i(\rho \mathbf{R}_k)}{1 + \lambda_i \left( \sum_{k=0}^{\infty} \tilde{\epsilon}_k^{t-1}(\rho) \mathbf{R}_k \, \mathbb{P}(k) \right)} + \frac{n_k}{M} \sum_{i=1}^{n_k} \frac{1}{\lambda_i(\mathbf{T}_k)} \right) \\ =& \ln\left(\frac{\rho n_k}{M}\right) \\ & - \ln\left( \frac{1}{M} \sum_{i=1}^{M} \frac{\lambda_i(\rho \mathbf{R}_k)}{1 + \sum_{j=0, j \neq k}^{\infty} \tilde{\epsilon}_j^{t-1}(\rho) \lambda_i\left(\mathbf{R}_k\right) \, \mathbb{P}(j) + e^{v_k^{t-1}} \lambda_i\left(\mathbf{R}_k\right)} + \frac{n_k}{M} \sum_{i=1}^{n_k} \frac{1}{\lambda_i(\mathbf{T}_k)} \right) \end{aligned}$$

$$= \ln\left(\frac{\rho n_k}{M}\right) - \ln\left(\frac{1}{M}\sum_{i=1}^{M}\frac{\rho}{\frac{1}{\lambda_i(\mathbf{R}_k)} + \sum_{j=0,j\neq k}^{\infty}\tilde{\epsilon}_j^{t-1}(\rho)\ \mathbb{P}(j) + e^{v_k^{t-1}}} + \frac{n_k}{M}\sum_{i=1}^{n_k}\frac{1}{\lambda_i(\mathbf{T}_k)}\right) \tag{3.56}$$

In the following, we will prove that the function $f(v_k^{t-1})$ converges. Firstly, we note that the function $f(v_k^{t-1})$ is obviously continuous. Secondly, we compute the first derivative of $f(v_k^{t-1})$ as

$$f^{'}(v_k^{t-1}) = \frac{\sum_{i=1}^{M}\frac{\rho e^{v_k^{t-1}}}{\left(\frac{1}{\lambda_i(\mathbf{R}_k)}+\sum_{j=0,j\neq k}^{\infty}\tilde{\epsilon}_j^{t-1}(\rho)\ \mathbb{P}(j)+e^{v_k^{t-1}}\right)^2}}{\sum_{i=1}^{M}\frac{\rho}{\frac{1}{\lambda_i(\mathbf{R}_k)}+\sum_{j=0,j\neq k}^{\infty}\tilde{\epsilon}_j^{t-1}(\rho)\ \mathbb{P}(j)+e^{v_k^{t-1}}} + n_k\sum_{i=1}^{n_k}\frac{1}{\lambda_i(\mathbf{T}_k)}} \tag{3.57}$$

At this point, it is obvious that

$$\frac{e^{v_k^{t-1}}}{\frac{1}{\lambda_i(\mathbf{R}_k)} + \sum_{j=0,j\neq k}^{\infty}\tilde{\epsilon}_j^{t-1}(\rho)\mathbb{P}(j) + e^{v_k^{t-1}}} \leq 1. \tag{3.58}$$

Accordingly, from (3.57) and (3.58), we have

$$\begin{aligned} f^{'}(v_k^{t-1}) &\leq \frac{\sum_{i=1}^{M}\frac{\rho}{\frac{1}{\lambda_i(\mathbf{R}_k)}+\sum_{j=0,j\neq k}^{\infty}\tilde{\epsilon}_j^{t-1}(\rho)\ \mathbb{P}(j)+e^{v_k^{t-1}}}}{\sum_{i=1}^{M}\frac{\rho}{\frac{1}{\lambda_i(\mathbf{R}_k)}+\sum_{j=0,j\neq k}^{\infty}\tilde{\epsilon}_j^{t-1}(\rho)\ \mathbb{P}(j)+e^{v_k^{t-1}}}} \\ &\leq 1. \end{aligned} \tag{3.59}$$

It is easy to show that the first derivative of $f(v_k^{t-1})$ is also positive, which means that the absolute value of $f^{'}(v_k^{t-1})$ is smaller than 1. Hence, using Lemma 3.3, given in Appendix 3.A we can state that $f(v_k^{t-1})$ is a contraction, which implies that it converges. This concludes the proof of uniqueness of eq. (3.15) and eq. (3.16)[7].

# Appendix 3.D Proof of Proposition 3.2

*Proof.* Let $\psi_k = \frac{M}{n_k}\epsilon_k(\rho)$. Then using (3.20)

$$\mathbb{E}_{\mathbf{u}}\left\{\log\det(\mathbf{I}_{n_k} + \mathcal{F}(\mathbf{u}_k)\psi_k\mathbf{T}_k)\right\}$$

[7]For the special case, when a single user is considered, a similar proof of convergence was shown in [61].

$$= \frac{2\kappa\pi}{\Gamma(k)} \sum_{i=1}^{n_k} \int_0^r \log(1+\psi_k\lambda_{ki}u^{-\alpha}) \exp(-\kappa\pi u^2) u^{2k} \mathrm{d}u$$
$$= \frac{2\kappa\pi}{\Gamma(k)} \sum_{i=1}^{n_k} \int_0^r G_{2,2}^{2,1}\left( \frac{1}{\psi_k\lambda_{ki}} u^{\alpha} \middle|_{0,0}^{0,1} \right) \exp(-\kappa\pi u^2) u^{2k} \mathrm{d}u \tag{3.60}$$

Substituting $y$ with $u\sqrt{\kappa\pi}$ and changing the limits of integration, (3.60) becomes

$$\frac{2}{\Gamma(k)} \sum_{i=1}^{n_k} \int_0^{r\sqrt{\kappa\pi}} G_{2,2}^{2,1}\left( \frac{1}{(\kappa\pi)^{\frac{\alpha}{2}}\psi_k\lambda_{ki}} y^{\alpha} \middle|_{0,0}^{0,1} \right) \times \exp(-y^2) \frac{y^{2k}}{(\sqrt{\kappa\pi})^{(k+1)}} \mathrm{d}y \tag{3.61}$$

Now, expanding $\exp(-y^2)$ with the help of Taylor's series expansion, we have

$$\exp(-y^2) = \sum_{n=0}^{\infty} (-1)^n \frac{y^{2n}}{n!} \tag{3.62}$$

Furthermore, using (3.62) in (3.61), we have

$$\frac{2\sum_{n=0}^{\infty}(-1)^n}{n!\Gamma(k)(\sqrt{\kappa\pi})^{(k+1)}} \sum_{i=1}^{n_k} \int_0^{r\sqrt{\kappa\pi}} G_{2,2}^{2,1}\left( \frac{1}{(\kappa\pi)^{\frac{\alpha}{2}}\psi_k\lambda_{ki}} y^{\alpha} \middle|_{0,0}^{0,1} \right) y^{2(n+k)} \mathrm{d}y. \tag{3.63}$$

Substituting $z$ with $\frac{y}{\sqrt{\kappa\pi}r}$ and changing the limits of integration, (3.63) becomes

$$\frac{2\sum_{n=0}^{\infty}(-1)^n(\sqrt{\kappa\pi})^{(2n+k)}r^{(2(n+k)+1)}}{n!\Gamma(1)} \times \sum_{i=1}^{n_k} \int_0^1 G_{2,2}^{2,1}\left( \frac{r^{\alpha}}{\psi_k\lambda_{ki}} z^{\alpha} \middle|_{0,0}^{0,1} \right) z^{2(n+k)} \mathrm{d}z \tag{3.64}$$

Simplifying (3.64) we get

$$\frac{2\sum_{n=0}^{\infty}(-1)^n(\sqrt{\kappa\pi})^{(2n+k)}r^{(2(n+k)+1)}}{\alpha n!\Gamma(k)} \times \sum_{i=1}^{n_k} \int_0^1 G_{2,2}^{2,1}\left( \frac{r^{\alpha}}{\psi_k\lambda_{ki}} z^{\alpha} \middle|_{0,0}^{0,1} \right) p^{\left(\frac{2(n+k)+1}{\alpha}-1\right)} \mathrm{d}p. \tag{3.65}$$

From (3.65) we have, $\rho = \frac{2(n+k)+1}{\alpha}$, $\sigma = 1$ and $\chi = \frac{r^{\alpha}}{\lambda_{ki}}$. Hence, (3.65) can be approximated as

$$\frac{2\sum_{n=0}^{\infty}(-1)^n(\sqrt{\kappa\pi})^{(2n+k)}r^{(2(n+k)+1)}}{\alpha n!\Gamma(k)}\Gamma(1)\sum_{i=1}^{n_k}G_{3,3}^{2,2}\left(\frac{r^{\alpha}}{\psi_k\lambda_{ki}}\middle|\begin{matrix}1-\frac{2(n+k)+1}{\alpha},0,\ 1\\ 0,\quad 0,-\frac{2(n+k)+1}{\alpha}\end{matrix}\right) \tag{3.66}$$

Plugging (3.66) into (3.42) for the $k$th user, we obtain (3.23). □

# Chapter 4

# Space-Constrained Massive MIMO Systems

## 4.1 Introduction

Due to the limited availability of wireless spectrum, massive multiple-input multiple-output (MIMO) can be truly exploited only by significantly increasing the number of antennas deployed per unit area [62]. A usual practice when deploying antenna elements is to space them by a distance equal to or greater than half the wavelength of the transmitted frequency [13], [58]. One of the constraints towards this end is the limited availability of physical area for deployment of a large number of antennas at the base station. Massively densified antenna deployment is a way out but it leads to two effects, namely spatial correlation and antenna mutual coupling. The proximity of the antenna elements as signal sources and electrical components causes antenna correlation and coupling respectively [63].

The nulls and the maximum of the radiation pattern of the antennas are shifted owing to the mutual coupling among them [64]. Mutual coupling effects among antenna elements in 2D linear arrays have widely been studied in [65]-[66]. While [65] and [66] focus on the performance of adaptive arrays when exerted to mutual coupling, [63] and [67] examine the performance of massive MIMO systems with antenna elements affected by mutual coupling owing to constrained physical space. Mutual coupling due to constrained antenna spacing has been stated to deteriorate the performance

of MIMO systems by influencing the correlation of the antennas in [68], [69]. Effects of mutual coupling on the radiation patterns of phased arrays were investigated in [70]. Effects of transmit correlation and mutual coupling on linear precoders were analyzed considering large scale MIMO transmitters in [63]. While a considerable amount of work has already been done with regards to antenna coupling in MIMO, its effects are still quite unknown when a massive MIMO scenario with hundreds of antennas at the base station (BS) are considered. Also to be noted is that most prior work on effects of antenna coupling on MIMO is based on linear arrays [66]-[71] as in cellular networks, the uniform linear array[1] is the most commonly deployed configuration. However, the uniform linear array can scan only the 2D space. On the other hand, the rectangular array can take both the azimuth and the elevation angles into consideration. This makes rectangular array the appropriate array configuration to exploit the 3D propagation space in the true sense.

Accordingly, since the need of the hour is to accommodate as many antennas as possible, we present a more realistic 3D rectangular antenna array configuration with increasing number of antennas. If antenna elements are rigged considering a spacing less than half the wavelength of transmission, a considerable number of antennas will be coupled affecting both the spectral efficiency (SE) and energy efficiency (EE) of the system. While mutual coupling models for 3D antenna arrays have been ever-present in the field of communications, most existing works on large-scale MIMO systems predict over-optimistic performance assuming arrays with unbounded physical space, the more relevant work in [63] considers only linear arrays and a simplified mutual coupling model. In this work, we consider a more realistic rectangular array bounded by a fixed physical space with an area of about $1m^2$ and analytically account for the full mutual coupling model of the array.

Any new system developed in the field of communication would demand energy saving as one of its primary design criteria. The advent of technology hasn't actually reduced the energy consumption of the BS and user equipments (UEs); instead energy consumption and power radiation has become a major health and economic hazard over the years [12]. [72] discusses the electrical power consumptions of the power amplifiers, the cooling systems and the associated circuits installed at the BS. While large antenna arrays have been stated to reduce uplink (UL) and downlink (DL) transmit powers due to coherent combining and an increased antenna aperture in [62], [15] claims such systems operate with a total output RF power of magnitude which is two times less

[1]Details on array geometry and in particular uniform linear and circular array configurations can be found in Chapter 6.

than the current technology. Thus, with the emergence of massive MIMO, we can claim to have taken a giant leap towards reducing the consumption of energy in the field of communication. But how massive is the leap and where will it lead us towards conservation of energy? We will try to analyze this question with respect to EE that can be considered to be a very proficient design goal when it comes to developing energy efficient communication systems.

The focus of this chapter is to consider realistic setups of massive MIMO and analyze how large MIMO systems bounded by fixed physical spaces fare to the demands of increasing EE while contributing towards high spectral efficiencies. We re-examine the question: "How many antennas do we need?" [7] by means of EE under a) realistic antenna deployments in fixed physical spaces and b) thorough and pragmatic power consumption models. We reflect on both the uplink and downlink of a multi-user MIMO system which models antenna correlation and coupling at the BS. We calculate the SE and transmitted power for both uplink and downlink and also the EE of this system with the help of a power consumption model similar to [49], incorporating parameters like power consumed by amplifiers and other digital circuits. Our analysis is based on the effect of increasing the number of BS antennas and reducing the antenna spacing on the EE of the system while taking into consideration two practical linear receivers/precoders in maximum ratio combining/transmission (MRC/MRT) and zero forcing (ZF). To obtain a fair comparison, we analyze the EE of massive MIMO systems considering the fixed power consumption for the cases of two current communication technologies: WIFI and LTE. While analytical expression for EE is obtained for ZF only, simulation results are provided for both MRC and ZF.

## 4.2 System Model

We consider the uplink and downlink of a single cell multi-user MIMO arrangement with one BS equipped with a uniform rectangular 3D antenna array located in a fixed physical space of area $\Delta$ as shown in Fig. 4.1. Each row and column of the antenna array consists of $n$ and $m$ dipole antennas respectively, with each element separated from the other by a distance $d$ within a row or a column. $M = n \times m$ is the total number of antennas receiving signals from $K$ single-antenna users with $M \gg K$. The users are assumed to transmit their data in the same time-frequency resource with $\lambda$ being the carrier wavelength. We also assume that $d < \lambda/2$ so that antenna coupling significantly impacts the performance of the system. Furthermore, the length and breadth of the

rectangular array are $\alpha\lambda$ and $\beta\lambda$ ($\alpha, \beta \in \mathbb{N}$) respectively, which leads to the following expressions

$$\Delta = \alpha\beta\lambda^2, \tag{4.1}$$

$$d = \frac{\alpha\lambda}{m-1} = \frac{\beta\lambda}{n-1}. \tag{4.2}$$

Hereinafter, in this chapter all the analysis performed with respect to the $n \times m$ rectangular array will take into consideration the following assumptions:

a) The antenna elements are placed at uniform intervals.

b) All the elements are identical to each other. In our case we consider dipoles of equal length.

c) All the elements have equal amplitude excitation.

d) The directions of arrivals (DOAs) or directions of departures (DODs) are randomly and independently distributed in angle spread $\phi$ as a $(D, \phi)$ channel ($D$ is explained later).

Perfect synchronization in time and frequency is considered between the BS and users, which operate in a time division duplex (TDD) protocol. The uplink and downlink channels are assumed to be reciprocal within a coherence block. Moreover, the uplink and downlink transmissions follow fixed transmission ratios, $\Upsilon^{UL}$ and $\Upsilon^{DL}$ respectively [58], with $\Upsilon^{UL} + \Upsilon^{DL} = 1$. Let $T$ be the length of the coherence time interval and $\tau^{UL}, \tau^{DL}$ are the number of symbols used for uplink and downlink pilots respectively. Uplink training utilizes $K\tau^{UL}$ of the coherence time interval while downlink training occupies $K\tau^{DL}$. The BS utilizes the uplink training to estimate the downlink channel.

Let $\mathbf{W}$ represent a semi-correlated frequency-flat channel matrix between the BS and the $K$ users which is modeled as $\mathbf{W} = \mathbf{H}\mathbf{F}^{\frac{1}{2}}$ for uplink with $\mathbf{H} \sim \mathcal{CN}(\mathbf{0}, \mathbf{\Sigma}_M^{UL} \otimes \mathbf{I}_K)$ representing the uplink channel and $\mathbf{W} = \mathbf{F}^{\frac{1}{2}}\mathbf{H}$ for downlink with $\mathbf{H} \sim \mathcal{CN}(\mathbf{0}, \mathbf{I}_K \otimes \mathbf{\Sigma}_M^{DL})$[2] representing the downlink channel, where $\mathbf{\Sigma}_M^{UL} = \mathbf{\Sigma}_M^{DL} = \mathbf{\Sigma}_M$ is the BS correlation matrix, $\otimes$ denotes the Kronecker product operator and $\mathbf{F}$ is a $K \times K$ diagonal matrix, where $[\mathbf{F}_{kk}] = f_k$. $\sqrt{f_k}$ models the geometric attenuation and shadow fading which is assumed to be independent over $M$ and constant over several coherence time

[2]It is to be noted that for simplicity of notation, we represent the uplink and downlink channel matrix with the same notation. However, wherever used, its property will be clearly mentioned.

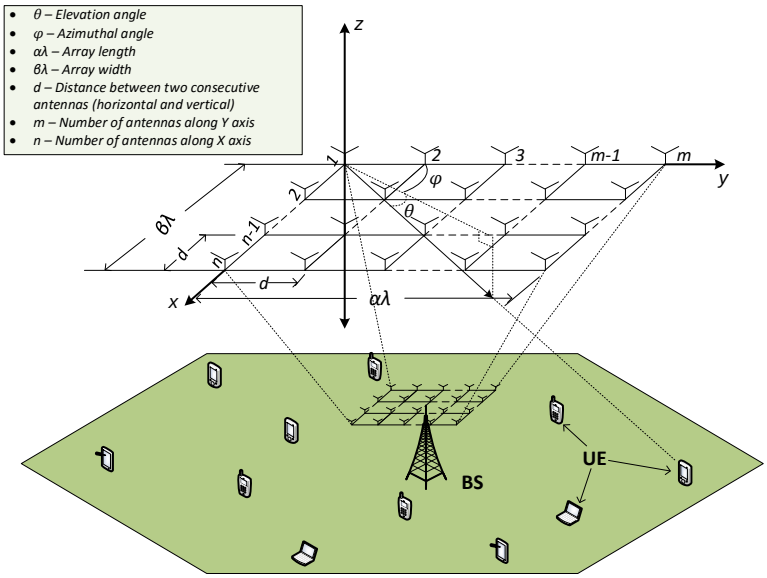


***Figure 4.1:*** *An illustration of a multi-user MIMO setup: A 3D rectangular array consisting of $M$ dipole antennas serving $K$ single-antenna users located uniformly within the cell diameter in the uplink and downlink.*

intervals. This holds true owing to the assumption that $d \ll r_u$, where $r_u$ is the minimum distance between an arbitrary user and the BS and $f_k$ changes very slowly with time.

### 4.2.1 Channel model with correlation and coupling

We examine a single-cell setup with an $M$-antenna BS and $K$ single-antenna users. The uplink and downlink channels are modeled as one-sided correlated Rayleigh flat fading channel with no line of sight. We assume the fading to be correlated only at the BS [73]. After incorporating the mutual coupling of the receiving antennas, we model $\mathbf{H}$ for uplink as [63]

$$\mathbf{H} = [\mathbf{h}_1, \mathbf{h}_2, \ldots, \mathbf{h}_k, \ldots, \mathbf{h}_K], \tag{4.3}$$

where $\mathbf{h}_k$ is the $M \times 1$ uplink channel vector of the $k$-th user; given as

$$\mathbf{h}_k = \mathbf{\Gamma} \mathbf{A}_k^{UL} \mathbf{g}_k \tag{4.4}$$

and for downlink as

$$\mathbf{H} = \left[\mathbf{h}_1^T, \quad \dots \quad \mathbf{h}_k^T, \quad \dots \quad \mathbf{h}_K^T\right]^T, \tag{4.5}$$

where $\mathbf{h}_k$ is the $1 \times M$ downlink channel vector of the $k$-th user; given as

$$\mathbf{h}_k = \mathbf{g}_k \mathbf{A}_k^{DL} \mathbf{\Gamma}, \tag{4.6}$$

where $\mathbf{\Gamma} \in \mathbb{C}^{M \times M}$ denotes mutual coupling, $\mathbf{A}_k^{UL} \in \mathbb{C}^{M \times D}$ denotes the receive steering matrix during uplink containing $D$ steering vectors of the receive antenna array with $D$ denoting the number of direction of arrivals (DOAs) while $\mathbf{A}_k^{DL} \in \mathbb{C}^{D \times M}$ denotes the transmit steering matrix during downlink containing $D$ steering vectors of the receive antenna array with $D$ denoting the number of direction of departures (DODs) and the vector $\mathbf{g}_k \sim \mathcal{CN}(\mathbf{0}, \mathbf{I}_D)$ whose dimensions for uplink and downlink are $D \times 1$ and $1 \times D$ respectively. For the sake of simplicity, the number of DOAs and DODs are considered to be equal. Furthermore, for the uplink transmission, $[\mathbf{H}^H \mathbf{H}] \sim \mathcal{CW}_K(M, \mathbf{\Sigma}_M)$ where $\mathcal{CW}_q(r, \mathbf{S})$ denotes a complex Wishart distribution with degrees of freedom $r$, dimension $q$ and covariance $\mathbf{S}$. Similarly for downlink transmission, $[\mathbf{H}\mathbf{H}^H] \sim \mathcal{CW}_K(M, \mathbf{\Sigma}_M)$.

### 4.2.2 Correlation at the BS

We consider the antenna array at the BS to be uniformly rectangular as shown in Fig. 4.1. As stated before, the spacing between two adjacent antennas within a row or a column is considered to be $d$. Thus without loss of generality, the steering matrix with respect to the $i$th direction of arrival can then be expressed as [74]

$$\mathbf{A}_i = \mathbf{a}_c(\phi_i, \theta) \mathbf{a}_r(\phi_i, \theta)^T, \tag{4.7}$$

where $\mathbf{a}_c(\theta, \phi) \in \mathbb{C}^{n \times 1}$ is the column array steering vector given as

$$\mathbf{a}_c(\phi_i, \theta) = \left[1, e^{j\frac{2\pi}{\lambda} d \cos\phi_i \sin\theta}, \dots, e^{j\frac{2\pi}{\lambda} d(n-1) \cos\phi_i \sin\theta}\right]^T \tag{4.8}$$

and $\mathbf{a}_r(\theta, \phi) \in \mathbb{C}^{m \times 1}$ is the row array steering vector given as

$$\mathbf{a}_r(\phi_i, \theta) = \left[1, e^{j\frac{2\pi}{\lambda} d \sin\phi_i \sin\theta}, \dots, e^{j\frac{2\pi}{\lambda} d(m-1) \sin\phi_i \sin\theta}\right]^T. \tag{4.9}$$

Using the vector valued operator vec$\{\cdot\}$, which maps a $m \times n$ matrix to a $mn \times 1$ column vector by stacking the columns of the matrix, the array steering matrix may

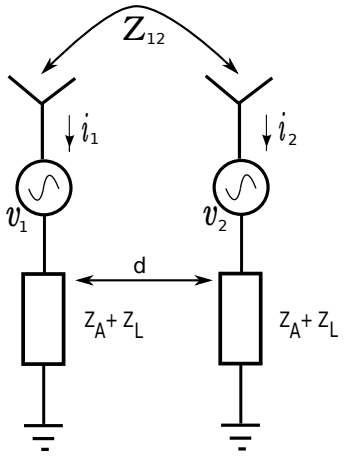


***Figure 4.2:*** *An example showing the effect of mutual coupling on two dipole antennas located adjacent to each other spaced at d distant apart.*

be transformed to a 2-D array steering vector as

$$\mathbf{a}(\phi_i, \theta) = \text{vec}\{\mathbf{A}_i\}. \tag{4.10}$$

The $M \times D$ steering matrix of the rectangular array for uplink can now be given as

$$\mathbf{A}^{UL} = [\mathbf{a}(\phi_1, \theta), \ldots, \mathbf{a}(\phi_i, \theta), \ldots, \mathbf{a}(\phi_D, \theta)], \tag{4.11}$$

where $\mathbf{a}(\phi_i, \theta) \in \mathbb{C}^{M \times 1}$ for $i \in 1, 2, 3 \ldots, D$. Similarly for downlink the $D \times M$ steering matrix is given as

$$\mathbf{A}^{DL} = [\mathbf{a}(\phi_1, \theta)^T, \ldots, \mathbf{a}(\phi_i, \theta)^T, \ldots, \mathbf{a}(\phi_D, \theta)^T]^T. \tag{4.12}$$

Hereinafter, for notational simplicity, we represent the uplink and downlink steering matrix with the same notation $\mathbf{A}$. However, the property of the matrix will be clearly mentioned, wherever used. Throughout this chapter we consider $d$ to be equidistant and the $D$ DOAs and DODs are randomly and independently distributed in an angle spread determined by the azimuth $\phi_i \in [-\frac{\pi}{2}, \frac{\pi}{2}], i = 1, 2, 3 \ldots, D$ and the same elevation $\theta \in [-\frac{\pi}{2}, \frac{\pi}{2}]$. Different degrees of transmit correlation are obtained by varying $\phi$ of the semi-correlated $(D, \phi)$ channel.

### 4.2.3 Mutual coupling at the BS

When multiple antennas radiating simultaneously are located in proximity of each other within a fixed physical space, the electric field of one antenna impacts the distribution of current of the adjacent antennas, which leads to the radiation pattern and input impedance of each antenna being disturbed [68]. This phenomenon is known as antenna coupling.

Our system model is characterized by mutual coupling among linear dipole antennas of length $l$ as shown in Fig. 4.2, which are arranged in a planar configuration with uniform square grids and rectangular boundary as described earlier. The mutual coupling matrix, $\mathbf{\Gamma}$ is defined as [64]

$$\mathbf{\Gamma} = (Z_L + Z_A)(\mathbf{Z} + Z_L\mathbf{I})^{-1}, \tag{4.13}$$

where $Z_L, Z_A$ and $\mathbf{Z}$ denote load impedance, antenna impedance and mutual impedance matrix respectively. $\mathbf{Z}$ can be constructed as a $M \times M$ matrix, which is given in (4.14) at the bottom of this page, where $Z_{(i,k)(j,l)}$ denotes the mutual impedance between antenna located at the $i$th row and $k$th column and the antenna located at the $j$th row and $l$th column of the rectangular array with $i, j \in 1, 2, \ldots, n$ and $k, l \in 1, 2, \ldots, m$.

The correlation matrix at the BS for uplink can now be given as

$$\begin{aligned} \mathbf{\Sigma}_M^{UL} &= \mathbb{E}\{\mathbf{H}\mathbf{H}^H\} \\ &= \mathbf{\Gamma}\mathbf{A}E\{\mathbf{g}_k\mathbf{g}_k^H\}\mathbf{A}^H\mathbf{\Gamma}^H \\ &= K\mathbf{\Gamma}\mathbf{A}\mathbf{A}^H\mathbf{\Gamma}^H. \end{aligned} \tag{4.15}$$

Similarly, the correlation matrix at the BS for downlink is given as

$$\mathbf{\Sigma}_M^{DL} = K\mathbf{\Gamma}^H\mathbf{A}^H\mathbf{A}\mathbf{\Gamma}. \tag{4.16}$$

$$\mathbf{Z} = \begin{bmatrix} Z_{(1,1)(1,1)} & \cdots & Z_{(1,1)(1,m)} & \cdots & Z_{(1,1)(2,1)} & \cdots & Z_{(1,1)(2,m)} & \cdots & Z_{(1,1)(n,1)} & \cdots & Z_{(1,1)(n,m)} \\ Z_{(1,2)(1,1)} & \cdots & Z_{(1,2)(1,m)} & \cdots & Z_{(1,2)(2,1)} & \cdots & Z_{(1,2)(2,m)} & \cdots & Z_{(1,2)(n,1)} & \cdots & Z_{(1,2)(n,m)} \\ \vdots & \ddots & \vdots & \ddots & \vdots & \ddots & \vdots & \ddots & \vdots & \ddots & \vdots \\ Z_{(1,m)(1,1)} & \cdots & Z_{(1,m)(1,m)} & \cdots & Z_{(1,m)(2,1)} & \cdots & Z_{(1,m)(2,m)} & \cdots & Z_{(1,m)(n,1)} & \cdots & Z_{(1,m)(n,m)} \\ \vdots & \ddots & \vdots & \ddots & \vdots & \ddots & \vdots & \ddots & \vdots & \ddots & \vdots \\ Z_{(n,1)(1,1)} & \cdots & Z_{(n,1)(1,m)} & \cdots & Z_{(n,1)(2,1)} & \cdots & Z_{(n,1)(2,m)} & \cdots & Z_{(n,1)(n,1)} & \cdots & Z_{(n,1)(n,m)} \\ \vdots & \ddots & \vdots & \ddots & \vdots & \ddots & \vdots & \ddots & \vdots & \ddots & \vdots \\ Z_{(n,m)(1,1)} & \cdots & Z_{(n,m)(1,m)} & \cdots & Z_{(n,m)(2,1)} & \cdots & Z_{(n,m)(2,m)} & \cdots & Z_{(n,m)(n,1)} & \cdots & Z_{(n,m)(n,m)} \end{bmatrix} \tag{4.14}$$

Since $\mathbf{\Sigma}_M^{UL} = \mathbf{\Sigma}_M^{DL} = \mathbf{\Sigma}_M$, we will ignore the superscripts $UL$ and $DL$ henceforth.

**Example 4.1.** *Assume that the antennas at the BS are rigged in a uniform planar array with square grids and rectangular boundary. Applying simple algebraic operations on the Cartesian co-ordinates of the rectangular array, the distance between any two antenna elements within the array can be given as*

$$d_{(i,k)(j,l)} = d\sqrt{(i-j)^2 + (k-l)^2}, \tag{4.17}$$

*where $i, j, k, l$ are described as before.*

$d_{(i,k)(j,l)}$ plays a significant role in determining the mutual impedance, $Z_{(i,k)(j,l)}$, which based on current maximum at the input antenna terminal is given by the electromotive force (EMF) method as [64]

$$Z_{(i,k)(j,l)} = R_{(i,k)(j,l)} + \mathrm{j}X_{(i,k)(j,l)}. \tag{4.18}$$

Here, $R_{(i,k)(j,l)}$ and $X_{(i,k)(j,l)}$ are self-mutual-resistance and self-mutual-reactance between antenna located at the $i$th row and $k$th column and the antenna located at the $j$th row and $l$th column respectively and given as [64]

$$R_{(i,k)(j,l)} = \frac{\sqrt{\mu_0}}{4\pi\sqrt{\epsilon_0}} \left[2C_{in}(u_0) - C_{in}(u_1) - C_{in}(u_2)\right] \tag{4.19}$$

and

$$X_{(i,k)(j,l)} = \frac{\sqrt{\mu_0}}{4\pi\sqrt{\epsilon_0}} \left[2S_{in}(u_0) - S_{in}(u_1) - S_{in}(u_2)\right], \tag{4.20}$$

where $\mu_0$ and $\epsilon_0$ denote the magnetic and electric constants,. Furthermore, the variables $u_0$, $u_1$, $u_2$ are respectively given as

$$\begin{aligned} u_0 &= 2\pi d_{(i,k)(j,l)}, \\ u_1 &= 2\pi\left(l + \sqrt{d_{(i,k)(j,l)}^2 + l^2}\right), \\ u_2 &= 2\pi\left(-l + \sqrt{d_{(i,k)(j,l)}^2 + l^2}\right), \end{aligned}$$

and $C_{in}(.)$ and $S_{in}(.)$ are cosine and sine integral functions respectively and are defined as

$$C_{in}(a) = \gamma + \ln(a) + \int_0^a \frac{\cos t - 1}{t} dt, \tag{4.21}$$

$$S_{in}(a) = \int_0^a \frac{\sin t}{t} dt, \tag{4.22}$$

where $\gamma$ is the Euler-Mascheroni constant and $l$ is the length of the dipole antenna.

The electrical and magnetic parameters of the antennas are considered to be equal for every antenna. Hence, considering equal spacing among the antennas along row and column of the rectangular array, the following properties for the mutual impedance matrix $\mathbf{Z}$ can be obtained -

a) $\mathbf{Z}$ is symmetric. Let $Z_{uv}$ be the element in the $u$th row and $v$th column of $\mathbf{Z}$. Then

$$Z_{uv} = Z_{vu}. \tag{4.23}$$

b) $\mathbf{Z}$ is a Toeplitz matrix. Thus

$$Z_{uv} = Z_{(u+1)(v+1)}. \tag{4.24}$$

c) $\mathbf{Z}$ has $2M - 1$ degrees of freedom.

**Remark 4.1.** *Let $Z_{pq} = Z_{(i,k)(j,l)}$, where $p, q \in 1, 2, \ldots, M$. If $p = q$, then $\Gamma_{pq} = Z_A$, where $Z_A$ denotes antenna or self impedance.*

## 4.3 Spectral Efficiency and Transmitted Power

### 4.3.1 Uplink

During uplink transmission, the $K$ users transmit their data in the same time-frequency resource. Thus, the $M \times 1$ received vector at the BS can be given as

$$\mathbf{y} = \mathbf{W}\mathbf{P}^{UL}\mathbf{x} + \mathbf{z}, \tag{4.25}$$

where $\mathbf{x} \in \mathbb{C}^{K\times 1}$ is the symbol transmitted by the $K$ users. $\mathbf{P}^{UL}$ is a $K \times K$ diagonal matrix with the vector $\mathbf{p}^{UL}$=$[p_1^{UL} \ldots p_k^{UL} \ldots p_K^{UL}]$ constituting the diagonal where $p_i^{UL}$ is the average transmitted power of each user and $p_i^{UL} \geq 0$ for $i = 1, 2, \ldots, K$ and $\mathbf{z}$ is a vector of additive white Gaussian noise with zero mean and variance[3] $\sigma^2\mathbf{I}_M$.

[3]Without loss of generality the variance of $\mathbf{z}$ is considered to be 1 in this chapter to reduce complexity.

For the detection of $\mathbf{x}$, the BS uses a $M \times K$ linear detector, $\mathbf{V}$ on $\mathbf{y}$. The signal and noise plus interference components of the processed received signal for the $k$th user after detection can thus be given as

$$r_k = \underbrace{p_k^{UL}\mathbf{v}_k^H\mathbf{w}_k x_k}_{\text{desired signal}} + \underbrace{\sum_{i=1,i\neq k}^{K} p_i^{UL}\mathbf{v}_k^H\mathbf{w}_i x_i}_{\text{interference}} + \underbrace{\mathbf{v}_k^H\mathbf{n}}_{\text{noise}}, \tag{4.26}$$

where $r_k$ and $x_k$ are the $k$th elements of vectors $\mathbf{r}$ and $\mathbf{x}$ respectively while $p_k^{UL}$ is the power transmitted by the $k$th user. We consider two low complexity detection schemes, namely MRC and ZF at the BS. Hence,

$$\mathbf{V} = \begin{cases} \mathbf{W}, & \text{for MRC} \\ \mathbf{W}\left(\mathbf{W}^H\mathbf{W}\right)^{-1}, & \text{for ZF.} \end{cases} \tag{4.27}$$

Assuming the channel to be ergodic, the ratio of the signal power of the $k$th user to the noise-plus-interference term (SINR) can be given as

$$\gamma_k^{UL} = \left( \frac{p_k^{UL}\left|\mathbf{v}_k^H\mathbf{w}_k\right|^2}{\sum_{i=1,i\neq k}^{K} p_i^{UL}|{\mathbf{v}_k}^H\mathbf{w}_i|^2 + \ ||\mathbf{v}_k||^2} \right). \tag{4.28}$$

Throughout this chapter, we assume the target SINR to be provided to each of the $K$ users to be equal. To achieve this equal SINR condition, we use the approach given in [75] for solving the power control problem in mobile scenarios using Perron's theorem[4]. Let us define a matrix $\mathbf{\Psi} \in \mathbb{C}^{K\times K}$, where

$$[\mathbf{\Psi}]_{k,i} = \begin{cases} \frac{|{\mathbf{v}_k}^H\mathbf{w}_i|^2}{\gamma_k^{UL}||\mathbf{v}_k||^2}, & \text{for } i \neq k \\ \frac{|{\mathbf{v}_k}^H\mathbf{w}_i|^2}{||\mathbf{v}_k||^2}, & \text{for } i = k. \end{cases} \tag{4.29}$$

Since in our analysis the variance of $\mathbf{z}$ is considered to be 1, therefore, to meet the equal SINR condition for the $K$ users, the uplink power vector $\mathbf{p}^{UL}$ has to satisfy the

[4]The model in [75] can be looked upon as a simplified generalization of our model without the mutual coupling effects. The power loss due to mutual coupling, $p^{coup}$ can be compensated for at the BS with additional circuitry. Moreover, any disparities in power distribution can be accounted for by properly designing efficient detector or precoder matrices to meet the specific power constraints of the system.

following condition [[75], eq. (29-33)]

$$\mathbf{p}^{UL}\mathbf{\Psi} = \mathbf{1}_{(1\times K)}. \tag{4.30}$$

Simplifying (4.29) and (4.30), the power assigned to each uplink user can be given as

$$p_k^{UL} = \frac{\gamma_k^{UL}}{q_k - \gamma_k^{UL} G_{ki}}, \tag{4.31}$$

where,

$$q_k = \frac{|\mathbf{v}_k{}^H \mathbf{w}_k|^2}{||\mathbf{v}_k||^2} \quad \text{and} \quad G_{ki} = \begin{cases} \frac{|\mathbf{v}_k{}^H \mathbf{w}_i|^2}{||\mathbf{v}_k||^2}, & \text{for } i \neq k \\ 0, & \text{for } i = k. \end{cases} \tag{4.32}$$

The total transmitted power for $K$ users during uplink can now be given as

$$p_t^{UL} = \mathbb{E}\{\mathbf{1}_{(1\times K)}\mathbf{p}^{UL}\}. \tag{4.33}$$

**Remark 4.2.** *The power allocation problem states that $p_k^{UL} > 0$. Hence, the necessary condition for $p_k^{UL}$ to have a positive solution is that $q_k - \gamma_k G_{ki}$ be non-negative for $\gamma_k > 0$.*

We now define the uplink SE for the $k$th user as [13]

$$R_k^{UL-A} = \left(\frac{T\Upsilon^{UL} - \tau^{UL}K}{T}\right)\tilde{R}_k^{UL-A}, \tag{4.34}$$

where $A \in \{MRC, ZF\}$, $T$ is the coherence interval in symbols, $\tau^{UL}$ is the transmitted uplink pilot sequence in symbols and $\Upsilon^{UL}$ is the fraction of uplink transmission as described earlier.

**Definition 4.1.** *Let a $p \times p$ matrix, $\mathbf{Q} \sim \mathcal{CW}_p(q, \mathbf{S})$, where $p$ is the dimension, $q$ is the degree of freedom and $\boldsymbol{S}$ is the covariance. Then from [76] for any integer $r > 0$,*

*1) $\mathbb{E}\{\mathbf{Q}^r\} = \tilde{c}(r, q, p)\mathbf{S}$, where $\tilde{c}(r, q, p)$ is a constant depending on $r, q, p$. If $r = 1$, then $\tilde{c}(1, q, p) = q$. Hence, $\mathbb{E}(\mathbf{Q}) = q\mathbf{S}$ and $\mathbb{E}[\mathrm{tr}(\mathbf{Q})] = pq\mathbf{S}$.*

*2) If $r = -1$, then $\mathbb{E}(\mathbf{Q}^r) = \tilde{c}(1, q, p)\mathbf{S}^{-1}$ and $\tilde{c}(1, q, p) = (p-q)^{-1}$. Hence, $\mathbb{E}(\mathbf{Q}^{-1}) = (p-q)^{-1}\mathbf{S}^{-1}$ and $\mathbb{E}[\mathrm{tr}(\mathbf{Q}^{-1})] = p(p-q)^{-1}\mathbf{S}^{-1}$.*

**Proposition 4.1.** *The first negative moment of the SINR for the kth user assuming $M \geq 2$, perfect CSI and MRC detection at the BS can be given as*

$$\mathbb{E}\{(\gamma_k^{UL-MRC})^{-1}\} = \frac{\mathrm{tr}[\mathbf{\Sigma}_M^{-1}]\left(\mathrm{tr}[\mathbf{\Sigma}_M]\sum_{i=1,i\neq k}^{K} p_i^{UL} f_i + 1\right)}{p_k^{UL}(M-1)f_k}. \tag{4.35}$$

*Accordingly, the uplink rate can be given as*

$$\begin{aligned} \tilde{R}_k^{UL-MRC} &= \log_2\left(1 + \left\{\mathbb{E}\{(\gamma_k^{-1})^{UL-MRC}\}\right\}^{-1}\right) \\ &= \log_2\left(1 + \frac{p_k^{UL}(M-1)f_k}{\mathrm{tr}[\mathbf{\Sigma}_M^{-1}]\left(\mathrm{tr}[\mathbf{\Sigma}_M]\sum_{i=1,i\neq k}^{K} p_i^{UL} f_i + 1\right)}\right). \end{aligned} \tag{4.36}$$

*Now if $\tilde{\gamma}_k$ is the minimum target SINR required to achieve a minimum rate of $\tilde{R}_k$ for the kth user, then the power required can be given as*

$$\tilde{p_k}^{UL-MRC} = \frac{\mathrm{tr}[\mathbf{\Sigma}_M^{-1}]\tilde{\gamma_k}^{UL-MRC}}{(M-1)f_k - \tilde{\gamma_k}^{UL-MRC}\mathrm{tr}[\mathbf{\Sigma}_M]\sum\limits_{i=1,i\neq k}^{K} f_i}. \tag{4.37}$$

*Proof.* The proof is given in Appendix 4.A. □

**Proposition 4.2.** *The first negative moment of the SINR for the kth user assuming $M \geq K+1$, perfect CSI and ZF detection at the BS can be given as*

$$\mathbb{E}\{(\gamma_k^{UL-ZF})^{-1}\} = \frac{\mathrm{tr}[\mathbf{\Sigma}_M^{-1}]}{p_k(M-K)f_k}. \tag{4.38}$$

*Accordingly, the uplink rate can be given as*

$$\begin{aligned} \tilde{R}_k^{UL-ZF} &= \mathbb{E}\left[\log_2\left(1 + \left\{\mathbb{E}\{(\gamma_k^{-1})^{UL-ZF}\}\right\}^{-1}\right)\right] \\ &= \log_2\left(1 + \frac{p_k^{UL}(M-K)f_k}{\mathrm{tr}[\mathbf{\Sigma}_M^{-1}]}\right). \end{aligned} \tag{4.39}$$

*If $\tilde{\gamma}_k$ is the minimum target SINR required to achieve a minimum rate of $\tilde{R}_k$ for the kth user, then the power required can be given as*

$$\tilde{p_k}^{UL-ZF} = \frac{\mathrm{tr}[\mathbf{\Sigma}_M^{-1}]\tilde{\gamma_k}^{UL-ZF}}{(M-K)f_k}. \tag{4.40}$$

*Proof.* The proof is given in Appendix 4.B. □

### 4.3.2 Downlink

Since we use TDD transmission technique, the downlink channel can be represented as a Hermitian transpose of the uplink channel. The BS transmits data streams simultaneously to all the $K$ users which creates an interfering broadcast channel. To counter the interference, we use $M \times K$ precoding matrix at the BS denoted by $\mathbf{T}$. The signal received by the $k$th user can be given as

$$r_k = \underbrace{p_k^{DL} f \mathbf{w}_k^H \mathbf{t}_k x_k}_{\text{desired signal}} + \underbrace{\sum_{i=1, i\neq k}^{K} p_i^{DL} f \mathbf{w}_k^H \mathbf{t}_i x_i}_{\text{interference}} + \underbrace{z_k}_{\text{noise}}, \tag{4.41}$$

where $\mathbf{x} \in \mathbb{C}^{M\times 1}$ is the symbol transmitted by $M$ antennas. $p_k^{DL} \subseteq \mathbf{p}^{DL} = [p_1^{DL} \ldots p_k^{DL} \ldots p_K^{DL}]^T$ is the power corresponding to the $k$th user similar to uplink with the same constraints while $z_k$ is the noise associated with the $k$th user. $\mathbf{t}_k$ is the vector of the precoding matrix associated with the $k$th user and $f = \frac{1}{\sqrt{(\mathbf{T}\mathbf{T}^H)}}$ is a normalization parameter to constrain the average transmitted power. Almost identical to the case of uplink, we consider two linear precoding schemes namely MRT and ZF. Accordingly,

$$\mathbf{T} = \begin{cases} \mathbf{W}, & \text{for MRT} \\ \mathbf{W}\left(\mathbf{W}^H\mathbf{W}\right)^{-1}, & \text{for ZF.} \end{cases} \tag{4.42}$$

The desired SINR can thus be given as

$$\gamma_k^{DL} = \left( \frac{p_k^{DL} \frac{|\mathbf{w}_k^H \mathbf{t}_k|^2}{||\mathbf{t}_k||^2}}{\sum_{i=1, i\neq k}^{K} p_i^{DL} \frac{|\mathbf{w}_k{}^H \mathbf{t}_i|^2}{||\mathbf{t}_i||^2} + 1} \right). \tag{4.43}$$

Similar to uplink, we assume the target SINR to be provided to each of the $K$ users to be equal. Following the same approach as used to derive (4.31), the downlink power for the $k$th user can be assigned as

$$p_k{}^{DL} = \frac{\gamma_k^{DL}}{q_k - \gamma_k G_{ki}}, \tag{4.44}$$

where

$$q_k = \frac{|\mathbf{w}_k{}^H \mathbf{t}_k|^2}{||\mathbf{t}_k||^2} \quad \text{and} \quad G_{ki} = \begin{cases} \frac{|\mathbf{w}_k{}^H \mathbf{t}_i|^2}{||\mathbf{t}_k||^2}, & \text{for } i \neq k \\ 0, & \text{for } i = k. \end{cases} \tag{4.45}$$

The total transmitted power for $K$ users during downlink can now be given as

$$p_t^{DL} = \mathbb{E}\{\mathbf{1}_{(1\times K)}\mathbf{p}^{DL}\}. \tag{4.46}$$

**Remark 4.3.** *Adhering to the power constraint $p_k^{DL} > 0$, the necessary condition for $p_k^{DL}$ to have a positive solution is that $q_k - {\gamma^{DL}}_k G_{ki}$ be non-negative for $\gamma_k^{DL} > 0$.*

The downlink rate similar to the uplink for the $k$th user can now be given as

$$R_k^{DL-A} = \left(\frac{T\Upsilon^{DL} - \tau^{DL}}{T}\right)\tilde{R}_k^{DL-A}, \tag{4.47}$$

where $A \in \{MRC, ZF\}$, $T$ is the coherence interval in symbols, $\tau^{DL}$ is the transmitted downlink pilot sequence and $\Upsilon^{DL}$ is the fraction of downlink transmission as described earlier.

**Proposition 4.3.** *With $M \geq 2$ and assuming perfect CSI and MRC detection at the BS, the first negative moment of the SINR for the $k$th user can be given as*

$$\mathbb{E}\{(\gamma_k^{DL-MRC})^{-1}\} = \frac{\mathrm{tr}[\mathbf{\Sigma}_M^{-1}]\left(\mathrm{tr}[\mathbf{\Sigma}_M]\sum_{i=1,i\neq k}^{K} p_i^{DL} f_i + 1\right)}{p_k^{DL}(M-1)f_k}. \tag{4.48}$$

*The downlink rate, $\tilde{R}_k^{DL-MRC}$ follows accordingly similar to Proposition 4.1. Also if $\tilde{\gamma}_k$ is the minimum target SINR required to achieve a minimum rate of $\tilde{R}_k$, then the power required can be given as*

$$\tilde{p_k}^{DL-MRC} = \frac{\mathrm{tr}[\mathbf{\Sigma}_M^{-1}]\tilde{\gamma_k}^{DL-MRC}}{(M-1)f_k - \tilde{\gamma_k}^{DL-MRC}\mathrm{tr}[\mathbf{\Sigma}_M]\sum\limits_{i=1,i\neq k}^{K} f_i}. \tag{4.49}$$

*Proof.* Following the same derivations as in Proposition 4.1 for the case of uplink, we can arrive at the above result. □

**Proposition 4.4.** *With $M \geq K+1$ and assuming perfect CSI and ZF detection at the BS, the first negative moment of the SINR for the $k$th user is given as*

$$\mathbb{E}\{(\gamma_k^{DL-ZF})^{-1}\} = \frac{\mathrm{tr}[\mathbf{\Sigma}_M^{-1}]}{p_k^{DL}(M-K)f_k}. \tag{4.50}$$

*The downlink rate, $\tilde{R}_k^{DL-ZF}$ follows accordingly similar to Proposition 4.2. Accordingly, if $\tilde{\gamma}_k$ is the minimum target SINR required to achieve a minimum rate of $\tilde{R}_k$, then the*

*power required can be given as*

$$\tilde{p_k}^{DL-ZF} = \frac{\mathrm{tr}[\mathbf{\Sigma}_M^{-1}]\tilde{\gamma_k}^{DL-ZF}}{(M-K)f_k}. \tag{4.51}$$

*Proof.* This proof can be obtained following an approach similar to the derivation of Proposition 4.2 for the case of uplink. □

## 4.4 Energy Efficiency

EE of a communication link as stated before is the total transmit energy consumption required per bit i.e., the ratio of the sum rate achieved to the consumed power, and can be expressed in bits/joule as [46, 13, 58, 77, 78][5].

$$\xi^A = \frac{R^A}{p^{PA} + p^{RF} + p^{Coup}}, \tag{4.52}$$

where

$$R^A = \sum_{k=1}^{K} (R_k^{UL-A} + R_k^{DL-A}) \tag{4.53}$$

is the total sum rate for the $K$ users through an entire process of uplink and downlink, $p^{PA}$ is the power consumed by the power amplifiers, $p^{RF}$ is the power consumed by the RF components of the systems, $p^{Coup}$ is the power loss due to mutual coupling among the antennas located in close proximity to each other and $A \in \{MRC, ZF\}$.

**Remark 4.4.** *In order to obtain insights on how the number of antennas, the physical space and the transmitted power affect the total EE of a massive MIMO system, it makes sense to look at the total rate and divide it by the total power. Hence, the EE metric used in this chapter focuses on the total rate and power of both uplink and downlink. Following [58, 77, 78], we look at the system as a whole, but with the*

[5]The definition of EE used in this chapter is in accordance with the mentioned literature. This approach of dividing the SE with the average total power consumption greatly simplifies the analysis and is comparable to the various recent literature on MIMO systems. The joint uplink-downlink optimization makes it favorable to attain a holistic and balanced optimization for the uplink and downlink resources, system parameters (such as antenna numbers) and to allow a performance guarantee vs power consumption on the full forward and reverse link between the base station (BS) and mobile users [79, 80, 80].

*important discrepancy that the increase in the number of BS antennas happens in a fixed physical space.*

### 4.4.1 Power amplifiers

The average power in watt consumed by the power amplifiers during uplink and downlink can be approximated as [46], [58]

$$p^{PA} = p_t^{UL}(\alpha^{UL} + 1) + p_t^{DL}(\alpha^{DL} + 1), \tag{4.54}$$

where $\alpha^{UL} = \frac{\zeta^{UL}}{\eta^{UL}} - 1$ and $\alpha^{DL} = \frac{\zeta^{DL}}{\eta^{DL}} - 1$ with $\zeta^{UL}$ and $\zeta^{DL}$ being the modulation-dependent peak to average power ratios (PAPR) for uplink and downlink respectively while $\eta^{UL}$ and $\eta^{DL}$ are the power amplifier efficiencies at the UE and BS respectively and $p_t^{UL}, p_t^{DL}$ are the transmitted powers in the uplink and downlink respectively as described earlier.

### 4.4.2 RF chains

The average power in watt consumed in the RF chains for a typical MIMO transmitter-receiver set can be given as [46]

$$p^{RF} = p_{fix}^{A} + Mp^{BS} + Kp^{UE} \tag{4.55}$$

where $p_{fix}^{A}$ is the fixed power consumption at the BS dependent on the processing scheme $A \in \{MRC, ZF\}$, $p^{BS}$ is the power required at the BS to run the circuit components, $p^{UE}$ is the power associated with the user equipments which are defined as follows

$$p^{BS} = p_{mix}^{BS} + p_{filt}^{BS} + p_{ADC}^{BS} + p_{DAC}^{BS} + p_{OSC}^{BS}, \tag{4.56}$$

$$p^{UE} = p_{mix}^{UE} + p_{filt}^{UE} + p_{ADC}^{UE} + p_{DAC}^{UE} + p_{OSC}^{UE}, \tag{4.57}$$

where $p_{mix}$, $p_{filt}$, $p_{ADC}$, $p_{DAC}$ and $p_{OSC}$ denote the power consumed by the mixers, filters, analog-to-digital converters, digital-to-analog converters and local oscillator

respectively[6].

### 4.4.3 Mutual coupling

The mutual coupling effect among antennas in the vicinity of each other as discussed earlier increases the power consumption of the system. Applying simple circuit theory analysis on Fig. 4.2, the terminal voltage for a particular antenna at the BS can be given as [65]

$$\mathrm{v}_i = \sum_{j=1, i\neq j}^{M} \mathrm{i}_j \Gamma_{i,j}, \tag{4.58}$$

where, $\mathrm{v}_i$ denotes the terminal voltage at the $i$th antenna element due to a unity current in the $j$th antenna element when the current in all other antenna elements is zero and $\Gamma_{i,j}$ is the total mutual coupling experienced by the $i$th antenna element due to all other antennas as discussed in Section 4.3. Furthermore, $\mathbf{i}_{BS} = [\mathrm{i}_1, \mathrm{i}_2, \mathrm{i}_3 \ldots\ldots \mathrm{i}_M]^T$, and $\mathbf{v}_{BS} = [\mathrm{v}_1, \mathrm{v}_2, \mathrm{v}_3 \ldots\ldots \mathrm{v}_M]^T$ where, $\mathbf{i}_{BS}$ and $\mathbf{v}_{BS}$ are vectors of currents and voltages respectively associated with the dipole antennas in the rectangular array. The power loss due to coupling based on the current maximum now follows as

$$p^{Coup} = \mathbf{v}_{\mathrm{BS}}^T \mathbf{i}_{\mathrm{BS}}. \tag{4.59}$$

In order to maintain a fixed SINR, this loss is compensated at the BS. Using (4.52)-(4.59) we now derive an analytical expression for $\xi$. For the sake of simplicity, we consider the minimum SINR, $\bar{\gamma}$ targeted for every users to be equal for both uplink and downlink.

Hereinafter, we consider a minimum fixed rate, $\tilde{R}$ to be provided to each and every user for both uplink and downlink which leads to the uplink and downlink rates being $\Upsilon^{UL}\tilde{R}$ and $\Upsilon^{DL}\tilde{R}$ respectively. Thus the total SE of the system for one complete cycle

[6]The components considered in this chapter may vary depending on set-ups used in practical scenarios. Any other components used can easily be included in the expressions of $p^{BS}$ and $p^{UE}$ while the ones that are not may be removed. It is to be noted that the uplink and downlink transmissions are separated by the fractions $\Upsilon^{UL}$ and $\Upsilon^{DL}$ respectively. Hence, by changing these parameters, the uplink and downlink power consumption parameters can be controlled to adjust to the requirement of the networks in consideration.

of uplink and downlink can be given as

$$\begin{aligned} R^A &= \sum_{k=1}^{K} \left[ \left( \frac{T\Upsilon^{UL} - K\tau^{UL}}{T} \right) \tilde{R}_k^{UL-A} + \left( \frac{T\Upsilon^{DL} - K\tau^{DL}}{T} \right) \tilde{R}_k^{DL-A} \right] \\ &= \frac{K\tilde{R}}{T} \left[ T - K(\tau^{UL} + \tau^{DL}) \right]. \end{aligned} \tag{4.60}$$

**Proposition 4.5.** *Taking into account the diversity loss due to mutual coupling, we aim at guaranteeing a minimum rate of $\tilde{R}$. We accomplish this by dynamically allocating power to the users and hence, define a parameter $\bar{p} = f(\gamma, \tilde{R})$. Therefore, considering ZF processing at the BS, with no loss of generality, we can define $\tilde{R}$ as*

$$\tilde{R} = \log_2(1 + \bar{p}(M - K)). \tag{4.61}$$

*Thus the total power consumed by the power amplifiers during one complete cycle of uplink and downlink when a ZF processing scheme is employed at the BS is*

$$p_{ZF}^{PA} = K\bar{p}\,\mathrm{tr}[\mathbf{\Sigma}_M^{-1}] \left( \frac{\zeta^{UL}}{\eta^{UL}} + \frac{\zeta^{DL}}{\eta^{DL}} \right). \tag{4.62}$$

*Proof.* The proof is given in Appendix 4.C. □

### 4.4.4 Energy efficiency and analytical optimum of $M$ for ZF

The EE of the system now follows from (50) as

$$\xi^{ZF} = \frac{\frac{K}{T}\left(T - K(\tau^{UL}\tau^{DL})\right)\log_2(1 + \bar{p}(M - K))}{K\bar{p}\,\mathrm{tr}[\mathbf{\Sigma}_M^{-1}]\left(\frac{\zeta^{UL}}{\eta^{UL}} + \frac{\zeta^{DL}}{\eta^{DL}}\right) + Mp^{BS} + Kp^{UE} + p^{Coup}} \tag{4.63}$$

**Definition 4.2.** *If a local maximum exists in a strictly quasi-concave function, it is also the global maximum [56]. This global optimum can then be obtained by setting the partial derivative of the quasi-concave function to zero.*

**Proposition 4.6.** *Considering ZF processing scheme at BS and power loss due to mutual coupling, the maximum number of antennas, $M$ that can be accommodated*

*within a fixed physical space, $\Delta$ which maximizes the EE, $\xi^{ZF}$ can be given as*

$$M_{max} = \frac{1}{\bar{p}} \left[ \exp\left\{ W\left( \frac{\bar{p}\left( K\bar{p}\,\mathrm{tr}[\mathbf{\Sigma}_M^{-1}]\left(\frac{\zeta^{UL}}{\eta^{UL}} + \frac{\zeta^{DL}}{\eta^{DL}}\right) + Kp^{UE} + p^{Coup}\right)}{p^{BS}e} - \frac{1-\bar{p}K}{e}\right) + 1 \right\} + \bar{p}K - 1 \right] \tag{4.64}$$

*where $W(*)$ is the product logarithm function and $e = 2.71828$ is the Euler's number and $p^{BS}$, $p^{UE}$, and $p^{Coup}$ are obtained from (53), (54) and (58) respectively.*

*Proof.* The proof is given in Appendix 4.D. □

Furthermore, it can also be shown that the stationary point $M_{max}$ is also a global maximum and the EE curve is quasi-concave, which increases for $K+1 \leq M \leq M_{max}$, attains a global maximum, $M_{max}$ and then decreases for $M_{max} \leq M \leq \infty$ (See Appendix 4.D).

At this point it is worth mentioning the relation between $\mathbf{\Sigma}_M$ and $M$. While there is no explicit mathematical expression relating these two parameters directly, from (15) it can be seen that $\mathbf{\Sigma}_M$ is related to $\Gamma$, which in turn is related to $Z$ through (13-16). However, $Z$ depends on $m, n$ and the distance $d$ through (17-22). Since the physical space $\Delta$ of the antenna array is constant, any changes made on $M$ will affect the mutual coupling $Z$ and subsequently the resulting correlation $\mathbf{\Sigma}_M$, which is indeed intuitive.

**Proposition 4.7.** *Considering ZF processing scheme at BS and power loss due to mutual coupling, the parameter $\bar{p}$ that maximizes the EE, $\xi^{ZF}$ provided $M$ is kept constant can be given as*

$$\bar{p}_{max} = \frac{1}{M-K} \left[ \exp\left\{ W\left( \frac{(M-K)(Mp^{BS} + Kp^{UE} + p^{Coup})}{K\,\mathrm{tr}[\mathbf{\Sigma}_M^{-1}]\left(\frac{\zeta^{UL}}{\eta^{UL}} + \frac{\zeta^{DL}}{\eta^{DL}}\right)e} - \frac{1}{e}\right) + 1 \right\} - 1 \right] \tag{4.65}$$

*Proof.* The proof is given in Appendix 4.E. □

## 4.5 Numerical Results

On the basis of the proposed system model for massive MIMO, we analyze the effect of mutual coupling and correlation on the SE and EE of massive MIMO systems through

Monte Carlo simulations (10000 realizations) for the small scale fading with respect to $M$, $\Delta$ and $d$, which is calculated as explained in Example 4.1. As previously mentioned, the fixed power consumption of two technologies, namely WIFI ($p_{fix}^{LTE} = 25$dBm) and LTE ($p_{fix}^{LTE} = 43$dBm) are considered to obtain a fair comparison.

We consider a single hexagonal cell with a diameter of $s_{max} = 3000$ meters which extends from vertex to vertex. The BS is located at the center of the cell with $K = 10$ users uniformly distributed in the cell. The minimum distance, $s_{min}$ between a user and the BS is 50 meters. The large scale fading as described in the system model is defined as $f_k = \frac{t_k}{(s_k/s_{min})^\nu}$, where $t_k$ is the log-normal random variable with a variance $\sigma_s^2$, $s_k$ is the distance between the $k$th user and the BS varying anywhere between $s_{min}$ and $s_{max}$ and $\nu$ is the path-loss exponent varying from 2 to 4 with 2 denoting free space propagation and 4 denoting a relatively lossy environment. For our simulations we choose $\sigma_s = 10dB$ and $\nu = 3.8$. In the above channel model, unless stated otherwise, a fixed total physical space is assumed with the dimensions (length:width) of the rectangular array following a fixed ratio of $\alpha : \beta = 1 : 1$. In other words, we consider a square array with equal number of antennas along the length and the width of the array. This ratio is just for our analytical tractability and can be modified according to the requirements of the set-up. Further, the area of this space is limited to $\alpha\beta\lambda^2$, where $\lambda$ is the carrier wavelength. To simplify the V-I characteristics calculations, the antenna elements are considered to be simple dipoles. The length of all the $M$ dipoles are considered to be $0.5\lambda$. Moreover, the peak-to- average power ratio

***Table 4.1:*** *Simulation Parameters [7, 58, 63, 77]*

| **Parameter** | **Value** | **Parameter** | **Value** |
|---|---|---|---|
| Length of coherence interval, $T$ | 196 | Length of the dipoles, $l$ | $0.5\lambda$ |
| Fraction of UL Transmission, $\Upsilon^{UL}$ | 0.4 | PAPR uplink, $\zeta^{UL}$ | 0.4 |
| Fraction of DL Transmission, $\Upsilon^{DL}$ | 0.6 | PAPR downlink, $\zeta^{DL}$ | 0.6 |
| Channel coherence time, $T_c$ | 1 ms | PA efficiency BS, $\eta^{DL}$ | 0.39 |
| Length of pilots, $\tau^{UL}, \tau^{DL}$ | 10 | PA efficiency UE, $\eta^{UL}$ | 0.3 |
| Array length, $\alpha\lambda$ | $5\lambda$ | $p_{fix}^{WIFI}$ | 25dBm |
| Array width, $\beta\lambda$ | $5\lambda$ | $p_{fix}^{LTE}$ | 43dBm |
| Antenna impedance, $Z_A$ | $50\Omega$ | $p_{OSC}^{BS}$ | 33dBm |
| Load impedance, $Z_L$ | $50\Omega$ | $p_{OSC}^{UE}$ | 17dBm |
| Length : Width ratio of array, $\alpha : \beta$ | 1:1 | $p_{mix}^{BS} + p_{filt}^{BS} + p_{DAC}^{BS} + p_{DAC}^{BS}$ | 30dBm |
| Number of DODs/DOAs, $D$ | 150 | $p_{mix}^{UE} + p_{filt}^{UE} + p_{DAC}^{UE} + p_{DAC}^{UE}$ | 16.9dBm |

(PAPR), is dependent on the modulation scheme and the associated constellation size. It is to be noted that the total PAPR for UL and DL is equal to 1 and the values of $\zeta^{DL}$ and $\zeta^{UL}$ are selected in such a way so that $\alpha^{DL} > \alpha^{UL}$. Also the power amplifier efficiency of the BS, $\eta^{DL}$ is considered to be greater than that of the power amplifier efficiency of the UE, $\eta^{UL}$. While this is not mandatory, the consideration is due to the fact that BS has more signal processing resources and can handle power management better than the UEs. All the simulation parameters used are given at the bottom of the previous page in Table 4.1.

### 4.5.1 Traditional model: Antenna spacing greater than half the carrier wavelength

To comprehend the effects of constrained physical spaces in a massive MIMO set-up, we first analyze its performance based on a system model where the spacing among the antennas is considered to be greater than half the carrier wavelength; thus negating any effects of mutual coupling and antenna correlation. For this scenario, we can consider $\mathbf{Z}$ as an all-ones matrix. This model will allow us to analyze the dependency of the correlation on $d$ and also lay a platform for our analysis of mutual coupling later. The curves in Fig. 4.4 labeled as 'without coupling' illustrate this scenario.

### 4.5.2 Proposed model: Antenna spacing less than half the carrier wavelength

In this sub-section we analyze the behaviour of the proposed model by increasing the number of antennas at the BS while keeping the area of the rectangular array fixed. Typically for a fixed physical spacing, increasing the number of antennas is associated with decreasing the antenna spacing; thus increasing mutual coupling which in turn reduces the EE. Therefore, there is a fundamental trade-off between the EE of the system and the number of antennas at the BS, which will be evident from the simulation results.

Fig. 4.3 illustrates the SE of the proposed system with a fixed physical space and shows its variation as a function of $M$. The spacing among the antennas varies depending on the number of antennas which in turn affects the mutual coupling matrix. Here we show the achievable SE in a massive MIMO system with coupling, considering MRC/MRT and ZF detection and precoding at the BS. The length and width of the array are constrained as $\alpha = 5$ and $\beta = 5$ which is kept fixed hereinafter unless stated otherwise. We increment the total number of antennas in squares. For example, $n = 1, 3, 5, \ldots$ and $m = 1, 3, 5, \ldots$ which implies, $M = 1, 9, 25, \ldots$ where $n$ and

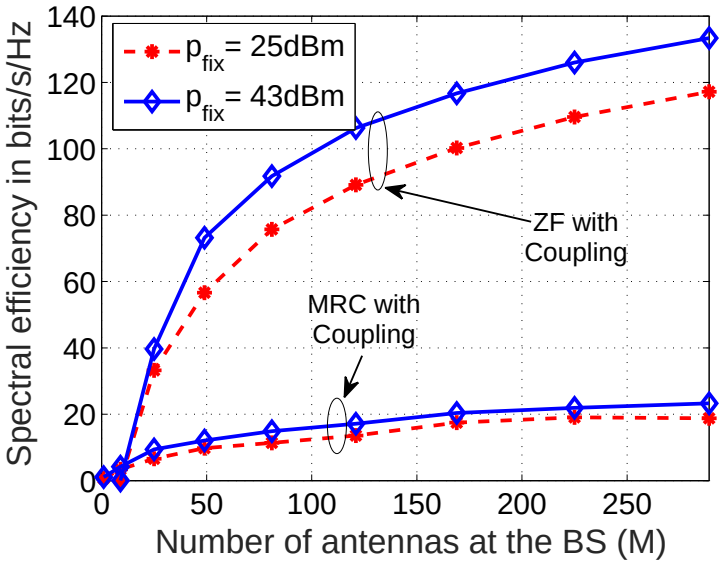


***Figure 4.3:*** *Spectral efficiency with respect to $M$ using MRC/MRT and ZF detection/precoding at the BS for two fixed power consumption schemes. In this example, $\alpha = 5$ and $\beta = 5$.*

$m$ are the number of antennas along the width and length respectively of the array. As expected with the increase in $M$, the SE of the system also increases. We note however, that the improvement in SE saturates for high numbers of antennas due to the significant correlation and coupling. For the same reason ZF outperforms MRC by a large extent. Also it can be seen that systems corresponding to fixed power consumption of LTE systems with a higher fixed transmission power offer higher SE as compared to fixed power consumption of WIFI systems with a lower fixed transmission power. For the case of ZF the difference in throughput for the two power schemes is higher than for the case of MRC where the gap between their respective performance is much less.

We next specifically examine the EE of such a system in detail. In Fig. 4.4, we consider two settings: one where the physical space is not bounded by any limitations while for the other, a setting similar to Fig. 4.3 is considered. For the first setting, the antennas are spaced far apart to negate any effects of coupling. This figure provides insights into EE of massive MIMO systems with and without coupling with MRC detection/precoding. We plot the EE with respect to the number of BS antennas $M$. The dashed lines show the performance of systems with fixed power consumption equivalent to that of WIFI systems while the continuous line represents the performance of systems with fixed power consumption equivalent to that of LTE systems like before.

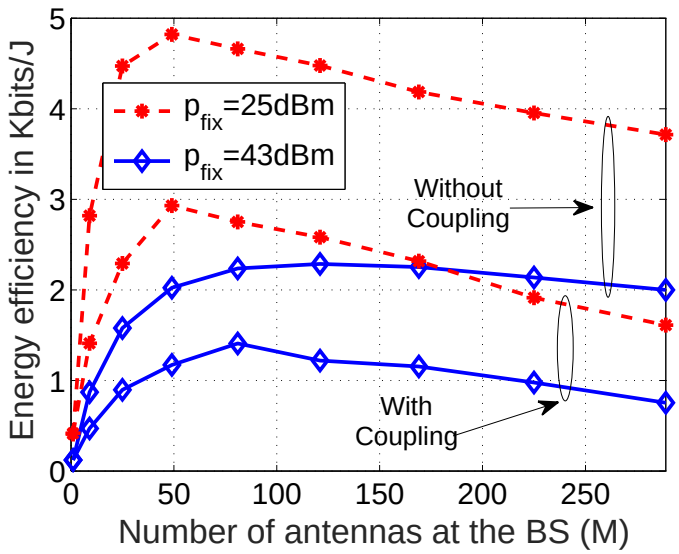


***Figure 4.4:*** *Energy efficiency with respect to $M$ with and without coupling at the BS using MRC detection/precoding at the BS for two fixed power consumption schemes. In this example, $\alpha = 5$ and $\beta = 5$.*

Now as $d$ is inversely proportional to $M$, it decreases with increasing $M$; thus also decreasing EE which is evident from the curve. For example, for $M = 100$ the EE falls from 4.8 Kbits/J (without coupling) to 2.7 Kbits/J when coupling is considered. Also to be noted is the shape of the EE curve. As stated in Proposition 4.6, the EE curve considering coupling is seen to be concave. However, the EE curve without coupling is also seen to be concave which eventually decreases with increasing $M$. This is due to the more accurate power consumption model we have used in the chapter, which is further exacerbated by the increasing correlation between the antennas. For example, each antenna at the BS has its individual circuitry, which has non-zero power consumption and hence the power consumed by the BS is a multiple of the number of antennas, $M$. Most existing works consider $p^{BS}$ to be constant and accordingly when M goes to infinity, the EE becomes unbounded. Our results on the contrary show that when the power at the BS is equal to $Mp^{BS}$ the EE does not always increase and is a concave function of $M$. Furthermore, when coupling is not considered, $p_k^{RF}$ in (52) still holds with $\xi^{ZF}$ in (60) staying the same but without the mutual coupling term, $\text{tr}[\mathbf{\Sigma}_M^{-1}]$ which can be shown to be concave similar to what was shown in Proposition 4.1.

Moreover, systems with fixed power consumption equivalent to that of WIFI systems with low power consumption naturally perform better from EE point of view like before but when coupling is considered the gap in their performance reduces with the

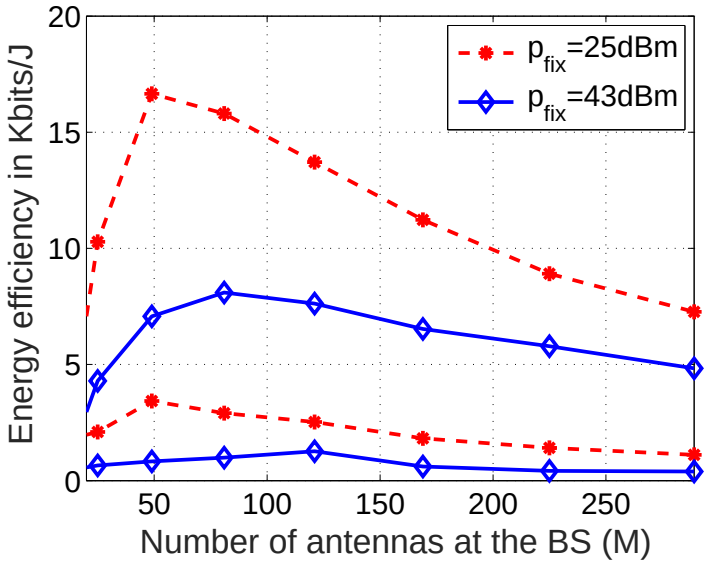


***Figure 4.5:*** *Energy efficiency with respect to $M$ with coupling at the BS using MRC and ZF detection/precoding at the BS for two fixed power consumption schemes. In this example, $\alpha = 3$ and $\beta = 3$.*

increase in the number of antennas, $M$. Furthermore, depending on the system model and channel detection/ precoding technique used, it is a concave or quasi-concave function of $M$.

Hereinafter, we consider three scenarios with three different physical spaces: (a) $\Delta = 3\lambda \times 3\lambda$, (b) $\Delta = 5\lambda \times 5\lambda$, and (c) $\Delta = 7\lambda \times 7\lambda$. Fig. 4.5 considers scenario (a) and compares the performance of MRC/MRT and ZF with respect to EE considering mutual coupling at the BS. The settings are kept exactly same as Fig. 4.3 except for $\Delta$. ZF outperforms MRC for both the cases of systems with fixed power consumption equivalent to that of WIFI and LTE as ZF is seen to give at least five times more throughput than MRC. Similar to Fig. 4.4, the performance gap between systems with fixed power consumption equivalent to that of WIFI and LTE systems reduces for both ZF and MRC. The optimal $M$ for ZF as calculated in Section 4.5 is also plotted. The figure shows that for WIFI systems 49 antennas and for LTE systems 81 antennas give a global optimum EE.

Fig. 4.6 considers scenario (b) while Fig. 4.7 considers scenario (c). The rest of the settings are kept exactly the same as Fig. 4.3. The results are similar to Fig. 4.5 as can be expected. The EE performance can be seen to improve due to the relaxation

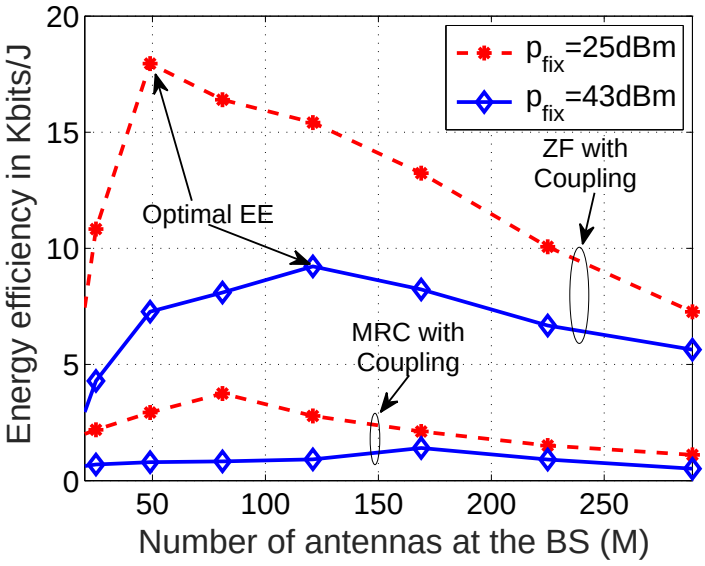


***Figure 4.6:*** *Energy efficiency with respect to $M$ with coupling at the BS using MRC and ZF detection/precoding at the BS for two fixed power consumption schemes. In this example, $\alpha = 5$ and $\beta = 5$.*

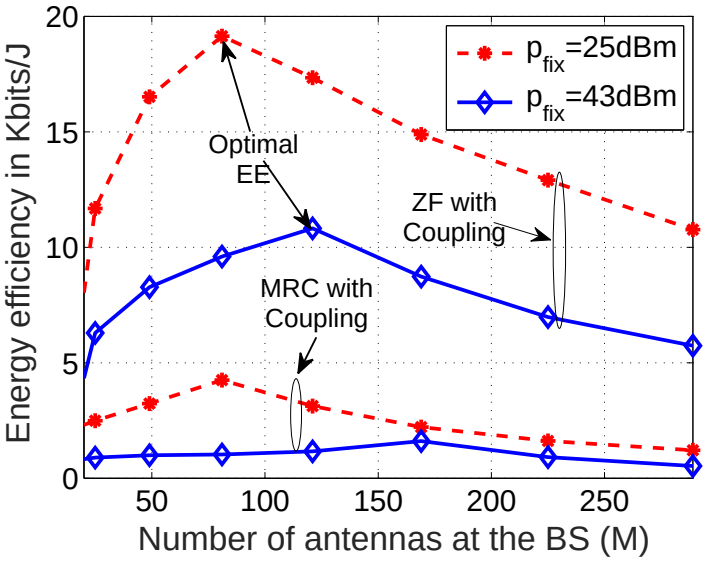


***Figure 4.7:*** *Energy efficiency with respect to $M$ with coupling at the BS using MRC and ZF detection/precoding at the BS for two fixed power consumption schemes. In this example, $\alpha = 7$ and $\beta = 7$.*

in BS physical area. However, it is to be noted that the optimal $M$ changes as the dimensions of $D$ increase. The optimality shifts towards the right as we increase the physical space. With a spacing of $\Delta = 5\lambda \times 5\lambda$, the number of antennas $M$ for systems with fixed power consumption equivalent to that of WIFI and LTE systems to give

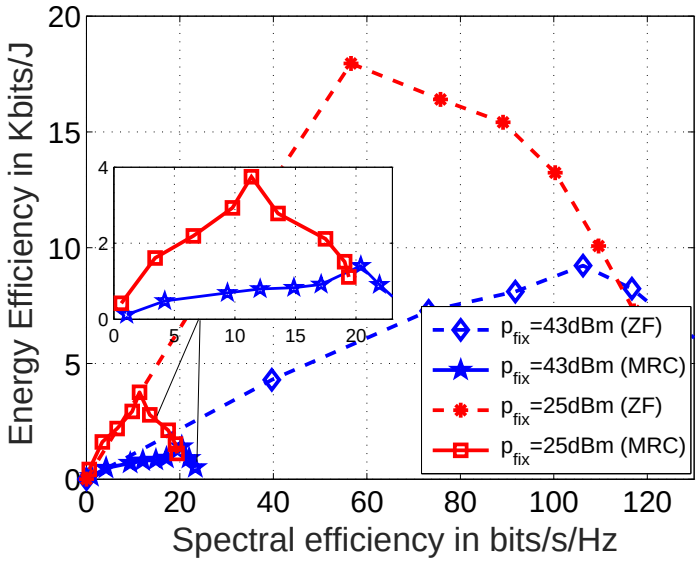


***Figure 4.8:*** *An illustration of the trade-off between energy efficiency and spectral efficiency. In this example,* $\alpha = 5$ *and* $\beta = 5$.

a global EE are 49 and 121 respectively while for $\Delta = 7\lambda \times 7\lambda$, M is 81 and 121 for systems with fixed power consumption equivalent to that of WIFI and LTE systems respectively. This is due to the changes in $\bar{p}_{max}$ owing to the effects of mutual coupling which accounts for $M_{max}$. This can be considered a trade-off between the number of antennas, $M$, the fixed physical space, $\Delta$ and EE.

At this point, it is worthwhile to note that there is a trade-off between the EE and SE of the system. This trade-off is in line with [13] and [49], where similar results were obtained but with different system models. Due to the consideration of the circuit power consumption at the BS which is a function of $M$, though the SE increases asymptotically, the EE does not. To explicitly show this trade-off, Fig. 4.8 considers the scenario with the bounded dimension of $\Delta = 5\lambda \times 5\lambda$. It can be seen from the figure that as the SE of the system increases, the EE of the system increases to a point before it starts to fall sharply. From (4.65) it is implicit that EE is a quasi concave function of the parameter $\bar{p}$. Additionally, $\bar{p}_{max}$ in (4.65) can be looked upon as the optimum power required to attain the maximum EE for a certain antenna array dimension. The SE on the other hand is a monotonically increasing function of $\bar{p}$ as can be seen from (58). This explains the quasi concavity of the of the plot between SE and EE. Furthermore, following the course of the previous figures, systems with fixed power consumption equivalent to that of WIFI systems show better performance than their

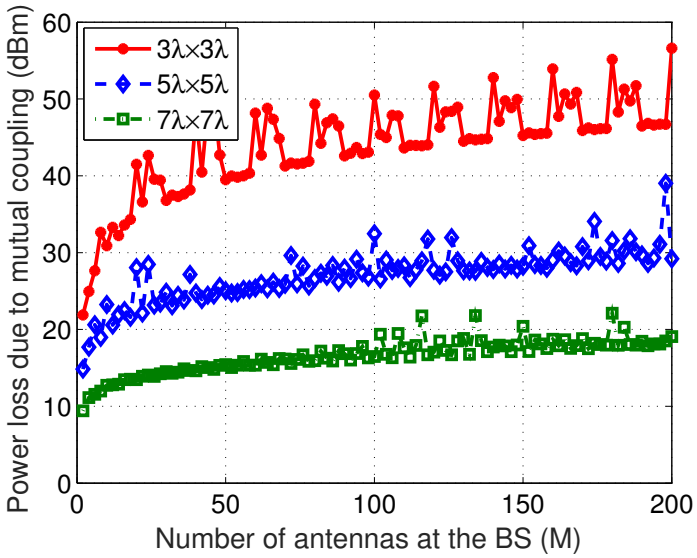


***Figure 4.9:*** *Power loss due to mutual coupling with respect to $M$ considering different array dimensions.*

LTE counterparts with respect to EE. $\bar{p}$ can be of paramount importance to network engineers while deciding on operating regimes where it is possible to jointly increase the SE and EE of the system. For other regimes however, $\bar{p}$ can be set according to the current traffic demands, for e.g., during night time when the traffic is low, $\bar{p}$ can be set to achieve high EE with a constraint on the SE.

Finally to further stress the impact of mutual coupling, in Fig. 4.9 we show the impact of the number of antennas, $M$ on the power loss due to coupling at the BS for different antenna spacings. Though the power loss due to coupling has already been taken into consideration in the previous results and figures, this figure specifically explains the variation of power loss due to mutual coupling. The settings are kept similar to Fig. 4.3. It can be seen from the figure that as the spacing between antennas is reduced, mutual coupling increases and so does the power loss due to coupling. The large variation between the $3\lambda \times 3\lambda$ and the other two curves is due to more compact physical spacing among the antennas, which results in more loss due to mutual coupling. As stated before, we aim at restricting the physical space to within $1m^2$. Hence, for example, considering about 100 antennas for the case of $3\lambda \times 3\lambda$ scenario, the spacing between any two adjacent antennas is equal to $0.1m$, which is less than half the wavelength of a 900 MHz GSM band and this introduces increasing amount of mutual coupling with increasing numbers of antennas. The constructive and destructive superposition of the signals due to mutual coupling is periodic with this decrease in

separation for a fixed wavelength, which contributes to the periodic behavior of the power loss.

## 4.6 Summary

Conventionally, massive MIMO systems are considered to achieve high EE with the increase in number of BS antennas which might be misleading when antenna coupling along with circuit power consumptions are considered. We have given an analysis of the effects of mutual coupling on the EE for realistic massive MIMO systems. Simulation results show that as the spacing between the antennas is reduced, the coupling among them increases, resulting in a dip in EE performance. We also reveal that the EE is a decreasing concave or quasi-concave function of $M$. A trade-off between the number of antennas, $M$, the fixed physical space, $\Delta$ and EE is found. Depending on the physical space, the optimum number of antennas are found with the objective of achieving high EE. It is evident that high EE can be obtained but at the cost of reducing $M$ or increasing $\Delta$. We would like to note that the optimum value of $M$ derived in this chapter may not directly relate to practical engineering designs, but is an illustration of the principle that increasing the number of antennas unboundedly is not beneficial when EE is considered as a design criteria.

The results of this chapter provide adequate insights into how future massive MIMO BSs can be setup within constrained physical spaces. However, when millimeter wave frequencies are considered, due to the smaller wavelength, the constraint on physical space is relaxed significantly and greater number of antennas can be incorporated within very small physical spacings. Hence, in order to fully realize the potential of massive MIMO systems, it is mandatory to shift the communication paradigm from micro wave ($\mu$Wave) to mmWave frequencies. Accordingly, while we study the rate and coverage of mmWave networks by assuming directional beamforming in Chapter 5, we study the performance analysis of a mmWave network, where the BSs are equipped with massive MIMO antenna arrays in Chapter 6 .

## Appendix 4.A Proof of Proposition 4.1

For MRC, $\gamma_k^{UL-MRC} = \left( \frac{p_k^{UL} ||\mathbf{w}_k||^4}{\sum\limits_{i=1, i\neq k}^{K} p_i^{UL} |\mathbf{w}_k{}^H \mathbf{w}_i|^2 + ||\mathbf{w}_k||^2} \right)$. Dividing both the numerator and denominator by $||\mathbf{w}_k||^2$ and defining $\bar{w}_i = \frac{\mathbf{w}_k{}^H \mathbf{w}_i}{||\mathbf{w}_k||}$, where $\bar{w}$ is a Gaussian random

variable with variance $\mathrm{tr}(\mathbf{\Sigma}_M)f_i$, we have

$$\mathbb{E}\{(\gamma_k^{UL-MRC})^{-1}\} = \left(\sum_{i=1,i\neq k}^{K} p_i^{UL}\mathbb{E}\{|\bar{w}_i|^2\}+1\right)\mathbb{E}\left(\frac{1}{p_k^{UL}||\mathbf{w}_k||^2}\right). \tag{4.66}$$

Now using the property $||\mathbf{A}|| = \sqrt{\mathrm{tr}(\mathbf{A}^H\mathbf{A})}$ and Definition 4.1, we have

$$\mathbb{E}\{(\gamma_k^{UL-MRC})^{-1}\} = \left(\mathrm{tr}(\mathbf{\Sigma}_M)\sum_{i=1,i\neq k}^{K} p_i^{UL}f_i+1\right)\frac{\mathrm{tr}\left[\mathbf{\Sigma}_M^{-1}\right]}{p_k^{UL}(M-1)f_k}. \tag{4.67}$$

Following a similar approach on (4.33), we obtain (4.37).

# Appendix 4.B Proof of Proposition 4.2

For ZF, $\gamma_k^{UL-ZF} = \frac{p_k^{UL}}{[(\mathbf{W}^H\mathbf{W})^{-1}]_{kk}}$. Hence

$$\begin{aligned}\mathbb{E}\left\{\left[(\mathbf{W}^H\mathbf{W})^{-1}\right]_{kk}\right\} &= \frac{1}{Kf_k}\mathbb{E}\left\{\mathrm{tr}\left[(\mathbf{W}^H\mathbf{W})^{-1}\right]\right\}\\ &= \frac{\mathrm{tr}\left[\mathbf{\Sigma}_M^{-1}\right]}{p_k^{UL}(M-K)f_k},\end{aligned} \tag{4.68}$$

which is obtained by using Definition 4.1. Now from (4.33) and (4.38) we obtain (4.40).

# Appendix 4.C Proof of Proposition 4.5

For ZF, $\gamma_k^{UL-ZF} = \frac{p_k^{UL}}{[(\mathbf{W}^H\mathbf{W})^{-1}]_{kk}}$. Hence, from (4.61) we have,

$$p_k^{ZF} = \bar{p}(M-K)\left[(\mathbf{W}^H\mathbf{W})^{-1}\right]_{kk}. \tag{4.69}$$

Therefore, using Definition 4.1 and from (4.40), (4.51) and (4.54) we have

$$\begin{aligned}p_{ZF}^{PA} &= K\bar{p}(M-K)\left(\frac{\zeta^{UL}}{\eta^{UL}}+\frac{\zeta^{DL}}{\eta^{DL}}\right)\mathbb{E}\left\{\mathrm{tr}\left[(\mathbf{W}^H\mathbf{W})^{-1}\right]\right\}\\ &= K\bar{p}(M-K)\left(\frac{\zeta^{UL}}{\eta^{UL}}+\frac{\zeta^{DL}}{\eta^{DL}}\right)\frac{\mathrm{tr}\left[\mathbf{\Sigma}_M^{-1}\right]}{M-K}\\ &= K\bar{p}\,\mathrm{tr}[\mathbf{\Sigma}_M^{-1}]\left(\frac{\zeta^{UL}}{\eta^{UL}}+\frac{\zeta^{DL}}{\eta^{DL}}\right).\end{aligned} \tag{4.70}$$

# Appendix 4.D Proof of Proposition 4.6

We rewrite (4.63) as

$$\xi^{ZF}(M) = \frac{\frac{K}{T}\left(T - K(\tau^{UL}\tau^{DL})\right)\log_2(1-\bar{p}K+\bar{p}M)}{K\bar{p}\,\mathrm{tr}[\mathbf{\Sigma}_M^{-1}]\left(\frac{\zeta^{UL}}{\eta^{UL}}+\frac{\zeta^{DL}}{\eta^{DL}}\right)+Kp^{UE}+p^{Coup}+Mp^{BS}}. \tag{4.71}$$

Let $(1-\bar{p}K)=a$, $\bar{p}=b$, $K\bar{p}\,\mathrm{tr}[\mathbf{\Sigma}_M^{-1}]\left(\frac{\zeta^{UL}}{\eta^{UL}}+\frac{\zeta^{DL}}{\eta^{DL}}\right)+Kp^{UE}+p^{Coup}=c$, $p^{BS}=d$ and $\frac{K}{T}\left(T-K(\tau^{UL}\tau^{DL})\right)=f$. Therefore, (4.71) implies

$$\xi^{ZF}(M) \;=\; \frac{f\log_2(a+bM)}{c+dM}. \tag{4.72}$$

In order to prove that the objective function, $\xi^{ZF}(M)$ is quasi-concave it is sufficient to prove that the upper contour sets $S_\psi = \{M \succeq 0 | \xi^{ZF}(M) \geq \psi\}$ of $\xi^{ZF}(M)$ are convex for any $\psi \in \mathbb{R}$ [81]. We investigate the cases when $\psi \leq 0$ and $\psi > 0$. When $\psi \leq 0$, the set is empty in the contour $\xi^{ZF}(M) = \psi$. Thus $\xi^{ZF}(M)$ is strictly quasi-convex when $\psi \leq 0$. Now when $\psi > 0$, $S_\psi$ is equivalent to

$$\begin{aligned} & \left\{ M \geq 0 \,\middle|\, \frac{f\log_2(a+bM)}{c+dM} \geq \psi \right\} \\ \Longrightarrow \quad & \left\{ M \geq 0 \,\middle|\, c\psi + dM\psi - f\log_2(a+bM) \leq 0 \right\}. \end{aligned}$$

Let $F = c\psi + dM\psi - f\log_2(a+bM)$. Now, $F$ is strictly convex within the range of $M$ as its Hessian is positive definite. Hence, $S_\psi$ is strictly convex, which concludes that $\xi^{ZF}(M)$ is a quasi-concave function of $M$.

Now using Definition 4.2, we can say that the local maximum of $\xi^{ZF}$ is also the global maximum. Furthermore, as $M \to \infty$, $\xi^{ZF} \to 0$. Since $M \nleq 0$, the local maximum is obtained by calculating the first derivative and setting it to zero as shown below. From (4.72) we have

$$\begin{aligned} \frac{\partial \xi^{ZF}(M)}{\partial M} &= \frac{\partial\left(\frac{f\log_2(a+bM)}{c+dM}\right)}{\partial M} \\ &= \frac{fb}{(a+bM)(c+dM)\ln 2} - \frac{fd\ln(a+bM)}{(c+dM)^2\ln 2}. \end{aligned}$$

(4.73)

Now equating the right hand side of (4.73) to zero, we have

$$\begin{aligned} \frac{b(c+dM)}{a+bM} &= d\ln(a+bM) \\ \implies \frac{bc-ad}{a+bM} &= d\left(\ln(a+bM)-1\right). \end{aligned} \tag{4.74}$$

Let $\ln(a+bM)-1=x$. Therefore $\exp(x+1)=a+bM$. Thus (4.74) implies

$$\begin{aligned} \frac{bc-ad}{\exp(x+1)} &= dx \\ \implies \frac{bc}{de}-\frac{a}{e} &= x\exp(x) \\ \implies x &= W\left(\frac{bc}{de}-\frac{a}{e}\right), \end{aligned} \tag{4.75}$$

where $W$, known as the product logarithm is the inverse function of $f(W)=We^W$ for any complex number $W$. Substituting $x$ with $\ln(a+bM)-1$ we have

$$M_{max}=\frac{\exp\left\{W\left(\frac{bc}{de}-\frac{a}{e}\right)+1\right\}-a}{b}. \tag{4.76}$$

Now, replacing $a,b,c,d$ with their equivalent parameters, we obtain (4.64). Quasi-concavity thus implies that $M_{max}$ is a global maximum and $\xi^{ZF}$ is increasing for $M<M_{max}$ and decreasing for $M>M_{max}$. Thus, $M_{max}$ is the unique optimal $M$ to attain a maximum $\xi^{ZF}$.

# Appendix 4.E Proof of Proposition 4.7

This result can be proved similarly to the proof of proposition 6 by changing the differentiation variable from $M$ to $\bar{p}$. Accordingly we can parameterize $a,b,c,d$ as $1,(M-K),(Kp^{UE}+p^{Coup}+Mp^{BS}),K\mathrm{tr}[\mathbf{\Sigma}_M^{-1}]\times\left(\frac{\zeta^{UL}}{\eta^{UL}}+\frac{\zeta^{DL}}{\eta^{DL}}\right)$ respectively. The quasi-concavity of $\xi^{ZF}(\bar{p})$ follows accordingly similar to the proof in Appendix 4.D. Hence, the local maximum will also be the global maximum which can be found by setting the first derivative to zero, i.e.,

$$\frac{\partial\xi^{ZF}(\bar{p})}{\partial\bar{p}}=0. \tag{4.77}$$

Solving (4.77) in a way similar to Appendix 4.D, we obtain the desired result. The details are omitted due to space limitations.

# Chapter 5

# Relay-Aided Millimeter Wave Networks

The availability of bands in the range of 20-100 GHz makes millimeter wave (mmWave) a lucrative prospect in the design of 5G networks [16, 20, 82, 83]. However one distinct disadvantage of mmWave communication is that the signals at mmWave frequencies cannot penetrate through obstacles like buildings, concrete walls, vehicles, trees, etc. These obstacles are usually termed as blockages in a wireless communications scenario. Among various ways to encounter blockages, one way is to go around the blockages by incorporating relays. In conventional communication systems, relay aided transmission has been regarded as an effective way to increase the coverage probability, throughput and transmission reliability of the networks [84]. The use of relays can be a promising solution for mmWave systems as well to combat the blockage effects and path losses that are encountered in mmWave networks. Accordingly, multiple relays can be deployed between the sources and the destination of a transmission link. Performance evaluation of relay aided networks has been widely studied in [85]-[86]. While [85] considers the deployment of relays as a network infrastructure without a wired backhaul connection, [87] explores the potential of deploying relays to design a cost effective network. Recently, cooperative relaying has been proposed in order to extend the coverage, increase the capacity and to provide cost effective solutions. In [88], authors have studied the coverage probability of relay aided cellular networks with different association criteria between the base station and mobile station. It has been shown that coverage probability highly depends on path loss exponents and den-

sity of relays. Similarly, the achievable transmission capacity has been analyzed in relay assisted device-to-device networks in [89]. Recently, the performance of Decode-and-Forward and Amplify-and-Forward strategies with high gain antenna arrays was characterized in [90]. The numerical results proved that directional antennas are useful for multi-hop relays. Hence, it is implicit that relays can prove to be an important tool in the design of mmWave cellular systems because coverage in such systems is a more acute problem, given the large difference between LOS and NLOS propagation characteristics.

Inspired by the stochastic geometry approach to analyze the performance of conventional cellular systems, we design a framework for evaluation of the coverage and rate performance in mmWave networks. However, applying the results of standard cellular systems to mmWave is non-trivial due to their differences in propagation characteristics and the use of highly directional beamforming. Directional beamforming was applied in [82] by considering a simplified path loss model. While in [91] a blockage model for mmWave is used to analyze the rate and coverage area of such systems, a distance dependent path loss model along with antenna gain parameters are considered in [18] to characterize the propagation environment in mmWave systems. Furthermore, we would like to refer the readers to [16, 17, 91, 18] which develop several mathematical frameworks to model the propagation characteristics of mmWave networks.

In this chapter, we incorporate relays to aid mmWave networks in order to provide better coverage and decrease blockage effects on the transmission link. We consider a stochastic geometry approach to characterize the spatially distributed relays and the sources. It is assumed that the sources and the relays in the mmWave network follow two PPPs but are independent of each other. Most works on relay-aided networks assume that the number of relays in the network is fixed and known. However, such fixed type network relays may not be suitable for practical outdoor environments when a network topology dynamically changes. Due to the fact that some relays are in outage because of blockages in the network, we consider the subset of relays which has lesser path loss. This consideration leads to a marked Poisson process. In general, however, one must contend with the mathematical challenges of working with such point processes.

Furthermore, we conform to two relay selection strategies for tractable analysis, namely random relay and best relay. The motivation behind the use of a random relay selection is to capture blockage effects on performance of active set of relays. Specifically, the end-to-end SNR is characterized using amplify and forward technique where

the relay obtains a noisy version of the signal transmitted by the source in presence of blockages and then amplifies its received signal and re-transmits it to the destination again in presence of blockages. After finding a best random path, it is possible to provide a bound on the active relays which can participate in the communication. These relay nodes are the ones that are minimally affected by blockages. Furthermore, we also consider the best relay selection in order to study the trade-off between performance and complexity of random relay selection techniques in mmWave networks.

The main contributions of this chapter can be summarized as in the following points:

- We have presented a relay modeling technique in mmWave networks considering blockages, in which we compute the density of active relays that aid the transmission.
- A closed form expression for end-to-end SNR is provided and the best random relay path in a mmWave network using order statistics is calculated.
- To investigate the asymptotic increase in the number of transmission paths, extreme value theory is used and accordingly the maximum end-to-end SNR of random relay paths is found to approach the Gumbel distribution.
- We have also provided the closed form expression of the SNR distribution for the best relay having maximum path gain in such a network.
- Finally, an analysis on the coverage probability and the transmission capacity of relay aided mmWave networks is provided. It is shown that relays improve the received SNR for mmWave networks for a specific coverage probability.

## 5.1 Mathematical Preliminaries

In this chapter, we extensively use log-normal random variables to model the shadowing effects caused due to random blockages in the mmWave network. A few important results are presented in this section for better understanding of this chapter. However, we avoid the proofs of any results provided here as they are well known in literature of probability theory.

**Definition 5.1.** *A log-normal random variable $X$ with parameters $\mu$ and $\sigma$ is defined as*

$$X = e^{\mu+\sigma Z}, \tag{5.1}$$

*where $\mu$ and $\sigma$ are the mean and standard deviation of the variable's natural logarithm respectively and $Z$ is a standard normal variable. The PDF of a log-normal distribution is given by*

$$f_X(x;\mu,\sigma) = \frac{1}{x\sigma\sqrt{2\pi}}\, e^{-\frac{(\ln x-\mu)^2}{2\sigma^2}} \tag{5.2}$$

*and the CDF is given by*

$$\begin{aligned} F_X(x;\mu,\sigma) &= \int_0^x f_X(p;\mu,\sigma)\,dp, \\ &= \frac{1}{2}\operatorname{erfc}\left(-\frac{\ln x-\mu}{\sigma\sqrt{2}}\right) = Q\left(\frac{\ln x-\mu}{\sigma}\right), \end{aligned} \tag{5.3}$$

*where* erfc *is the complementary error function, and $Q$ is the cumulative distribution function of the standard normal distribution.*

**Lemma 5.1.** *Let $X_j \sim \ln\mathcal{N}(\mu_j,\sigma_j^2)$ be $n$ statistical independent log-normally distributed variables, and $Y = \prod_{j=1}^n X_j$, then $Y$ is also log-normally distributed with parameters $\sum_{j=1}^n \mu_j$, and $\sum_{j=1}^n \sigma_j^2$.*

**Lemma 5.2.** *Let $X_j \sim \ln\mathcal{N}(\mu_j,\sigma_j^2)$ are independent log-normally distributed variables with varying $\sigma$ and $\mu$ parameters, and $Y = \sum_{j=1}^n X_j$. Then the distribution of $Y$ has no closed form expression, but can be reasonably approximated by another log-normal distribution $Z$ with parameters[92]*

$$\mu_Z = \ln\left[\sum e^{\mu_j+\sigma_j^2/2}\right] - \frac{\sigma_Z^2}{2}, \tag{5.4}$$

$$\sigma_Z^2 = \ln\left[\frac{\sum e^{2\mu_j+\sigma_j^2}(e^{\sigma_j^2}-1)}{(\sum e^{\mu_j+\sigma_j^2/2})^2}+1\right]. \tag{5.5}$$

**Lemma 5.3.** *Let $X \sim \ln\mathcal{N}(\mu,\sigma^2)$, then $aX \sim \ln\mathcal{N}(\mu+\ln a,\ \sigma^2)$, $a \in \mathbb{R}$.*

**Lemma 5.4.** *If $X \sim \ln\mathcal{N}(\mu,\sigma^2)$, then $\frac{1}{X} \sim \ln\mathcal{N}(-\mu,\ \sigma^2)$.*

## 5.2 System Model

In this section, we illustrate our system model for a relay assisted mmWave network. We focus on the communication from multiple mmWave BSs, aided by multiple relays

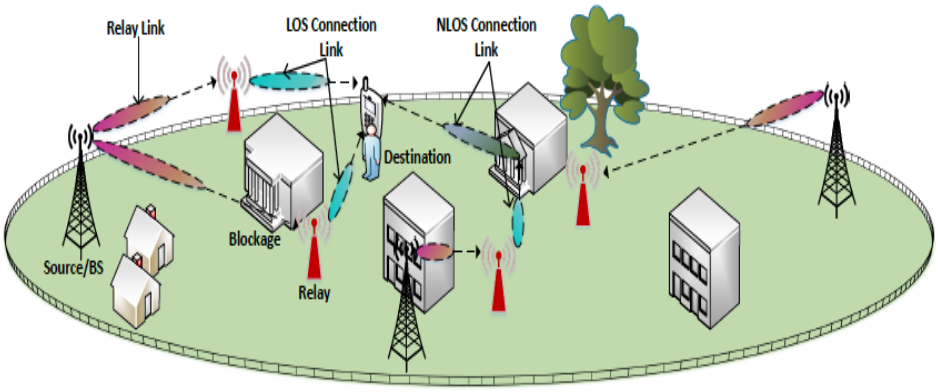


***Figure 5.1:*** *An illustration of an outdoor mmWave network aided by relays.*

to a typical user in the presence of blockages. The user is assumed to be located at the origin $\mathcal{O}$. We term the direct link between a BS and the user or a relay and the user as connection link. The link between a BS and a relay is termed as the relay link. Hereinafter, we use the terms source and destination to represent the mmWave BS and the user respectively. The specifics of the model are described below.

### 5.2.1 Network modeling

We consider a relay-aided mmWave ad hoc network consisting of multiple sources transmitting to a typical destination (reference point) as shown in Fig. 5.1. The sources in the network are modeled as points in $\mathbb{R}^2$ which are distributed uniformly as a homogeneous PPP $\Phi_{\mathrm{S}}$ with intensity $\lambda_{\mathrm{S}}$. The relays are also modeled as points of a uniform PPP, denoted by $\Phi_{\mathrm{R}}$, with intensity $\lambda_{\mathrm{R}}$ in $\mathbb{R}^2$.

### 5.2.2 Path loss modeling

It is well known that shadow fading heavily depends on the site-specific details of an environment. More specifically, path loss dependent shadow fading is typically a result of regression analysis on a signal level measurement represented on a distance dependent path loss scatter plot. In other words, a path loss law is fitted to the measurement, and the residual error of the model fit is called shadow fading. The path loss can be modeled in several ways from practical data accumulated from field measurements. In this chapter, for analytic tractability, we use the alpha plus beta model (based on the traditional free space path loss model) given in [16], which takes into consideration the log-normal shadowing. Accordingly, in a mmWave transmission,

the path loss (in dB) associated with the transmission between any two nodes $x_i$ and $x_j$ can be given as

$$L(x_i, x_j) = \eta + 10\alpha \log_{10} ||x_i - x_j|| + \mathcal{X}_{\mathcal{N}}, \tag{5.6}$$

where $||x_i - x_j||$ is the distance between the $i$th and $j$th nodes with $\{i, j\} \in \mathbb{Z}^+$ and $\mathcal{X}_{\mathcal{N}} \sim \mathcal{N}(0, \sigma^2)$. However, it is to be noted that the sources and the relays can be either LOS or NLOS. Let the path loss at a fixed small reference distance, $x_i - x_j = 1$ be $\eta$. Then for such a model, $\alpha$ can be physically interpreted as the path loss exponent. Moreover, the parameters $(\alpha, \eta)$ can be looked upon as the floating intercept and slope of the best linear fit data. In that case, it may not be necessary to attribute $(\alpha, \eta)$ with any specific physical interpretation. The deviation in fitting (in dB) is modeled as a Gaussian random variable $\mathcal{X}_{\mathcal{N}}$ (Lognormal in linear scale) with zero mean and variance $\sigma^2$. Accordingly, $\alpha$, $\eta$ and $\sigma^2$ are altered for each of the two scenarios.

According to [83, 16], the alpha plus beta model can be compared to the free space path loss model for a certain range of distances (30m-200m). For millimeter wave networks, due to path loss sensitivity, the typical communication range falls under 200m. Therefore, considering the alpha plus beta model is a viable approximation for such high frequency communications.

In mmWave networks, small scale fading does not have as much impact on transmitted signals as compared to lower frequency systems. However, blockages and shadowing are more significant in such systems. It is extensively mentioned in literature [16, 20] that in mmWave analysis, small scale fading can be ignored. Hence, ignoring fading and considering only shadowing, the probability density function of $\mathcal{X}_{\mathcal{N}}$ in (5.6) can be defined as

$$\mathcal{X}_{\mathcal{N}} \sim f_{\mathcal{X}_{\mathcal{N}}}(x; \mu_c, \sigma_c) = \frac{1}{x\sqrt{2\pi}\sigma_c} \exp\left( - \frac{(\log x - \mu_c)^2}{2\sigma_c^2} \right), \tag{5.7}$$

where the parameters, $\mu_c$ and $\sigma_c^2$ follows from [18] and $x > 0$.

### 5.2.3 Directional beamforming modeling

Due to the small wavelength of mmWaves, directional beamforming can be exploited for compensating the path loss and additional noise. Accordingly, antenna arrays are deployed at the source, relays and the destination. In our model, we assume all the sources and the relays to be equipped with directional antennas with sectorized gain

pattern. Let $\theta$ be the beamwidth of the main lobe. Then the antenna gain pattern for a source, relay or destination node about some angle $\phi$ is given as [17]

$$G_q(\phi) = \left\{ \begin{array}{ll} G_q^{\max} & \text{if} |\phi| \leq \theta \\ G_q^{\min} & \text{if} |\phi| \geq \theta \end{array} \right\}, \tag{5.8}$$

where $q \in \mathrm{S}, \mathrm{R}, \mathrm{D}$, $\phi \in [0, 2\pi)$ is the angle of boresight direction, $G_q^{(max)}$ and $G_q^{(min)}$ are the array gains of main and side lobes, respectively. The typical user does not have the same directional gain pattern but can be modeled similarly[1]. For simplicity, in this work only the source and the relays are considered to have directional gains, while the user is assumed to have omni directional antennas similar to [18]. Hereinafter, we assume the antenna beams of the connection link and the relay link to be aligned. Hence, the total gain on a desired connection link is $G^{\max}$ and the relay link is $(G^{\max})^2$.

### 5.2.4 Blockage modeling

Blockages in the network are usually concrete buildings which cannot be penetrated by mmWave signals. In particular, the blockages form a process of random shapes, e.g. a Boolean scheme of rectangles [91], on the plane. We consider the blockages to be stationary blocks which are invariant with respect to direction [94]. The link between a BS and a typical user can be either LOS or NLOS[2]. Different researchers have tried to model blockages with varied level of success based on different geographical scenarios. In [95] a PPP based random blockage model is used, where $e^{-\beta r}$ is considered to be the probability of LOS with $\beta$ being the blockage density and $r$ the distance between the transmitting and receiving nodes. Another model that has been considered in literature is a fixed LOS probability model as was depicted in [18]. Leveraging the modeling of blockages from this later model, we consider a two state statistical model for each and every link. The link can be either LOS or NLOS. LOS link occurs when there is a direct propagation path between a source and the destination while NLOS occurs when the link is blocked and the destination receives the signal through reflection from a blockage. Due to the presence of blockages, only a subset of the BSs $\Phi_{\mathrm{BS}}$ are LOS to the typical user. Let the LOS area within a circular ball of radius $r_D$ be centered around the reference point. Then, if the LOS link is of length $r$, the probability of the

[1]Several existing analytical models for single user analog beamforming enabled mmWave networks also assume an equivalent single input single output (SISO) like system with directional antenna gains by abstracting underlying signal level details [93].

[2]The notations {L, N} and {LOS, NLOS} will be interchangeably used hereinafter and both sets signify the same meaning.

connection link to be LOS is given by $p_{\mathrm{L}}$ if $r < r_D$ and 0 otherwise. Similarly, the NLOS probability is represented by $p_{\mathrm{N}}$. The parameters $r$ and $r_D$ are dependent on the geographical and deployment scenario of the network. The analytical results derived in this chapter are based on the blockage model proposed in [18] and the numerical analyses are done based on the data accumulated by [18] and [95].

We would like to note that the LOS probabilities are assumed to be independent between different links, i.e., we ignore potential correlations of blockage effects between links. However, in reality the LOS probabilities for different links may not be independent. Essentially in an urban area, neighbouring BSs might simultaneously be blocked by a large building. Nonetheless, in [91], it was shown that ignoring such correlations cause only a minor loss of accuracy in the SINR evaluation. Furthermore, the PPP based random blockage model will be considered in Chapter 6.

### 5.2.5 SNR modeling

Recent studies on mmWave networks [16, 18, 20], state that in contrast to conventional cellular networks which are usually strongly interference limited, mmWave networks in urban settings are more noise limited. This is due to the fact that in the presence of blockages, the signals received from unintentional sources are close to negligible. In such densely blocked scenarios (typical for urban settings), SNR provides a good enough approximation to signal to interference plus noise ratio (SINR) for directional mmWave networks. Additionally, such an assumption also aids us in deriving closed form expressions and hence, interference at the destination is ignored hereinafter.

In order to characterize the SNR distribution, we assume a two slot synchronous communication throughout the chapter. While the active relay nodes are allowed to receive from the sources in the first time slot, the destination is allowed to receive from the active relay nodes and the sources in the second time slot. We also assume that all relays co-operate with each other while transmitting and are deployed with a guard zone[3].

[3]The guard zone resembles a specific SNR which must be fulfilled in order for the relay node to be deployed. This is explained in Section 5.3 of this chapter.

**First time slot**

Consider that the relay nodes are served by the sources during this time slot. The SNR at any specific relay, $R$ can then be formulated as

$$\gamma_{\mathrm{SR}}^{i} = \frac{P_{\mathrm{S}}(G^{\max})^2 \mathcal{X}_{\mathcal{N}} r_{\mathrm{SR}}^{-\alpha_i}}{N_0}, \tag{5.9}$$

where $P_{\mathrm{S}}$ is the transmit power of the source, $r_{\mathrm{SR}}$[4] is the length of the link from the source to relay, $\alpha$ is the path loss exponent, $i \in \{\mathrm{L},\ \mathrm{N}\}$ and $N_0$ is the noise power.

**Second time slot**

Consider that the destination, $D$ is served by a source with or without the help of relay $R$ during this time slot[5]. Then the SNR at the destination $D$ receiving signal only from the source, $S$ can be given as

$$\gamma_{\mathrm{SD}}^{i} = \frac{P_{\mathrm{S}} G^{\max} \mathcal{X}_{\mathcal{N}} r_{\mathrm{SD}}^{-\alpha_i}}{N_0}. \tag{5.10}$$

Similarly, the SNR at the destination $D$ receiving signal only from the relay, $R$ can be given as

$$\gamma_{\mathrm{RD}}^{i} = \frac{P_{\mathrm{R}} G^{\max} \mathcal{X}_{\mathcal{N}} r_{\mathrm{RD}}^{-\alpha_i}}{N_0}, \tag{5.11}$$

where $P_{\mathrm{R}}$ is the transmit power of the relay. Note that for simplicity, we have omitted the subscript 'max' from $G$ in all our subsequent discussions. Hereinafter, for analytical tractability, we consider that the transmitted power at the source and relay is the same and given as $P$.

Now, considering that the source transmits to the destination only through the aid of the relay, the coverage probability of such a relay-aided transmission link with a target SNR, $T$ is given by

$$\mathcal{P}_{\mathrm{R}}^{c} = 1 - \mathbb{P}\{\gamma_{\mathrm{SR}} < T\}\mathbb{P}\{\gamma_{\mathrm{RD}} < T\}. \tag{5.12}$$

[4] $r_{\mathrm{AB}}$ is the distance between the A-th and B-th nodes.

[5] This model of considering the destination to receive the signal from the source as well as relay in the second time slot can be useful when considering a maximal ratio combining scheme at the destination which would take into consideration both the signals from the relay and the source provided that the strength of the signal is above a certain threshold.

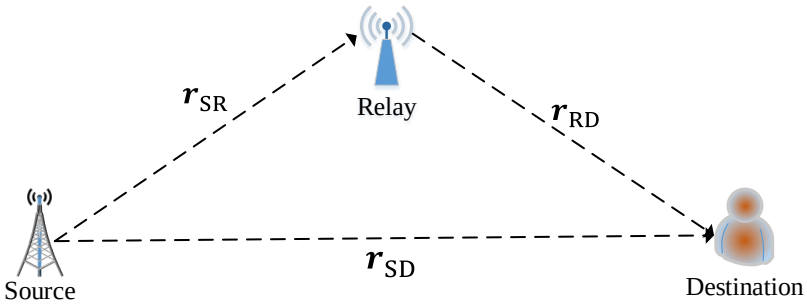


***Figure 5.2:*** *Topology of a relay assisted network link.*

## 5.3 Relay aided MmWave Transmission

Fig. 5.2 shows an example of a transmission from a source to a destination through the aid of a relay. With the assistance of relays, it is possible to act on the constraints of path loss in a mmWave network and also extend the communication distance, while also improving the quality of communication. In this section we characterize the conditions for relay aided transmission in mmWave communication networks. Further, we would like to note that relay cooperation takes place if and only if the SNR at the destination from the source through a direct link is not good enough and falls below a certain threshold. In order to avoid the aid of relay, we define a required outage constraint $\gamma_{\text{out}}$ for the source-to-destination link as

$$\mathcal{P}_{\text{out}} = \mathbb{P}\left\{\gamma_{\text{SD}}^{i} < \gamma_{\text{out}}\right\}. \tag{5.13}$$

### 5.3.1 Preliminaries on active relays

Due to the impact of blockages, some of the relay nodes may not be available or capable to support the transmission from source node to destination node and only a subset of the relay nodes may participate in the communication. In this subsection we give an insight on such active relays which are available to aid the communication from the source to the destination.

Consider the distribution of relays follows a terrain according to its coverage probability, which depends on the blockages and deployment constraints. Hence, the distri-

bution is far from being spatially uniform. Such conditions are clearly distinct from the random and uniformly distributed network assumptions that lead to a Poisson number of nodes per unit area *i.e.*, the PPP model – commonly adopted in current literature [88, 96, 86]. Some recent works such as [97, 98] focus on the impact of topological models on random networks. To elaborate, in [97] hard core point processes (HCPPs) are proposed to model networks with carrier-sensing multiple access (CSMA) techniques, and in [98] the coverage probability of cellular systems are analyzed under PPP, HCPP and Strauss Process (SP) models. These models are further compared against field data, which demonstrate that indeed HCPP and SP lead to significantly more accurate results than the PPP model commonly used earlier. All in all, it is now an established fact that as far as the topological models for random networks are concerned, the PPP alone is not sufficient, and hence alternative models need to be considered. Motivated by such recent results [98, 97, 99], we consider the Matérn HCPP (MHCPP) model in order to characterize the distribution of active relays in the following analysis[6].

Since we model the distribution of relays in our network with a MHCPP, it is worthwhile to mention here some properties of MHCPP. In the MHCPP Type I, all the points obtained from a stationary PPP of intensity $\lambda_p$ are retained if and only if they are at a distance of at least $d$ from all other points. Whereas, in MHCPP Type II model, points are obtained by deleting the primary points that co-exist within a distance less than the hard core distance from another primary point having a lower mark.

For a MHCPP model, which is generated from a homogenous PPP, $\Phi_p$, with intensity $\lambda_p$ and repulsive distance d, the intensity $\lambda_m$ of the MHCPP is given by [97, 99]

$$\lambda_m = \frac{1 - \exp\left(-\lambda_p \pi d^2\right)}{\pi d^2}. \tag{5.14}$$

Consequently, the probability of a point being retained from $\Phi_p$ is

$$\mathcal{P} = \frac{\lambda_m}{\lambda_p} = \frac{1 - \exp\left(-\lambda_p \pi d^2\right)}{\lambda_p \pi d^2}. \tag{5.15}$$

These hardcore models (Type I and Type II) of point processes are not directly applicable to fading and blockage environments. This is due to the fact that the density

[6]The HCPP is considered in this chapter to find the density of active relays only.

of active number of nodes depends on random fading gains and blockage processes. To tackle the impact of fading, [99] extends the hard core process analysis for the case of Rayleigh fading and [97] derives the active number of transmitters under generalized fading channel by employing MHCPP Type II model. In this chapter, we leverage the results from [97] and incorporate additional blockage effects. It is a well known fact that the characterization of non-PPP models (general topologies) via the Laplace Functional and probability generating functionals is in reality a challenging problem. Therefore, the hard-core point processes are quite difficult to analyze due to the simple reason that their probability generating functionals do not exist [100, 99, 101]. However, it has been argued in [100, 99] that the nodes further away from the hard core distance, $d$ can still be modeled as a PPP. Furthermore, it has been shown in [101] that MHCPP type II is better approximated with a PPP rather than Type I. Hence, we take into account such an approximation for analytical tractability and consider that the distribution of relay nodes follows a PPP, while the density of the relay nodes is approximated by that of a modified hard-core PPP with density $\bar{\lambda}_{\mathrm{R}}$.

### 5.3.2 Density of active relays

In this subsection, we aim to find the intensity of active relays by generalizing the traditional MHCPP for blockage environments in mmWave. To overcome underestimation flaw, in [97], authors made an assumption of a bounded region, a circle with a deterministic radius, where the nodes contribute to the event of interest. In our model, the contribution of each relay node to the event of interest will be Bernoulli distributed with a parameter that accounts for both shadowing and blockage process. The procedure to find active density of relay nodes follows similar steps as in [97]. However, the neighborhood success probability varies due to the addition of a blockage process in our system.

Let $\Phi_{\mathrm{R}}$ be the primary point process and $\bar{\Phi}_{\mathrm{R}}$ be the generalized MHCPP. In order to generalize the traditional MHCPP with respect to SNR, the hard-core distance $d$ is replaced with the received SNR. A relay node is retained in $\bar{\Phi}_{\mathrm{R}}$ if and only if it has the lowest mark in its neighborhood set of relays $N(x_i)$ which is determined by dynamically changing the random-shaped region defined by instantaneous path gains.

**Lemma 5.5.** *Let $\mathcal{P}_\zeta$ be the neighborhood success probability. Now, if the retaining probability of a relay node is $\mathcal{P}_{\mathrm{R}} = \frac{1-e^{-N\mathcal{P}_\zeta}}{N\mathcal{P}_\zeta}$ with the expected number of nodes in the disc $N$, then the intensity of active number of relays is given by $\bar{\lambda}_{\mathrm{R}} = \lambda_{\mathrm{R}}\mathcal{P}_{\mathrm{R}}$ [97,*

*Theorem 4.1].*

Therefore, in order to find the retaining probability, $\mathcal{P}_{\mathrm{R}}$ in Lemma 5.5, one must compute the neighborhood success probability, $\mathcal{P}_{\zeta}$. As mentioned earlier, the neighborhood set of any relay node is determined by bounding the observation region by $\mathcal{B}_{x_i}(r_d)$, where $r_d$ is a sufficiently large distance, such that the probability for a relay located beyond $r_d$ to become a neighbor of $x_i$ is a very small number, $\varrho$. Therefore,

$$\mathbb{P}\left\{\frac{P\,(G^{\max})^2\mathcal{X}_{\mathcal{N}}}{N_0||x_i-x_j||^{\alpha}} > \gamma_{\mathrm{R}}|\,||x_i-x_j|| > r_d\right\} \leq \varrho, \tag{5.16}$$

where $\gamma_{\mathrm{R}}$ is the minimum required target SNR.

Hence, $r_d$ can be determined as

$$r_d = \left(\tfrac{P\,(G^{\max})^2}{N_0\gamma_{\mathrm{R}}}F^{-1}_{\mathcal{X}_{\mathcal{N}}}(\varrho)\right)^{1/\alpha}, \tag{5.17}$$

where, $F^{-1}$ denotes the inverse of the CDF of $\mathcal{X}_{\mathcal{N}}$.

Then the neighborhood success probability within the bounded region can be defined as

$$\mathcal{P}_{\zeta} = \mathbb{P}\{\gamma_{x_i,x_j} \geq \gamma_{\mathrm{R}}|x_j \in \mathcal{B}_{x_i}(r_d)\}. \tag{5.18}$$

Therefore, considering blockages (5.18) can be written as

$$\begin{aligned}\mathcal{P}_{\zeta} &= \sum_{i\in\mathrm{L,N}} p_i \int_0^{r_d}\left(1-F_{\mathcal{X}_{\mathcal{N}}}\left(\frac{N_0\gamma_{\mathrm{R}}r^{\alpha_i}}{P\,(G^{\max})^2}\right)\right)r\mathrm{d}r,\\ &= \sum_{i\in\mathrm{L,N}} p_i \int_0^{r_d}\left[1-Q\left(\frac{\log\left(\frac{N_0\gamma_{\mathrm{R}}r^{\alpha_i}}{P\,(G^{\max})^2}\right)-\mu_c}{\sigma_c}\right)\right]r\mathrm{d}r,\end{aligned} \tag{5.19}$$

where, $Q(.)$ is the cumulative distribution function of the standard normal distribution. A closed form expression for $\mathcal{P}_{\zeta}$ can be given as

Using (5.20), we can derive the generalized MHCPP process of the relays and their active nodes which can withstand the blockage effects in the network to transfer the information with less outage probability. In practical scenarios, selecting a relay from an observation (or defined) region with a small neighborhood set of relays is opti-

$$\mathcal{P}_\zeta = \frac{1}{4} {r_d}^2 \sum_{i \in \mathrm{L,\ N}} p_i \left[ -\exp\left(\frac{2\left(\alpha_i \mu_c + \sigma_c^2\right)}{\alpha_i^2}\right) \left(\frac{N_0 \gamma_R}{P(G^{\max})^2} r_d^{\alpha_i}\right)^{\frac{-2}{\alpha_i}} \right. \tag{5.20}$$
$$\left. \operatorname{erf}\left(\frac{\alpha_i \mu_c - \alpha \log\left(\frac{N_0 \gamma_R}{P(G^{\max})^2} r_d^{\alpha_i}\right) + 2\sigma_c^2}{\sqrt{2}\alpha_i \sigma_c}\right) + \operatorname{erf}\left(\frac{\mu_c - \log\left(\frac{N_0 \gamma_R}{P(G^{\max})^2} r_d^{\alpha_i}\right)}{\sqrt{2}\sigma_c}\right) \right].$$

mal. Since the computational complexity increases with number of relays, a carefully designed region can be taken into consideration.

From the above analysis, it is clear that the achievable capacity of relay assisted link depends on the distance between the relay and the reference point. Assume that our communication is taking place within radius $r_d$, then source-destination pair should select the optimal relay with distance less than $r_d$. In the subsequent section, we discuss relay selection techniques based on the best end-to-end SNR[7] and minimum path loss.

Here, we follow two strategies for tractable analysis, namely, random relay and best relay while taking into consideration the blockage effects. The random relay selection technique is used to capture the blockage effects on the performance of active set of relays while, the best relay selection is studied in order to weigh on the trade-off between performance and complexity of random relay selection techniques in mmWave networks.

## 5.4 SNR Analysis of the Relay Schemes

In this section, we analyze the SNRs of two relay selection techniques in order to determine the best technique suitable for a mmWave communication. In the first technique, we select the path with the best SNR from a set of random paths. The random paths can be looked upon as the end-to-end SNR from the source to the destination through the aid of relay. In the second case, we select the best relay first based on the minimum path loss and then use that relay to transmit the signal to the destination from the source.

[7]The end-to-end SNR signifies the total SNR from source to the destination through the aid of relay using amplify and forward technique [86].

### 5.4.1 Best path selection based on end-to-end SNR

In this subsection, in order to select any random path, we first select a random relay and then compute the end-to-end SNR[8] distribution of that path. Subsequently, we select the path with the best SNR distribution from an asymptotic point of view (when the number of links tend to infinity in a dense network) by using extreme value theory.

As stated before, any node can receive a signal either through LOS or NLOS link. We now compute the SNR distribution accounting for both the LOS and NLOS links. Thus the achievable SNR between the source and the destination can be given as[9]

$$\gamma_{\mathrm{SD}} = \gamma_{\mathrm{SD}}^{\mathrm{L}} p_{\mathrm{L}} + \gamma_{\mathrm{SD}}^{\mathrm{N}} p_{\mathrm{N}}, \tag{5.21}$$

where $\gamma_{\mathrm{SD}}^{\mathrm{L}}$ and $\gamma_{\mathrm{SD}}^{\mathrm{N}}$ are the LOS and NLOS SNRs respectively for the links from source to destination and $p_{\mathrm{L}}$ and $p_{\mathrm{N}}$ are the probabilities that the links are LOS and NLOS respectively. Similarly, the achievable SNR between the source and relay and the relay and destination are given respectively as

$$\gamma_{\mathrm{SR}} = \gamma_{\mathrm{SR}}^{\mathrm{L}} p_{\mathrm{L}} + \gamma_{\mathrm{SR}}^{\mathrm{N}} p_{\mathrm{N}} \text{ and} \tag{5.22}$$

$$\gamma_{\mathrm{RD}} = \gamma_{\mathrm{RD}}^{\mathrm{L}} p_{\mathrm{L}} + \gamma_{\mathrm{RD}}^{\mathrm{N}} p_{\mathrm{N}}. \tag{5.23}$$

Considering the LOS regime, the SNR distribution can be formulated as

$$\begin{aligned} F_{\gamma_{SD}^{\mathrm{L}}}(z) &= \mathbb{P}\left\{\frac{P\,G^{\max}\mathcal{X}_{\mathcal{N}}}{r^{\alpha_{\mathrm{L}}}N_0} < z\right\}, \\ &= \mathbb{P}\left\{\mathcal{X}_{\mathcal{N}} < \frac{z r^{\alpha_{\mathrm{L}}} N_0}{P\,G^{\max}}\right\}, \\ &= Q\left(\frac{\log\left(\frac{z N_0 r^{\alpha_{\mathrm{L}}}}{P\,G^{\max}}\right) - \mu_{\mathrm{SD}}^{\mathrm{L}}}{\sigma_{\mathrm{SD}}^{\mathrm{L}}}\right), \end{aligned} \tag{5.24}$$

where, $Q(.)$ is the cumulative distribution function of the standard normal distribution.

[8] We would like to refer the readers to [86, 102] for an elaborate description on this technique.

[9] Since we model the links between the sources and the destination as LOS and NLOS which are independent of each other, we leverage the notion of mark from stochastic geometry to further split the Poisson Point Processes into two independent LOS and NLOS sub processes.

Using Lemma 5.3, the distribution of $\gamma_{\mathrm{SD}}^{L} p_{\mathrm{L}}$ can now be expressed as

$$F_{\gamma_{SD}^{\mathrm{L}}}(z) = Q\left(\frac{\log\left(\frac{zN_0 r^{\alpha_{\mathrm{L}}}}{P\,G^{\max}}\right) - (\mu_{\mathrm{SD}}^{\mathrm{L}} + p_{\mathrm{L}})}{\sigma_{\mathrm{SD}}^{\mathrm{L}}}\right). \tag{5.25}$$

Similarly the $\gamma_{\mathrm{SD}}^{\mathrm{N}}$ can be characterized. Therefore, now the total SNR can be calculated using equation (5.21). However, $\gamma_{\mathrm{SD}}^{\mathrm{L}}$ and $\gamma_{\mathrm{SD}}^{\mathrm{N}}$ are two independent log-normally distributed variables with different $\mu$ and $\sigma$ parameters. In this scenario, the distribution of the total SNR $\gamma_{\mathrm{SD}}$ has no closed form expression, but it can be approximated by another log-normal distribution using Lemma 5.2 with parameters $\mu_{\mathrm{SD}}$ and $\sigma_{\mathrm{SD}}^2$.

In order to capture the blockage effects on both sides of relay (Source-to-Relay and Relay-to-Destination), we consider the end-to-end SNR to find the path with the best SNR distribution.

For practical systems, the relay gain is given by $\mathcal{G}^2 = (1/(P(G^{\max})^2 \mathcal{X}_{\mathcal{N}} r^{\alpha_i} + N_0))$. However, assuming the ideal relaying gain[10] i.e., $\mathcal{G}^2 = (1/(P(G^{\max})^2 \mathcal{X} r^{\alpha_i}))$, the end-to-end SNR of the link through the aid of relay can now be given as [86, 102]

$$\hat{\gamma}_{\mathrm{SRD}} = \frac{\gamma_{\mathrm{SR}}\gamma_{\mathrm{RD}}}{\gamma_{\mathrm{SR}} + \gamma_{\mathrm{RD}}}, \tag{5.26}$$

where the subscript SRD stands for the path from the source to the relay to the destination.

**Proposition 5.1.** *The end-to-end SNR in a relay aided mmWave network $\hat{\gamma}_{\mathrm{SRD}}$ is log-normally distributed with new parameters $\hat{\mu}_{\mathrm{SRD}}$ and $\hat{\sigma}_{\mathrm{SRD}}$.*

*Proof.* Let $X = \gamma_{\mathrm{SR}}\gamma_{\mathrm{RD}}$ and $Y = \gamma_{\mathrm{SR}} + \gamma_{\mathrm{RD}}$, then in order to prove that $Z = \frac{X}{Y}$ is log-normally distributed, it is sufficient to prove that $Z$ is a log-normal random variable with parameters $\mu_Z$ and $\sigma_Z$.

Now, from Lemma 5.1, we have

$$X \sim \log\mathcal{N}(\mu_X, \sigma_X^2), \tag{5.27}$$

[10]The adoption of the ideal relaying gain is mainly for analytical tractability and can act as a tight upper bound for the practical relaying gain. This method is widely used in literature [86, 102] to approximate relay gains.

where

$$\mu_X = \mu_{\mathrm{SR}} + \mu_{\mathrm{RD}}, \tag{5.28}$$

$$\sigma_X^2 = \sigma_{\mathrm{SR}}^2 + \sigma_{\mathrm{RD}}^2. \tag{5.29}$$

Using Lemma 5.2, $Y$ can be tightly approximated with another log-normal random variable with parameters

$$\mu_Y = \ln\left[\sum e^{\mu_j + \sigma_j^2/2}\right] - \frac{\sigma_{\mathrm{SD}}^2}{2}, \tag{5.30}$$

$$\sigma_Y^2 = \ln\left[\frac{\sum e^{2\mu_j + \sigma_j^2}(e^{\sigma_j^2} - 1)}{(\sum e^{\mu_j + \sigma_j^2/2})^2} + 1\right]. \tag{5.31}$$

Again, using Lemma 5.1, the distribution of $\bar{\gamma}_R = \frac{X}{Y}$ can be given as another log normal variable which is the required result. □

**Proposition 5.2.** *Let $\bar{\gamma} = \max\{\hat{\gamma}_{\mathrm{SRD}_i}\}$. Then the probability distribution of the best path from source to the destination which exhibits the maximum end-to-end SNR can be given as*

$$F_{\bar{\gamma}} = \prod_{i=1}^{n} F_{\hat{\gamma}_{\mathrm{SRD}_i}} = (F_{\hat{\gamma}_{\mathrm{SRD}_i}})^n, \tag{5.32}$$

*where $n = K \times N$ gives the total number of paths available for a given $K$ number of sources and $N$ number of relays.*

*Proof.* Let $F_Y(y)$ denote the CDF of $Y$, then the CDF of the maximum of identically distributed random variables $X_1, X_2, \cdots, X_n$ can be given as

$$F_Y(y) = \mathbb{P}\{Y < y\} = \mathbb{P}\{x_1 < y, x_2 < y \cdots x_n < y\} \tag{5.33}$$

Therefore, $F_Y(y)$ can be obtained using order statistics [103] as follows

$$F_Y(y) = \mathbb{P}\{Y < y\} = \prod_{k=1}^{n} \mathbb{P}\{x_k < y\} = (F_{X_k}(y))^n. \tag{5.34}$$

Proposition 5.2 thus follows from (5.34). Furthermore, the parameters $K$ and $N$ can be computed from the mean of the expected number of source and relay nodes.

*Mean of Expected Number of Source Nodes:* For given values of propagation pa-

rameters in bounded region, one can obtain the expected number of source nodes present in the communication vicinity by describing the propagation process. Let $\Phi_{\mathrm{S}} = \{\frac{r^{\alpha_i} N_0}{\mathcal{X} P (G^{\max})^2}, r \in \phi\}$ be the path loss process, where $i \in \{LOS,\ NLOS\}$. Then the expected number of nodes can be given as

$$\Lambda_{\mathrm{S}}((0,t]) = 2\pi\lambda_{\mathrm{S}} \int_{\mathbb{R}^+} \mathbb{P}\left\{\frac{r^{\alpha_i} N_0}{\mathcal{X}_{\mathcal{N}} P (G^{\max})^2} < t\right\} r \mathrm{dr} \tag{5.35}$$

The closed form expression for the above integral follows as in [18]. The mean of the expected number of the relay nodes follows similarly with density $\bar{\lambda}_{\mathrm{R}}$. □

#### 5.4.1.1 Asymptotic analysis

We now investigate the asymptotic behavior of the distribution of the maximum SNR $\hat{\gamma}$ of the best relay path with the help of extreme value theory. This is to obtain insights into coverage in very dense networks. In general, extreme value theory is used to deal with extreme values, such as maxima or minima of distributions when the number of random variables increases asymptotically. Let $\varphi_i$s be the realizations of a random variable $\bar{\varphi}$, where $\varphi_i$s are independent and identically distributed with $i = 1, 2, \ldots, n$. By extreme value theory [104], if there exist constants $a \in \mathbb{R}, b > 0$, and some non-degenerate distribution function $F(k)$ such that the distribution of $\frac{\bar{\varphi}_{max} - a}{b}$ scales to $F(k)$, then $F(k)$ converges to one of the three standard extreme value distributions: Gumbel, Frechet and Weibull distributions, where $\bar{\varphi}_{max} = \max(\varphi_1, \varphi_2, \ldots, \varphi_n)$. There are only three possible non-degenerate limiting distributions for maxima, which can be expressed as

1. $F_1(k) = e^{-e^{-k}}, \qquad -\infty < k < \infty$
2. $F_2(k) = e^{-k^{-\alpha}} u(k), \quad \alpha > 0$
3. $F_3(k) = \begin{cases} e^{-(-k)^{\alpha}}, & \alpha > 0,\ k \leq 0 \\ 1, & k > 0 \end{cases}$

where $u(k)$ is the step function.

**Proposition 5.3.** *Let $\bar{\gamma} = \max(\hat{\gamma}_{\mathrm{SRD}_1}, \hat{\gamma}_{\mathrm{SRD}_2}, \ldots, \hat{\gamma}_{\mathrm{SRD}_n})$ denote the maximum end-to-end SNR where $\hat{\gamma}_{\mathrm{SRD}_i}$s are independent and identically distributed and $n \in \mathbb{Z}^+$. Then, the distribution of $\bar{\gamma}$, $\mathcal{F}_n$ converges to reduced type 1 asymptotic distribution, $F_1(k)$*

*given as*

$$\mathcal{F}_n(a_n k + b_n) = e^{(-e)^{(-k)}}, \iota \tag{5.36}$$

*where*

$$a_n = \iota_n \sigma e^{\hat{\mu}_{\mathrm{SRD}} + \kappa_n \hat{\sigma}_{\mathrm{SRD}}} \tag{5.37}$$

*and*

$$b_n = e^{\hat{\mu}_{\mathrm{SRD}} + \kappa_n \hat{\sigma}_{\mathrm{SRD}}}, \tag{5.38}$$

*with* $\kappa_n = \frac{2\iota_n^2 - (2\log \iota_n - \log 2 + \log 4\pi)}{2\iota_n}$ *and* $\iota_n = \sqrt{2\log n}$.

*Proof.* The proof of this proposition follows from Proposition 5.1 where it was proved that $\bar{\gamma}$ follows lognormal distribution. The distribution of $\bar{\gamma}$, $\mathcal{F}_n(k)$ belongs to the domain of attraction of the limiting distribution, if it results in one limiting distribution for extreme. The limit law for $\mathcal{F}_n(a_n k + b_n)$ when $\mathcal{F}(n)$ has the lognormal law is $F_1(k)$. This can be verified by ascertaining that the Von-Mises criterion is satisfied. The Von-Mises condition [104, 105] associated with the quantity $\bar{\gamma} = \max(\hat{\gamma}_{\mathrm{SRD}_1}, \hat{\gamma}_{\mathrm{SRD}_2}, \ldots, \hat{\gamma}_{\mathrm{SRD}_n})$ requires that

$$\lim_{k\to\infty} \frac{d}{dk}\left[\frac{1 - F_{\hat{\gamma}_{\mathrm{SRD}}}(k)}{f_{\hat{\gamma}_{\mathrm{SRD}}}(k)}\right] = 0, \tag{5.39}$$

which indicates that $\bar{\gamma}$ follows a Gumbel Distribution. Similarly, our result follows from [106], where it was also verified that the limit law for a distribution function when it follows lognormal law is of type $F_1(k)$. The derivation of parameters $a_n$ and $b_n$ are given in Appendix 5.A. □

### 5.4.2 Best relay selection based on least path loss

The motivation behind the use of best and random relay selection is to study the trade-off between performance and complexity of relay selection techniques in mmWave networks. The active relays which can participate in the communication are the ones that are minimally affected by blockages. Such a relay with the least path loss can be considered to be the best relay.

**Proposition 5.4.** *In a relay aided mmWave network, the SNR distribution for the best relay can be given as*

$$F_{\gamma_{best}}(t) = \exp\left( - \sum_{i \in \mathrm{L,N}} \frac{p_i}{\alpha_i} 2\pi\lambda \left( \frac{P(G^{\max})^2}{N_0} \right)^{\frac{2}{\alpha_i}} \times \int_t^{\infty} y^{\frac{-2}{\alpha_i}-1} \Xi_{\left(\frac{2}{\alpha_i}\right)}(y/r_d) \mathrm{dy} \right), \tag{5.40}$$

*where* $\Xi_j(y) = \exp(\sigma^2 j^2/2 + \mu j) Q\left(-\frac{\sigma^2 - \log(y) + \mu}{\sigma}\right)$ *is the* $j$*-th truncated moment of* $\mathcal{X}$*.*

*Proof.* The proof is given in Appendix 5.B. □

Hence, using the above proposition, we select the best relay from a set of active relays which are obtained as stated in section 5.3. At this point it is worthwhile to mention that compared to the decode and forward relaying technique, the amplify and forward relaying may amplify the noise as well. Considering a NLOS condition (dense blockage environment), best relay scheme may not be suitable in amplify and forward systems as it will select the best among the worst channels and amplify the noise. In such a condition, decode and forward relay is advantageous over amplify and forward although it has higher complexity.

## 5.5 Coverage Probability and Transmission Capacity

The relays which are located at larger distances can suffer from large path loss and incur high maintenance costs. Thus, the relay selection method should be carefully designed in order to achieve higher coverage rates. In this section, we analyze the performance of our system based on two performance metrics, namely coverage probability and transmission capacity. The coverage probability is defined as the probability that the destination is able to receive a signal with some threshold SNR $T$, i.e., $P_c = \mathbb{P}[\gamma > T]$. That is, the probability of coverage is the complementary cumulative distribution function (CCDF) of the SNRs over the network. On the other hand, the transmission capacity of a network can be defined as the achievable rate of successful transmission per unit area, given the constraints of certain connection outage. This metric is of interest since the characterization of the capacity of every individual active link in a large random network is impractical. Mathematically, the transmission capacity of a

***Table 5.1:*** *Simulation Parameters*

| Notation | Parameter | Values |
|---|---|---|
| $r_d$ | Radius of the bounded region | 200 meters |
| $\lambda_s$ | Density of source nodes | 0.001 |
| $p_{LOS}$ | LOS probability | 0.12 |
| $G_{\max}$ | Antenna Gain | 18dB |
| $\alpha$ | Path loss exponent | LOS-2, NLOS-4 |
| $P$ | Node transmit power | 1 Watt |
| $N_0$ | Noise power | Thermal noise + 10dB noise figure. |
| $r_{\mathrm{SD}}$ | Link distance | 35 meter |

relay aided system is defined as

$$\tau = (\lambda_{\mathrm{R}} + \lambda_{\mathrm{S}})\mathcal{R}(1 - \mathbb{P}(\gamma > T)), \tag{5.41}$$

where $\mathcal{R}$ is the rate of a random end-to-end link defined as

$$\mathcal{R} = \log_2(1 + T), \tag{5.42}$$

where $T$ is the minimum threshold SNR. $\mathbb{P}(\gamma > T)$ follows from Proposition 5.3 and Proposition 5.4 depending on the relay selection scheme. However, for the case of decode and forward technique, the average rate, $\mathcal{R}$ is calculated as in [84].

## 5.6 Numerical Results

In this section, we validate the system model and also verify the results mentioned in the propositions. In general, the computations are done through Monte Carlo simulations which is then used to validate the analytical results[11].

We consider the mmWave bandwidth of 2 GHz and carrier frequency 73 GHz. Unless stated otherwise, most of the values of the parameters used are inspired from literature mentioned in the references [18, 17]. For the system guidelines, we mention these parameters and their corresponding values in Table 5.1.

Fig. 5.3 shows the variation of the active number of relays with respect to the

[11]The parameters considered for simulation in this chapter have been taken from recent mmWave studies [16, 20, 18].

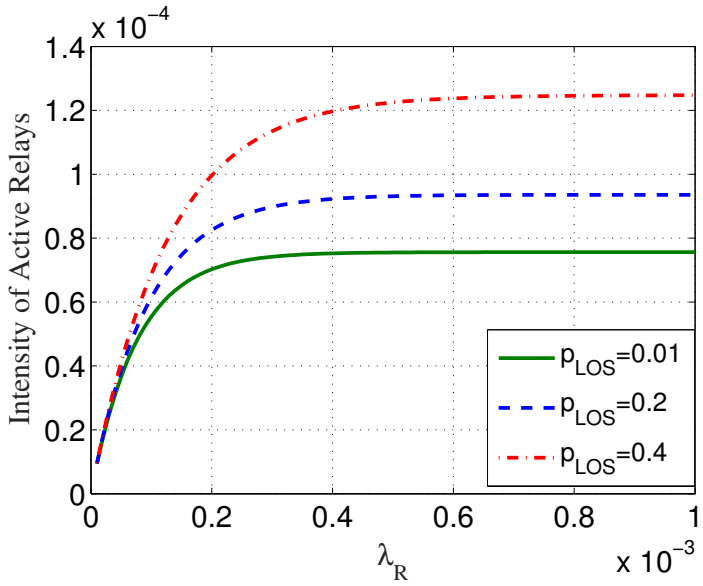


***Figure 5.3:*** *Intensity of active relays versus $\lambda_R$. The minimum required target SNR was kept at 5dB.*

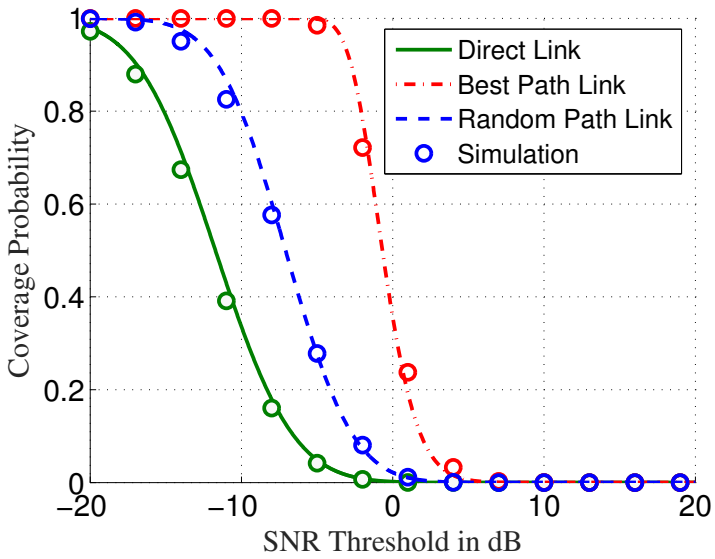


***Figure 5.4:*** *Comparison of the SNR coverage among the direct link, best path link and any random link from the source to the destination.*

intensity of the relays before thinning for different blockage outage probabilities. In order to find the active number of relays, we need to find the retaining probability which can be evaluated by (5.20). For a given blockage probability and given density of the relays, one can identify the required number of active relays in order to meet the transmission requirement in the mmWave network.

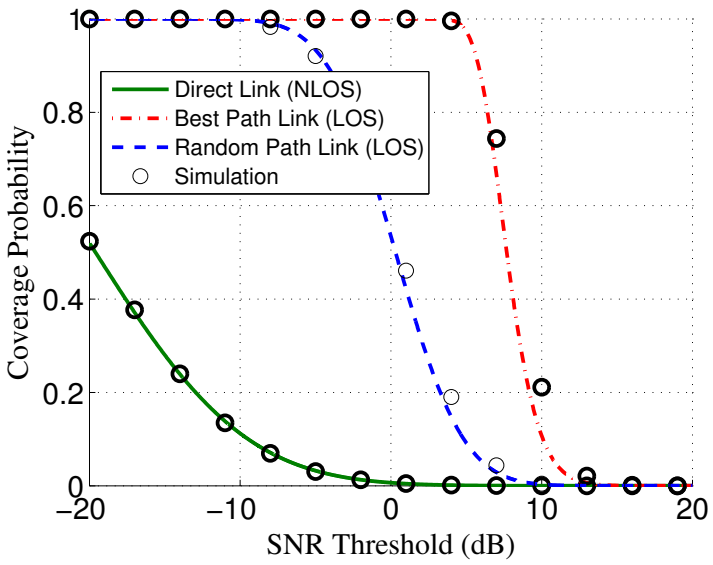


***Figure 5.5:*** *Comparison of the SNR coverage between the best path link and any random link from the source to the destination for LOS scenario.*

In Fig. 5.4 we show the comparison of the coverage probability of the SNR among three links, namely the direct link between the source and the destination, the best path link from the source to the destination through the aid of relays and any random path link which also takes relay into consideration. It is evident from the figure that relay aided transmission has a better coverage probability when compared to a direct link between a source and a destination. It can also be seen that the best end-to-end link has a better coverage probability compared to any random link. Furthermore, we would like to stress on the fact that there is a steep fall on the coverage probability due to the shadowing effects caused by blockages.

Fig. 5.5 and Fig. 5.6 show the coverage probability for LOS and NLOS relay links respectively. The LOS scenario arises when we consider that all NLOS links are completely attenuated due to blockages and vice versa. In other words the path loss exponent for such links is very large for the respective scenarios and hence these links can be ignored when calculating the coverage probability of the system. The direct link from source to destination without the aid of the relay for NLOS is shown in the figure just for the sake of comparison. It is evident from the figures that relay aided transmission has better coverage probability to a direct link between the source and destination.

In Fig. 5.7 we give insights into the coverage probability of the system in very dense networks. This figure is an attempt at validating Proposition 5.3 where we state

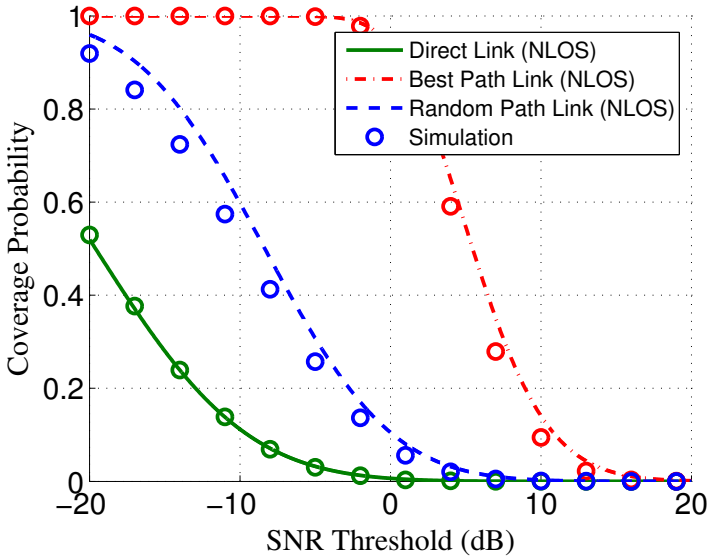


***Figure 5.6:*** *Comparison of the SNR coverage between the best path link and any random link from the source to the destination for NLOS scenario.*

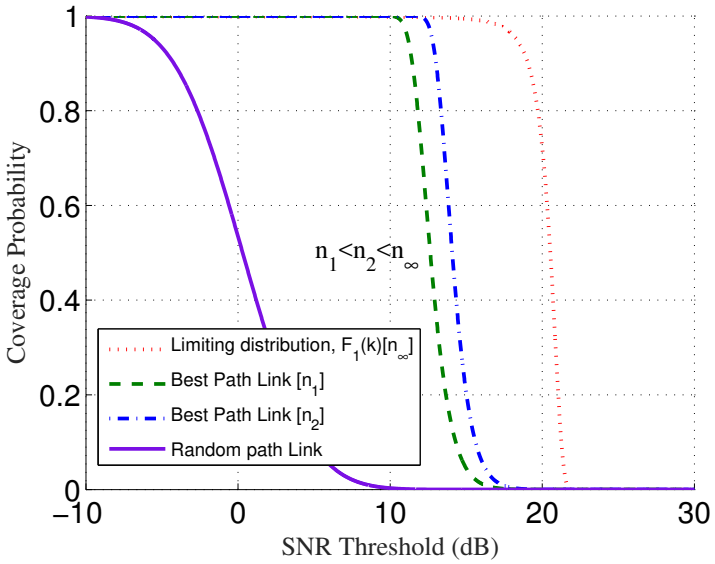


***Figure 5.7:*** *Comparison of the SNR coverage among the best path links when the number of links increase asymptotically.*

that when the number of SNR links tend to infinity the distribution tends toward the non-degenerate limiting distribution $F_1(k)$. From the figure it can be seen that as we increase the value of $n$, the curves converge towards the asymptotic curve which represents the Gumbel distribution. In the figure, $n_1$, $n_2$ and $n_\infty$ correspond to one, two and infinite number of paths respectively. Increasing $n$ can be looked upon as

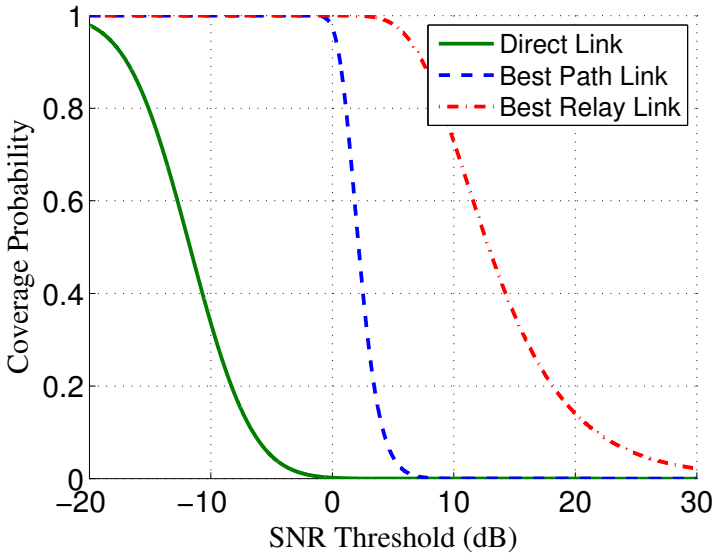


***Figure 5.8:*** *Coverage probability comparison between the direct link, the best path link and best relay link from the source to the destination.*

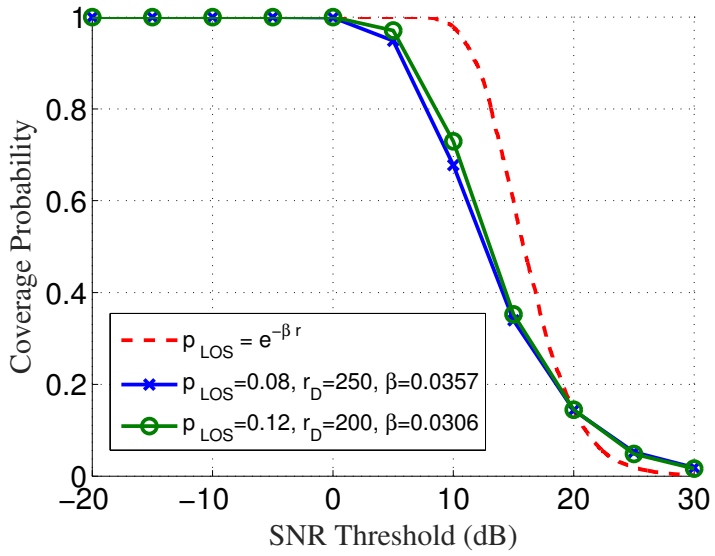


***Figure 5.9:*** *Coverage probability comparison of different blockage models under best relay strategy.*

increasing the density of the nodes which in turn increases the coverage probability of the system.

While the best path link is conditioned on the best end-to-end SNR between the source and the destination, the best relay is conditioned on the least path loss. Accordingly, Fig. 5.8 shows the trade-offs of the coverage probability of the SNR among

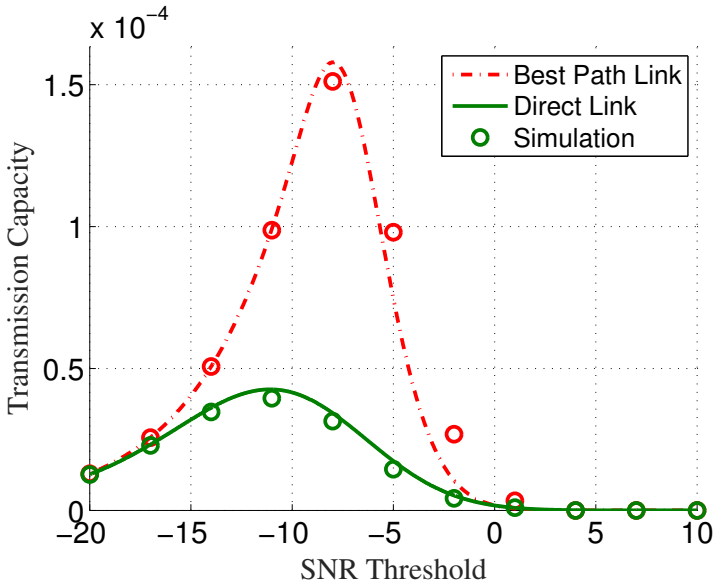


***Figure 5.10:*** *Transmission capacity comparison between the direct link and the best path link from the source to the destination generated through the aid of relays.*

three links, namely the direct link, the best path link and the best relay link. It can be seen from the figure that the best relay transmission scheme out performs the other two links. However, the best relay scheme has a high implementation complexity, since it requires high signaling overheads and channel state information from all potential relays. For systems with limited computational capabilities, the best path link is a viable option, but at the expense of reduced coverage. Furthermore, it is worth noting that the performance of the best relay is always an upper bound for the best path.

Fig. 5.9 gives the comparison between our model and a general blockage model, for e.g., the ones considered in [17, 93]. It is evident from the figure that for a given relay and blockage density, performance gap of the coverage probability considering the best relay strategy between our model (fixed $p_{\mathrm{L}}$) and the $e^{-\beta r}$ model [17] is minimal. This is comparable to the model considered in [17, 93]. We note that the adoption of step function in our analysis enables faster calculations of the coverage probability, as it simplifies expressions for the evaluation of the numerical integrals. In dense mmWave networks, the error due to such an approximation (LOS step model) is generally small and simplifies the dense network analysis. The step function approximation generally provides a lower bound of the SINR distribution corresponding to $e^{-\beta r}$ blockage model and the errors due to the approximation become smaller when the base station density increases.

Finally, in Fig. 5.10 we compare the transmission capacity between the direct link

and the best path link from the source to the destination generated through the aid of relays. In this case, we have considered the low complexity case of the best path link. The figure shows the existence of an optimal SNR threshold which depends on the operating conditions of the network. The convexity of the curve can be understood from Fig. 5.3 where it was seen that the active number of relays reach a saturation point after a certain density. Hence, it is quite obvious for the transmission capacity to reach a optimal point.

## 5.7 Summary

Blockages can be quite detrimental to the performance of outdoor mmWave networks. A possible fix for this is to go around the blockages by creating alternative propagation paths with the aid of relays. Accordingly, potential benefits of deploying relays in outdoor mmWave networks were investigated in this chapter. Coverage probability from sources to a destination aided by relays which were modeled as independent PPPs were studied. By considering blockages in a mmWave network, a relay modeling technique was given. New relay nodes from a set of relays were derived using generalized MHCPP. These active nodes are the ones that can withstand the blockage effects in the network to transfer information with less outage probability. In practical scenarios, selecting a relay from an observation (or defined) region with a small neighborhood set of relays is quite optimal. Since the computational complexity increases with the number of relays, a carefully designed region can be taken into consideration. Relay aided transmission was seen to improve the SNR by around 5dB for a specific coverage probability. Furthermore, closed form expression for end-to-end signal to noise ratio (SNR) was provided along with the computation of the best random relay path using order statistics. In very dense networks, the number of links can be quite large. To investigate such a scenario, extreme value theory was used to analyze the maximum end-to-end SNR of random relay paths. It is quite evident from our analysis that the use of relays can prevent the attenuation of the desired signal by negating the effects of blockages, which in turn also increases the coverage probability and transmission capacity of mmWave networks.

We would like to note that this chapter relies on a directional gain model for the relays to understand the impact of relay deployment and blockages in the environment on the coverage and rate performance of mmWave networks. The analytical directional gain model assumes an equivalent SISO-like system with directional antenna gains by

abstracting underlying signal level details. Accordingly, in Chapter 6 we consider a multi-user MIMO mmWave network with multiple BSs, where the BSs are equipped with very large antenna arrays. Further, while in this chapter, the fixed blockage model is considered to analyze the rate and coverage area of mmWave systems, the exponential blockage path loss model will be considered in the following chapter to characterize the propagation environment in such systems.

# Appendix 5.A Proof of Proposition 5.3

In order to evaluate the constant $a_n$ and $b_n$ we first define $\bar{\xi}_n = (\log \bar{\gamma}_n - \hat{\mu}_{\text{SRD}})\hat{\sigma}_{\text{SRD}}$, where $\hat{\mu}_{\text{SRD}}$ and $\hat{\sigma}_{\text{SRD}}$ follows from Proposition 5.1. We also define $\zeta_n = n[1 - F_{\hat{\xi}}(\hat{\xi}_n)]$, where $\hat{\xi}_i$ is a realization of $\bar{\xi}$ with $i \in \mathbb{Z}^+$ and $F_{\hat{\xi}}(\hat{\gamma}_{\text{SRD}}) = \int_{-\infty}^{\hat{\gamma}_{\text{SRD}}} (2\pi)^{\frac{-1}{2}} e^{(\frac{-\hat{\gamma}_{\text{SRD}}{}^2}{2})} \mathrm{d}\hat{\gamma}_{\text{SRD}}$. Now, we have from [107] that as $n \to \infty$, $\bar{\xi}_n = \kappa_n - \iota_n \log \zeta$, where

$$\kappa_n = \frac{2\iota_n^2 - (2\log \iota_n - \log 2 + \log 4\pi)}{2\iota_n}, \tag{5.43}$$

and

$$\iota_n = \sqrt{2\log n}. \tag{5.44}$$

Also, $\mathbb{P}\{\zeta \leq u\} = 1 - e^{-u},\ u \geq 0$. Therefore,

$$\mathbb{P}\{\bar{\xi}_n \leq \hat{\xi}\} = e^{-e^{\frac{-(\hat{\xi}-\kappa_n)}{\iota_n}}} \text{ for } \infty < \hat{\xi} < \infty. \tag{5.45}$$

Now, from the definition of $\bar{\xi}_n$ we have

$$\mathbb{P}\{\bar{\gamma}_n \leq \hat{\gamma}_{\text{SRD}}\} = e^{-\left(\hat{\gamma}^{\frac{-1}{\iota_n \hat{\sigma}_{\text{SRD}}}} e^{\left(\frac{-(\hat{\mu}_{\text{SRD}})}{\iota_n \hat{\sigma}_{\text{SRD}}} + \frac{\kappa_n}{\iota_n}\right)}\right)} \text{ for } \hat{\gamma}_{\text{SRD}} \geq 0. \tag{5.46}$$

Let $k_i$ be a realization of a new random variable $\psi_n$. Then, defining

$$\psi_n = \epsilon_n(\bar{\gamma}_n - 1), \tag{5.47}$$

where $\epsilon_n = \frac{1}{\iota_n \hat{\sigma}_{\text{SRD}}}$, we have

$$\begin{aligned} \mathbb{P}\{\psi_n < k\} &= \mathbb{P}\left\{\bar{\gamma}_n < 1 + \frac{k}{\epsilon_n}\right\} \\ &= e^{\left\{-\left(1+\frac{k}{\epsilon_n}\right)^{-\epsilon_n} e^{\left(\frac{\hat{\mu}_{\text{SRD}}}{\iota_n \hat{\sigma}_{\text{SRD}}} + \frac{\kappa_n}{\iota_n}\right)}\right\}}. \end{aligned} \tag{5.48}$$

Also, for $-\infty < k < \infty$, we have

$$\mathbb{P}\left\{\bar{\gamma}_n \leq e^{(\hat{\mu}_{\text{SRD}} + \kappa_n \hat{\sigma}_{\text{SRD}})}\left(1 + \frac{k}{\epsilon_n}\right)\right\} = e^{\left\{-\left(1+\frac{k}{\epsilon_n}\right)^{-\epsilon_n}\right\}}. \tag{5.49}$$

Now, as $n \to \infty$, $\epsilon_n \to \infty$. Therefore,

$$\lim_{n\to\infty} \mathbb{P}\left\{\bar{\gamma}_n \leq e^{\left(\frac{\hat{\mu}_{\text{SRD}}}{\iota_n \hat{\sigma}_{\text{SRD}}} + \frac{\kappa_n}{\iota_n}\right)\frac{1}{\epsilon_n}}\left(1 + \frac{k}{\epsilon_n}\right)\right\} = e^{-e^{-k}}. \tag{5.50}$$

Hence, the constants $a_n$ and $b_n$ can respectively be identified from (5.50) as

$$a_n = \iota_n \hat{\sigma}_{\text{SRD}} e^{\hat{\mu}_{\text{SRD}} + \kappa_n \hat{\sigma}_{\text{SRD}}} \tag{5.51}$$

and

$$b_n = e^{\hat{\mu}_{\text{SRD}} + \kappa_n \hat{\sigma}_{\text{SRD}}}. \tag{5.52}$$

# Appendix 5.B Proof of Proposition 5.4

Let $\Phi = \left\{x_i = \frac{P(G^{\max})^2}{N_0} r^{-\alpha_i}\right\}$ be path gain process, where $i \in \{\text{L, N}\}$. By using Mapping theorem [43], the density function under the effect of blockages can be given as

$$\lambda(x) = \sum_{i \in \text{L,N}} \frac{p_i 2\pi\lambda}{\alpha_i} \left(\frac{P(G^{\max})^2}{N_0}\right)^{\frac{2}{\alpha_i}} x^{\frac{-2}{\alpha_i}-1}. \tag{5.53}$$

Since our propagation process $\Phi$ is also effected by shadowing, using the displacement theorem [43], the updated density in bounded region can be given as

$$\hat{\lambda}(y) = \int_0^{r_d} \lambda(x)\rho(x,y)\ \mathrm{d}x, \tag{5.54}$$

where

$$\rho(x,y) \;=\; \frac{\mathrm{d}}{\mathrm{dy}}(1 - F_{\mathcal{X}_\mathcal{N}}(y/x)) = -\tfrac{1}{x} f_{\mathcal{X}_\mathcal{N}}(y/x). \tag{5.55}$$

Now, using (5.53) and (5.55), (5.54) can be evaluated as

$$\begin{aligned}
\hat{\lambda}(y) \;&=\; \sum_{i\in \mathrm{L,N}} \frac{p_i}{\alpha_i} \int_0^{r_d} 2\pi\lambda \left(\frac{P(G^{\max})^2}{N_0}\right)^{\frac{2}{\alpha_i}} x^{\frac{-2}{\alpha_i}-1} \rho(x,y)\,\mathrm{d}x \\
&=\; \sum_{i\in \mathrm{L,N}} \frac{p_i}{\alpha_i} \int_0^{r_d} 2\pi\lambda \left(\frac{P(G^{\max})^2}{N_0}\right)^{\frac{2}{\alpha_i}} x^{\frac{-2}{\alpha_i}-1} (-f_{\mathcal{X}}(y/x)\tfrac{1}{x})\ \mathrm{d}x \\
&=\; \sum_{i\in \mathrm{L,N}} \frac{p_i}{\alpha_i} \int_0^{r_d} 2\pi\lambda \left(\frac{P(G^{\max})^2}{N_0}\right)^{\frac{2}{\alpha_i}} \frac{x^{\frac{-2}{\alpha_i}}}{y} f_{\mathcal{X}}(y/x)(-\tfrac{y}{x^2})\ \mathrm{d}x \\
&\overset{(z=\frac{y}{x})}{=}\; \sum_{i\in \mathrm{L,N}} \frac{p_i}{\alpha_i} 2\pi\lambda \left(\frac{P(G^{\max})^2}{N_0}\right)^{\frac{2}{\alpha_i}} y^{\frac{-2}{\alpha_i}-1} \int_{y/r_d}^{\infty} z^{\frac{2}{\alpha_i}} f_{\mathcal{X}}(z)\,\mathrm{d}z.
\end{aligned} \tag{5.56}$$

Using the void probability of a PPP, the path gain distribution for best relay in interval of $(t,\infty)$ can thus be given as

$$\begin{aligned}
F_{\gamma_{best}}(t) \;&=\; \exp\left(-\int_t^{\infty} \hat{\lambda}(y)\mathrm{dy}\right) \\
&=\; \exp\left(-\sum_{i\in \mathrm{L,N}} \frac{p_i}{\alpha_i} 2\pi\lambda \left(\frac{P(G^{\max})^2}{N_0}\right)^{\frac{2}{\alpha_i}} \int_t^{\infty} y^{\frac{-2}{\alpha_i}-1} \int_{y/r_d}^{\infty} z^{\frac{2}{\alpha_i}} f_{\mathcal{X}}(z)\,\mathrm{d}z\mathrm{dy}\right).
\end{aligned} \tag{5.57}$$

# Chapter 6

# Millimeter Wave Systems with Massive MIMO Array

Due to the high frequencies used in millimeter wave (mmWave), the path-loss with omni-directional antennas increases with frequency. Large antenna arrays or massive multiple-input multiple-output (MIMO) arrays when utilized at one side of the link, can be used to keep the antenna aperture constant [5], which eliminates the frequency dependence of path loss relative to omnidirectional antennas. Massive MIMO arrays when utilized at both sides of the link, can also provide a net array gain to counter the larger thermal noise bandwidth.

Hence, massive MIMO technology can be considered to be an integral setup in the implementation of mmWave networks. But, the presence of spatial correlation in realistic propagation channels significantly deteriorates the system performance of MIMO communications [108]. One way to achieve high performance in a correlated environment is to separate the antennas sufficiently so that a large diversity order can be obtained. However, accommodating a large number of antennas with sufficient antenna spacing poses several constraints for practical implementation, given the limited space at the BS and at the user device. As a consequence, several compact antenna array topologies have emerged that pack the antennas intelligently to minimize the overall correlation in the MIMO channel [109]. As discussed in Chapter 4, two such antenna array configurations that have been proposed in literature are the uniform linear array (ULA) and the uniform circular array (UCA). The initial 3GPP LTE releases defined MIMO channels in the azimuth only. Accordingly, most prior work [110, 111, 112]

considered 2D cellular layouts to evaluate spatial correlation for the ULA and UCA configurations. Furthermore, the correlation in these works was investigated in the azimuth only. These works do not take into consideration the explicit relationship between the spatial correlation and the angular domain consisting of both the azimuth and the elevation dimensions. Since real world transmission channels are 3D in nature, beamforming in the azimuth dimension alone cannot fully exploit all the degrees of freedom (DOF) of the channel.

Recent results have revealed the potential of 3D beamforming to enhance system performance. Encouraged by this, 3GPP is carrying out research to develop and standardize channel models for 3D MIMO systems [113, 114]. Moreover, the absence of elevation dimension is not the only limitation of the existing correlation models. Authors in [109, 115, 116, 117] do consider the spatial correlation in 3D propagation scenarios. However, certain assumptions on the nature of the underlying angular distributions do not represent the attributes of mmWave propagation scenarios accurately. In a mmWave transmission, the spatial degrees of freedom offered by the channel depend on both the channel conditions and the number of antennas deployed. Hence, to obtain the system performance, the effects of the channel conditions and the type of antenna array have to be considered in conjunction with each other. Most recent works that study the impact of different channel conditions do not take into account the choice of the antenna array, which may affect the performance analysis. This problem is further elevated in very large MIMO systems, where a larger number of antennas are rigged in a limited space [116]. In general, the choice of the array geometry to be deployed at the BS is made based on numerous factors, such as cost, availability and compatibility of the array with the existing system. In cellular networks, the ULA is the most commonly deployed configuration. However, the ULA can scan only the 2D space. On the other hand, the UCA can take both the azimuth and the elevation angles into consideration. This makes UCA the appropriate array configuration to exploit the 3D propagation space in the true sense.

Considering the limitations of the current analysis and inspired by the stochastic geometry approach to analyze the performance of large scale MIMO systems and mmWave networks, in this chapter we consider a realistic propagation scenario of the downlink of such a system with spatially distributed BSs with UCA serving single-antenna users within a fixed coverage area of a densely built up urban environment. In particular, it is assumed that the BSs and users inside the coverage area follow two independent Poisson point processes (PPPs). We then analyze the performance of the

system based on important metrics, namely coverage probability, average rate and area spectral efficiency with respect to varying number of antennas at the BS as well as the intensity of the BSs and users within the coverage area.

In particular, we provide an analytical framework for a mmWave system by considering 3D circular antenna array at the BS, which enables us to take both the azimuth and elevation dimensions into account. Accordingly, we find the optimal beamformer in a local sense to achieve the maximum signal-to-interference-plus-noise ratio (SINR) that can be provided to a user. We then derive a closed-form expression for the SINR when the number of antennas at the UCA grows without bound. Further, to model the blockages, we carry out our analysis by incorporating the exponential blockage model. Accordingly, we derive the coverage probability of the system. We also extend our analysis for multiple BSs scenario, where a user may be associated to the nearest BS. In order to analyze the performance of our model, we begin by calculating the average rate of the system. With the help of this rate and a certain outage probability, we analyze the transmission capacity of the network. Via numerical results, we provide a detailed analysis on the effect of the number of BS antennas, blockage density, path loss coefficient, node density, and SINR threshold on a mmWave network, where BSs are equipped with very large antenna arrays.

## 6.1 Mathematical Preliminaries

In this section, we discuss and present a few important mathematical results that will be integral in deriving a few of the analytical results presented in the chapter.

**Lemma 6.1.** *The Bessel function of order zero, $J_0(x)$ can be upper bounded as*

$$|J_0(x)| \leq w x^{\frac{-1}{3}}, \tag{6.1}$$

*where $w = 0.7857$.*

**Lemma 6.2.** *The Bessel function of order one, $J_1(x)$ can be given as [118]*

$$J_1(x) = \sum_{i=0}^{\infty} \frac{(-1)^i}{i!\,\Gamma(i+2)} \left(\frac{x}{2}\right)^{(2i+1)}, \tag{6.2}$$

*where $\Gamma(.)$ is the Gamma function.*

**Lemma 6.3.** *Let an integral function $\mathcal{I}$ be denoted as*

$$\mathcal{I}(x,y) = -x \int_{\Phi_{min}}^{\Phi_{max}} \frac{J_0(y\sin(\Phi))\sin(\Phi)}{\cos^3(\Phi)} d\Phi, \tag{6.3}$$

*where $[x,y] \in \mathbb{R}^+$ and $[\Phi_{min}, \Phi_{max}] \in [\pi/2, \pi]$. Then a solution for the above integral is given as*

$$\begin{aligned}\mathcal{I}(x,y) = -\frac{x}{2}\Bigg[\frac{J_0(y\sin(\Phi_{min}))}{1-\sin^2(\Phi_{min})} - \frac{J_0(y\sin(\Phi_{max}))}{1-\sin^2(\Phi_{max})} + \sum_{i=0}^{\infty}\frac{(-1)^i}{i!\,\Gamma(i+2)}\left(\frac{y}{2}\right)^{2(i+1)} \\ \times\Bigg(-\Bigg(\log(1-\sin^2(\Phi_{min})) + \sum_{k=1}^{i}\frac{\sin^{2k}(\Phi_{min})}{k}\Bigg) + \log(1-\sin^2(\Phi_{max})) \\ + \sum_{k=1}^{i}\frac{\sin^{2k}(\Phi_{max})}{k}\Bigg)\Bigg],\end{aligned} \tag{6.4}$$

where $J_0(x)$ the Bessel function of order zero.

*Proof.* The proof is given in Appendix 6.A. □

## 6.2 System Model

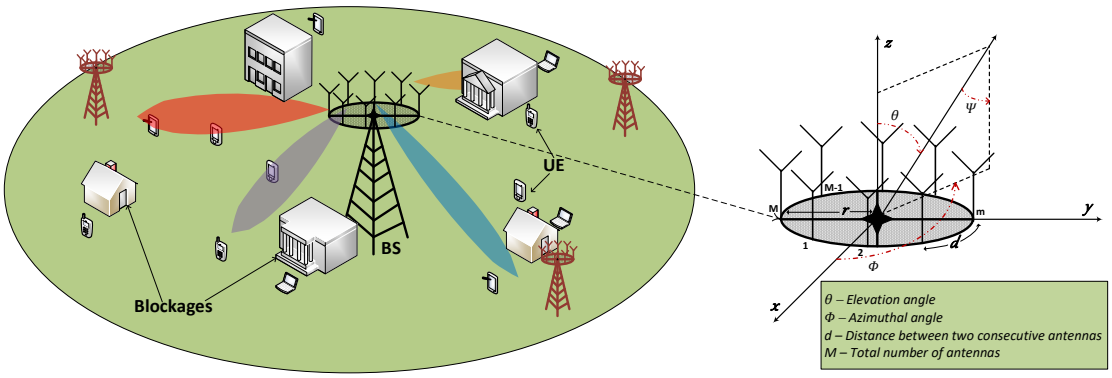


***Figure 6.1:*** *An illustration of an outdoor mmWave cellular network with 3D circular antenna array.*

In this section, we illustrate our system model of an outdoor mmWave network, where the base station (BS) is equipped with a large antenna array configured as UCA. In particular, for analytical tractability, we begin the analysis for a single BS setup, which

***Table 6.1:*** *Notations*

| Notation | Description |
|---|---|
| $r_c$ | Radius of the circular coverage area |
| $r_h$ | Minimum distance between BS and user |
| $r_k$ | Distance from the $k$th user to the BS |
| $h$ | Height of the BS |
| $M$ | Number of antennas in the UCA |
| $\theta$ | Elevation angle |
| $\phi$ | Azimuthal angle |
| $d$ | Distance between two consecutive antennas |
| $\Phi_{\text{BS}}$ | PPP of BS |
| $\lambda_{\text{BS}}$ | Density of BS |
| $\Phi_{\text{U}}$ | PPP of users |
| $\lambda_{\text{U}}$ | Density of users |
| $\alpha$ | Path loss exponent |
| $m$ | Nakagami fading parameter |

will then be extended to multiple BSs setup in Section 6.4 and thereafter. We consider the downlink of this system, as shown in Fig. 6.1, where the BS is equipped with $M$ antennas transmitting simultaneously to spatially distributed single antenna users. The users in this network are modeled as points of a uniform PPP, denoted by $\Phi_{\text{U}}$, with density $\lambda_{\text{U}}$ in $\mathbb{R}^2$. Let, $\mathcal{K}$ be the set of all users in $\Phi_{\text{U}}$, which are connected at the same time to the BS[1] in consideration. Also, let the cardinality of $\mathcal{K}$ be $K$. The number of users connected at a particular time is given as $K = \min(U_{max}, N)$, where $U_{max}$ is the maximum number of users that can be scheduled in a time slot and $N$ is the total number of users connected to the BS. Further specifications regarding the model are presented in Table 6.1. Moreover, in mmWave signal propagation, signal corruption is mainly caused by small scale fading, shadowing and blockages. The modeling of these effects are discussed in details in the following subsections.

### 6.2.1 Channel modeling

Let $\mathbf{w}_k$ represents the semi-correlated frequency-flat channel vector between the BS and the $k$th user. Then, $\mathbf{w}_k$ can be modeled as $\mathbf{w}_k = \sqrt{\Xi_k^{\iota}}\eta_k\mathbf{h}_k$, where $\mathbf{h}_k$ models the small scale fading channel vector between the BS and the $k$th user, $\eta$ denotes

[1]As of now, we do not give any index for the BS. However, later in the chapter, for the multiple BS scenario, this will be considered as the $l$ th BS, with $\Phi_{\text{BS}}$ being the BS process.

the complex gain, which is assumed to follow Nakagami fading, and is modeled as $\eta \sim f_\eta(t;m) \triangleq \frac{m^m t^{m-1} e^{-mt}}{\Gamma(m)}$. Here, $m$ is the Nakagami fading parameter with $\Gamma(m)$ being the upper incomplete Gamma function and $\Xi_k^\iota$ models the path loss attenuation given as

$$\Xi_k^\iota = \frac{1}{(r_k/r_h)^{\alpha_\iota}}. \tag{6.5}$$

Here, $\alpha_\iota$, with $\iota \in \{\mathrm{L}, \mathrm{N}\}$ is the path loss exponent, where 2 denotes a free space propagation and 4 a relatively lossy environment. L here refers to a line of sight (LOS) link while N refers to a non line of sight (NLOS) link.

We assume the antenna array at the BS to be UCA. The advantage of using a UCA is that it can exploit the real life 3D propagation space. As shown in Fig. 6.1, the BS with UCA configuration consists of $M$ antennas placed uniformly in a circular array configuration with radius $r$, angle of elevation $\theta$ and angle of azimuth $\phi$. Then without loss of generality, the channel vector, $\mathbf{h}_k$ for the $k$th user can be given as

$$\mathbf{h}_k = \left[1, e^{j\frac{2\pi}{\lambda} r \sin\theta_k \cos(\phi_k - \bar{\phi}_1)}, \ldots, e^{j\frac{2\pi}{\lambda} r(M-1)\sin\theta_k \cos(\phi_k - \bar{\phi}_{M-1})}\right]^T. \tag{6.6}$$

Here, $\bar{\phi}_m = \frac{2m\pi}{M}$ is the angle between the $m$th antenna element and the $y$ axis of the array.

Now, in order to model the distribution of the angle of departures (AoDs) for a UCA, we need the distributions of both the azimuth and elevation angles. Since the BS array is deployed at a certain height from the ground and the users are randomly located on a circle, the azimuth angles are uniformly distributed within the interval $[0, 2\pi]$.

**Lemma 6.4.** *The pdf of the azimuth angles $\phi_{k_{\forall k=\{1,\ldots,K\}}}$ for a UCA, when the users are uniformly distributed within a circular coverage area can be given as*

$$f_\phi = \frac{1}{2\pi}. \tag{6.7}$$

However, unlike the azimuth angles, the PDF of the elevation angles $\phi_{k_{\forall k=\{1,\ldots,K\}}}$ does not follow a uniform distribution and can be given by the following lemma.

**Lemma 6.5.** *The PDF of the elevation angles $\theta_{k_{\forall k=\{1,\ldots,K\}}}$ for a UCA, when the users*

*are uniformly distributed within a circular coverage area can be given as*

$$f_\theta = \begin{cases} -\frac{2h^2}{(r_c^2 - r_h^2)} \frac{\sin(\theta_k)}{\cos^3(\theta_k)}, & \theta_{min} \leq \theta_k \leq \theta_{max} \\ 0 & otherwise, \end{cases} \tag{6.8}$$

*where* $\theta_{min} = \frac{\pi}{2} + \tan^{-1} \frac{h}{r_c}$, $\theta_{max} = \frac{\pi}{2} + \tan^{-1} \frac{h}{r_h}$.

*Proof.* The proof is given in Appendix 6.B. □

### 6.2.2 Blockage modeling

In Chapter 5, we considered the fixed blockage probability model to analyze the mmWave network. Another blockage model that has been extensively considered in literature is the PPP based random blockage model. Let the LOS link be of length $x$, then the probabilities of occurrence for LOS and NLOS can be denoted as $p_{\mathrm{L}}(x)$ and $p_{\mathrm{N}}(x) = 1 - p_{\mathrm{L}}(x)$ respectively. The probability function for LOS in the network can be derived from field measurements as was given in [20] or stochastic blockage models in [91, 119], where the blockage parameters are characterized by some random distributions. Essentially, when the blockages are modeled as a rectangle boolean scheme, the probabilities of LOS and NLOS links can respectively be given as a function of $x$ as

$$p_{\mathrm{L}}(x) = e^{-\beta x}, \quad p_{\mathrm{N}}(x) = 1 - e^{-\beta x}, \tag{6.9}$$

where $\beta$ is the blockage density.

### 6.2.3 Performance metrics

Three important metrics, namely coverage probability, average rate and the area spectral efficiency of the mmWave network will be studied. Due to the impact of blockages, these parameters tend to be of paramount importance in the characterization of mmWave systems. Furthermore, these metrics have received considerable attention during the last decade in the analysis of cellular networks. Accordingly, while the coverage probability is the probability that a typical user receives a specific fixed signal to interference plus noise ratio, the area spectral efficiency of a network can be defined as the maximum achievable average data rate per unit bandwidth per unit area, given the constraints of certain connection outage. Accordingly, in order to characterize the

area spectral efficiency, one needs to calculate the average/expected rate. While rate coverage probability has been studied in recent literature [17, 93], average rate has not yet been properly evaluated in stochastic geometry related mmWave literature. Finding a closed-form expression becomes very challenging when we consider other uncertainties such as blockages, interference and shadowing. Recent papers [120, 121] use a two-step methodological approach to compute the average rate: i) first, the coverage probability is computed; and ii) then, the average rate is obtained by integrating the coverage probability over the positive real axis. Accordingly, for general fading channels, a four-fold integral needs to be computed. To overcome this limitation, authors in [122, 123] propose a new analytical framework, which reduces the number of integrals and is also flexible enough for application to arbitrary fading distributions. Therefore, in this chapter, leveraging the analysis from [123], we give a generalized expression to evaluate the average rate in terms of MGFs as

$$\mathbb{E}[R] = \int_0^\infty (1 - \mathcal{L}_S(z))\mathcal{L}_\mathcal{I}(z)\frac{e^{-z}}{z}\,\mathrm{dz}, \tag{6.10}$$

where $R$ is the instantaneous rate and $\mathcal{L}_X(z) = \mathbb{E}[e^{-zX}]$.

## 6.3 Signal to Interference plus Noise Ratio (SINR)

The BS transmits data streams simultaneously to all the connected $K$ users which creates an interfering broadcast channel. To encounter its effect we use a $M \times K$ beamforming matrix at the BS denoted by $\mathbf{T}$. The signal received by the user at $k \in \mathcal{K}$ can be given as

$$y_k = \underbrace{\sqrt{\rho_k}\,\mathbf{w}_k^H \mathbf{t}_k s_k}_{\text{desired signal}} + \underbrace{\sum_{i\in\mathcal{K}, i\neq k} \sqrt{\rho_i}\mathbf{w}_k^H \mathbf{t}_i s_i}_{\text{interference}} + \underbrace{z_k}_{\text{noise}}, \tag{6.11}$$

where $\mathbf{s} = [s_1, \ldots, s_k, \ldots, \ldots s_K] \in \mathbb{C}^{M\times 1}$ is the symbol transmitted by $M$ antennas, $\rho_k \subseteq [\rho_1, \ldots \rho_k, \ldots, \rho_K]$ is the transmitted power corresponding to the $k$th user, $z_k$ is the complex circular symmetric Gaussian noise with zero mean and a variance of $\sigma^2$, which is associated with the $k$th user and $\mathbf{t}_k$ is the vector of the beamforming matrix associated with the $k$th user. Now, assuming the channel to be ergodic, the SINR at

the $k$th user can be given as

$$\begin{aligned}\gamma_k &= \frac{\rho_k|\mathbf{w}_k^H\mathbf{t}_k|^2}{\sum\limits_{i\in\mathcal{K},i\neq k}\rho_i|\mathbf{w}_k{}^H\mathbf{t}_i|^2+\ \sigma^2}, \\ &= \frac{\frac{\rho_k}{M}\Xi_k^\iota\eta_k^2\,|\mathbf{h}_k^H\mathbf{t}_k|^2}{\sum\limits_{i\in\mathcal{K},i\neq k}\frac{\rho_i}{M}\Xi_i^\iota\eta_i^2|\mathbf{h}_k{}^H\mathbf{t}_i|^2+\ \frac{\sigma^2}{M}},\ \forall\iota\in\{\mathrm{L},\mathrm{N}\}.\end{aligned} \tag{6.12}$$

Our aim now is to design the precoders/beamformers that maximize the received SINR on each of the BS-UE links. Accordingly, for the case of fixed antenna spacing $d$, in order to achieve the maximum SINR, we explore over the asymptotic regime when $M\to\infty$ by finding the optimal beamforming vector $\mathbf{t}_k^*$.

**Lemma 6.6.** *In UCA, when $M\to\infty$, radius of the circular array $r\sim\frac{Md}{2\pi}$ [124].*

**Proposition 6.1.** *Assume perfect CSI at the BS and the users, and fixed antenna spacing. Now, when $M$ grows without bound, then the first negative moment of the maximum SINR for the $k$th user in a mmWave network can be given as*

$$\mathbb{E}[\gamma_k^{-1}]=\frac{(K-1)\,\Psi_k\sum\limits_{i\in\mathcal{K},i\neq k}\rho_i\Xi_i^\iota\eta_i^2+\ \sigma^2}{\rho_k\Xi_k^\iota\eta_k^2M},\ \forall\iota\in\{\mathrm{L},\mathrm{N}\}, \tag{6.13}$$

*where*

$$\begin{aligned}\Psi_k = 1+\frac{2}{M}\sum_{t=1}^{M-1}(M-t)\left(\frac{2h^2}{2(r_c^2-r_h^2)}\right)^2\Bigg[&\frac{J_0(\frac{2^{\frac{3}{2}}\pi}{\lambda}r\sqrt{1-\cos\left(\frac{2\pi t}{M}\right)}\sin(\theta_{min}))}{1-\sin^2(\theta_{min})} \\ -&\frac{J_0(\frac{2^{\frac{3}{2}}\pi}{\lambda}r\sqrt{1-\cos\left(\frac{2\pi t}{M}\right)}\sin(\theta_{max}))}{1-\sin^2(\theta_{max})}+\sum_{i=0}^{\infty}\frac{(-1)^i}{i!\,\Gamma(i+2)}\left(\frac{\frac{2^{\frac{3}{2}}\pi}{\lambda}r\sqrt{1-\cos\left(\frac{2\pi t}{M}\right)}}{2}\right)^{2(i+1)} \\ &\left(-\left(\log(1-\sin^2(\theta_{min}))+\sum_{l=1}^{i}\frac{\sin^{2k}(\theta_{min})}{l}\right)+\left(\log(1-\sin^2(\theta_{max}))+\sum_{l=1}^{i}\frac{\sin^{2k}(\theta_{max})}{l}\right)\right)\Bigg]^2.\end{aligned} \tag{6.14}$$

*Proof.* In order to prove this proposition, we split it into two parts. First, we maximize the SINR $\gamma_k$ in (6.12). Then, we calculate the expectation of $\gamma_k^{-1}$ to obtain (6.13). In order to maximize $\gamma_k$ in (6.12), we have to maximize the numerator and minimize the

denominator. Using the Rayleigh quotient law, $|\mathbf{h}_k^H \mathbf{t}_k|^2$ can be bounded as [13]

$$|\mathbf{h}_k^H \mathbf{t}_k|^2 \;\leq\; \lambda_{max}(\mathbf{h}_k \mathbf{h}_k^H) = M. \tag{6.15}$$

The above inequality holds only when $\mathbf{t}_k$ is an eigenvector of $|\mathbf{h}_k \mathbf{h}_k^H|$ corresponding to the maximum eigenvalue $\lambda_{max}$. In other words,

$$\mathbf{t}_k = \frac{\mathbf{h}_k}{||\mathbf{h}_k||}. \tag{6.16}$$

Furthermore, the denominator in (6.12) can be minimized if

$$\frac{|\mathbf{h}_k^H \mathbf{t}_i|}{\sqrt{M}} \to 0. \tag{6.17}$$

For the case of UCA at the BS, we have

$$\frac{|\mathbf{h}_k^H \mathbf{t}_i|}{\sqrt{M}} = \frac{1}{M} \left| \sum_{m=0}^{M-1} e^{j\frac{2\pi}{\lambda} r\left(\delta_1 \cos(\frac{2\pi m}{M}) + \delta_2 \sin(\frac{2\pi m}{M})\right)} \right|, \tag{6.18}$$

where, $\delta_1 \triangleq \sin\theta_k \cos\phi_k - \sin\theta_j \cos\phi_j$ and $\delta_2 \triangleq \sin\theta_k \sin\phi_k - \sin\theta_j \sin\phi_j$. When the number of antennas at the BS grows without bound, the integral in (6.18) tends to a finite integral can be expressed as

$$\frac{|\mathbf{h}_k^H \mathbf{t}_i|}{\sqrt{M}} \to \left| \frac{1}{2\pi} \int_0^{2\pi} e^{j\frac{2\pi}{\lambda} r(\delta_1 \cos x + \delta_2 \sin x)} dx \right|. \tag{6.19}$$

Now, using ([53], Eq. (3.338.4)), the above integral can be analytically solved and when $M \to \infty$, we have

$$\lim_{M\to\infty} \frac{|\mathbf{h}_k^H \mathbf{t}_i|}{\sqrt{M}} \to \lim_{M\to\infty} \left| J_0\left(\frac{2\pi}{\lambda} r \sqrt{\delta_1^2 + \delta_2^2}\right) \right|. \tag{6.20}$$

With fixed antenna spacing $d$, when $r \to \infty$, the right hand side of (6.20) equals to zero, which validates (6.17). However, for a fixed total physical space at the BS (fixed $r$), increasing $M$ will lead to the decrease in $d$. Accordingly, the RHS of (6.20) converges to a constant non-zero limit. Hence, the optimal beamforming vector that maximizes the SINR as $M \to \infty$ can be given as

$$\mathbf{t}_k^* = \frac{\mathbf{h_k}}{\sqrt{M}}. \tag{6.21}$$

The SINR for the $k$th user can now be given as

$$\gamma_k = \frac{\rho_k \Xi_k^{\iota} \eta_k^2 M}{\sum\limits_{i \in \mathcal{K}, i \neq k} \rho_i \Xi_i^{\iota} \eta_i^2 \left| \frac{\mathbf{h}_k{}^H \mathbf{h}_i}{\sqrt{M}} \right|^2 + \sigma^2}, \ \forall \iota \in \{\mathrm{L}, \mathrm{N}\}. \tag{6.22}$$

In order to calculate the first negative moment of the SINR, the expectation should be taken over the channel vectors, which is related to the azimuth and elevation AoDs of all the users. Accordingly, the first negative moment of the maximum SINR for the $k$th user can be given as

$$\begin{aligned} \mathbb{E}[\gamma_k^{-1}] &= \mathbb{E}\left\{ \frac{\frac{1}{M} \sum\limits_{i \in \mathcal{K}, i \neq k} \rho_i \Xi_i^{\iota} \eta_i^2 \left| \mathbf{h}_k{}^H \mathbf{h}_i \right|^2 + \sigma^2}{\rho_k \Xi_k^{\iota} \eta_k^2 M} \right\}, \\ &= \left\{ \frac{1}{M} \sum_{i \in \mathcal{K}, i \neq k} \rho_i \Xi_i^{\iota} \eta_i^2 \mathbb{E}\left\{ |\mathbf{h}_k{}^H \mathbf{h}_i|^2 \right\} + \sigma^2 \right\} \frac{1}{\rho_k \Xi_k^{\iota} \eta_k^2 M}, \ \forall \iota \in \{\mathrm{L}, \mathrm{N}\}. \end{aligned} \tag{6.23}$$

Let $\Psi_k \triangleq \frac{1}{M} \mathbb{E}\left\{ |\mathbf{h}_k{}^H \mathbf{h}_i|^2 \right\}$. Therefore, using (6.6), we have

$$\begin{aligned} \Psi_k &= \frac{1}{M} \mathbb{E}\left\{ \left| \sum_{m=1}^{M} e^{j \frac{2\pi}{\lambda} r\left( \delta_1 \cos(\frac{2\pi m}{M}) + \delta_2 \sin(\frac{2\pi m}{M}) \right)} \right|^2 \right\}, \\ &= \frac{1}{M} \mathbb{E}\left\{ \sum_{n=1}^{M} \sum_{m=1}^{M} e^{j \frac{2\pi}{\lambda} r\left( \delta_1 \cos(\frac{2\pi n}{M}) + \delta_2 \sin(\frac{2\pi n}{M}) \right)} e^{-j \frac{2\pi}{\lambda} r\left( \delta_1 \cos(\frac{2\pi m}{M}) + \delta_2 \sin(\frac{2\pi m}{M}) \right)} \right\}, \\ &= \frac{1}{M} \mathbb{E}\left\{ \sum_{n=1}^{M} \sum_{m=1}^{M} e^{j \frac{2\pi}{\lambda} r\left( \delta_1 \cos(\frac{2\pi n}{M}) + \delta_2 \sin(\frac{2\pi n}{M}) - \delta_1 \cos(\frac{2\pi m}{M}) - \delta_2 \sin(\frac{2\pi m}{M}) \right)} \right\}, \\ &= \frac{1}{M} \mathbb{E}\left\{ \sum_{n=1}^{M} \sum_{m=1}^{M} e^{j \frac{2\pi}{\lambda} r\left( \delta_1 (\cos(\frac{2\pi n}{M}) - \cos(\frac{2\pi m}{M})) - \delta_2 (\sin(\frac{2\pi m}{M}) - \sin(\frac{2\pi n}{M})) \right)} \right\}, \\ &= \frac{1}{M} \mathbb{E}\left\{ \sum_{n=1}^{M} \sum_{m=1}^{M} e^{j \frac{2\pi}{\lambda} r\left( \delta_1 \bar{a} - \delta_2 \bar{b} \right)} \right\}. \end{aligned} \tag{6.24}$$

Here, $\bar{a} = \cos(\frac{2\pi n}{M}) - \cos(\frac{2\pi m}{M})$ and $\bar{b} = \sin(\frac{2\pi m}{M}) - \sin(\frac{2\pi n}{M})$. Now substituting $\delta_1 \triangleq \sin\theta_k \cos\phi_k - \sin\theta_j \cos\phi_j$ and $\delta_2 \triangleq \sin\theta_k \sin\phi_k - \sin\theta_j \sin\phi_j$, we have

$$\Psi_k = \frac{1}{M} \sum_{n=1}^{M} \sum_{m=1}^{M} \underbrace{\mathbb{E}\left\{ e^{j \frac{2\pi}{\lambda} r(\bar{a} \sin\theta_k \cos\phi_k + \bar{b} \sin\theta_k \sin\phi_k)} \right\}}_{E_1} \underbrace{\mathbb{E}\left\{ e^{-j \frac{2\pi}{\lambda} r(\bar{a} \sin\theta_j \cos\phi_j + \bar{b} \sin\theta_j \sin\phi_j)} \right\}}_{E_2}. \tag{6.25}$$

Let $a = \bar{a}\sin\theta_k$ and $b = \bar{b}\sin\theta_k$. Therefore,

$$\begin{aligned} E_1 &= \mathbb{E}\left\{e^{j\frac{2\pi}{\lambda}r\sqrt{a^2+b^2}(\cos(A)\cos\phi_k+\sin A\sin\phi_k)}\right\} \\ &= \int_{\theta_{min}}^{\theta_{max}}\int_0^{2\pi} e^{j\frac{2\pi}{\lambda}r\sqrt{a^2+b^2}\cos(\phi_k-A)} f_\phi(\phi_k) f_\theta(\theta_k) d\phi_k d\theta_k. \end{aligned} \tag{6.26}$$

This integral can now be solved in two parts. Solving for the inner integral first, the detailed mathematical steps of which are deferred to Appendix 6.C, we have

$$E_1 = -\frac{2h^2}{r_c^2 - r_h^2}\int_{\theta_{min}}^{\theta_{max}} J_0\left(\zeta\sin(\theta_k)\right)\frac{\sin(\theta_k)}{\cos^3(\theta_k)}d\theta_k, \tag{6.27}$$

where $\zeta = \frac{2^{\frac{3}{2}}\pi}{\lambda}r\sqrt{1-\cos\left(\frac{2\pi(n-m)}{M}\right)}$. Now, rewriting the summations in (6.25) using $t = n - m$ and using (6.27), $\Psi_k$ can be rewritten as

$$\begin{aligned} \Psi_k &= -\frac{2h^2}{M(r_c^2 - r_h^2)}\sum_{t=-(M-1)}^{M-1}(M-|t|)\left[\int_{\theta_{min}}^{\theta_{max}} J_0\left(\zeta\sin(\theta_k)\right)\frac{\sin(\theta_k)}{\cos^3(\theta_k)}d\theta_k\right]^2, \\ &\overset{(a)}{=} -\frac{2h^2}{M(r_c^2 - r_h^2)}\left\{M + 2\sum_{t=1}^{M-1}(M-t)\left[\int_{\theta_{min}}^{\theta_{max}} J_0\left(\zeta\sin(\theta_k)\right)\frac{\sin(\theta_k)}{\cos^3(\theta_k)}d\theta_k\right]^2\right\}, \end{aligned} \tag{6.28}$$

where $\bar{\zeta} = \frac{2^{\frac{3}{2}}\pi}{\lambda}r\sqrt{1-\cos\left(\frac{2\pi t}{M}\right)}$ and $(a)$ is obtained by putting $J_0(0) = 1$. Now, let

$$x = \frac{2h^2}{r_c^2 - r_h^2} \text{ and } y = \frac{2^{\frac{3}{2}}\pi}{\lambda}r\sqrt{1-\cos\left(\frac{2\pi t}{M}\right)}. \tag{6.29}$$

Therefore, comparing (6.29) with Lemma 6.3, the integral in (6.28) can be evaluated, which further leads to the solution of $\Psi_k$ as given in (6.14). Now, substituting the value of $\Psi_k$ in (6.23), we obtain the proof of Proposition 6.1. □

Accordingly, the downlink SINR for the user $k \in \mathcal{K}$ when the number of antennas at the BS for a UCA grows very large, can be given as

$$\gamma_k = \{\mathbb{E}[\gamma_k^{-1}]\}^{-1} = \frac{\rho_k \Xi_k^\iota \eta_k^2 M}{(K-1)\,\Psi_k \sum\limits_{i\in\mathcal{K}, i\neq k}\rho_i \Xi_i^\iota \eta_i^2 + \sigma^2}, \ \forall \iota \in \{\mathrm{L}, \mathrm{N}\}. \tag{6.30}$$

However, as discussed before, mmWave networks are often affected by blockages. Hence, it may not be possible to provide the user $k \in \mathcal{K}$ with the SINR in (6.30).

In the following section, the effect of blockages on this system will be analyzed with respect to various performance metrics.

**Remark 6.1.** *The asymptotically optimal beamforming vector* $\mathbf{t}_k^*$ *in* (6.21) *for the ULA is an approach similar to the MRT scheme. When* $M$ *becomes very large, the channel response vectors between different users are asymptotically orthogonal to each other resulting in the suppression of the interference between different users. Then, the SINR achieves its maximum value. Though many other optimal schemes have been proposed in literature for MIMO networks, this can at least be considered to be one of the low-complexity optimal schemes in local sense, when the number of BS antennas in a UCA grows without bound.*

## 6.4 SINR Distribution

In this section, we derive the SINR distribution for a single BS scenario as well as multiple BSs scenario. We begin by characterizing the overall complimentary cumulative distribution function (CCDF) of the SINR $\gamma_k$, when the desired link is either LOS or NLOS. Next we extend the analysis for multiple BSs scenario by incorporating interference from other BSs followed by the characterization of the SINR for this scenario.

### 6.4.1 Single BS scenario

We begin by analyzing the coverage probability for the current set up, where a single BS serves the spatially distributed users within the circular coverage area. Let $T$ be the target SINR. The CCDF of the SINR for the $k$th user can then be given as

$$P_{\gamma_k}(T) = 1 - \mathbb{P}[\gamma_k \leq T]. \tag{6.31}$$

Now considering the multi-path components and using the law of total probability, the CCDF of the SINR for the $k$th user can be rewritten as

$$P_{\gamma_k}(T) = P_{\gamma_k}^{\mathrm{L}}(T)P_{\mathrm{L}} + P_{\gamma_k}^{\mathrm{N}}(T)P_{\mathrm{N}}, \tag{6.32}$$

In the above, $P_{\gamma_k}^{\mathrm{L}}(T)$ and $P_{\gamma_k}^{\mathrm{N}}(T)$ are the conditional CCDFs on the event that the link between the BS and the $k$th user is LOS and NLOS, respectively. As such, the CCDF

of the SINR of the $k$th user conditioned on the fact that the link is LOS is given as

$$P^{\mathrm{L}}_{\gamma_k}(T) = 1 - \mathbb{P}[\gamma_k \leq T|\mathrm{L}]. \tag{6.33}$$

The CCDF of the SINR for the NLOS link can be given similarly. It is worthwhile to note that (6.31) is sometimes referred to in literature as the coverage probability of the network. In particular, the coverage probability is defined as the probability that the destination is able to receive a signal with some threshold SINR $T$. That is, the probability of coverage is actually the CCDF of the SINRs over the network.

**Proposition 6.2.** *Let $p_k = \rho_k r_h^{\alpha_\iota}$. Then the SINR coverage probability for a mmWave BS equipped with a very large UCA can be given as*

$$\mathcal{P}_{\gamma_k}(T) = P_{\mathrm{L}}\mathcal{P}^{\mathrm{L}}_{\gamma_k}(T) + P_{\mathrm{N}}\mathcal{P}^{\mathrm{N}}_{\gamma_k}(T), \tag{6.34}$$

*where*

$$\mathcal{P}^{\mathrm{L}}_{\gamma_k}(T) = \sum_{l=1}^{m} \binom{m}{l} (-1)^{l+1} \exp\left(\frac{-A\,l\,T\,r_k^{\alpha_{\mathrm{L}}}\sigma^2}{p_k M}\right) \prod_{\iota\in\mathrm{L,N}} \exp\left[-2\pi\lambda_{\mathrm{U}}\right. \tag{6.35}$$
$$\left. \times \int_0^\infty x \left(1 - \left(\frac{1}{1 + \frac{AlTr_k^{\alpha_{\mathrm{L}}}(K-1)\Psi_k p_i}{m p_k M} x^{-\alpha_j}}\right)^m\right) P_\iota(x)\,dx\right],$$

*and $\mathcal{P}^{\mathrm{N}}_{\gamma_k}(T)$ follows similarly. Here, $T$ is the SINR threshold, $p_{\mathrm{L}}$ and $p_{\mathrm{N}}$ are the probabilities for LOS and NLOS respectively, and $A = m(m!)^{\frac{-1}{m}}$.*

*Proof.* The proof of this proposition is given in Appendix 6.D.

□

#### 6.4.1.1 Multiple BSs scenario

Next, we consider the scenario where multiple BSs are located within a particular service area, where each BS serves multiple users. Accordingly, the BSs in the network are modeled as points in $\mathbb{R}^2$ which are distributed uniformly as a homogeneous PPP $\Phi_{\mathrm{BS}}$ with intensity $\lambda_{\mathrm{BS}}$. Also, let the number of users connected at a particular time to the $l$th BS be given as $K_l = \min(U_{max}, N_l)$, where $U_{max}$ is the maximum number of users that can be scheduled in a time slot and $N_l$ is the total number of users connected to the $l$th BS. The additional BSs result in extra interference for the typical user at

the origin of $\mathbb{R}^2$. Accordingly, the signal received by the typical user from the BS at $l \in \Phi_{\mathrm{BS}}$ can be given as

$$y_{k_l} = \mathbf{w}_{k_l,l}^H \mathbf{t}_{k_l} x_{k_l} + \sum_{i \in \mathcal{K}_l, i \neq k} \mathbf{w}_{k_l,l}^H \mathbf{t}_{i_l} x_{i_l} + \text{ OBI} + z_{k_l}, \tag{6.36}$$

where OBI is the other BSs' interference to the $k$th user from all other BSs except the $l$th BS.

Accordingly, by a slight abuse of notation, the SINR of the user at $k \in \mathcal{K}$ served by the BS at $l \in \Phi_{\mathrm{BS}}$ can be given as

$$\bar{\gamma}_{k_l} = \frac{|\mathbf{w}_{k_l,l}^H \mathbf{t}_{k_l}|^2}{\sum\limits_{i \in \mathcal{K}, i \neq k} |\mathbf{w}_{k_l,l}^H \mathbf{t}_{i_l}|^2 + \sum\limits_{j \in \Phi_{\mathrm{BS}}, j \neq l} \sum\limits_{w \in \mathcal{K}} |\mathbf{w}_{k_j,j}^H \mathbf{t}_{w_j}|^2 + \sigma^2}. \tag{6.37}$$

Now, in order to model the OBI, the notion of side lobe gain $\tau_{\mathrm{BS}}$ can be introduced by considering an approximation as in [125], where the angular space in the azimuth is quantized into sectors equivalent to the number of BS antennas. Accordingly, the SINR in (6.37) can be approximated as[2]

$$\bar{\gamma}_k = \frac{\rho_k \Xi_k^{\iota} \eta_k^2 M}{(K-1)\ \Psi_k \sum\limits_{i \in \mathcal{K}, i \neq k} \rho_i \Xi_i^{\iota} \eta_i^2 + I_{\mathrm{BS}} + \sigma^2} \ \forall \iota \in \{\mathrm{L}, \mathrm{N}\}, \tag{6.38}$$

where $I_{\mathrm{BS}}$ is the OBI and can be given as

$$I_{\mathrm{BS}} = \sum_{j \in \Phi_{\mathrm{BS}}, j \neq l} M \rho_j \Xi_j^{\iota} \eta_j^2 \times \sum_{w \in \mathcal{K}_j} ||\mathbf{t}^{\dagger}(\theta_{k_j}, \phi_{k_j}) \mathbf{t}(\theta_{w_j}, \phi_{w_j})||^2. \tag{6.39}$$

Now, leveraging the analysis from [125], the $I_{\mathrm{BS}}$ can further be modeled as

$$I_{\mathrm{BS}} = \sum_{j \in \Phi_{\mathrm{BS}}, j \neq l} M \rho_j \Xi_j^{\iota} \eta_j^2 \Upsilon_j, \tag{6.40}$$

where

$$\Upsilon_j = \begin{cases} 1, & \theta_{k_j} = \theta_{w_j} \text{ and } \phi_{k_j} = \phi_{w_j} \\ \tau_{\mathrm{BS}}, & \text{otherwise,} \end{cases} \tag{6.41}$$

with $\tau_{\mathrm{BS}} < 1$.

[2]For brevity, hereinafter we have removed the subscript $l$ from all subsequent variables.

**Proposition 6.3.** *The SINR coverage probability for a mmWave network with multiple BSs, each equipped with very large UCAs can be given as*

$$\mathcal{P}_{\bar{\gamma}_k}(T) = P_{\mathrm{L}}\mathcal{P}^{\mathrm{L}}_{\bar{\gamma}_k}(T) + P_{\mathrm{N}}\mathcal{P}^{\mathrm{N}}_{\bar{\gamma}_k}(T), \tag{6.42}$$

*where*

$$\mathcal{P}^{\mathrm{L}}_{\bar{\gamma}_k}(T) = \sum_{l=1}^{m} \binom{m}{l} (-1)^{l+1} \exp\left(\frac{-A\, l\, T\, r_k^{\alpha_{\mathrm{L}}}\sigma^2}{p_k M}\right) \prod_{\iota\in \mathrm{L,N}} \mathbb{E}_{I^{\iota}_{\mathcal{K}}}\left[\exp\left(\frac{-A\, l\, T r_k^{\alpha_{\mathrm{L}}} I^{\iota}_{\mathcal{K}}}{p_k M}\right)\right] \mathbb{E}_{I^{\iota}_{\Phi_{\mathrm{BS}}}}\left[\exp\left(\frac{-A\, l\, T r_k^{\alpha_{\mathrm{L}}} I^{\iota}_{\Phi_{\mathrm{BS}}}}{p_k M}\right)\right]. \tag{6.43}$$

$\mathcal{P}^{\mathrm{N}}_{\bar{\gamma}_k}(T)$ *follows similarly. Here,* $p_{\mathrm{L}}$ *and* $p_{\mathrm{N}}$ *are the probabilities for LOS and NLOS respectively,* $p_k = \rho_k r_h^{\alpha}$ *and the rest of the parameters are as defined before.*

*Proof.* The proof of this proposition can be obtained by similarly following the steps of the proof of Proposition 6.2. For better understanding, we give a sketch of the proof in Appendix 6.E. □

Furthermore, we would like to note that in the above two propositions, the typical user is conditioned on a random BS association. This may not be the case every time and the typical user may be associated to its nearest BS to maximize its received SINR.

**Lemma 6.7.** *The SINR coverage probability for a mmWave network with multiple BSs, each equipped with very large UCAs conditioned on nearest BS association can be given as*

$$\mathcal{P}_{\hat{\gamma}_k}(T) = \int_{r>0} \mathcal{P}_{\bar{\gamma}_k}(T, r_k) f(r_k)\, dr_k, \tag{6.44}$$

*where* $f(r_k)$ *is the nearest distance distribution of the BSs, which is given by*

$$f(r_k) = 2\pi\lambda_{\mathrm{BS}} r_k e^{-\pi\lambda_{\mathrm{BS}} r_k^2}. \tag{6.45}$$

## 6.5 Average Rate and Area Spectral Efficiency

In this section, we characterize the average rate in mmWave networks considering MGF of channel gains. To this point, the received signal gain at the user can be denoted

as $\zeta_k = p_k r_k^{-\alpha_\iota} \eta_k^2 M/\sigma^2$, where $p_k = \rho_k r_h^{\alpha_\iota}$, with $\iota \in \{\mathrm{L}, \mathrm{N}\}$. In order to characterize the average rate, we need the moment generating functions of $\zeta_k$. Before deriving the corresponding MGF's, we first characterize their corresponding distributions. Thus, the required SNR distribution without taking interference into account can be given as

$$\begin{aligned} F_{\zeta_k}(T) &= P_{\mathrm{L}}\mathbb{P}\{\zeta_k < T|\mathrm{L}\} + P_{\mathrm{N}}\mathbb{P}\{\zeta_k < T|\mathrm{N}\}, \\ &= \sum_{k=0}^{m} \binom{m}{k} (-1)^{k+1} \exp\left(\frac{-A\,k\,T\,r_k^{\alpha_{\mathrm{L}}}\sigma^2}{p_k M}\right) e^{-\beta r_k} \\ &+ \sum_{k=0}^{m} \binom{m}{k} (-1)^{k+1} \exp\left(\frac{-A\,k\,T\,r_k^{\alpha_{\mathrm{N}}}\sigma^2}{p_k M}\right) (1 - e^{-\beta r_k}). \end{aligned} \tag{6.46}$$

Therefore, the MGF of this distribution is given as

$$\begin{aligned} \mathcal{L}_{\zeta_k}(z) &= \sum_{k=0}^{m} \binom{m}{k} (-1)^{k+1} \left(1 + \frac{z p_k M l}{A\,k\,T\,r_k^{\alpha_{\mathrm{L}}}\sigma^2}\right)^{-1} e^{-\beta r_k} \\ &+ \sum_{k=0}^{m} \binom{m}{k} (-1)^{k+1} \left(1 + \frac{z p_k M}{A\,k\,T\,r_k^{\alpha_{\mathrm{N}}}\sigma^2}\right)^{-1} (1 - e^{-\beta r_k}). \end{aligned} \tag{6.47}$$

Now, an integral-form expression for the average rate is given in the following proposition using (6.10) and (6.38).

**Proposition 6.4.** *The gross average rate for a typical user in a mmWave network with multiple BSs equipped with very large UCAs can be given as*

$$\bar{\mathcal{R}} = B_{\mathrm{total}} \int_0^{\infty} (1 - \mathcal{L}_{\zeta_k}(z)) \mathcal{L}_{\mathcal{I}_{\mathrm{U}}}(\tfrac{z}{\sigma^2}) \mathcal{L}_{\mathcal{I}_{\mathrm{BS}}}(\tfrac{z}{\sigma^2}) \frac{e^{-z}}{z}\, \mathrm{dz}, \tag{6.48}$$

*where, $\mathcal{L}_{\zeta_k}(.)$ is given in* (6.47)*, and*

$$\mathcal{L}_{\mathcal{I}_{\mathrm{U}}}(z) = \prod_{\iota \in \mathrm{L},\mathrm{N}} \exp\left[-2\pi\lambda_{\mathrm{U}} \int_0^{\infty} x \left(1 - \left(\frac{1}{1 + \frac{z\,(K-1)\Psi_k p_i}{m} x^{-\alpha_\iota}}\right)^m\right) P_\iota(x)\, dx\right], \tag{6.49}$$

$$\mathcal{L}_{\mathcal{I}_{\mathrm{BS}}}(z) = \prod_{\iota \in \mathrm{L},\mathrm{N}} \exp\left[-2\pi\lambda_{\mathrm{BS}} \int_0^{\infty} x \left(1 - \left(\frac{1}{1 + \frac{z\,M p_j \tau_{\mathrm{BS}}^2}{m} x^{-\alpha_\iota}}\right)^m\right) P_\iota(x)\, dx\right]. \tag{6.50}$$

*where $p_j = \rho_j r_h^{\alpha_\iota}$ and $B_{\mathrm{total}}$ is the total bandwidth of the mmWave transmission.*

*Proof.* This proof follows from equation (6.10) and by using the integral-form expressions of $\mathcal{L}_{\mathcal{I}_{\mathrm{U}}}(\frac{z}{\sigma^2})$ and $\mathcal{L}_{\mathcal{I}_{\mathrm{BS}}}(\frac{z}{\sigma^2})$ from the proof of Proposition 6.3. □

For the network as a whole, it is now necessary to determine the outage $\mathbb{P}[\bar{\gamma}_k < \epsilon]$, where $\epsilon$ is the outage probability. However, this depends on the distance between the BSs and the users, and the locations of the active[3] BSs. If fewer transmitters are active, then the SINR and accordingly the outage probability can be decreased, but the overall network throughput would also decrease. Hence, it is mandatory to balance these two effects with a metric that can take into consideration both the average rate and outage into consideration. One such metric is the area spectral efficiency. In particular, the area spectral efficiency of a network is defined as the sum of the maximum average data rates per unit bandwidth per unit area for a specific outage constraint leading to a successful transmission resulting from an average number active BSs. Mathematically, the area spectral efficiency of a mmWave network can be given as [17, 126, 127]

$$\nu_s = \frac{\lambda_{\mathrm{BS}}\, \bar{\mathcal{R}}\, (1-\epsilon)}{B_{\mathrm{total}}}, \tag{6.51}$$

where $\lambda_{\mathrm{BS}}$ is the average number of active BSs[4] sending a gross average rate of $\bar{\mathcal{R}}$ for an outage probability $\epsilon$ and $B_{\mathrm{total}}$ is the total bandwidth of the mmWave transmission.

## 6.6 Numerical Results

In this section, we validate our system model and also verify the accuracy of the results mentioned in the propositions. In general, the computations are done through Monte Carlo simulations, which are then used to validate the analytical results. We consider the mmWave bandwidth of 2 GHz [128] and carrier frequency 23 GHz. Unless stated otherwise, most of the values of the parameters used are inspired from literature mentioned in the references [128, 18, 17]. A few of the parameters and their corresponding values are given in Table 6.2. All other parameters and values will be explicitly mentioned wherever used.

We begin by analyzing the coverage probability of the system with respect to SINR

[3]The active BSs are the ones that are not totally blocked by the blockages and can associate with a user either through LOS or NLOS.

[4]Obtaining a closed-form expression for $\lambda_{\mathrm{BS}}$ is not tractable, but can be computed numerically from (6.42) for a given $\epsilon$.

***Table 6.2:*** *Simulation Parameters*

| **Notation** | **Parameter** | **Values** |
|---|---|---|
| $r_c$ | Radius of the circular coverage area | 250m |
| $r_k$ | Distance from the $k$th user to the BS | 25m |
| $h$ | Height of the BS | 15m |
| $M$ | Number of antennas in the UCA | 200 |
| $\lambda_{\text{BS}}$ | Density of BSs | 0.00005 |
| $\lambda_{\text{U}}$ | Density of users | 0.00001 |
| $\beta$ | Blockage density | 0.001 |
| $G$ | Interferer antenna gain | 10 dB |
| $\alpha$ | Path loss exponent | LOS-2.5, NLOS-3.5 |
| $m$ | Nakagami fading figure | 6 |
| $\rho$ | BS transmit power | 30 dBm |
| $\sigma^2$ | Noise power | Thermal noise + 10dB noise figure. |

threshold for different numbers of antennas at the BS, $M$ in Fig 6.2. In particular, this result is a validation of Proposition 6.2. It can be seen from the figure that the gap between the analytical and simulation results obtained after numerical evaluation is quite tight. The figure shows that the number of antennas $M$ has a considerable impact on the coverage probability. As we increase the number of antennas at the BS, the probability of coverage for a BS with respect to a typical user for a fixed transmit power increases.

Next, in Fig. 6.3 we consider the scenario where multiple BSs are located within the service area. Hereinafter, unless stated otherwise, this scenario will be considered in all subsequent analyses. This figure compares the coverage probability for varying BS's densities. As can be observed from the figure, increasing density of BSs leads to lower coverage. Although this result appears counter-intuitive at first, it can be explained by the fact that deployment of more BSs increases the probability for interfering BSs. The effect of interference from BSs can however be alleviated with the help of BS cooperation, where a set of BSs cooperate to improve the coverage of the network. Under such a scenario, the user can associate itself with the best BS (conditioned on distance). Accordingly, Fig. 6.4 shows the coverage probability as a function of BS density for the nearest BS association.

As expected, the figure shows that an increase in BS density leads to an increase in coverage probability.

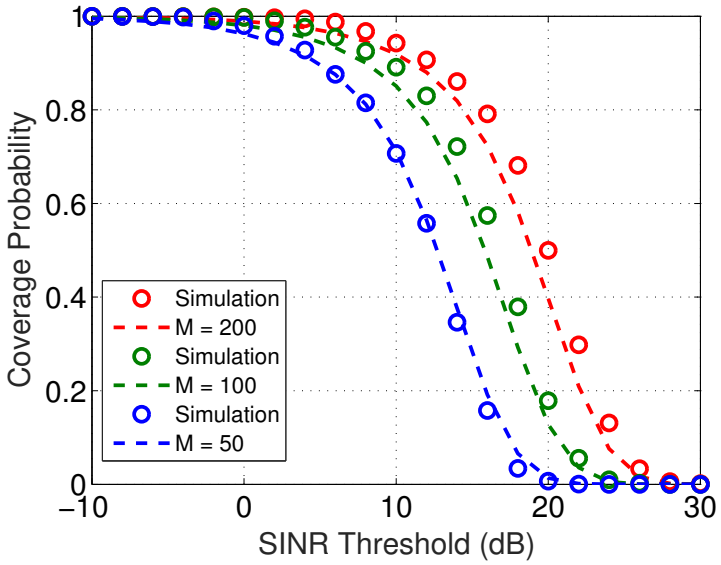


***Figure 6.2:*** *Coverage probability as a function of $M$. Here, $\lambda_{\mathrm{U}} = 0.0001$.*

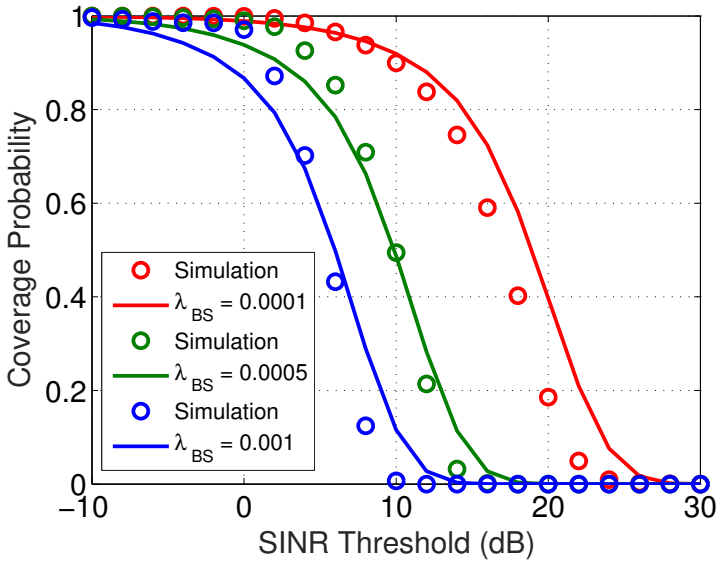


***Figure 6.3:*** *Coverage probability as a function of $\lambda_{\mathrm{BS}}$. Here, $\lambda_{\mathrm{U}} = 0.0001$.*

In Fig. 6.5, we show the coverage probability against SINR threshold for different blockage densities. In this figure, the density of BS is kept constant, while the blockage density is varied. It is shown from the figure that higher blockages lead to better coverage. Although blockages might not ordinarily be expected to improve coverage, in this figure, this outcome is not so unusual considering the fact that increased blockages in the network also limit the interference from interfering BSs. This in turn improves the SINR, which leads to better coverage probability.

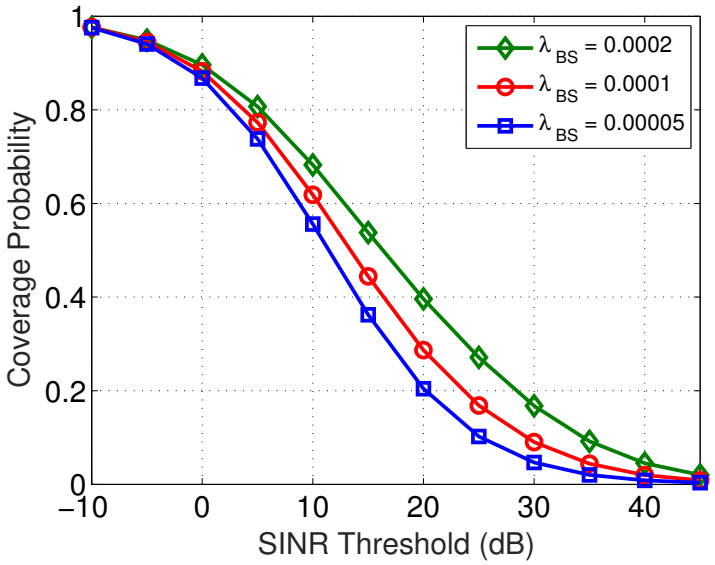


***Figure 6.4:*** *Coverage probability as a function of* $\lambda_{\mathrm{BS}}$ *under nearest BS association. Here,* $\lambda_{\mathrm{U}} = 0.00005$ *and* $M = 250$.

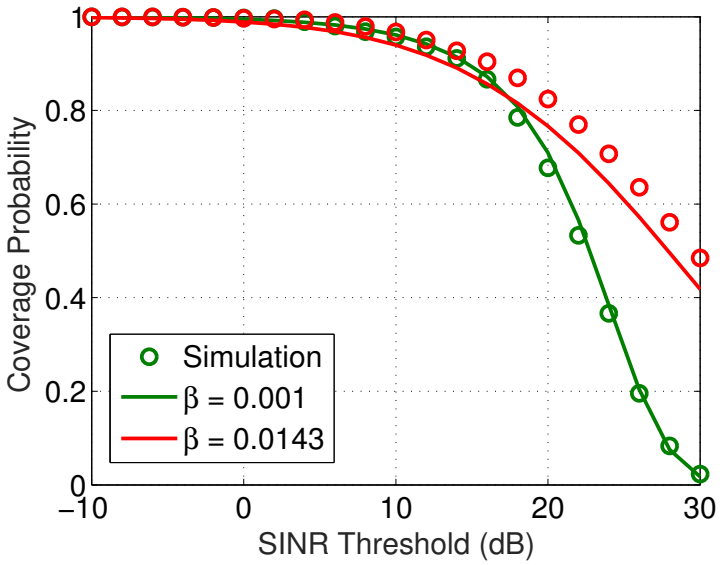


***Figure 6.5:*** *Coverage probability as a function of* $\beta$. *Here,* $\lambda_{\mathrm{U}} = 0.00005$ *and* $M = 250$.

After establishing the effect of various parameters with respect to coverage probability in the previous figures, we now look into the average rate analysis of the mmWave network. Similar to Fig. 6.2, we analyze the average rate for different $M$ as a function of user densities in Fig. 6.6. As expected, the average rate increases (logarithmically) as the value of $M$ increases. However, as $M$ grows unboundedly, the rate saturates

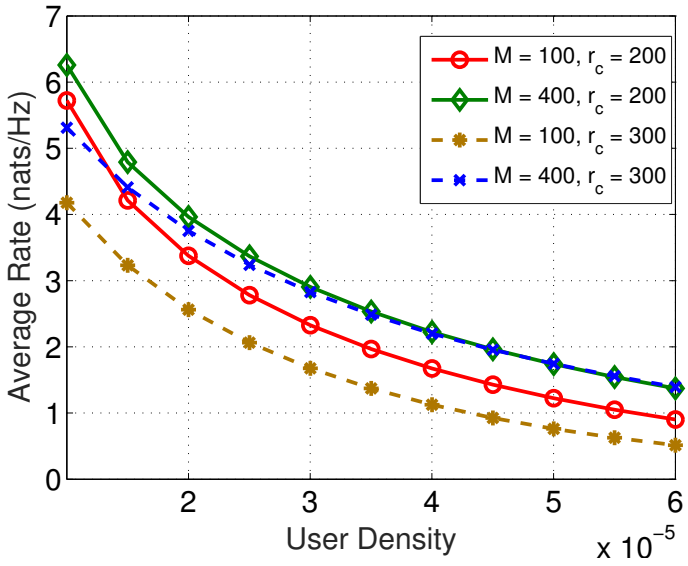


***Figure 6.6:*** *Average rate as a function of $M$. Here, $\alpha = 2.1$ and $\lambda_{\text{BS}} = 0.00001$.*

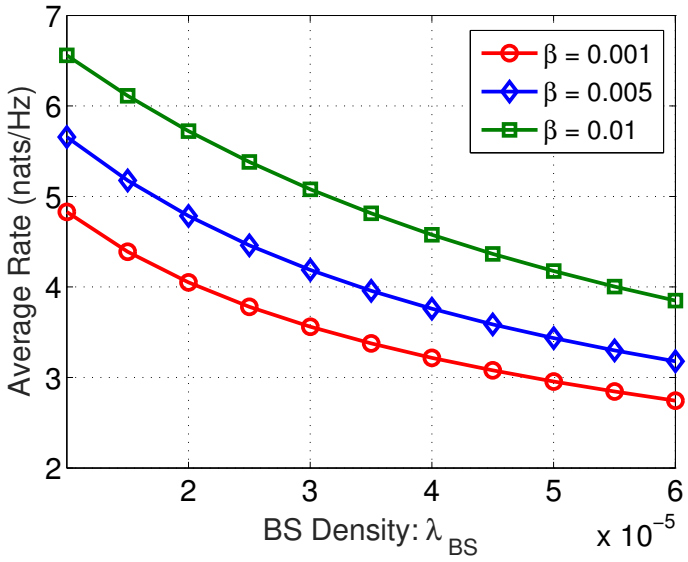


***Figure 6.7:*** *Average rate as a function of $\beta$. Here, $M = 100$.*

and almost converges to a nonzero limit. This can be explained by the fact that as the number of antennas increases the correlation among the antennas also increases in the UCA. It can be also seen that the performance decreases with the increase the value of radius ($r_c$). This can be explained from the fact that the higher radii allow more blockages and BSs which leads to more attenuation and interference respectively, consequently decreasing the average rate.

Next, we investigate the average rate as a function of BS density in Fig. 6.7. The

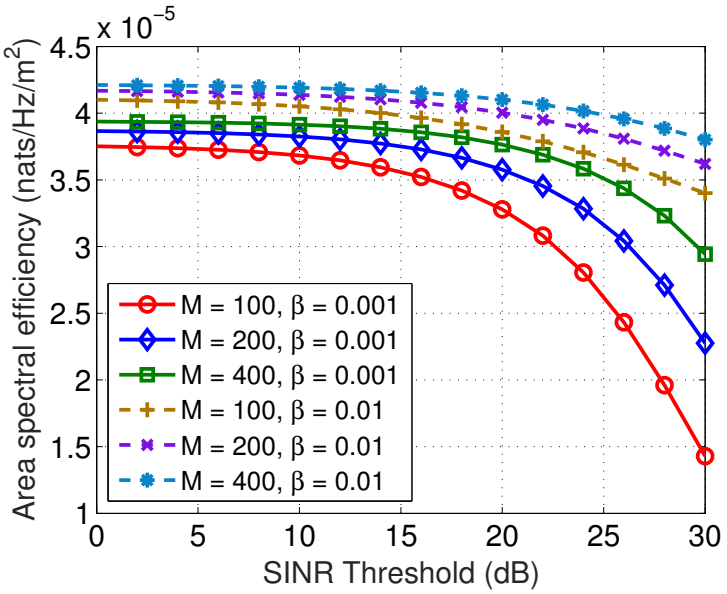


***Figure 6.8:*** *Area spectral efficiency as a function of $M$ and $\beta$. Here, $r_c = 200$.*

figure shows a decrease in average rate as BS density is increased. This result matches the trend from the plots in Fig. 6.3, where the extra interference from the BSs decreases the average rate. In addition, we consider the average rate performance for different blockage densities and observe that increasing blockages produces better average rates. This confirms our observation from Fig. 6.5 where increasing blockages had a positive effect on the coverage performance of mmWave networks.

Furthermore, Fig. 6.8 shows the performance gains in terms of area spectral efficiency that can be achieved by increasing the number of antennas in the UCA of the BSs. It can be seen from the figure that the area spectral efficiency increases as the value of $M$ increases. However, a linear increase in SINR results in an exponential decrease of the area spectral efficiency of the network. This can be explained due to the fact that the increase in SINR threshold results in the increase in outage probability, which in turn reduces the area spectral efficiency. Furthermore, a tractable derivation of the optimal density of BSs is an open optimization problem, the exploration of the analytical solutions of which are deferred for future work.

## 6.7 Summary

In a mmWave transmission, the spatial degrees of freedom offered by the channel depends on both the channel conditions and the number of antennas deployed. Hence,

to obtain the system performance, the effects of the channel conditions and the type of antenna array need to be considered in conjunction with each other. If not taken into consideration, this can result into an elevated problem in massive MIMO systems, where a larger number of antennas are rigged within a limited physical space. Though the ULA is the most commonly deployed configuration, it can scan only the 2D space. On the other hand, the UCA can take both the azimuth and the elevation angles into consideration. This makes UCA the appropriate array configuration to exploit the 3D propagation space in the true sense. Accordingly, this chapter deals with the downlink of a mmWave network equipped with large 3D circular antenna array.

In particular we characterize the SINR of the system based on array geometry at the BS. Furthermore, stochastic geometric tools are employed while modeling the interference. Thereby, expressions for coverage probability and average rate are derived and validated in the numerical section. Using this average rate, the area spectral efficiency of the mmWave network was calculated followed by the area spectral efficiency. With the help of numerical results, we provided a detailed analysis on the effect of the number of BS antennas, blockage density, path loss coefficient, node density, and SINR threshold on a mmWave network, where BSs are equipped with very large antenna arrays. It was found that increasing $M$ in the UCA deployed at the BS in the network can lead to better area spectral efficiency in mmWave networks. Also, though increasing $\beta$ results in the attenuation of the desired signal, it also helps to attenuate the interference from non-intended sources, thus increasing the resultant SINR, which in turn increases the area spectral efficiency. However, the attenuation of the desired signal may not be desirable and may lead to loss of transmitted information. This can be dealt with by the use of relays, which was discussed in the previous chapter.

# Appendix 6.A Proof of Lemma 6.3

*Proof.* Let $p = \sin\Phi$. Therefore, $d\Phi = dp/\cos(\Phi)$. Now, substituting these values in (6.3), we have

$$\mathcal{I}(x,y) = -x\int_{p_{min}}^{p_{max}} \frac{J_0(yp)p}{(1-p^2)^2}dp. \tag{6.52}$$

Integrating (6.52) by parts, we have

$$\mathcal{I}(x,y) = \frac{xJ_0(yp)}{2(p^2-1)}\Big|_{p_{min}}^{p_{max}} + xy\underbrace{\int_{p_{min}}^{p_{max}} \frac{J_1(yp)}{2(p^2-1)}dp}_{\bar{\mathcal{I}}(y)}. \tag{6.53}$$

Using Lemma 6.2, we have

$$\bar{\mathcal{I}}(y) = \sum_{i=0}^{\infty} \frac{(-1)^i}{i!\,\Gamma(i+2)}\left(\frac{y}{2}\right)^{(2i+1)} \int_{p_{min}}^{p_{max}} \frac{p^{(2i+1)}}{2(p^2-1)}dp, \tag{6.54}$$

Now, let $q = p^2$. Therefore, (6.54) becomes

$$\begin{aligned}
\bar{\mathcal{I}}(y) &= \frac{1}{4}\sum_{i=0}^{\infty} \frac{(-1)^i}{i!\,\Gamma(i+2)}\left(\frac{y}{2}\right)^{(2i+1)} \left(\int_0^{p_{max}^2} \frac{q^i}{q-1}dq - \int_0^{p_{min}^2} \frac{q^i}{q-1}dq\right), \\
&\overset{(a)}{=} \frac{1}{4}\sum_{i=0}^{\infty} \frac{(-1)^i}{i!\,\Gamma(i+2)}\left(\frac{y}{2}\right)^{(2i+1)} \left(\frac{p_{max}^{2(i+1)}}{i+1}{}_2F_1(1,i+1;i+2;p_{max}^2)\right. \\
&- \left.\frac{p_{min}^{2(i+1)}}{i+1}{}_2F_1(1,i+1;i+2;p_{min}^2)\right), \qquad (6.55) \\
&\overset{(b)}{=} \frac{1}{4}\sum_{i=0}^{\infty} \frac{(-1)^i}{i!\,\Gamma(i+2)}\left(\frac{y}{2}\right)^{(2i+1)} \qquad (6.56) \\
&\times \left(-\left(\log(1-p_{max}^2) + \sum_{k=1}^{i}\frac{p_{max}^{2k}}{k}\right) + \log(1-p_{min}^2) + \sum_{k=1}^{i}\frac{p_{min}^{2k}}{k}\right),
\end{aligned}$$

where $(a)$ is obtained using the integration identity from [53, Eq. (3.194.5)] and $(b)$ is obtained using the integration identity from [129, Eq. 07.23.03.0224.01]. Further, $F$ is a Hypergeometric function. □

# Appendix 6.B Proof of Lemma 6.5

*Proof.* Let $\psi_k$ denote the supplementary of the elevation angle $\theta_k$. Then the CDF of the elevation angle can be given as

$$F(\theta) = \mathbb{P}(\theta_k < \theta) = \mathbb{P}(\psi_k + \pi/2 < \theta). \tag{6.57}$$

From Fig. 1, we have $\tan\psi_k = h/r_0$. When $\theta < \pi/2 + \tan^{-1}\frac{h}{r_c}$,

$$\mathbb{P}(\theta_k < \theta) = 0. \tag{6.58}$$

Similarly, when $\pi/2 + \tan^{-1}\frac{h}{r_c} \leq \theta \leq \pi/2 + \tan^{-1}\frac{h}{r_h}$,

$$\begin{aligned}\mathbb{P}(\theta_K < \theta) &= \mathbb{P}\left(\tan^{-1}\frac{h}{r_0} < \theta - \pi/2\right) \\ &= 1 - \mathbb{P}\left(r_0 < \frac{h}{\tan(\theta - \pi/2)}\right). \end{aligned} \tag{6.59}$$

Moreover, when the users are uniformly distributed within the coverage area, the CDF of the distance of any random user can be given as [130]

$$\mathbb{P}(r_0 < x) = \frac{x^2 - r^h}{r_c^2 - r_h^2}. \tag{6.60}$$

Therefore, from (6.58) and (6.60) we have

$$\mathbb{P}(\theta_k < \theta) = 1 - \frac{1}{r_c^2 - r_h^2}\left(\frac{h^2}{\tan^2(\theta - \pi/2)} - r_h^2\right). \tag{6.61}$$

Finally, when $\theta > \pi/2 + \tan^{-1}\frac{h}{r_h}$,

$$\mathbb{P}(\theta_k < \theta) = 1. \tag{6.62}$$

Therefore, from (6.58), (6.61) and (6.62) we have

$$F(\theta) = \begin{cases} 0, & \theta < \Theta_1 \\ 1 - \frac{1}{(r_c^2 - r_h^2)}\left(\frac{h^2}{\tan^2(\theta - \pi/2)} - r_h^2\right), & \Theta_1 \leq \theta \leq \Theta_2 \\ 1, & \theta > \Theta_2, \end{cases} \tag{6.63}$$

where, $\Theta_1 = \pi/2 + \tan^{-1}\frac{h}{r_c}$ and $\Theta_2 = \pi/2 + \tan^{-1}\frac{h}{r_h}$. Now differentiating (6.63) with respect to $\theta$, we obtain (6.8). □

# Appendix 6.C Calculation of Integral in (6.26)

The integral in (6.26) can be solved in two parts. Solving for the inner integral, we have

$$\int_0^{2\pi} e^{j\frac{2\pi}{\lambda} r\sqrt{a^2+b^2}\cos(\phi_k - A)} \frac{1}{2\pi} d\phi_k$$

$$\begin{aligned}
&\overset{(a)}{=} I_0\left(j\frac{2\pi}{\lambda}r\sqrt{a^2+b^2}\right)\\
&\overset{(b)}{=} J_0\left(\frac{2\pi}{\lambda}r\sqrt{a^2+b^2}\right),\\
&= J_0\left(\frac{2\pi}{\lambda}r\sqrt{\left(\cos(\frac{2\pi n}{M})-\cos(\frac{2\pi m}{M})\right)^2+\left(\sin(\frac{2\pi m}{M})-\sin(\frac{2\pi n}{M})\right)^2}\sin\theta_k\right),\\
&= J_0\left(\frac{2^{\frac{3}{2}}\pi}{\lambda}r\sqrt{1-\cos\left(\frac{2\pi(n-m)}{M}\right)}\sin\theta_k\right). \qquad (6.64)
\end{aligned}$$

In the above, (a) is obtained by using the integral identity [53, Eq. (3.339)] and (b) is obtained using the identity $J_0(z) = I_0(jz)$. Now, substituting the values of the inner integral in (6.26) with (6.64) and solving for the outer integral, we have

$$E_1 = \int_{\theta_{min}}^{\theta_{max}} J_0\left(\frac{2^{\frac{3}{2}}\pi}{\lambda}r\sqrt{1-\cos\left(\frac{2\pi(n-m)}{M}\right)}\sin\theta_k\right) f_\theta(\theta_k)d\theta_k. \qquad (6.65)$$

Now, using Lemma 6.5, we have

$$E_1 = -\frac{2h^2}{r_c^2-r_h^2}\int_{\theta_{min}}^{\theta_{max}} J_0\left(\zeta\sin(\theta_k)\right)\frac{\sin(\theta_k)}{\cos^3(\theta_k)}d\theta_k, \qquad (6.66)$$

where $\zeta = \frac{2^{\frac{3}{2}}\pi}{\lambda}r\sqrt{1-\cos\left(\frac{2\pi(n-m)}{M}\right)}$. Similarly, $E_2$ can be evaluated. Since $\theta_k$ and $\theta_j$ are random variables in the same real domain, they evaluate to the same result.

# Appendix 6.D Proof of Proposition 6.2

Let $p_k = \rho_k r_h^{\alpha_\iota}$. Therefore, from equation (6.30), we have

$$\begin{aligned}
\gamma_k &= \frac{\rho_k \Xi_k^\iota \eta_k^2 M}{(K-1)\,\Psi_k \sum\limits_{i\in\mathcal{K},i\neq k}\rho_i\Xi_i^\iota\eta_i^2 + \sigma^2} \qquad (6.67)\\
&= \frac{p_k r_k^{-\alpha_\iota}\eta_k^2 M}{(K-1)\,\Psi_k \sum\limits_{i\in\mathcal{K},i\neq k} p_i\eta_i^2 r_i^{-\alpha_\iota} + \sigma^2},
\end{aligned}$$

where $\iota \in \{\mathrm{L},\mathrm{N}\}$.

Using (6.67), the CCDF of conditional SINR $\gamma_k$ on the event that the link between the BS and the $k$th user is LOS can be given as

$$\mathcal{P}^{\mathrm{L}}_{\gamma_k}(T) = \mathbb{P}\left[\frac{p_k r_k^{-\alpha_{\mathrm{L}}}\eta_k^2 M}{(K-1)\ \Psi_k \sum\limits_{i\in\mathcal{K},i\neq k} p_i\eta_i^2 r_i^{-\alpha_\iota} +\ \sigma^2} > T\right], \tag{6.68}$$

$$= \mathbb{P}\left[\eta_k^2 > \frac{T\, r_k^{\alpha_{\mathrm{L}}}}{p_k M}\left(\sigma^2 + I_{\mathcal{K}}\right)\right],$$

$$= \mathbb{P}\left[\eta_k^2 > \frac{T\, r_k^{\alpha_{\mathrm{L}}}}{p_k M}\left(\sigma^2 + I_{\mathcal{K}}\right)\right],$$

$$= 1 - \mathbb{P}\left[\eta_k^2 < \frac{T\, r_k^{\alpha_{\mathrm{L}}}}{p_k M}\left(\sigma^2 + I_{\mathcal{K}}\right)\right], \tag{6.69}$$

where $I_{\mathcal{K}} = (K-1)\ \Psi_k \sum\limits_{i\in\mathcal{K},i\neq k} p_i\eta_i^2 r_i^{-\alpha_\iota}$ is the received aggregate interference from all the users. In the following analysis, we employ stochastic geometry tools to model such interference.

Leveraging the tight lower bound of a Gamma random variable of parameter $m$ as $\mathbb{P}[z > \gamma] < (1 - e^{-A\gamma})^m$ with $A = m(m!)^{\frac{-1}{m}}$, we can bound (6.69) as

$$\mathcal{P}^{\mathrm{L}}_{\gamma_k}(T) \ \ < \ \ 1 - \mathbb{E}_{I_{\mathcal{K}}}\left[\left(1 - \exp\left(\frac{-A\,T\, r_k^{\alpha_{\mathrm{L}}}}{p_k M}(\sigma^2 + I_{\mathcal{K}})\right)\right)^m\right] \tag{6.70}$$

Now using the Binomial theorem [93], (6.70) can be given as

$$\mathcal{P}^{\mathrm{L}}_{\gamma_k}(T) \ \ \approx \ \ \sum_{l=1}^{m}\binom{m}{l}(-1)^{l+1}\mathbb{E}_{I_{\mathcal{K}}}\left[\exp\left(\frac{-A\,l\,T\, r_k^{\alpha_{\mathrm{L}}}}{p_k M}(\sigma^2 + I_{\mathcal{K}})\right)\right]. \tag{6.71}$$

Now considering both LOS and NLOS users and leveraging the notion of mark of stochastic geometry, we consider the interference as two independent PPPs such that

$$I_{\mathcal{K}} = I^{\mathrm{L}}_{\mathcal{K}} + I^{\mathrm{N}}_{\mathcal{K}}. \tag{6.72}$$

Accordingly, we can rewrite (6.71) as

$$\mathcal{P}^{\mathrm{L}}_{\gamma_k}(T) = \sum_{l=1}^{m}\binom{m}{l}(-1)^{l+1}\exp\left(\frac{-A\,l\,T\, r_k^{\alpha_{\mathrm{L}}}\sigma^2}{p_k M}\right)\prod_{\iota\in\mathrm{L,N}}\mathbb{E}_{I^\iota_{\mathcal{K}}}\left[e^{\frac{-A\,l\,T r_k^{\alpha_{\mathrm{L}}} I^\iota_{\mathcal{K}}}{p_k M}}\right], \tag{6.73}$$

where each expectation in (6.73) is the Laplace transform of the associated sub-PPP. Now, using stochastic geometry and a slight abuse of notation, the expectation in (6.73)

for the LOS case with respect to $I_{\mathcal{K}}^{\mathrm{L}}$ can be given as

$$\begin{aligned}\mathbb{E}[\exp(-sI_{\mathcal{K}}^{\mathrm{L}})] &= \mathbb{E}_{I_{\mathcal{K}},\eta_i}\left[\exp\left(-s\sum_{i\in\mathcal{K}} p_i\eta_i^2 x_i^{-\alpha_{\mathrm{L}}}(K-1)\Psi_k\right)\right], \\ &\overset{(a)}{=} \mathbb{E}_{I_{\mathcal{K}}}\left\{\prod_{i\in\mathcal{K}}\mathbb{E}_{\eta_i}\left[\exp\left(-s\,p_i\eta_i^2 x_i^{-\alpha_{\mathrm{L}}}(K-1)\Psi_k\right)\right]\right\}, \\ &\overset{(b)}{=} \mathbb{E}_{I_{\mathcal{K}}}\left\{\prod_{i\in\mathcal{K}}\left(\frac{1}{1+\frac{s\,(K-1)\Psi_k p_i}{m}x_i^{-\alpha_{\mathrm{L}}}}\right)^m\right\}, \\ &\overset{(c)}{=} \exp\left[-2\pi\lambda_{\mathrm{U}}\int_0^\infty x\left(1-\left(\frac{1}{1+\frac{s\,(K-1)\Psi_k p_i}{m}x^{-\alpha_{\mathrm{L}}}}\right)^m\right)e^{-\beta x}\mathrm{d}x\right],\end{aligned} \tag{6.74}$$

where (a) follows from the assumption of independent small scale fading, (b) follows from the use of the moment generating function of Nakagami-$m$ random variable and (c) follows due to the use of probability generating functionals of PPPs. Similarly, the Laplace transform of interference in the NLOS case can be derived. Following footprints of the derivation of $\mathcal{P}_{\gamma_k}^{\mathrm{L}}(T)$, $\mathcal{P}_{\gamma_k}^{\mathrm{N}}(T)$ can be calculated, which concludes this proof.

# Appendix 6.E Proof of Proposition 6.3

The CCDF of conditional SINR $\bar{\gamma}_k$ in LOS can be given from (6.38) as

$$\mathcal{P}_{\bar{\gamma}_k}^{\mathrm{L}}(T) = \mathbb{P}\left[\eta_k^2 > \frac{T\,r_k^{\alpha_{\mathrm{L}}}}{p_k M}\left(\sigma^2 + I_{\mathcal{K}} + I_{\mathrm{BS}}\right)\right], \tag{6.75}$$

Similar to the proof of Proposition 6.2, we approximate (6.75) as

$$\mathcal{P}_{\bar{\gamma}_k}^{\mathrm{L}}(T) \approx \ \sum_{l=1}^{m}\binom{m}{l}(-1)^{l+1}\mathbb{E}_{I_{\mathcal{K}}}\left[\exp\left(\frac{-A\,l\,T\,r_k^{\alpha_{\mathrm{L}}}}{p_k M}(\sigma^2 + I_{\mathcal{K}} + I_{\mathrm{BS}})\right)\right]. \tag{6.76}$$

Now considering both LOS and NLOS BSs, and users and leveraging the notion of mark of stochastic geometry, we have

$$I_{\mathcal{K}} = I_{\mathcal{K}}^{\mathrm{L}} + I_{\mathcal{K}}^{\mathrm{N}}, \text{ and } I_{\Phi_{\mathrm{BS}}} = I_{\Phi_{\mathrm{BS}}}^{\mathrm{L}} + I_{\Phi_{\mathrm{BS}}}^{\mathrm{N}}. \tag{6.77}$$

Accordingly, we can rewrite (6.76) as

$$\begin{aligned}\mathcal{P}^{\mathrm{L}}_{\bar{\gamma}_k}(T) &= \sum_{l=1}^{m}\binom{m}{l}(-1)^{l+1}e^{\frac{-A\,l\,T\,r_k^{\alpha_{\mathrm{L}}}\sigma^2}{p_k M}} \\ &\times \prod_{\iota\in\{\mathrm{L},\mathrm{N}\}}\mathbb{E}_{I^{\iota}_{\mathcal{K}}}\left[e^{\frac{-A\,l\,T r_k^{\alpha_{\mathrm{L}}} I^{\iota}_{\mathcal{K}}}{p_k M}}\right]\mathbb{E}_{I^{\iota}_{\mathrm{BS}}}\left[e^{\frac{-A\,l\,T r^{\alpha_{\mathrm{L}}} I^{\iota}_{\Phi_{\mathrm{BS}}}}{p_k M}}\right], \end{aligned} \tag{6.78}$$

where $\mathbb{E}_{I^{j}_{\mathcal{K}}}[.]$ follows from the proof of Proposition 6.2 and is given as

$$\mathbb{E}[\exp(-sI^{\iota}_{\mathcal{K}})] = \prod_{\iota\in\mathrm{L},\mathrm{N}}\exp\left[-2\pi\lambda_{\mathrm{U}}\int_0^{\infty}x\left(1-\left(\frac{1}{1+\frac{s\,(K-1)\Psi_k p_i}{m}x^{-\alpha_\iota}}\right)^{m}\right)P_\iota(x)\mathrm{d}x\right], \tag{6.79}$$

Similarly, considering $I^{\mathrm{L}}_{\Phi_{\mathrm{BS}}}$

$$\begin{aligned}\mathbb{E}[\exp(-sI^{\mathrm{L}}_{\Phi_{\mathrm{BS}}})] &= \mathbb{E}_{\eta,\Upsilon_j}\left[\exp\left(-sMp_j x_j^{-\alpha_{\mathrm{L}}}\eta_j^2\Upsilon_j\right)\right] \\ &\overset{(a)}{\leq} \mathbb{E}_{\eta}\left[\exp\left(-sMp_j x_j^{\alpha_{\mathrm{L}}}\eta_j^2\tau^2_{\mathrm{BS}}\right)\right], \\ &\overset{(b)}{=} \exp\left[-2\pi\lambda_{\mathrm{BS}}\int_0^{\infty}x\left(1-\left(\frac{1}{1+\frac{s\,Mp_j\tau^2_{\mathrm{BS}}}{m}x^{-\alpha_{\mathrm{L}}}}\right)^{m}\right)e^{-\beta x}\mathrm{d}x\right], \end{aligned} \tag{6.80}$$

where $(a)$ follows by taking the upper bound on the Laplace functional with $\Upsilon_j \geq \tau_{\mathrm{BS}}$ and $(b)$ is obtained by following a similar approach as the proof of Proposition 6.2. Similarly, $I^{\mathrm{N}}_{\Phi_{\mathrm{BS}}}$ case can be derived. This proof concludes by deriving the closed-form expression for $\mathcal{P}^{\mathrm{N}}_{\bar{\gamma}_k}(T)$.

# Chapter 7

# Full-Duplex MIMO Cognitive Radios

## 7.1 Introduction

Among the emerging technologies for next-generation wireless networks, full duplex (FD) communication is considered a way to potentially double the speed of wireless communication, and is a potential candidate for 5G systems since it enables available spectral resources to be fully utilized in time and frequency.

Many feasible solutions including antenna, analog and digital cancellation have been demonstrated experimentally to mitigate the overwhelming self-interference (SI), which is the fundamental challenge in implementing a full-duplex radio [24, 25]. However, the performance is limited by the residual self-interference to be induced by the imperfection of the transmit and receive front-end chain [26, 27]. In addition to self-interference, co-channel interference (CCI) from uplink (UL) users to downlink (DL) users is another challenge in full-duplex networks that needs to be overcome to fully exploit the multi-access nature of the wireless medium in conjunction with full-duplex systems. To optimize the system performance, self-interference and CCI in FD systems should be addressed jointly through beamforming [28, 29, 30, 31].

In addition to FD systems, cognitive radio system is also a promising technology to enhance spectrum efficiency [131]. Accordingly, cognitive radios can be deployed in FD mode. A FD cognitive radio (CR) can simultaneously transmit and sense the

transmission status of other nodes [132, 133]. In underlay cognitive radio systems, a set of unlicensed secondary users (SUs) operate within the service range of licensed primary users (PUs) where the amount of interference from SUs to PUs must be constrained to meet the Quality-of-Service (QoS) requirements for the PUs. Since it is difficult to obtain the estimates of the channels between SUs and PUs (due to the lack of full SU-PU cooperation), it is important to consider the imperfect channel estimates, and develop robust beamforming schemes that ensure constrained interference on PUs [134, 135].

There are two classes of models frequently used to characterize the imperfect channel state information (CSI): the stochastic and the deterministic (or worst-case) models. In the stochastic model, the channel is usually modeled as a complex random matrix with normally distributed elements, and the transmitter knows the mean and/or the covariance [136]. In the norm-bounded deterministic model, the instantaneous channel lies in a known set of possible values, which represents the amount of uncertainty on the channel, i.e., the bigger the set is, the more uncertainty there is [134, 135].

A sum mean squared error (MSE) minimization problem for a multiple-input multiple-output (MIMO) FD cognitive radio system has been studied in [79], in which the optimization problem has been cast as a second-order cone programming (SOCP). However, the authors have not taken the channel estimation errors into account, and the SOCP-based algorithm proposed in [79] cannot be applied under norm-bounded deterministic imperfect CSI. Therefore, it is important to design robust transceivers for FD underlay cognitive radio systems that take into account imperfect channel knowledge.

Motivated by the above, in this chapter, we consider a scenario where a secondary BS operating in FD mode communicates with UL and DL SUs operating in HD mode simultaneously within the service range of multiple PUs. In addition to self-interference, CCI is also taken into account to design the optimum robust beamformers under a norm-bounded-error model. We study the sum-MSE as the objective function to minimize, subject to power constraints at the UL SUs and secondary BS, and interfering power constraints at the PUs. Since this problem is semi-infinite and non-convex, two methods are proposed to jointly design the transceiver matrices at the secondary BS and users. In the first method, the semi-infinite constraints are first transformed into the tractable forms, and an iterative Semidefinite programming (SDP) algorithm which optimizes the transmit and receiving beamforming matrices in alternating manner is proposed. At each iteration, sum-MSE decreases monotonically, and is guaranteed to converge. On the other hand, to further reduce the design complexity, the cutting-set

method [137, 138] is adopted in the second method, where the sum-MSE optimization problem is solved by employing an iterative procedure which consists of alternating transceiver design and channel determination steps. In particular, the former step involves the transceiver design with a given worst-case channel set, and the latter step involves the calculation of worst-case channels in the uncertainty regions given transceiver designs. Simulation results demonstrate that the proposed robust designs can significantly increase robustness to the CSI errors and can provide the improved performance over the non-robust design. Moreover, it is shown that the proposed FD system can achieve a significant improvement of throughput over a HD system.

## 7.2 System Model

We consider a FD cognitive cellular system, in which a secondary FD BS communicates with HD mode UL and DL SUs, simultaneously within the service range of PUs as illustrated in Fig. 7.1. The BS equipped with $M_0$ transmit and $N_0$ receive antennas serves $K$ UL and $J$ DL users simultaneously. The number of antennas of the $k$-th UL and the $j$-th DL user are denoted by $M_k$ and $N_j$, respectively. The channels $\mathbf{H}_k^{UL} \in \mathbb{C}^{N_0 \times M_k}$ and $\mathbf{H}_j^{DL} \in \mathbb{C}^{N_j \times M_0}$ represent the $k$-th UL and the $j$-th DL channel, respectively. $\mathbf{H}_0 \in \mathbb{C}^{N_0 \times M_0}$ is the self-interference channel from the transmitter antennas of BS to the receiver antennas of BS. $\mathbf{H}_{jk}^{DU} \in \mathbb{C}^{N_j \times M_k}$ denotes the CCI channel from the $k$-th UL user to the $j$-th DL user.

We also take into account the limited dynamic range (DR), which is caused by non-ideal amplifiers, oscillators, analog-to-digital converters (ADCs), and digital-to-analog converters (DACs). We adopt the limited DR model in [139], which has also been commonly used in [140]-[27]. Particularly, at each receive antenna an additive white Gaussian "receiver distortion" with variance $\beta$ times the energy of the undistorted received signal on that receive antenna is applied, and at each transmit antenna, an additive white Gaussian "transmitter noise" with variance $\kappa$ times the energy of the intended transmit signal is applied. This transmitter/receiver distortion model is valid, since it was shown by hardware measurements in [141] and [142] that the non-ideality of the transmitter and receiver chain can be approximated by an independent Gaussian noise model, respectively.

The vector of source symbols of length $d_k^{UL}$ transmitted by the $k$-th UL user is denoted as $\mathbf{s}_k^{UL} \in \mathbb{C}^{d_k^{UL} \times 1}$. It is assumed that the symbols are independent and identically distributed (i.i.d.) with unit power, i.e., $\mathbb{E}\left[\mathbf{s}_k^{UL}\left(\mathbf{s}_k^{UL}\right)^H\right] = \mathbf{I}_{d_k^{UL}}$. Similarly, the

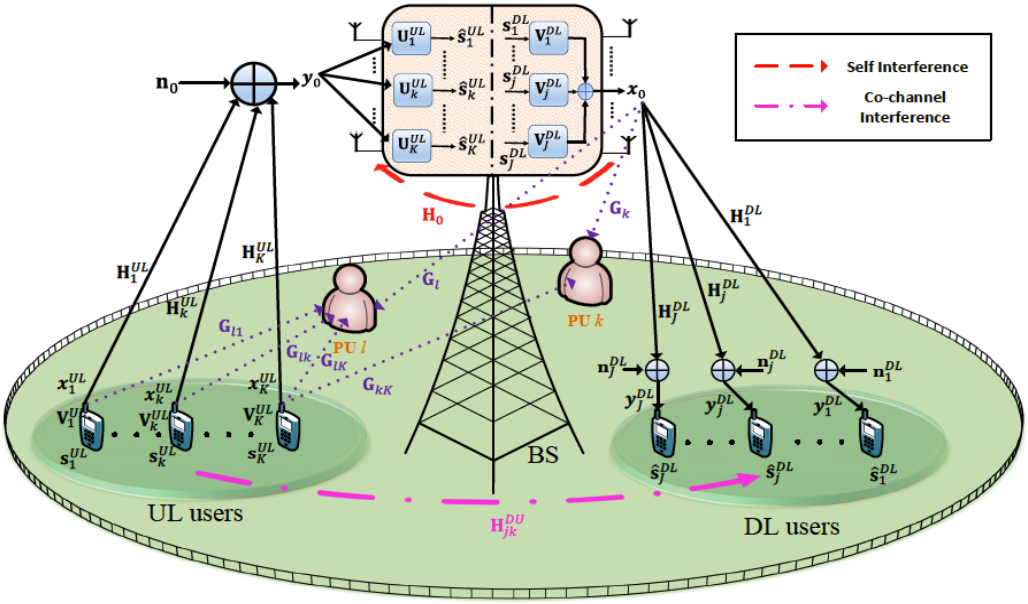


***Figure 7.1:*** *An illustration of a FD multi-user MIMO CR cellular system.*

transmit symbols of length $d_j^{DL}$ for the $j$-th DL user is denoted by $\mathbf{s}_j^{DL} \in \mathbb{C}^{d_j^{DL}\times 1}$, with $\mathbb{E}\left[\mathbf{s}_j^{DL}\left(\mathbf{s}_j^{DL}\right)^H\right] = \mathbf{I}_{d_j^{DL}}$. Denoting the precoders for the data streams of the $k$-th UL and $j$-th DL user as $\mathbf{V}_k^{UL} \in \mathbb{C}^{M_k\times d_k^{UL}}$, and $\mathbf{V}_j^{DL} \in \mathbb{C}^{M_0\times d_j^{DL}}$, respectively, the transmitted signal of the $k$-th UL user and that of the BS can be written respectively, as

$$\mathbf{x}_k^{UL} = \mathbf{V}_k^{UL}\mathbf{s}_k^{UL}, \qquad \mathbf{x}_0 = \sum_{j=1}^{J}\mathbf{V}_j^{DL}\mathbf{s}_j^{DL}. \tag{7.1}$$

We consider a FD multi-user MIMO system that suffers from self-interference and CCI. The signal received by the BS and that received by the $j$-th DL user can be written respectively, as

$$\mathbf{y}_0 = \sum_{k=1}^{K}\mathbf{H}_k^{UL}\left(\mathbf{x}_k^{UL}+\mathbf{c}_k^{UL}\right) + \mathbf{H}_0\left(\mathbf{x}_0+\mathbf{c}_0\right) + \mathbf{e}_0 + \mathbf{n}_0, \tag{7.2}$$

$$\mathbf{y}_j^{DL} = \mathbf{H}_j^{DL}\left(\mathbf{x}_0+\mathbf{c}_0\right) + \sum_{k=1}^{K}\mathbf{H}_{jk}^{DU}\left(\mathbf{x}_k^{UL}+\mathbf{c}_k^{UL}\right) + \mathbf{e}_j^{DL} + \mathbf{n}_j^{DL}, \tag{7.3}$$

where $\mathbf{n}_0 \in \mathbb{C}^{N_0}$ and $\mathbf{n}_j^{DL} \in \mathbb{C}^{N_j}$ denote the additive white Gaussian noise (AWGN) vector with zero mean and covariance matrix $\mathbf{R}_0 = \sigma_0^2\mathbf{I}_{N_0}$ and $\mathbf{R}_j^{DL} = \sigma_j^2\mathbf{I}_{N_j}$ at the BS

and the $j$-th DL user, respectively.[1]

In (7.2)-(7.3), $\mathbf{c}_k^{UL}$ ($\mathbf{c}_0$) is the transmitter distortion at the $k$-th UL user (BS), which models the effect of limited transmitter DR, and closely approximates the effects of additive power-amplifier noise, non-linearities in the DAC and phase noise. The covariance matrix of $\mathbf{c}_k^{UL}$ is given by $\kappa$ ($\kappa \ll 1$) times the energy of the intended signal at each transmit antenna [139]. In particular $\mathbf{c}_k^{UL}$ can be modeled as

$$\mathbf{c}_k^{UL} \sim \mathcal{CN}\left(\mathbf{0}, \kappa \,\mathrm{diag}\left(\mathbf{V}_k^{UL}\left(\mathbf{V}_k^{UL}\right)^H\right)\right), \tag{7.4}$$

$$\mathbf{c}_k^{UL} \perp \mathbf{x}_k^{UL}. \tag{7.5}$$

Finally, in (7.3)((7.2)), $\mathbf{e}_j^{DL}$ ($\mathbf{e}_0$) is the receiver distortion at the $j$-th DL user (BS), which models the effect of limited receiver DR, and closely approximates the combined effects of additive gain-control noise, non-linearities in the ADC and phase noise. The covariance matrix of $\mathbf{e}_j^{DL}$ is given by $\beta$ ($\beta \ll 1$) times the energy of the undistorted received signal at each receive antenna [139]. In particular, $\mathbf{e}_j^{DL}$ can be modeled as

$$\mathbf{e}_j^{DL} \sim \mathcal{CN}\left(\mathbf{0}, \beta \mathrm{diag}\left(\mathbf{\Phi}_j^{DL}\right)\right), \tag{7.6}$$

$$\mathbf{e}_j^{DL} \perp \mathbf{u}_j^{DL}, \tag{7.7}$$

where $\mathbf{\Phi}_j^{DL} = \mathrm{Cov}\{\mathbf{u}_j^{DL}\}$ and $\mathbf{u}_j^{DL}$ is the undistorted received vector at the $j$-th DL user, i.e., $\mathbf{u}_j^{DL} = \mathbf{y}_j^{DL} - \mathbf{e}_j^{DL}$. The discussion on the transmitter/receiver distortion model holds for $\mathbf{c}_0$ and $\mathbf{e}_0$, as well.

The received signals are processed by linear decoders, denoted as $\mathbf{U}_k^{UL} \in \mathbb{C}^{N_0 \times d_k^{UL}}$, and $\mathbf{U}_j^{DL} \in \mathbb{C}^{N_j \times d_j^{DL}}$ by the BS and $j$-th DL user, respectively. Therefore the estimate of data streams of the $k$-th UL user at the BS is given as $\hat{\mathbf{s}}_k^{UL} = \left(\mathbf{U}_k^{UL}\right)^H \mathbf{y}_0$, and similarly, the estimate of data streams of the $j$-th DL user is $\hat{\mathbf{s}}_j^{DL} = \left(\mathbf{U}_j^{DL}\right)^H \mathbf{y}_j^{DL}$. Using these estimates, the MSE of the $k$-th UL and $j$-th DL user, can be respectively given as[2] [79]

$$\begin{aligned}\mathbf{MSE}_k^{UL} &= \mathbb{E}\left\{(\hat{\mathbf{s}}_k^{UL} - \mathbf{s}_k^{UL})(\hat{\mathbf{s}}_k^{UL} - \mathbf{s}_k^{UL})^H\right\} \\ &= \mathbb{E}\left\{\left(\left(\mathbf{U}_k^{UL}\right)^H \mathbf{y}_0 - \mathbf{s}_k^{UL}\right)\left(\left(\mathbf{U}_k^{UL}\right)^H \mathbf{y}_0 - \mathbf{s}_k^{UL}\right)^H\right\}\end{aligned}$$

[1]Since the SU receiver cannot differentiate the interference generated by the PUs from the background thermal noise, the noise vectors in (7.2) and (7.3) captures the background thermal noise as well as the interference generated by the PUs. This assumption is also adopted in [134] and [143]-[144], and the noise is modeled as zero mean with unit variance in [134, 145] as we have assumed in this chapter.

[2]The details on how to calculate the MSE is given in Section 2.5.2.

$$
\begin{aligned}
&= \left(\left(\mathbf{U}_k^{UL}\right)^H \mathbf{H}_k^{UL}\mathbf{V}_k^{UL} - \mathbf{I}_{d_k^{UL}}\right)\left(\left(\mathbf{U}_k^{UL}\right)^H \mathbf{H}_k^{UL}\mathbf{V}_k^{UL} - \mathbf{I}_{d_k^{UL}}\right)^H \\
&\quad + \left(\mathbf{U}_k^{UL}\right)^H \mathbf{\Sigma}_k^{UL}\mathbf{U}_k^{UL}, \qquad (7.8)\\
\mathbf{MSE}_j^{DL} &= \mathbb{E}\left\{(\hat{\mathbf{s}}_j^{DL} - \mathbf{s}_j^{DL})(\hat{\mathbf{s}}_j^{DL} - \mathbf{s}_j^{DL})^H\right\} \\
&= \mathbb{E}\left\{\left(\left(\mathbf{U}_j^{DL}\right)^H \mathbf{y}_j^{DL} - \mathbf{s}_j^{DL}\right)\left(\left(\mathbf{U}_j^{DL}\right)^H \mathbf{y}_j^{DL} - \mathbf{s}_j^{DL}\right)^H\right\} \\
&= \left(\left(\mathbf{U}_j^{DL}\right)^H \mathbf{H}_j^{DL}\mathbf{V}_j^{DL} - \mathbf{I}_{d_j^{DL}}\right)\left(\left(\mathbf{U}_j^{DL}\right)^H \mathbf{H}_j^{DL}\mathbf{V}_j^{DL} - \mathbf{I}_{d_j^{DL}}\right)^H \\
&\quad + \left(\mathbf{U}_j^{DL}\right)^H \mathbf{\Sigma}_j^{DL}\mathbf{U}_j^{DL}. \qquad (7.9)
\end{aligned}
$$

In (7.8) and (7.9), $\mathbf{\Sigma}_k^{UL}$ and $\mathbf{\Sigma}_j^{DL}$ are the approximated aggregate interference-plus-noise terms[3] [4] at the $k$-th UL and $j$-th DL user, respectively, and are expressed as [139]

$$
\begin{aligned}
\mathbf{\Sigma}_k^{UL} &\approx \sum_{j\neq k}^{K} \mathbf{H}_j^{UL}\mathbf{V}_j^{UL}\left(\mathbf{V}_j^{UL}\right)^H\left(\mathbf{H}_j^{UL}\right)^H + \kappa\sum_{j=1}^{K}\mathbf{H}_j^{UL}\mathrm{diag}\left(\mathbf{V}_j^{UL}\left(\mathbf{V}_j^{UL}\right)^H\right)\left(\mathbf{H}_j^{UL}\right)^H \\
&+ \sum_{j=1}^{J}\mathbf{H}_0\left(\mathbf{V}_j^{DL}\left(\mathbf{V}_j^{DL}\right)^H + \kappa\mathrm{diag}\left(\mathbf{V}_j^{DL}\left(\mathbf{V}_j^{DL}\right)^H\right)\right)\mathbf{H}_0^H \\
&+ \beta\sum_{j=1}^{K}\mathrm{diag}\left(\mathbf{H}_j^{UL}\mathbf{V}_j^{UL}\left(\mathbf{V}_j^{UL}\right)^H\left(\mathbf{H}_j^{UL}\right)^H\right) + \beta\sum_{j=1}^{J}\mathrm{diag}\left(\mathbf{H}_0\mathbf{V}_j^{DL}\left(\mathbf{V}_j^{DL}\right)^H\mathbf{H}_0^H\right) \\
&+ \sigma_0^2\mathbf{I}_{N_0}, \qquad (7.10)\\
\mathbf{\Sigma}_j^{DL} &\approx \sum_{i\neq j}^{J}\mathbf{H}_j^{DL}\mathbf{V}_i^{DL}\left(\mathbf{V}_i^{DL}\right)^H\left(\mathbf{H}_j^{DL}\right)^H + \kappa\sum_{i=1}^{J}\mathbf{H}_j^{DL}\mathrm{diag}\left(\mathbf{V}_i^{DL}\left(\mathbf{V}_i^{DL}\right)^H\right)\left(\mathbf{H}_j^{DL}\right)^H \\
&+ \sum_{k=1}^{K}\mathbf{H}_{jk}^{DU}\left(\mathbf{V}_k^{UL}\left(\mathbf{V}_k^{UL}\right)^H + \kappa\mathrm{diag}\left(\mathbf{V}_k^{UL}\left(\mathbf{V}_k^{UL}\right)^H\right)\right)\left(\mathbf{H}_{jk}^{DU}\right)^H \\
&+ \beta\sum_{i=1}^{J}\mathrm{diag}\left(\mathbf{H}_j^{DL}\mathbf{V}_i^{DL}\left(\mathbf{V}_i^{DL}\right)^H\left(\mathbf{H}_j^{DL}\right)^H\right) + \beta\sum_{k=1}^{K}\mathrm{diag}\left(\mathbf{H}_{jk}^{DU}\mathbf{V}_k^{UL}\left(\mathbf{V}_k^{UL}\right)^H\left(\mathbf{H}_{jk}^{DU}\right)^H\right) \\
&+ \sigma_j^2\mathbf{I}_{N_j}. \qquad (7.11)
\end{aligned}
$$

Without loss of generality, we assume that there is only DL transmission over the considered frequency band in the primary network. Therefore, the power of the interference resulting from the secondary UL users and BS at the $l$-th PU equipped with $T_l$

[3] Note that $\mathbf{\Sigma}_k^{UL}$ and $\mathbf{\Sigma}_j^{DL}$ are approximated under $\kappa \ll 1$ and $\beta \ll 1$, which is a practical assumption [146, 139]. Therefore, the terms including the multiplication of $\kappa$ and $\beta$ are negligible, and have been ignored in the approximation.

[4] In practice, since the BS knows the codeword $\mathbf{x}_0$ (its own transmitted signal), and the self-interference channel $\mathbf{H}_0$, the term $\mathbf{H}_0\mathbf{x}_0$ can be canceled out in (7.2). In the following sections, we will keep this term merely to be able to use the simplification in the next subsection. However, in the performance simulations, this term will not be considered.

receive antennas can be written as

$$I_l^{PU} = \sum_{k=1}^{K} \mathrm{tr}\left\{\mathbf{G}_{lk}\left(\mathbf{V}_k^{UL}\left(\mathbf{V}_k^{UL}\right)^H + \kappa \mathrm{diag}\left(\mathbf{V}_k^{UL}\left(\mathbf{V}_k^{UL}\right)^H\right)\right)\mathbf{G}_{lk}^H\right\} + \sum_{j=1}^{J} \mathrm{tr}\left\{\mathbf{G}_l\left(\mathbf{V}_j^{DL}\left(\mathbf{V}_j^{DL}\right)^H + \kappa \mathrm{diag}\left(\mathbf{V}_j^{DL}\left(\mathbf{V}_j^{DL}\right)^H\right)\right)\mathbf{G}_l^H\right\}, \tag{7.12}$$

where $\mathbf{G}_{lk} \in \mathbb{C}^{T_l \times M_k}$ $\left(\mathbf{G}_l \in \mathbb{C}^{T_l \times M_0}\right)$ is the channel between the $l$-th PU and $k$-th UL user ($l$-th PU and the BS).

### 7.2.1 Joint beamforming design

In this chapter, we tackle the sum-MSE minimization problem, which is formulated as

$$\min_{\mathbf{V},\mathbf{U}} \quad \sum_{k=1}^{K} \mathrm{tr}\left\{\mathbf{MSE}_k^{UL}\right\} + \sum_{j=1}^{J} \mathrm{tr}\left\{\mathbf{MSE}_j^{DL}\right\} \tag{7.13}$$

$$\text{s.t.} \quad \mathrm{tr}\left\{\mathbf{V}_k^{UL}\left(\mathbf{V}_k^{UL}\right)^H\right\} \le P_k,\ k = 1, \ldots, K, \tag{7.14}$$

$$\sum_{j=1}^{J} \mathrm{tr}\left\{\mathbf{V}_j^{DL}\left(\mathbf{V}_j^{DL}\right)^H\right\} \le P_0, \tag{7.15}$$

$$I_l^{PU} \le \lambda_l,\ l = 1, \ldots, L, \tag{7.16}$$

where $P_k$ in (7.14) is the transmit power constraint at the $k$-th UL user, $P_0$ in (7.15) is the total power constraint at the BS, and $\lambda_l$ in (7.16) is the upper limit of the interference allowed to be imposed on the $l$-th PU. Here,

$$\mathbf{V} = \left\{\mathbf{V}_k^{UL},\ k = 1, \ldots, K,\ \mathbf{V}_j^{DL},\ j = 1, \ldots, J\right\}$$

and

$$\mathbf{U} = \left\{\mathbf{U}_k^{UL},\ k = 1, \ldots, K,\ \mathbf{U}_j^{DL},\ j = 1, \ldots, J\right\}$$

are the set of all transmit and receive beamforming matrices, respectively.

*Simplification of Notation:* To simplify the notation, we will combine UL and DL channels, similar to [31]. Let us use $\mathcal{S}^{UL}$ and $\mathcal{S}^{DL}$ to represent the set of $K$ UL and $J$ DL channels, respectively. Denoting $\mathbf{H}_{ij}$, $\mathbf{G}_{lj}$, $\mathbf{n}_i$ and receive (transmit) antenna

numbers $\tilde{N}_i\left(\tilde{M}_i\right)$ as

$$\begin{aligned}
\mathbf{H}_{ij} &= \begin{cases} \mathbf{H}_j^{UL},\, i \in \mathcal{S}^{UL},\ j \in \mathcal{S}^{UL}, \\ \mathbf{H}_0,\quad i \in \mathcal{S}^{UL},\ j \in \mathcal{S}^{DL}, \\ \mathbf{H}_{ij}^{DU},\, i \in \mathcal{S}^{DL},\ j \in \mathcal{S}^{UL}, \\ \mathbf{H}_i^{DL},\, i \in \mathcal{S}^{DL},\ j \in \mathcal{S}^{DL}, \end{cases} \\
\mathbf{G}_{lj} &= \begin{cases} \mathbf{G}_{lj},\quad j \in \mathcal{S}^{UL}, \\ \mathbf{G}_l,\quad j \in \mathcal{S}^{DL}, \end{cases} \\
\mathbf{n}_i &= \begin{cases} \mathbf{n}_0,\quad i \in \mathcal{S}^{UL}, \\ \mathbf{n}_i^{DL},\quad i \in \mathcal{S}^{DL}, \end{cases} \\
\tilde{N}_i\left(\tilde{M}_i\right) &= \begin{cases} N_0\left(M_i\right),\quad i \in \mathcal{S}^{UL}, \\ N_i\left(M_0\right),\quad i \in \mathcal{S}^{DL}, \end{cases}
\end{aligned}$$

and referring to $\mathbf{V}_i^X$, $\mathbf{U}_i^X$, $d_i^X$ and $\mathbf{\Sigma}_i^X$, $X \in \{UL, DL\}$ as $\mathbf{V}_i$, $\mathbf{U}_i$, $d_i$ and $\mathbf{\Sigma}_i$, respectively, the MSE of the $i$-th link, $i \in \mathcal{S} \triangleq \mathcal{S}^{UL} \bigcup \mathcal{S}^{DL}$ can be written as

$$\mathbf{MSE}_i = \left(\mathbf{U}_i^H \mathbf{H}_{ii} \mathbf{V}_i - \mathbf{I}_{d_i}\right)\left(\mathbf{U}_i^H \mathbf{H}_{ii} \mathbf{V}_i - \mathbf{I}_{d_i}\right)^H + \mathbf{U}_i^H \mathbf{\Sigma}_i \mathbf{U}_i, \tag{7.17}$$

where

$$\begin{aligned}
\mathbf{\Sigma}_i &= \sum_{j \in \mathcal{S}, j \neq i} \mathbf{H}_{ij} \mathbf{V}_j \mathbf{V}_j^H \mathbf{H}_{ij}^H + \kappa \sum_{j \in \mathcal{S}} \mathbf{H}_{ij} \mathrm{diag}\left(\mathbf{V}_j \mathbf{V}_j^H\right) \mathbf{H}_{ij}^H \, \beta \sum_{j \in \mathcal{S}} \mathrm{diag}\left(\mathbf{H}_{ij} \mathbf{V}_j \mathbf{V}_j^H \mathbf{H}_{ij}^H\right) \\
&+ \sigma_i^2 \mathbf{I}_{\tilde{N}_i},
\end{aligned} \tag{7.18}$$

and the interference power at the $l$-th PU, $I_l^{PU}$ in (7.12) can be rewritten as

$$I_l^{PU} = \sum_{j \in \mathcal{S}} \mathrm{tr}\left\{\mathbf{G}_{lj}\left(\mathbf{V}_j \mathbf{V}_j^H + \kappa \mathrm{diag}\left(\mathbf{V}_j \mathbf{V}_j^H\right)\right) \mathbf{G}_{lj}^H\right\}. \tag{7.19}$$

Using the simplified notation, the problem (7.13)-(7.16) can be rewritten as

$$\min_{\mathbf{V},\mathbf{U}} \quad \sum_{i \in \mathcal{S}} \mathrm{tr}\left\{\mathbf{MSE}_i\right\} \tag{7.20}$$

$$\text{s.t.} \quad \mathrm{tr}\left\{\mathbf{V}_i \mathbf{V}_i^H\right\} \leq P_i,\ i \in \mathcal{S}^{UL}, \tag{7.21}$$

$$\sum_{i\in\mathcal{S}^{DL}} \mathrm{tr}\left\{\mathbf{V}_i\mathbf{V}_i^H\right\} \le P_0, \tag{7.22}$$

$$I_l^{PU} \le \lambda_l,\ l=1,\ldots,L, \tag{7.23}$$

### 7.2.2 Imperfect CSI model

In this chapter, the CSI for both the channels in secondary network, and the channels between secondary and primary network are assumed to be imperfectly known. The imperfect CSI is modelled using a deterministic norm-bounded error model [134]-[135], which is expressed as

$$\mathbf{H}_{ij} \in \mathcal{H}_{ij} = \left\{\tilde{\mathbf{H}}_{ij} + \boldsymbol{\Delta_i} : \|\boldsymbol{\Delta_i}\|_F \le \delta_i,\ j\in\mathcal{S}\right\}, \tag{7.24}$$

$$\mathbf{G}_{lj} \in \mathcal{G}_{lj} = \left\{\tilde{\mathbf{G}}_{lj} + \boldsymbol{\Lambda_l} : \|\boldsymbol{\Lambda_l}\|_F \le \theta_l,\ j\in\mathcal{S}\right\}, \tag{7.25}$$

where $\tilde{\mathbf{H}}_{ij}$, $\tilde{\mathbf{G}}_{lj}$, and $\delta_i$, $\theta_l$ denote the nominal value of the CSI and uncertainty bounds, respectively.

Under channel uncertainties, the optimization problem (7.20)-(7.23) can be rewritten as

$$\min_{\mathbf{V},\mathbf{U}} \max_{\forall\mathbf{H}_{ij}\in\mathcal{H}_{ij}} \quad \sum_{i\in\mathcal{S}} \mathrm{tr}\left\{\mathbf{MSE}_i\right\} \tag{7.26}$$

$$\text{s.t.} \quad \mathrm{tr}\left\{\mathbf{V}_i\mathbf{V}_i^H\right\} \le P_i,\ i\in\mathcal{S}^{UL}, \tag{7.27}$$

$$\sum_{i\in\mathcal{S}^{DL}} \mathrm{tr}\left\{\mathbf{V}_i\mathbf{V}_i^H\right\} \le P_0, \tag{7.28}$$

$$I_l^{PU} \le \lambda_l,\ \forall\mathbf{G}_{lj}\in\mathcal{G}_{lj},\ l=1,\ldots,L. \tag{7.29}$$

Due to the constraint (7.29), the problem (7.26) is a semi-infinite program [147, Ch. 3], and we will derive an equivalent constraint in linear matrix inequality (LMI) form in Section 7.3, so that the problem (7.26) will turn into an equivalent SDP, which can be efficiently solved by standard interior point methods. Then, in an attempt to further reduce the complexity of the SDP algorithm, in Section 7.4, we will develop a cutting-set based algorithm to solve the non-convex problem (7.26).

## 7.3 Robust Transceiver Design based on SDP Method

Since the problem (7.26) is an intractable semi-infinite optimization problem [148], in the following, we will turn it into a tractable form. Using epigraph form and introducing slack variables $\tau_i$, the minimax problem (7.26) can be equivalently rewritten as the following minimization problem:

$$\min_{\mathbf{V},\mathbf{U},\boldsymbol{\tau}} \quad \sum_{i\in\mathcal{S}} \tau_i \tag{7.30}$$

$$\text{s.t.} \quad \operatorname{tr}\{\mathbf{MSE}_i\} \le \tau_i,\ \forall \mathbf{H}_{ij} \in \mathcal{H}_{ij},\ i \in \mathcal{S}, \tag{7.31}$$

$$\operatorname{tr}\left\{\mathbf{V}_i\mathbf{V}_i^H\right\} \le P_i,\ i \in \mathcal{S}^{UL}, \tag{7.32}$$

$$\sum_{i\in\mathcal{S}^{DL}} \operatorname{tr}\left\{\mathbf{V}_i\mathbf{V}_i^H\right\} \le P_0, \tag{7.33}$$

$$I_l^{PU} \le \lambda_l,\ \forall \mathbf{G}_{lj} \in \mathcal{G}_{lj},\ l = 1,\ldots,L, \tag{7.34}$$

where $\boldsymbol{\tau}$ is a stacked vector composed of $\tau_i,\ i \in \mathcal{S}$.

The problem (7.30) can be formulated as a standard SDP, which is defined as minimizing a linear objective under LMI constraints, which is a matrix constraint in the form of $\mathbf{A}(\mathbf{x}) \succeq \mathbf{0}$, where the matrix $\mathbf{A}$ depends linearly on $\mathbf{x}$. Thanks to this formulation, many well known algorithms for solving SDPs, for example, interior point methods [81] can be exploited to solve the optimization problem efficiently in polynomial time. To solve the optimization problem (7.30), we need to write $\operatorname{tr}\{\mathbf{MSE}_i\}$ and $I_l^{PU}$ in vector forms, the derivation of which are given in Appendix 7.C. Now, using the vector forms, the SDP formulation, equivalent to the problem (7.30) is expressed as below, the lengthy proof of which is relegated to Appendix 7.B.

$$\min_{\mathbf{V},\mathbf{U},\boldsymbol{\tau},\epsilon_i\ge 0,\eta_l\ge 0} \quad \sum_{i\in\mathcal{S}} \tau_i \tag{7.35}$$

$$\text{s.t.} \quad \begin{bmatrix} \tau_i - \epsilon_i & \tilde{\boldsymbol{\mu}}_i^H & \mathbf{0}_{1\times\tilde{N}_i\tilde{M}} \\ \tilde{\boldsymbol{\mu}}_i & \mathbf{I}_{A_i} & -\delta_i\mathbf{D}_{\Delta_i} \\ \mathbf{0}_{\tilde{N}_i\tilde{M}\times 1} & -\delta_i\mathbf{D}_{\Delta_i}^H & \epsilon_i\mathbf{I}_{\tilde{N}_i\tilde{M}} \end{bmatrix} \succeq 0,\ i \in \mathcal{S}, \tag{7.36}$$

$$\|\operatorname{vec}(\mathbf{V}_i)\|_2^2 \le P_i,\ i \in \mathcal{S}^{UL}, \tag{7.37}$$

$$\|\lfloor \operatorname{vec}(\mathbf{V}_i)\rfloor_{i\in\mathcal{S}^{DL}}\|_2^2 \le P_0, \tag{7.38}$$

$$\begin{bmatrix} \lambda_l - \eta_l & \tilde{\boldsymbol{\iota}}_l^H & \mathbf{0}_{1\times T_l\tilde{M}} \\ \tilde{\boldsymbol{\iota}}_l & \mathbf{I}_{B_l} & -\theta_l \mathbf{E}_{\Lambda_l} \\ \mathbf{0}_{T_l\tilde{M}\times 1} & -\theta_l \mathbf{E}_{\Lambda_l}^H & \eta_l \mathbf{I}_{T_l\tilde{M}} \end{bmatrix} \succeq 0,\ l=1,\ldots,L. \tag{7.39}$$

The variables $A_i$, $B_l$, $\tilde{\boldsymbol{\mu}}_i$, $\mathbf{D}_{\Delta_i}$, $\tilde{\boldsymbol{\iota}}_l$, and $\mathbf{E}_{\Lambda_l}$ are respectively defined as

$$A_i = d_i \left( \sum_{j\in\mathcal{S}} \left( d_j + \tilde{M}_j \right) + \tilde{N}_i \right) + \tilde{N}_i \sum_{j\in\mathcal{S}} d_j, \tag{7.40}$$

$$B_l = T_l \sum_{j\in\mathcal{S}} \left( d_j + \tilde{M}_j \right), \tag{7.41}$$

$$\tilde{\boldsymbol{\mu}}_i = \begin{bmatrix} \left(\mathbf{V}_i^T \otimes \mathbf{U}_i^H\right) \mathrm{vec}\left(\tilde{\mathbf{H}}_{ii}\right) - \mathrm{vec}\left(\mathbf{I}_{d_i}\right) \\ \left\lfloor \left(\mathbf{V}_j^T \otimes \mathbf{U}_i^H\right) \mathrm{vec}\left(\tilde{\mathbf{H}}_{ij}\right) \right\rfloor_{j\in\mathcal{S}, j\neq i} \\ \left\lfloor \left\lfloor \sqrt{\kappa} \left( (\boldsymbol{\Gamma}_\ell \mathbf{V}_j)^T \otimes \mathbf{U}_i^H \right) \mathrm{vec}\left(\tilde{\mathbf{H}}_{ij}\right) \right\rfloor_{\ell\in\mathcal{D}_j^{(T)}} \right\rfloor_{j\in\mathcal{S}} \\ \left\lfloor \left\lfloor \sqrt{\beta} \left( \mathbf{V}_j^T \otimes (\mathbf{U}_i^H \boldsymbol{\Gamma}_\ell) \right) \mathrm{vec}\left(\tilde{\mathbf{H}}_{ij}\right) \right\rfloor_{\ell\in\mathcal{D}_i^{(R)}} \right\rfloor_{j\in\mathcal{S}} \\ \sigma_i \mathrm{vec}\left(\mathbf{U}_i\right) \end{bmatrix}, \tag{7.42}$$

$$\boldsymbol{\mu}_{\Delta_i} = \underbrace{\begin{bmatrix} \left(\mathbf{V}_i^T \otimes \mathbf{U}_i^H\right) \\ \left\lfloor \left(\mathbf{V}_j^T \otimes \mathbf{U}_i^H\right) \right\rfloor_{j\in\mathcal{S}, j\neq i} \\ \left\lfloor \left\lfloor \sqrt{\kappa} \left( (\boldsymbol{\Gamma}_\ell \mathbf{V}_j)^T \otimes \mathbf{U}_i^H \right) \right\rfloor_{\ell\in\mathcal{D}_j^{(T)}} \right\rfloor_{j\in\mathcal{S}} \\ \left\lfloor \left\lfloor \sqrt{\beta} \left( \mathbf{V}_j^T \otimes (\mathbf{U}_i^H \boldsymbol{\Gamma}_\ell) \right) \right\rfloor_{\ell\in\mathcal{D}_i^{(R)}} \right\rfloor_{j\in\mathcal{S}} \\ \mathbf{0}_{d_i\tilde{N}_i \times \tilde{N}_i\tilde{M}} \end{bmatrix}}_{\mathbf{D}_{\Delta_i}} \mathrm{vec}\left(\boldsymbol{\Delta_i}\right), \tag{7.43}$$

$$\tilde{\boldsymbol{\iota}}_l = \begin{bmatrix} \left\lfloor \left(\mathbf{V}_j^T \otimes \mathbf{I}_{T_l}\right) \mathrm{vec}\left(\tilde{\mathbf{G}}_{lj}\right) \right\rfloor_{j\in\mathcal{S}} \\ \sqrt{\kappa} \left\lfloor \left\lfloor \left( (\boldsymbol{\Gamma}_\ell \mathbf{V}_j)^T \otimes \mathbf{I}_{T_l} \right) \mathrm{vec}\left(\tilde{\mathbf{G}}_{lj}\right) \right\rfloor_{\ell\in\mathcal{D}_j^{(T)}} \right\rfloor_{j\in\mathcal{S}} \end{bmatrix}, \tag{7.44}$$

$$\boldsymbol{\iota}_{\Lambda_l} = \underbrace{\begin{bmatrix} \left\lfloor \left(\mathbf{V}_j^T \otimes \mathbf{I}_{T_l}\right) \right\rfloor_{j\in\mathcal{S}} \\ \sqrt{\kappa} \left\lfloor \left\lfloor \left( (\boldsymbol{\Gamma}_\ell \mathbf{V}_j)^T \otimes \mathbf{I}_{T_l} \right) \right\rfloor_{\ell\in\mathcal{D}_j^{(T)}} \right\rfloor_{j\in\mathcal{S}} \end{bmatrix}}_{\mathbf{E}_{\Lambda_l}} \mathrm{vec}\left(\boldsymbol{\Lambda_l}\right). \tag{7.45}$$

As it can be seen from (7.36), the problem (7.35) does not hold a jointly convex

***Table 7.1:*** *Sum-MSE Minimization using SDP Algorithm*

| |
|---|
| 1) Set the iteration number $n = 0$ and initialize $\mathbf{V}^{[n]}$. |
| 2) $n \leftarrow n + 1$. Update $\mathbf{U}_i^{[n]},\ i \in \mathcal{S}$ by solving the convex SDP problem (7.35) under fixed $\mathbf{V}^{[n-1]}$. |
| 3) Update $\mathbf{V}_i^{[n]},\ i \in \mathcal{S}$ by solving the convex SDP (7.35) under fixed $\mathbf{U}^{[n]}$. |
| 4) Repeat steps 2 and 3 until convergence. |

structure over the optimization variables. Nevertheless it is a separately convex optimization problem over the transmit beamforming matrices $\mathbf{V}$, and the receiving beamforming matrices $\mathbf{U}$, once the other variables are fixed. This facilitates an alternating optimization algorithm where in each iteration the solution to (7.35) is calculated, as a convex optimization problem, assuming an alternatively fixed $\mathbf{V}$ or $\mathbf{U}$. The described optimization iterations continue until a stationary point is obtained, or a pre-defined number of iterations is reached. Please see Table 7.1 for a detailed algorithm description.

The proposed sum-MSE algorithm monotonically decreases the total MSE over each iteration by updating the transceivers in an alternating fashion. Also the fact that MSE is bounded below (at least by zero), it is quite obvious that the proposed sum-MSE minimization algorithm is convergent [149, 150]. However, the sum-MSE optimization problem is not jointly convex. Hence, the proposed algorithm is not guaranteed to converge to a global optimum point. As a result, it is important to select good initialization points to ensure a suboptimal solution with a good performance. For the simulations, we use right singular matrices as the initialization technique [151].

### 7.3.1 Computational complexity

In this subsection, the computational complexity of the proposed SDP method in Table 7.1 is discussed. The number of arithmetic operations required to solve a standard real-valued SDP problem

$$\min_{\mathbf{x}\in\mathcal{R}^n} \quad \mathbf{c}^T\mathbf{x} \tag{7.46}$$

$$\text{s.t.} \quad \mathbf{A}_0 + \sum_{i=1}^{n} x_i\mathbf{A}_i \succeq \mathbf{0}, \tag{7.47}$$

$$\|\mathbf{x}\|_2 \leq R, \tag{7.48}$$

***Table 7.2:*** *Complexity Parameters of SDP-based Method*

| | **Number of variables** ($n$) | **Dimension of blocks** ($a_i$) |
|---|---|---|
| $\mathbf{V}$ | $\sum_{i\in\mathcal{S}} 2\tilde{M}d_i + 2\lvert\mathcal{S}\rvert + L$ | $a_i = A_i + \tilde{N}_i\tilde{M} + 1,\ i \in \mathcal{S}$<br>$a_i = \tilde{M}d_i^{UL} + 1,\ i \in \mathcal{S}^{UL}$<br>$a_i = \tilde{M}\sum_{i\in\mathcal{S}^{DL}} d_i^{DL} + 1$<br>$a_l = B_l + T_l\tilde{M} + 1,\ l, \ldots, L$ |
| $\mathbf{U}_i$ | $2\tilde{N}_i d_i + 2$ | $a_i = A_i + \tilde{N}_i\tilde{M} + 1,\ i \in \mathcal{S}$ |

where $\mathbf{A}_i$ denotes the symmetric block-diagonal matrices with $P$ diagonal blocks of size $a_l \times a_l,\ l = 1, \ldots, P$, is upper-bounded by [148]

$$\mathcal{O}(1)\left(1 + \sum_{l=1}^{P} a_l\right)^{1/2} n\left(n^2 + n\sum_{l=1}^{P} a_l^2 + \sum_{l=1}^{P} a_l^3\right). \tag{7.49}$$

Since the proposed algorithm in Table 7.1 solves a SDP problem in Step 2 and Step 3, the number of arithmetic operations required to compute optimal $\mathbf{V}_i$ and $\mathbf{U}_i$ is calculated from (7.49) as follows. In computing $\mathbf{V}_i$, the number of diagonal blocks $P$ is equal to $|\mathcal{S}| + \left|\mathcal{S}^{UL}\right| + L + 1$. For the MSE constraint of each user, the dimension of blocks are $a_i = A_i + \tilde{N}_i\tilde{M} + 1,\ i \in \mathcal{S}$. For the UL SU power constraint, the dimension of the blocks are $a_i = \tilde{M}d_i^{UL} + 1,\ i \in \mathcal{S}^{UL}$. For the BS power constraint, the dimension of the block is $a_i = \tilde{M}\sum_{i\in\mathcal{S}^{DL}} d_i^{DL} + 1$, and for the PU interference constraint, the dimension of the blocks are $a_l = B_l + T_l\tilde{M} + 1,\ l, \ldots, L$. The unknown variables to be determined are of size $n = \sum_{i\in\mathcal{S}} 2\tilde{M}d_i + 2|\mathcal{S}| + L$, where the first term corresponds to the real and image parts of $\mathbf{V}_i$ and the other terms represent the additional slack variables. The calculation of the number of arithmetic operations required to compute $\mathbf{U}_i$ can be carried out similarly. The computational complexity parameters for solving the sum-MSE minimization problem using SDP method are given in Table 7.2. It is observed that when the number of users and transmit/receive antennas increase, the computational complexity of the SDP-based method can be unacceptably high.

### 7.3.2 CSI acquisition

We assume that the secondary BS has the knowledge of nominal channels and the radius of uncertainty regions. We undertake a centralized approach where the secondary BS coordinates the calibration of channel matrices, collects all channel matrices, computes the beamforming matrices based on the imperfect CSI, and then distributes them to the

SUs. The estimation of CSI matrices in the secondary network follows a similar strategy to that of traditional systems, as the secondary nodes cooperate with the secondary BS. This is performed via the exchange of the training sequences and feedback, and the application of usual CSI estimation methods [152]. On the other hand, it is more challenging to obtain an accurate estimate for the CSI between the secondary and primary networks, as the primary network is usually not willing to cooperate with the secondary network. In this regard, few methods have been suggested to combat this problem. Firstly, in case the primary system adopts the TDD scheme, the secondary network can obtain the CSI to the primary nodes by taking advantage of the channel reciprocity, and overhearing the transmissions from the primary network [152]-[153]. Secondly, a partial CSI can be obtained via blind environmental learning [154, 155]. Third, an estimate of CSI can be obtained via the realization of a *band manager* with the ability to exchange the CSI between the secondary and primary networks [156, 157, 158], and finally, if possible, the primary system can cooperate with the secondary network to exchange the channel estimates [152]. Of course, since the primary and secondary systems are not fully coordinated, the quality of these channel estimates will be degraded. Hence, we choose to model these imperfections by considering norm-bounded estimation errors for the links between the secondary transmitters and primary receivers. Note that after secondary network obtain the CSIs of the channels, they report them to the central scheduler to perform resource allocation/transceiver design in each time slot [159].

## 7.4 Robust Transceiver Design based on Cutting-Set Method

Although the SDP-based iterative design improves the system performance, it has a high computational complexity. In this section, we propose a low complexity algorithm, the cutting-set method [137], which provides a new way to deal with the channel uncertainties by separating CSI errors from the robust transceiver design problem. In particular, the original problem is solved through a two step alternating algorithm, namely transceiver design and worst-case channel determination steps. In the first step (transceiver design), the optimal beamforming matrices are computed under the assumption that the errors belong to a certain known uncertainty region (fixed set of CSI), whereas the second step (worst-case channel determination) computes the worst-case channel error matrices that maximize the constraint functions under the

assumption that transceiver beamforming matrices computed in the first step are fixed. In the following, we give both steps of the cutting-set algorithm in detail to solve the robust MSE-based optimization problem.

### 7.4.1 Transceiver design for fixed CSI

In the transceiver design step, a version of the semi-infinite problem is solved over finite subsets of the uncertainty regions. Assuming that the worst-case channels are given (fixed CSI), the optimal $\mathbf{V}_i$ and $\mathbf{U}_i$ are computed through solving the following optimization problem:

$$\min_{\mathbf{V},\mathbf{U},\boldsymbol{\tau}} \quad \sum_{i\in\mathcal{S}} \tau_i \tag{7.50}$$

$$\text{s.t.} \quad \|\boldsymbol{\mu}_i\|_2^2 \leq \tau_i,\ i \in \mathcal{S}, \tag{7.51}$$

$$\|\mathrm{vec}\,(\mathbf{V}_i)\|_2^2 \leq P_i,\ i \in \mathcal{S}^{UL}, \tag{7.52}$$

$$\|\lfloor \mathrm{vec}\,(\mathbf{V}_i)\rfloor_{i\in\mathcal{S}^{DL}}\|_2^2 \leq P_0, \tag{7.53}$$

$$\|\boldsymbol{\iota}_l\|_2^2 \leq \lambda_l,\ l = 1,\ldots,L. \tag{7.54}$$

Note that this problem is similar to the optimization problem (7.74) (without CSI errors) given in Appendix 7.B, and with straightforward manipulation, it is easy to show that the SDP formulation without CSI errors would reduce to the SOCP formulation. Hence, we can reformulate the problem (7.50) as a SOCP problem under fixed $\mathbf{V}$ or fixed $\mathbf{U}$ [79].

### 7.4.2 Worst-case channel determination for given transceivers

In the second step, worst-case analysis is carried out where channels that violate the constraints are determined and appended to the finite uncertainty subsets. For fixed transceiver beamforming matrices computed in the first step, the worst-case channels, which maximize the MSE and PU interference constraints given in (7.51) and (7.54), respectively, are computed in the bounded uncertainty regions. Note that under fixed transceiver beamforming matrices, the MSE and PU interference constraints are independent of each other with respect to the CSI errors. For a fixed transceiver design, the worst-case CSI errors that maximize the MSE of the $i$-th user can be obtained by

solving the following problem

$$\max_{\boldsymbol{\Delta_i}} \quad \mathrm{tr}\left\{\mathbf{MSE}_i\right\} \tag{7.55}$$

$$\text{s.t.} \quad \|\boldsymbol{\Delta_i}\|_F \leq \delta_i. \tag{7.56}$$

Since the objective function (7.55) is non-convex, the problem is intractable, and thus to simplify the computation, we adopt a first order approximation by neglecting all the terms that involve the second orders of CSI errors in (7.17). The approximation is expressed as

$$\begin{aligned}
\mathrm{tr}\left\{\mathbf{MSE}_i\right\} &\approx \mathrm{tr}\left\{\tilde{\mathbf{MSE}}_i\right\} + 2\Re\left\{\mathrm{tr}\left\{\mathbf{U}_i^H\boldsymbol{\Delta_i}\mathbf{V}_i\left(\mathbf{U}_i^H\tilde{\mathbf{H}}_{ii}\mathbf{V}_i - \mathbf{I}_{d_i}\right)^H\right\}\right\} \\
&+ \sum_{j\in\mathcal{S},j\neq i} 2\Re\left\{\mathrm{tr}\left\{\mathbf{U}_i^H\boldsymbol{\Delta_i}\mathbf{V}_j\mathbf{V}_j^H\tilde{\mathbf{H}}_{ij}^H\mathbf{U}_i\right\}\right\} \\
&+ \kappa\sum_{j\in\mathcal{S}} 2\Re\left\{\mathrm{tr}\left\{\mathbf{U}_i^H\boldsymbol{\Delta_i}\mathrm{diag}\left(\mathbf{V}_j\mathbf{V}_j^H\right)\tilde{\mathbf{H}}_{ij}^H\mathbf{U}_i\right\}\right\} \\
&+ \beta\sum_{j\in\mathcal{S}} 2\Re\left\{\mathrm{tr}\left\{\mathbf{V}_j\mathbf{V}_j^H\tilde{\mathbf{H}}_{ij}^H\mathrm{diag}\left(\mathbf{U}_i\mathbf{U}_i^H\right)\boldsymbol{\Delta_i}\right\}\right\} \\
&\overset{(a)}{=} \mathrm{tr}\left\{\tilde{\mathbf{MSE}}_i\right\} + 2\Re\left\{\mathrm{vec}^H\left(\mathbf{B}_i^H\right)\mathrm{vec}\left(\boldsymbol{\Delta_i}\right)\right\},
\end{aligned} \tag{7.57}$$

where $\mathrm{tr}\left\{\tilde{\mathbf{MSE}}_i\right\}$ is obtained by setting all CSI errors in (7.17) to zero, $(a)$ is obtained by using the identity $\mathrm{tr}\left\{\mathbf{AB}\right\} = \mathrm{vec}^H\left(\mathbf{A}^H\right)\mathrm{vec}\left(\mathbf{B}\right)$, and $\mathbf{B}_i$ is expressed as

$$\begin{aligned}
\mathbf{B}_i &= \mathbf{V}_i\left(\mathbf{U}_i^H\tilde{\mathbf{H}}_{ii}\mathbf{V}_i - \mathbf{I}_{d_i}\right)^H\mathbf{U}_i^H + \sum_{j\in\mathcal{S},j\neq i}\mathbf{V}_j\mathbf{V}_j^H\tilde{\mathbf{H}}_{ij}^H\mathbf{U}_i\mathbf{U}_i^H \\
&+ \kappa\sum_{j\in\mathcal{S}}\mathrm{diag}\left(\mathbf{V}_j\mathbf{V}_j^H\right)\tilde{\mathbf{H}}_{ij}^H\mathbf{U}_i\mathbf{U}_i^H + \beta\sum_{j\in\mathcal{S}}\mathbf{V}_j\mathbf{V}_j^H\tilde{\mathbf{H}}_{ij}^H\mathrm{diag}\left(\mathbf{U}_i\mathbf{U}_i^H\right).
\end{aligned} \tag{7.58}$$

Using Cauchy-Schwarz inequality in the approximate MSE expression in (7.57), the worst-case CSI errors corresponding to the MSE constraints are computed as (Please see Appendix 7.D for the complete derivation.)

$$\boldsymbol{\Delta_i} = \frac{\delta_i}{\|\mathrm{vec}\left(\mathbf{B}_i\right)\|_2}\mathbf{B}_i^H. \tag{7.59}$$

After computing the worst-case CSI errors, the corresponding worst-case channels can be written as $\mathbf{H}_{ij} = \tilde{\mathbf{H}}_{ij} + \boldsymbol{\Delta_i},\ j \in \mathcal{S}$. Note that since the worst-case CSI error in (7.59) is computed based on the approximation in (7.57), the MSE constraints in (7.51) may

be violated even if the corresponding worst-case channels are in the given uncertainty regions. However, this violation is negligible, since the effect of the second order terms of CSI errors on the performance are insignificant when the CSI error is small [160].

Next, we compute the worst-case CSI errors corresponding to the PU interference (7.34). Specifically, for a fixed transceiver matrices, the worst-case CSI errors that maximize the interference power at the $l$-th PU is computed by solving the following problem

$$\max_{\boldsymbol{\Lambda_l}} \quad I_l^{PU} \tag{7.60}$$

$$\text{s.t.} \quad \|\boldsymbol{\Lambda_l}\|_F \leq \theta_l, \tag{7.61}$$

which is, again, difficult to solve. Similar to (7.57), to simplify the analysis and computation, an approximation for (7.19) involving only the first-order errors (ignoring the second-order terms) is adopted, and the approximation is expressed as

$$\begin{aligned} I_l^{PU} &\approx \tilde{I}_l^{PU} + \sum_{j\in\mathcal{S}} 2\Re\left\{\text{tr}\left\{\boldsymbol{\Lambda_l}\mathbf{V}_j\mathbf{V}_j^H\tilde{\mathbf{G}}_{lj}^H\right\}\right\} + \kappa\sum_{j\in\mathcal{S}} 2\Re\left\{\text{tr}\left\{\boldsymbol{\Lambda_l}\text{diag}\left(\mathbf{V}_j\mathbf{V}_j^H\right)\tilde{\mathbf{G}}_{lj}^H\right\}\right\} \\ &= \tilde{I}_l^{PU} + 2\Re\left\{\text{vec}^H\left(\mathbf{C}_l^H\right)\text{vec}\left(\boldsymbol{\Lambda_l}\right)\right\}, \end{aligned} \tag{7.62}$$

where $\tilde{I}_l^{PU}$ is obtained by setting all CSI errors in (7.19) to zero, and $\mathbf{C}_l$ is defined as

$$\mathbf{C}_l = \sum_{j\in\mathcal{S}}\left(\mathbf{V}_j\mathbf{V}_j^H + \kappa\text{diag}\left(\mathbf{V}_j\mathbf{V}_j^H\right)\right)\tilde{\mathbf{G}}_{lj}^H. \tag{7.63}$$

Using Cauchy-Schwarz inequality in the approximate expression (7.62), the worst-case errors corresponding to the $l$-th PU interference are obtained similarly as that of (7.59) as

$$\boldsymbol{\Lambda_l} = \frac{\theta_l}{\|\text{vec}\left(\mathbf{C}_l\right)\|_2}\mathbf{C}_l^H. \tag{7.64}$$

The corresponding worst-case channels can be expressed as $\mathbf{G}_{lj} = \tilde{\mathbf{G}}_{lj} + \boldsymbol{\Lambda_l},\ j \in \mathcal{S}$.

### 7.4.3 Iterative algorithm for the robust design

The proposed cutting-set algorithm to solve the robust MSE-based problem involves a two-step algorithm alternating over transceiver design and worst-case channel determination steps described in the previous two subsections. The algorithm starts

***Table 7.3:*** *Sum-MSE Minimization using Cutting-Set Method*

| |
|---|
| 1) Set the iteration number $n = 0$ and initialize $\mathcal{H}^{[n]}$. |
| 2) Update $\mathbf{U}_i^{[n]}$ and $\mathbf{V}_i^{[n]}$ by solving the problem (7.50) with the given set $\mathcal{H}^{[n]}$ utilizing a similar iterative algorithm given in Table 7.1. |
| 3) Compute the worst-case channels, denoted as $\tilde{\mathcal{H}}_{[n]}$ using (7.59) and (7.64). |
| 4) Find the violating channels and append them to the set, i.e., $\mathcal{H}^{[n+1]} = \left\{\tilde{\mathcal{H}}_{[n]}, \mathcal{H}^{[n]}\right\}$. |
| 5) If the termination criterion is satisfied, then end. Otherwise, set $n \leftarrow n + 1$ and go to Step 2. |

with the set of channel matrices $\mathcal{H}$, which initially contains only the imperfect CSI $\tilde{\mathbf{H}}_{ij},\ \{i,j\} \in \mathcal{S}$ and $\tilde{\mathbf{G}}_{lj},\ j \in \mathcal{S},\ l = 1,\ldots,L$. In the first (transceiver design) step, the problem (7.50) is solved with all the given channels in the set $\mathcal{H}$ (the constraints should involve all the elements of $\mathcal{H}$).

In the worst-case channel determination step, the worst-case channels are obtained by solving the problems (7.55) and (7.60). If the resulting channels for all links, i.e., $\tilde{\mathbf{H}}_{ij} + \boldsymbol{\Delta}_{\boldsymbol{i}}$ and $\tilde{\mathbf{G}}_{lj} + \boldsymbol{\Lambda}_{\boldsymbol{l}}$ violate the constraints in (7.51) and/or (7.54) for the fixed transceiver matrices calculated in the previous step, these worst-channels are added to the set $\mathcal{H}$. The algorithm alternates between these two steps until it does not produce any violating channel, i.e., the maximum constraint violation is below a specified threshold. Note that during the worst-case channel determination step, the set $\mathcal{H}$ may be expanded (or remain the same) depending on the constraint violations. During the minimization step (first step), the precoder and receive beamforming matrices are computed to meet MSE and PU interference constraints for increasing number of worst-case channels in $\mathcal{H}$ (MSE and PU interference constraints must include all the channels in $\mathcal{H}$) resulting in increased robustness. Particularly, as the size of the set $\mathcal{H}$ increases, the number of effective constraints in the transceiver design problem increases.

It has been demonstrated in [137] that the iterative procedure can be terminated within a few iterations. When the worst-case analysis problem has an exact solution, the iterations of the cutting-set algorithm lead to the optimal solution, whereas the iterations lead to a suboptimal solution if the worst-case analysis makes use of approximations [137]. Due to the MSE and interference approximations in (7.57) and (7.62), respectively, the proposed iterative algorithm is not guaranteed to lead to the robust optimal solution, and generally leads to the locally optimal solution. The proposed algorithm is outlined in Table 7.3.

***Table 7.4:*** *Complexity Parameters of Cutting-Set Method*

| | **Number of variables** ($n$) | **Dimension of blocks** ($a_i$) |
|---|---|---|
| $\mathbf{V}$ | $\sum_{i\in\mathcal{S}} 2\tilde{M}d_i + \lvert\mathcal{S}\rvert$ | $a_i = A_i - \tilde{N}_i d_i,\ i \in \mathcal{S}$<br>$a_i = \tilde{M} d_i^{UL},\ i \in \mathcal{S}^{UL}$<br>$a_i = \tilde{M} \sum_{i\in\mathcal{S}^{DL}} d_i^{DL}$<br>$a_l = B_l,\ l, \ldots, L$ |
| $\mathbf{U}_i$ | $2\tilde{N}_i d_i + 1$ | $a_i = A_i,\ i \in \mathcal{S}$ |

### 7.4.4 Computational complexity

The computation complexity of the cutting-set method mainly depends on solving the SOCP problem (7.50), since the computation complexity to update the worst-case channels set is negligible. Consider the real-valued problem

$$\min_{\mathbf{x}\in\mathcal{R}^n} \quad \mathbf{c}^T\mathbf{x} \tag{7.65}$$

$$\text{s.t.} \quad \|\mathbf{A}_i\mathbf{x} + \mathbf{b}_i\| \leq \mathbf{c}_i^T\mathbf{x} + d_i,\ i = 1, \ldots, P, \tag{7.66}$$

$$\|\mathbf{x}\|_2 \leq R, \tag{7.67}$$

where $\mathbf{b}_i \in \mathcal{R}^{a_i}$. The number of elementary arithmetic operations necessary for solving this problem is upper-bounded by [148]

$$\mathcal{O}(1)(1+P)^{1/2} n \left(n^2 + P + \sum_{i=0}^{P} a_i^2\right). \tag{7.68}$$

The number of inequalities $P+1$ is equal to $|\mathcal{S}| + \left|\mathcal{S}^{UL}\right| + L + 1$. For the MSE constraint of each user, the dimension of blocks are $a_i = A_i - \tilde{N}_i d_i,\ i \in \mathcal{S}$. For the UL SU power constraint, the dimension of the blocks are $a_i = \tilde{M} d_i^{UL},\ i \in \mathcal{S}^{UL}$. For the BS power constraint, the dimension of the block is $a_i = \tilde{M} \sum_{i\in\mathcal{S}^{DL}} d_i^{DL}$, and for the PU interference constraint, the dimension of the blocks are $a_l = B_l,\ l, \ldots, L$. The unknown variables to be determined are of size $n = \sum_{i\in\mathcal{S}} 2\tilde{M}d_i + |\mathcal{S}|$. It is worth noting that the complexity of the other subproblems can be determined in a similar manner. Then, the complexity parameters for sum-MSE minimization problem based on cutting-set method is given in Table 7.4. Compared to the analytical results in Table 7.2, the computational complexity of the cutting-set method in each iteration has much lower complexity than that of the SDP-based method.

## 7.5 Numerical Results

In this section, we numerically investigate the sum-MSE minimization problem for a FD MIMO cognitive cellular system. We start by comparing the sum MSE performance of the two algorithms, proposed in the chapter as a function of transmitter/receiver distortion, $\kappa/\beta$ and channel uncertainty size, $\delta/\theta$. We then analyze the sum-rate performance of the FD system as a function of the number of antennas $\tilde{N}$, transmitter/receiver distortion, $\kappa/\beta$, channel uncertainty size, $\delta/\theta$ and CCI attenuation factor[5], $\nu$. The tolerance (the difference between MSE of two iterations) of the proposed iterative algorithm is set to $10^{-4}$, the maximum number of iterations is set to 50, and the results are averaged over 100 independent channel realizations. Since the optimization problems we are dealing with are non-convex, we need to choose good initialization points to have a suboptimal solution with good performance. In this chapter, we use right singular matrices initialization [151].

We consider small cell deployments [161] and compare the FD system with the HD system under the 3GPP LTE specifications. Small cell is considered to be suitable for deployment of FD technology due to its low transmit power, short transmission distances and low mobility [30, 162]. We consider a single hexagonal cell consisting of a BS in the center with $M_0$ transmit and $N_0$ receive antennas. $K = 2$ UL and $J = 2$ DL users equipped with $N$ antennas randomly distributed in the cell[6]. For simplicity, we assume $M_0 = N_0 = N = \tilde{N}$. The CR system has $L = 2$ PUs, with the same maximum allowed interfering power (i.e., $\lambda_l = 0$dB).

The channel between BS and users (both SUs and PUs) are assumed to experience the path loss model for line-of-sight (LOS), and the channel between UL and DL users are assumed to experience the path loss model for non-line-of-sight (NLOS) communications. Detailed simulation parameters are shown in Table 7.5.

[5]It is important to note that while the channel matrices are assumed to be given for each user, it is essential for a practical system to exploit a smart channel assignment algorithm prior to precoder/decoder design. This is particularly essential for a FD setup as the CCI can be reduced by assigning the users with weaker interference paths into the same channel. In order to incorporate the effect of channel assignment into our simulation, we assume an attenuation coefficient, namely $\nu$, on the CCI channels, which represent the degree of isolation among UL and DL users due to channel assignment.

[6]Although the BS has $N_0 + M_0$ antennas in total, we assume that only $M_0$ ($N_0$) antennas can be used for transmission (reception) in HD mode. This assumption is similar to [31]. The reason is that in practical systems RF front-ends are scarce resources, since they are much more expensive than antennas. Therefore, we assume that BS only has $M_0$ transmission front-ends and $N_0$ receiving front-ends, and do not carry out antenna partitioning.

***Table 7.5:*** *Simulation Parameters*

| **Parameter** | **Settings** |
|---|---|
| Cell Radius | 40m |
| Carrier Frequency | 2GHz |
| Bandwidth | 10MHz |
| Thermal Noise Density | $-174$dBm/Hz |
| Noise Figure | BS: 13dB, User: 9dB |
| Path Loss (dB) between BS and users ($d$ in km) | $103.8 + 20.9 \log_{10} d$ |
| Path Loss (dB) between users ($d$ in km) | $145.4 + 37.5 \log_{10} d$ |
| Shadowing Standard Deviation | LOS: 3dB, NLOS: 4dB |

The estimated channel gain between the BS to $k$th UL user is given by $\tilde{\mathbf{H}}_k^{UL} = \sqrt{\kappa_k^{UL}}\hat{\mathbf{H}}_k^{UL}$, where $\hat{\mathbf{H}}_k^{UL}$ denotes the small scale fading following a complex Gaussian distribution with zero mean and unit variance, and $\kappa_k^{UL} = 10^{(-\mathrm{X}/10)},\ X \in \{\mathrm{LOS}, \mathrm{NLOS}\}$ represents the large scale fading consisting of path loss and shadowing, where LOS and NLOS are calculated from a specific path loss model given in Table 7.5. The channels between BS and DL users, between UL users and DL users, between BS and PUs, and between UL users and PUs are defined similarly. We adopt the Rician model in [163], in which the self-interference channel is distributed as $\tilde{\mathbf{H}}_0 \sim \mathcal{CN}\left(\sqrt{\frac{K_R}{1+K_R}}\hat{\mathbf{H}}_0, \frac{1}{1+K_R}\mathbf{I}_{N_0} \otimes \mathbf{I}_{M_0}\right)$, where $K_R$ is the Rician factor, and $\hat{\mathbf{H}}_0$ is a deterministic matrix[7]. Unless stated otherwise, we consider, $\tilde{N} = 2,\ \kappa = \beta = -70$dB, $\nu = 0.5$ and $\delta = \theta = 0.1$.

Fig. 7.2 shows the evolution of the proposed algorithms, i.e., the convergence of the algorithms in Table 7.1 and Table 7.3. The monotonic decrease of the sum-MSE can be verified, and is seen that the cutting set algorithm converges more rapidly than SDP.

After establishing the convergence of the two algorithms, we now present a thorough comparison of the SDP and cutting-set methods in terms of computational complexity (complex multiplications) and CPU time (time in secs required for convergence)/iteration number (number of iterations required to converge) in Fig. 7.3a and Fig. 7.3b, respectively with respect to different number of antennas. Similarly, in Fig. 7.4a and Fig. 7.4b, computational complexity and CPU time/iteration number are plotted with respect to different number of users for the two algorithms, respec-

[7]Similar to [30], without loss of generality, we set $K_R = 1$ and $\tilde{\mathbf{H}}_0$ to be the matrix of all ones for all experiments.

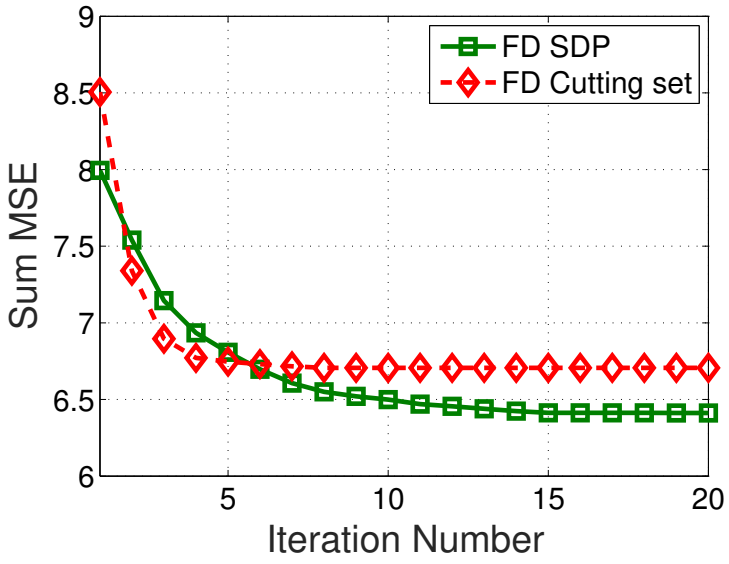


***Figure 7.2:*** *Convergence behavior of the proposed algorithms.*

tively.[8] Note that in Fig. 7.3b and Fig. 7.4b, the bar plots represent the CPU time and lines represent the number of iterations. As expected, cutting-set algorithm always has the lowest complexity and requires less computational time than SDP, especially at high number of antennas and users, which is inline with our computational complexity analysis in Table 7.2 and 7.4.

We now compare the proposed SDP and cutting set algorithms in terms of sum-MSE performance for different $\kappa = \beta$ values in Fig. 7.5. From the figure, it can be seen that the cutting set algorithm performs as well as the SDP based one with a nominal performance gap. This loss in performance is well compensated from the computational point of view as the cutting set based method provides affordable computational complexity with respect to its SDP counterpart. Hence, the cutting set method can be considered as a good alternative to the SDP method, which offers a decent trade-off between performance and computational complexity.

To further highlight the similarities between the two algorithms, in Fig. 7.6, we compare both SDP and cutting set in terms of sum-MSE performance for various channel uncertainty sizes. When the size of the channel uncertainty is low, the performance of both the algorithms are quite similar, whereas with an increase in $\delta = \theta$ values, the performance gap between the two algorithm increases. The reason is that cutting-set

[8]For system guidelines we note that, the proposed algorithms are evaluated centrally using MATLAB R20015a on a Linux server with Intel Xeon processor (16 cores, each clocked at 2 GHz) and 31.4 GiB of memory.

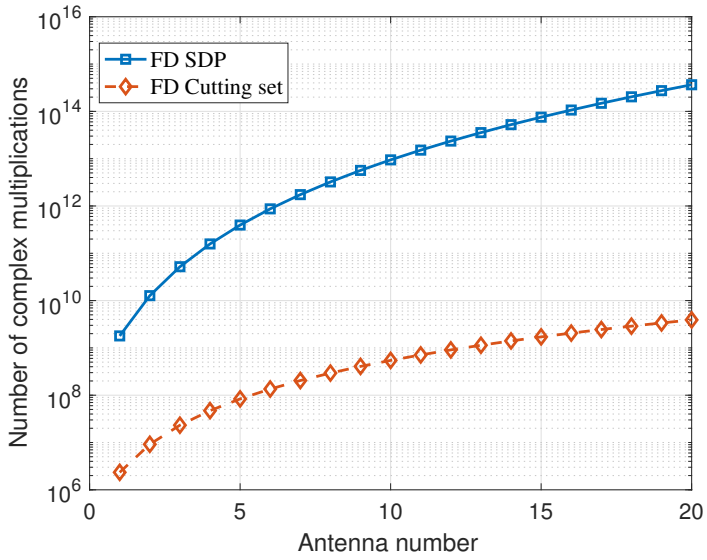


**(a)** Complexity comparison.

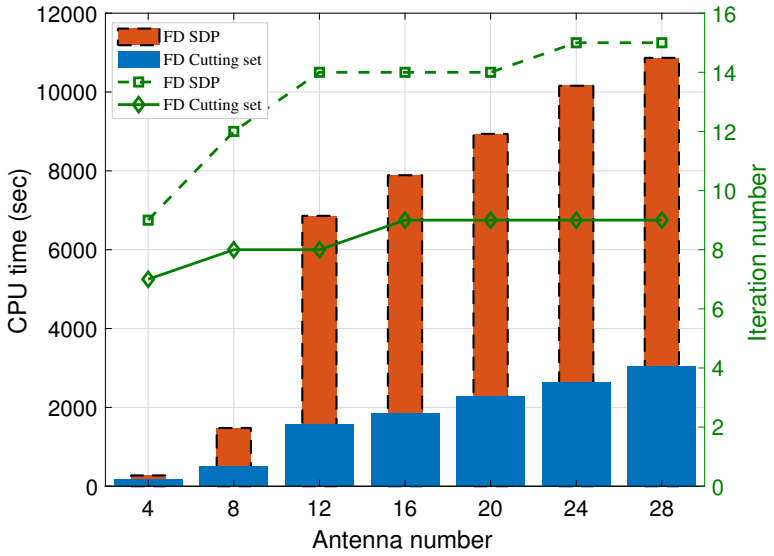


**(b)** CPU time and iteration number comparisons.

***Figure 7.3:*** *Complexity, CPU time and iteration number comparisons of SDP and cutting-set algorithm systems with respect to different number of antennas. In (a), 3 UL, 3 DL, 2 PU equipped with 3 antennas, and $d = 2$ data stream transmission is assumed.*

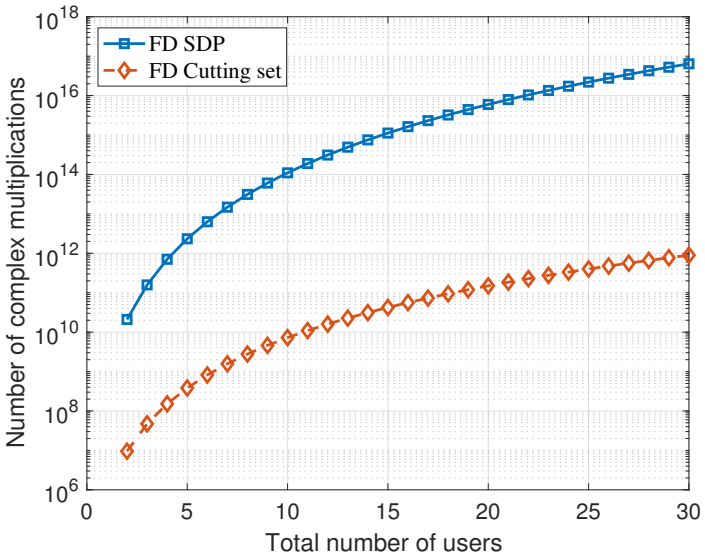


**(a)** Complexity comparison.

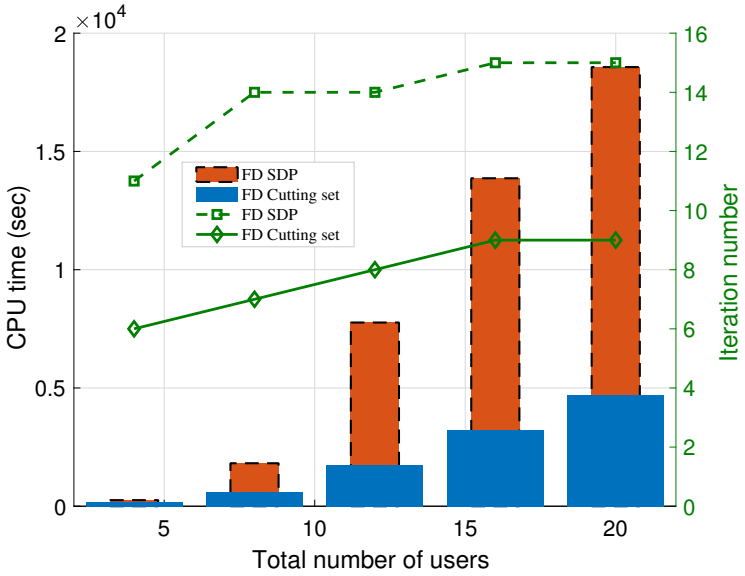


**(b)** CPU time and iteration number comparisons.

***Figure 7.4:*** *Complexity, CPU time and iteration number comparisons of SDP and cutting-set algorithm systems with respect to different number of users. In (a), 4 transmit/receive antennas, 2 PU equipped with 3 antennas, and $d = 2$ data stream transmission is assumed.*

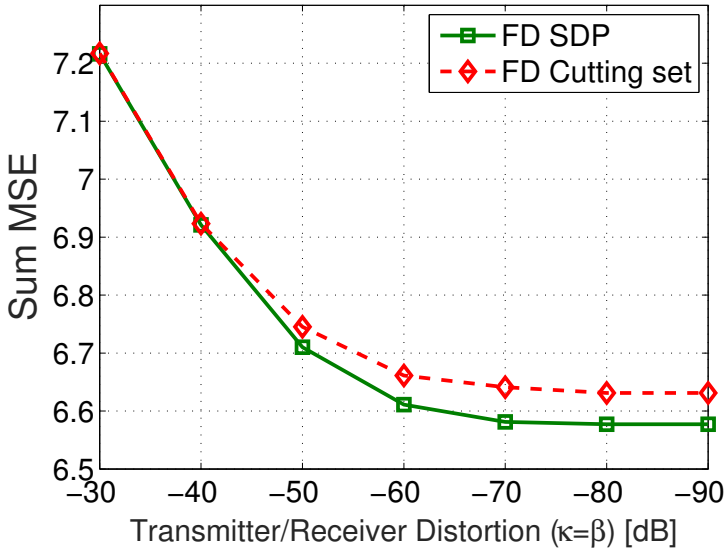


***Figure 7.5:*** *Sum-MSE comparison of SDP and cutting-set algorithms for an FD system with respect to transmitter/receiver distortion, i.e., $\kappa$, $\beta$.*

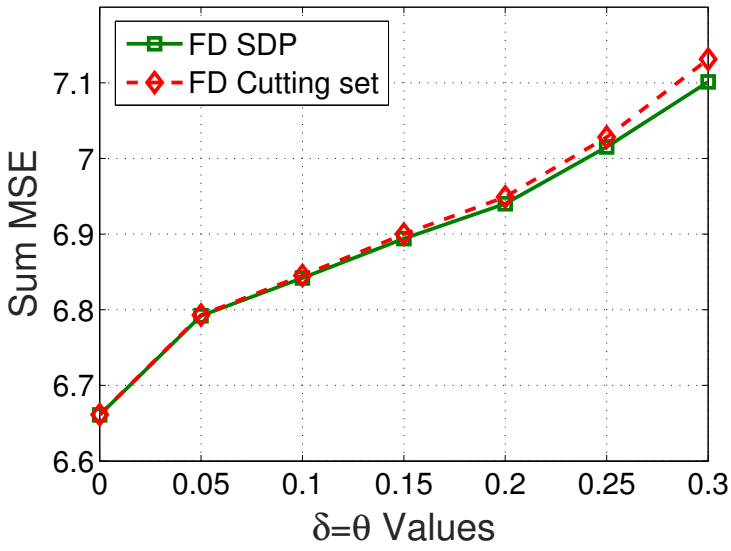


***Figure 7.6:*** *Sum-MSE comparison of SDP and cutting-set algorithms for an FD system with respect to channel uncertainty, $\delta = \theta$. Here, $\kappa = \beta = -40dB$.*

algorithm is derived based on the approximations given in (7.57) and (7.62), where the second-order CSI errors are ignored. But as the channel uncertainty size increases, the effect of second-order CSI errors become more apparent.

In our next example, we show the complementary cumulative distribution (CCD) of the total interference power from the secondary users to the primary users, i.e.,

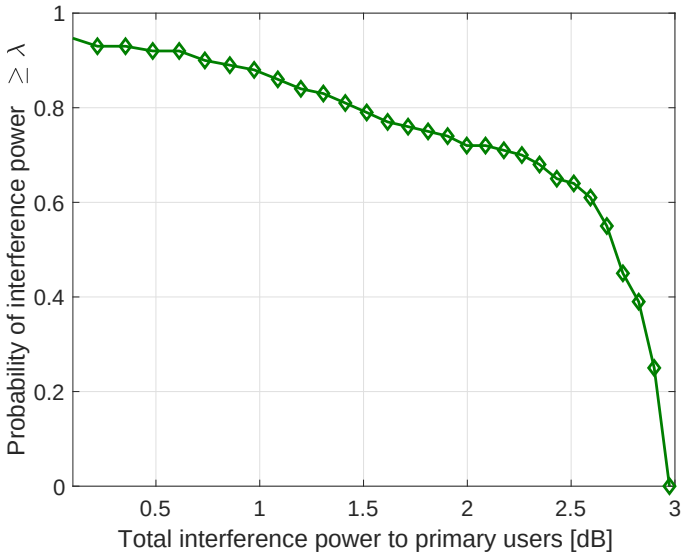


***Figure 7.7:*** *Probability of interference power from secondary to primary network with respect to the maximum allowed total interfering power, $\lambda$.*

$\mathbb{P}[I^{PU} \geq \lambda]$, where $I^{PU} = \sum_{l=1}^{L} I_l^{PU}$ and $\lambda = \sum_{l=1}^{L} \lambda_l$. Here, the precoders/decoders are designed based on the SDP based algorithm. It can be seen from Fig. 7.7 that the probability of total interference power from the secondary network to the PUs is zero when it is higher than $\lambda = 3$dB, which is the maximum allowed total interfering power (considering 2 PUs, with each allowing 0dB interference). This is in conjunction to constraint (7.34), which ensures that the interference to the primary users is always kept below or equal to the maximum allowed total interfering power. While achieving the equality condition in (7.34) will ensure maximum sum rate for the secondary users, the proposed algorithm mainly operates below the maximum allowed interfering power to protect the primary users, but still satisfying the required quality of service of the secondary users. Moreover, the area under the CCD curve can be contemplated as the region, under which the proposed algorithm is always feasible.

Hereinafter, we will compare FD with HD systems in terms of sum-rate performance as a function of $\kappa = \beta$ values for different numbers of antennas based on the SDP algorithm (We haven't included the performance of the cutting-set algorithm hereinafter, since we have observed both SDP and cutting-set algorithms give very similar performance). The sum-rate of the MIMO FD cellular system can be expressed as

$$I_{sum} = \sum_{i \in \mathcal{S}} \sum_{k=1}^{d_i} \log_2 \left(1 + \mathrm{SINR}_{i_k}\right), \tag{7.69}$$

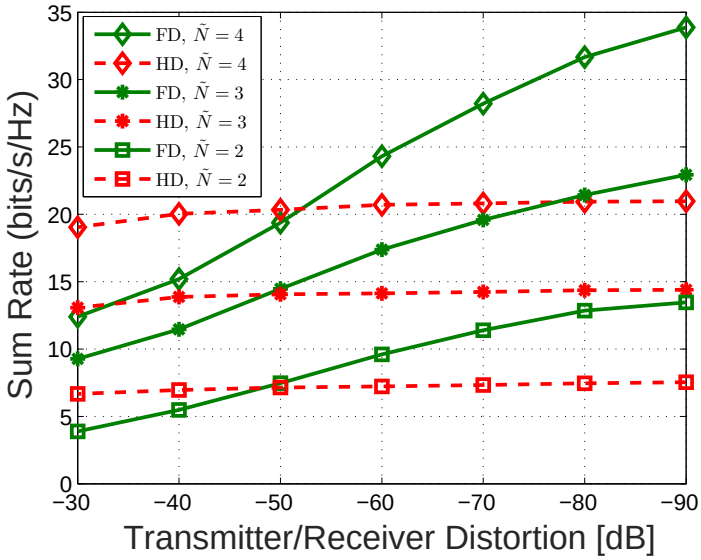


***Figure 7.8:*** *Sum-rate comparison of FD and HD systems with respect to transmitter/receiver distortion, i.e., $\kappa$, $\beta$. Here, $\kappa = \beta$.*

where $\text{SINR}_{i_k}$ is the SINR of the $k$-th stream of user $i$ and can be given as defined in Section 2.5.2 as

$$\text{SINR}_{i_k} = \frac{1}{\text{MSE}_{i_k}} - 1. \tag{7.70}$$

In (7.70), $\mathbf{u}_{i_k}$ and $\mathbf{v}_{i_k}$ are the $k$-th column of $\mathbf{U}_i$, and $\mathbf{V}_i$, respectively. As seen in Fig. 7.8, the performance of HD system is not affected with $\kappa$ and $\beta$ values, and at high self-interference cancellation levels, FD system achieves around 1.6 times more sum-rate than that of HD. However, at low self-interference cancellation levels (below around $\kappa = \beta = -55$dB), the distortion is magnified with the increasing number of antennas and the performance of FD system drops below that of HD scheme.

In Fig. 7.9, the importance of the smart channel assignment, as a stage prior to the precoder/decoder design is depicted for the SDP algorithm. The CCI attenuation represents the provided isolation among the UL and DL users. It is seen that as the suppression level of CCI increases, the FD system starts outperforming the HD system, and thus isolation among the UL and DL users is essential for a successful coexistence of UL and DL users in a FD setup.

In Fig. 7.10, we compare FD with HD systems in terms of sum-rate performance for different $\kappa = \beta$ values as a function of $\delta = \theta$ based on the SDP algorithm. From the figure, it can be seen that the performance of both the FD and HD systems degrades as

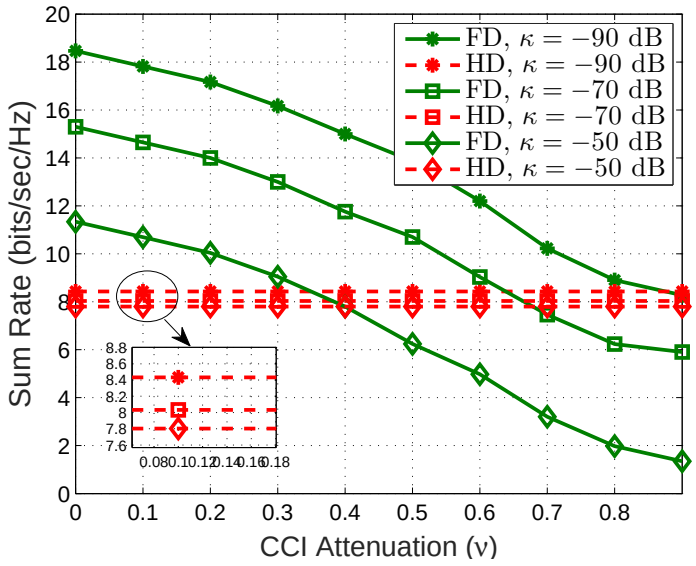


***Figure 7.9:*** *Sum-rate comparison of FD and HD systems with respect to CCI attenuation factor, i.e., $\nu$.*

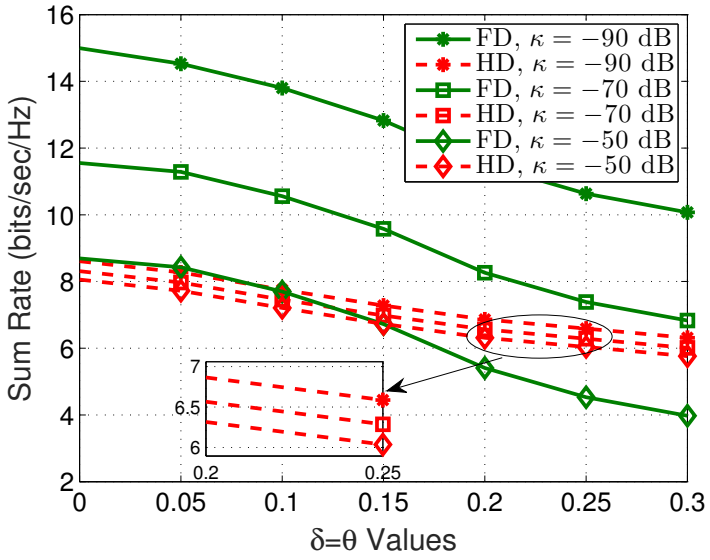


***Figure 7.10:*** *Sum-rate comparison of FD and HD systems with respect to channel uncertainty, $\delta = \theta$.*

the size of the uncertainty region increases. However, the FD system suffers more as a result of that and the gap between the FD and HD system decreases. But, if the channel uncertainty is nominal along with a low distortion level (around -70 dB), FD systems achieve around 1.4 times more sum-rate than that of HD systems. This degradation in performance of the FD system is explained as follows. Since there are more interference

channels (self-interference and CCI) in FD systems, as the uncertainty level of the channels increases, the system performance of the FD system degrades more. This indicates that the channel estimation is a critical factor for successful deployment of FD systems.

## 7.6 Summary

In this chapter, we have studied the robust MSE-based transceiver design problem for a FD MIMO cognitive cellular system that suffers from self-interference and CCI under the limited DR at the transmitters and receivers, and norm-bounded channel uncertainties. Since the globally optimal solution is difficult to obtain due to the non-convex nature of the problems, an alternating SDP-based algorithm that iterates between transmit and receiving beamforming matrices while keeping the other fixed is first proposed. Second, an efficient cutting-set method was proposed to solve the original complicated problems by applying an alternating sequence of transceiver design and channel determination steps. As simulation results demonstrate, compared to the SDP-based method, the cutting-set method achieves a similar performance with a lower computational complexity. Moreover, it has been shown in simulations that the sum-rate achieved by FD system is higher than that of HD system under reasonable self-interference cancellation and/or CCI attenuation values.

Furthermore, in this chapter, sophisticated transmit and receive filters were used to cancel the self interference. However, the advent of massive MIMO systems has opened up possibilities to suppress the self interference to the desired 110dB by simply leveraging the excess antennas used in a large MIMO antenna array. Accordingly, discussion on designs of simple precoders/detectors to cancel the self interference at the BS are provided in the following chapter.

## Appendix 7.A Useful Lemmas

**Lemma 7.1.** *[164] Given matrices* $\mathbf{P}$, $\mathbf{Q}$, $\mathbf{A}$ *with* $\mathbf{A} = \mathbf{A}^H$, *the semi-infinite LMI of the form of*

$$\mathbf{A} \succeq \mathbf{P}^H \mathbf{X} \mathbf{Q} + \mathbf{Q}^H \mathbf{X}^H \mathbf{P}, \qquad \forall \mathbf{X} : \|\mathbf{X}\|_F \leq \rho,$$

*holds if and only if* $\exists \epsilon \geq 0$ *such that*

$$\begin{bmatrix} \mathbf{A} - \epsilon \mathbf{Q}^H \mathbf{Q} & -\rho \mathbf{P}^H \\ -\rho \mathbf{P} & \epsilon \mathbf{I} \end{bmatrix} \succeq 0. \tag{7.71}$$

**Lemma 7.2.** *Schur Complement Lemma [81]: Let* $\mathbf{Q}$ *and* $\mathbf{R}$ *be symmetric matrices. Then the following two expressions are equivalent.*

$$\begin{bmatrix} \mathbf{Q} & \mathbf{S} \\ \mathbf{S}^* & \mathbf{R} \end{bmatrix} \succeq \mathbf{0} \quad \triangleq \quad \mathbf{R} \succeq \mathbf{0},\ \mathbf{Q} - \mathbf{S}\mathbf{R}^{-1}\mathbf{S}^* \succeq \mathbf{0}.$$

# Appendix 7.B Problem Reformulation

To solve the optimization problem (7.30), we first write it in a more compact form for ease of exposition. To that end, we write $\text{tr}\{\mathbf{MSE}_i\}$ and $I_l^{PU}$ in vector forms. As shown in Appendix 7.C, the vector forms of $\text{tr}\{\mathbf{MSE}_i\}$ and $I_l^{PU}$ can be written as $\text{tr}\{\mathbf{MSE}_i\} = \|\boldsymbol{\mu}_i\|_2^2$ and $I_l^{PU} = \|\boldsymbol{\iota}_l\|_2^2$, where $\boldsymbol{\mu}_i$ and $\boldsymbol{\iota}_l$ are given as

$$\boldsymbol{\mu}_i = \begin{bmatrix} \left(\mathbf{V}_i^T \otimes \mathbf{U}_i^H\right) \text{vec}\left(\mathbf{H}_{ii}\right) - \text{vec}\left(\mathbf{I}_{d_i}\right) \\ \left\lfloor \left(\mathbf{V}_j^T \otimes \mathbf{U}_i^H\right) \text{vec}\left(\mathbf{H}_{ij}\right) \right\rfloor_{j\in\mathcal{S}, j\neq i} \\ \left\lfloor \left\lfloor \sqrt{\kappa} \left((\boldsymbol{\Gamma}_\ell \mathbf{V}_j)^T \otimes \mathbf{U}_i^H\right) \text{vec}\left(\mathbf{H}_{ij}\right) \right\rfloor_{\ell \in \mathcal{D}_j^{(T)}} \right\rfloor_{j\in\mathcal{S}} \\ \left\lfloor \left\lfloor \sqrt{\beta} \left(\mathbf{V}_j^T \otimes (\mathbf{U}_i^H \boldsymbol{\Gamma}_\ell)\right) \text{vec}\left(\mathbf{H}_{ij}\right) \right\rfloor_{\ell \in \mathcal{D}_i^{(R)}} \right\rfloor_{j\in\mathcal{S}} \\ \sigma_i \text{vec}\left(\mathbf{U}_i\right) \end{bmatrix} \tag{7.72}$$

$$\boldsymbol{\iota}_l = \begin{bmatrix} \left\lfloor \left(\mathbf{V}_j^T \otimes \mathbf{I}_{T_l}\right) \text{vec}\left(\mathbf{G}_{lj}\right) \right\rfloor_{j\in\mathcal{S}} \\ \sqrt{\kappa} \left\lfloor \left\lfloor \left((\boldsymbol{\Gamma}_\ell \mathbf{V}_j)^T \otimes \mathbf{I}_{T_l}\right) \text{vec}\left(\mathbf{G}_{lj}\right) \right\rfloor_{\ell \in \mathcal{D}_j^{(T)}} \right\rfloor_{j\in\mathcal{S}} \end{bmatrix}, \tag{7.73}$$

where $\mathcal{D}_j^{(R)}$ represents the set $\{1 \cdots \tilde{N}_j\}$, $\mathcal{D}_j^{(T)}$ represents the set $\{1 \cdots \tilde{M}_j\}$ and $\boldsymbol{\Gamma}_\ell$ is a square matrix with zero elements, except for the $\ell$-th diagonal element, equal to 1. Using the vector forms (7.72) and (7.73), the problem (7.30) can be rewritten as

$$\min_{\mathbf{V},\mathbf{U},\boldsymbol{\tau}} \quad \sum_{i\in\mathcal{S}} \tau_i \tag{7.74}$$

$$\text{s.t.} \quad \|\boldsymbol{\mu}_i\|_2^2 \leq \tau_i,\ \|\boldsymbol{\Delta}_i\|_F \leq \delta_i,\ i \in \mathcal{S}, \tag{7.75}$$

$$\|\text{vec}\left(\mathbf{V}_i\right)\|_2^2 \leq P_i,\ i \in \mathcal{S}^{UL}, \tag{7.76}$$

$$\|\left\lfloor \text{vec}\left(\mathbf{V}_i\right) \right\rfloor_{i\in\mathcal{S}^{DL}}\|_2^2 \leq P_0, \tag{7.77}$$

$$\|\boldsymbol{\iota}_l\|_2^2 \leq \lambda_l,\ \|\boldsymbol{\Lambda_l}\|_F \leq \theta_l,\ l = 1, \ldots, L. \tag{7.78}$$

Semi-infinite optimization problems can be formulated in terms of LMIs. Such a reduction, if possible, has important practical consequences: It means that those semi-infinite problems can be solved efficiently with interior-point methods for LMI problems [81]. Note that the constraints (7.75) and (7.78) are not in the form of an LMI because the optimization variables do not appear linearly in these constraints. To recast the semi-infinite problem (7.74) as a SDP problem, the Schur complement lemma given in Lemma 7.2 is used to rewrite the constraints (7.75) and (7.78) in LMI form. Accordingly, the resulting optimization problem is written as

$$\min_{\mathbf{V},\mathbf{U},\boldsymbol{\tau}} \quad \sum_{i\in\mathcal{S}} \tau_i \tag{7.79}$$

$$\text{s.t.} \quad \begin{bmatrix} \tau_i & \boldsymbol{\mu}_i^H \\ \boldsymbol{\mu}_i & \mathbf{I}_{A_i} \end{bmatrix} \succeq 0,\ \|\boldsymbol{\Delta_i}\|_F \leq \delta_i,\ i \in \mathcal{S}, \tag{7.80}$$

$$\|\mathrm{vec}\,(\mathbf{V}_i)\|_2^2 \leq P_i,\ i \in \mathcal{S}^{UL}, \tag{7.81}$$

$$\|\lfloor \mathrm{vec}\,(\mathbf{V}_i)\rfloor_{i\in\mathcal{S}^{DL}}\|_2^2 \leq P_0, \tag{7.82}$$

$$\begin{bmatrix} \lambda_l & \boldsymbol{\iota}_l^H \\ \boldsymbol{\iota}_l & \mathbf{I}_{B_l} \end{bmatrix} \succeq 0,\ \|\boldsymbol{\Lambda_l}\|_F \leq \theta_l,\ l = 1, \ldots, L, \tag{7.83}$$

where the dimensions of the identity matrices in (7.80) and (7.83) are given, respectively, as

$$A_i = d_i \left( \sum_{j\in\mathcal{S}} \left( d_j + \tilde{M}_j \right) + \tilde{N}_i \right) + \tilde{N}_i \sum_{j\in\mathcal{S}} d_j, \tag{7.84}$$

$$B_l = T_l \sum_{j\in\mathcal{S}} \left( d_j + \tilde{M}_j \right). \tag{7.85}$$

To further simplify the problem (7.79) , Lemma 7.1 is used to relax the semi-infiniteness of the constraints (7.80) and (7.83).

However, to apply Lemma 7.1, we need to separate the estimated channel and the channel estimation error. To this end, the LMI in (7.80) is first expressed as

$$\begin{bmatrix} \tau_i & \tilde{\boldsymbol{\mu}}_i^H \\ \tilde{\boldsymbol{\mu}}_i & \mathbf{I}_{A_i} \end{bmatrix} + \begin{bmatrix} 0 & \boldsymbol{\mu}_{\Delta_i}^H \\ \boldsymbol{\mu}_{\Delta_i} & \mathbf{0}_{A_i\times A_i} \end{bmatrix} \succeq 0, \tag{7.86}$$

where[9]

$$\tilde{\boldsymbol{\mu}}_i = \begin{bmatrix} \left(\mathbf{V}_i^T \otimes \mathbf{U}_i^H\right) \mathrm{vec}\left(\tilde{\mathbf{H}}_{ii}\right) - \mathrm{vec}\left(\mathbf{I}_{d_i}\right) \\ \left\lfloor \left(\mathbf{V}_j^T \otimes \mathbf{U}_i^H\right) \mathrm{vec}\left(\tilde{\mathbf{H}}_{ij}\right) \right\rfloor_{j\in\mathcal{S}, j\neq i} \\ \left\lfloor \left\lfloor \sqrt{\kappa}\left((\boldsymbol{\Gamma}_\ell \mathbf{V}_j)^T \otimes \mathbf{U}_i^H\right) \mathrm{vec}\left(\tilde{\mathbf{H}}_{ij}\right) \right\rfloor_{\ell\in\mathcal{D}_j^{(T)}} \right\rfloor_{j\in\mathcal{S}} \\ \left\lfloor \left\lfloor \sqrt{\beta}\left(\mathbf{V}_j^T \otimes (\mathbf{U}_i^H \boldsymbol{\Gamma}_\ell)\right) \mathrm{vec}\left(\tilde{\mathbf{H}}_{ij}\right) \right\rfloor_{\ell\in\mathcal{D}_i^{(R)}} \right\rfloor_{j\in\mathcal{S}} \\ \sigma_i \mathrm{vec}\left(\mathbf{U}_i\right) \end{bmatrix}, \tag{7.87}$$

$$\boldsymbol{\mu}_{\Delta_i} = \underbrace{\begin{bmatrix} \left(\mathbf{V}_i^T \otimes \mathbf{U}_i^H\right) \\ \left\lfloor \left(\mathbf{V}_j^T \otimes \mathbf{U}_i^H\right) \right\rfloor_{j\in\mathcal{S}, j\neq i} \\ \left\lfloor \left\lfloor \sqrt{\kappa}\left((\boldsymbol{\Gamma}_\ell \mathbf{V}_j)^T \otimes \mathbf{U}_i^H\right) \right\rfloor_{\ell\in\mathcal{D}_j^{(T)}} \right\rfloor_{j\in\mathcal{S}} \\ \left\lfloor \left\lfloor \sqrt{\beta}\left(\mathbf{V}_j^T \otimes (\mathbf{U}_i^H \boldsymbol{\Gamma}_\ell)\right) \right\rfloor_{\ell\in\mathcal{D}_i^{(R)}} \right\rfloor_{j\in\mathcal{S}} \\ \mathbf{0}_{d_i \tilde{N}_i \times \tilde{N}_i \tilde{M}} \end{bmatrix}}_{\mathbf{D}_{\Delta_i}} \mathrm{vec}\left(\boldsymbol{\Delta}_{\boldsymbol{i}}\right). \tag{7.88}$$

By choosing

$$\mathbf{A} = \begin{bmatrix} \tau_i & \tilde{\boldsymbol{\mu}}_i^H \\ \tilde{\boldsymbol{\mu}}_i & \mathbf{I}_{A_i} \end{bmatrix}, \ \mathbf{P} = \left[\mathbf{0}_{\tilde{N}_i \tilde{M} \times 1}, \ \mathbf{D}_{\Delta_i}^H\right], \tag{7.89}$$

$$\mathbf{X} = \mathrm{vec}\left(\boldsymbol{\Delta}_{\boldsymbol{i}}\right), \ \mathbf{Q} = \left[-1, \mathbf{0}_{1\times A_i}\right], \tag{7.90}$$

and applying Lemma 7.1, the LMI in (7.80) is relaxed as

$$\begin{bmatrix} \tau_i - \epsilon_i & \tilde{\boldsymbol{\mu}}_i^H & \mathbf{0}_{1\times \tilde{N}_i \tilde{M}} \\ \tilde{\boldsymbol{\mu}}_i & \mathbf{I}_{A_i} & -\delta_i \mathbf{D}_{\Delta_i} \\ \mathbf{0}_{\tilde{N}_i \tilde{M} \times 1} & -\delta_i \mathbf{D}_{\Delta_i}^H & \epsilon_i \mathbf{I}_{\tilde{N}_i \tilde{M}} \end{bmatrix} \succeq 0, \ i \in \mathcal{S}, \tag{7.91}$$

$$\epsilon_i \geq 0, \ i \in \mathcal{S}. \tag{7.92}$$

Using a similar procedure, the LMI in (7.83) is expressed as

$$\begin{bmatrix} \lambda_l & \tilde{\boldsymbol{\iota}}_l^H \\ \tilde{\boldsymbol{\iota}}_l & \mathbf{I}_{B_l} \end{bmatrix} + \begin{bmatrix} 0 & \boldsymbol{\iota}_{\Lambda_l}^H \\ \boldsymbol{\iota}_{\Lambda_l} & \mathbf{0}_{B_l \times B_l} \end{bmatrix} \succeq 0, \tag{7.93}$$

[9]To simplify the presentation, from now on we will assume the number of transmit antennas at the BS is equal to number of transmit antennas at the UL users, i.e., $\tilde{M} = M_0 = M_i, \ i \in \mathcal{S}^{UL}$.

where

$$\tilde{\boldsymbol{\iota}}_l = \begin{bmatrix} \left\lfloor \left(\mathbf{V}_j^T \otimes \mathbf{I}_{T_l}\right) \mathrm{vec}\left(\tilde{\mathbf{G}}_{lj}\right) \right\rfloor_{j\in\mathcal{S}} \\ \sqrt{\kappa} \left\lfloor \left\lfloor \left((\boldsymbol{\Gamma}_\ell \mathbf{V}_j)^T \otimes \mathbf{I}_{T_l}\right) \mathrm{vec}\left(\tilde{\mathbf{G}}_{lj}\right) \right\rfloor_{\ell\in\mathcal{D}_j^{(T)}} \right\rfloor_{j\in\mathcal{S}} \end{bmatrix}, \tag{7.94}$$

$$\boldsymbol{\iota}_{\Lambda_l} = \underbrace{\begin{bmatrix} \left\lfloor \left(\mathbf{V}_j^T \otimes \mathbf{I}_{T_l}\right) \right\rfloor_{j\in\mathcal{S}} \\ \sqrt{\kappa} \left\lfloor \left\lfloor \left((\boldsymbol{\Gamma}_\ell \mathbf{V}_j)^T \otimes \mathbf{I}_{T_l}\right) \right\rfloor_{\ell\in\mathcal{D}_j^{(T)}} \right\rfloor_{j\in\mathcal{S}} \end{bmatrix}}_{\mathbf{E}_{\Lambda_l}} \mathrm{vec}\left(\boldsymbol{\Lambda_l}\right). \tag{7.95}$$

Then the LMI in (7.83) is relaxed as

$$\begin{bmatrix} \lambda_l - \eta_l & \tilde{\boldsymbol{\iota}}_l^H & \mathbf{0}_{1\times T_l\tilde{M}} \\ \tilde{\boldsymbol{\iota}}_l & \mathbf{I}_{B_l} & -\theta_l \mathbf{E}_{\Lambda_l} \\ \mathbf{0}_{T_l\tilde{M}\times 1} & -\theta_l \mathbf{E}_{\Lambda_l}^H & \eta_l \mathbf{I}_{T_l\tilde{M}} \end{bmatrix} \succeq 0,\ l = 1,\ldots,L, \tag{7.96}$$

$$\eta_l \geq 0,\ l = 1,\ldots,L. \tag{7.97}$$

Using the relaxed LMIs in (7.91) and (7.96), the SDP problem, which is equivalent to (7.26) can be formulated as (7.35).

# Appendix 7.C MSE Computation

Using (7.17), $\mathrm{tr}\{\mathbf{MSE}_i\}$ can be written as

$$\begin{aligned}
&\mathrm{tr}\{\mathbf{MSE}_i\} = \mathrm{tr}\left\{\left(\mathbf{U}_i^H\mathbf{H}_{ii}\mathbf{V}_i - \mathbf{I}_{d_i}\right)\left(\mathbf{U}_i^H\mathbf{H}_{ii}\mathbf{V}_i - \mathbf{I}_{d_i}\right)^H + \mathbf{U}_i^H\boldsymbol{\Sigma}_i\mathbf{U}_i\right\} \\
=\ & \mathrm{tr}\left\{\left(\mathbf{U}_i^H\mathbf{H}_{ii}\mathbf{V}_i - \mathbf{I}_{d_i}\right)\left(\mathbf{U}_i^H\mathbf{H}_{ii}\mathbf{V}_i - \mathbf{I}_{d_i}\right)^H\right\} \\
+\ & \sum_{j\in\mathcal{S},j\neq i} \mathrm{tr}\left\{\mathbf{U}_i^H\mathbf{H}_{ij}\mathbf{V}_j\mathbf{V}_j^H\mathbf{H}_{ij}^H\mathbf{U}_i\right\} + \sum_{j\in\mathcal{S}} \kappa\mathrm{tr}\left\{\mathbf{U}_i^H\mathbf{H}_{ij}\mathrm{diag}\left(\mathbf{V}_j\mathbf{V}_j^H\right)\mathbf{H}_{ij}^H\mathbf{U}_i\right\} \\
+\ & \sum_{j\in\mathcal{S}} \beta\mathrm{tr}\left\{\mathbf{U}_i^H\mathrm{diag}\left(\mathbf{H}_{ij}\mathbf{V}_j\mathbf{V}_j^H\mathbf{H}_{ij}^H\right)\mathbf{U}_i\right\} + \sigma_i^2\mathrm{tr}\left\{\mathbf{U}_i^H\mathbf{U}_i\right\} \\
=\ & \mathrm{tr}\left\{\left(\mathbf{U}_i^H\mathbf{H}_{ii}\mathbf{V}_i - \mathbf{I}_{d_i}\right)\left(\mathbf{U}_i^H\mathbf{H}_{ii}\mathbf{V}_i - \mathbf{I}_{d_i}\right)^H\right\} + \sum_{j\in\mathcal{S},j\neq i} \mathrm{tr}\left\{\mathbf{U}_i^H\mathbf{H}_{ij}\mathbf{V}_j\mathbf{V}_j^H\mathbf{H}_{ij}^H\mathbf{U}_i\right\} \\
+\ & \sum_{j\in\mathcal{S}}\sum_{\ell\in\mathcal{D}_j^{(T)}} \kappa\mathrm{tr}\left\{\mathbf{U}_i^H\mathbf{H}_{ij}\boldsymbol{\Gamma}_\ell\mathbf{V}_j\mathbf{V}_j^H\boldsymbol{\Gamma}_\ell^H\mathbf{H}_{ij}^H\mathbf{U}_i\right\} \\
+\ & \sum_{j\in\mathcal{S}}\sum_{\ell\in\mathcal{D}_i^{(R)}} \beta\mathrm{tr}\left\{\mathbf{U}_i^H\boldsymbol{\Gamma}_\ell\mathbf{H}_{ij}\mathbf{V}_j\mathbf{V}_j^H\mathbf{H}_{ij}^H\boldsymbol{\Gamma}_\ell^H\mathbf{U}_i\right\} + \sigma_i^2\mathrm{tr}\left\{\mathbf{U}_i^H\mathbf{U}_i\right\},
\end{aligned} \tag{7.98}$$

where $\mathcal{D}_j^{(R)}$ represents the set $\{1 \cdots \tilde{N}_j\}$, $\mathcal{D}_j^{(T)}$ represents the set $\{1 \cdots \tilde{M}_j\}$ and $\mathbf{\Gamma}_\ell$ is a square matrix with zero elements, except for the $\ell$-th diagonal element, equal to 1. Applying the vec$(\cdot)$ operation, and the identity $\|\text{vec}\,(\mathbf{A})\|_2^2 = \text{tr}\left\{\mathbf{A}\mathbf{A}^H\right\}$, (7.98) can be rewritten as

$$\begin{aligned} & \text{tr}\{\mathbf{MSE}_i\} \\ = \; & \left\|\text{vec}\left(\mathbf{U}_i^H\mathbf{H}_{ii}\mathbf{V}_i\right) - \text{vec}(\mathbf{I}_{d_i})\right\|_2^2 + \sum_{j\in\mathcal{S}, j\neq i} \left\|\text{vec}\left(\mathbf{U}_i^H\mathbf{H}_{ij}\mathbf{V}_j\right)\right\|_2^2 + \sigma_i^2 \left\|\text{vec}\,(\mathbf{U}_i)\right\|_2^2 \\ + \; & \sum_{j\in\mathcal{S}} \sum_{\ell\in\mathcal{D}_j^{(T)}} \kappa \left\|\text{vec}\left(\mathbf{U}_i^H\mathbf{H}_{ij}\mathbf{\Gamma}_\ell\mathbf{V}_j\right)\right\|_2^2 + \sum_{j\in\mathcal{S}} \sum_{\ell\in\mathcal{D}_i^{(R)}} \beta \left\|\text{vec}\left(\mathbf{U}_i^H\mathbf{\Gamma}_\ell\mathbf{H}_{ij}\mathbf{V}_j\right)\right\|_2^2. \quad (7.99) \end{aligned}$$

Using the identity $\text{vec}(\mathbf{ABC}) = \left(\mathbf{C}^T \otimes \mathbf{A}\right)\text{vec}\,(\mathbf{B})$, (7.99) can be written as $\|\boldsymbol{\mu}_i\|_2^2$, where $\boldsymbol{\mu}_i$ is given in (7.72).

Similar to (7.99), $I_l^{PU}$ can be written as

$$I_l^{PU} = \sum_{j\in\mathcal{S}} \left( \|\text{vec}\,(\mathbf{G}_{lj}\mathbf{V}_j)\|_2^2 + \sum_{\ell\in\mathcal{D}_j^{(T)}} \kappa \|\text{vec}\,(\mathbf{G}_{lj}\mathbf{\Gamma}_\ell\mathbf{V}_j)\|_2^2 \right). \quad (7.100)$$

Using the identity $\text{vec}(\mathbf{ABC}) = \left(\mathbf{C}^T \otimes \mathbf{A}\right)\text{vec}\,(\mathbf{B})$, (7.100) can be written as $\|\boldsymbol{\iota}_l\|_2^2$, where $\boldsymbol{\iota}_l$ is given in (7.73).

# Appendix 7.D Calculation of Worst Case CSI Error

The approximate MSE expression in (7.57) can be rewritten as

$$\begin{aligned} \text{vec}^H\left(\mathbf{B}_i^H\right)\text{vec}\,(\mathbf{\Delta_i}) &= ||\text{vec}\left(\mathbf{B}_i^H\right) \cdot \text{vec}\,(\mathbf{\Delta_i})\,|| \\ &\leq ||\text{vec}\left(\mathbf{B}_i^H\right)||\,||\text{vec}\,(\mathbf{\Delta_i})\,|| \quad (7.101) \\ &= ||\text{vec}\left(\mathbf{B}_i^H\right)||\delta_i, \quad (7.102) \end{aligned}$$

where $(\cdot)$ denotes the dot product operator and (7.101) is obtained by using the Cauchy-Schwarz inequality, $||\mathbf{ab}|| \leq ||\mathbf{a}||\,||\mathbf{b}||$. Now equality is achieved for $s \in \mathbb{R}$ when

$$\text{vec}\,(\mathbf{\Delta_i}) = s\ \text{vec}\left(\mathbf{B}_i^H\right) \quad (7.103)$$

Now plugging (7.103) in (7.102), we have

$$\begin{aligned} s\ ||\text{vec}\big(\mathbf{B}_i^H\big)\,||^2 &= ||\text{vec}\big(\mathbf{B}_i^H\big)\,||\delta_i \\ \implies s &= \frac{\delta_i}{||\text{vec}(\mathbf{B}_i^H)\,||} \\ \implies \text{vec}\,(\boldsymbol{\Delta_i}) &= \frac{\delta_i \text{vec}\big(\mathbf{B}_i^H\big)}{||\text{vec}(\mathbf{B}_i^H)\,||} \\ \implies \boldsymbol{\Delta_i} &= \frac{\delta_i\big(\mathbf{B}_i^H\big)}{||\text{vec}(\mathbf{B}_i^H)\,||}. \end{aligned} \tag{7.104}$$

# Chapter 8

# Conclusions

## 8.1 Summary

Future wireless communication networks will predominantly be formed with mobile devices such as smart phones, tablets, wearables, internet of things (IoTs) etc. This has resulted in an exponential growth in the amount of wireless data being created. However, spectrum resources in the current microwave regime is almost expended and it is evident that the wave of data requirement will not be met with the current state-of-the-art technologies. Hence, spectrum and energy efficient design of future wireless networks become extremely important. Accordingly, it is imperative to shift the communication paradigm to beyond 20GHz, where more than 100GHz of unused millimeter wave (mmWave) bandwidth is available. Furthermore, advanced and optimized communication and signal processing techniques also need to be developed to meet the demands future cellular networks. In this thesis, we provided a holistic study of three promising technologies (massive multiple-input multiple-output (MIMO), mmWave and full duplex (FD)), which have the potential to meet three primary requirements of future 5G wireless communication systems: i) delivering very high (10X more than current state-of-the-art) and increasing energy efficiency (on the order of 100X), ii) serving a large number of users simultaneously and iii) providing higher bandwidths. We have provided several advantages and corresponding trade-offs of these technologies with respect to several real-life implementation constraints, such as physical space for massive MIMO, blockages for mmWave, and self-interference for FD.

In Chapter 3, the uplink performance of a massive MIMO system was analysed. Stochastic geometry was used to characterise the spatially distributed users while large

dimensional random matrix theory (RMT) was used to achieve deterministic approximations of the sum rate of the system. Approximations for the analytical sum rate were provided along with closed-form expressions at the low and high signal to noise ratio (SNR) regimes. The approximations were further validated with Monte-Carlo simulations. The performance was evaluated with respect to the number of antennas at the base station (BS) and the intensity of the users. We also provided an analysis of the energy efficiency of the system by taking into consideration the circuit power consumption, which was shown to be a function of the number of antennas and the users. The relative EE of the system was plotted with respect to varying BS antennas for different SNR ranges. It was shown that the energy efficiency is a quasi-concave function of the number of base station antennas and does not always increase linearly with it. Accordingly, in Chapter 4 the optimum number of antennas that can be rigged in a space-constrained massive MIMO system when energy efficiency (EE) is considered as a design criteria was derived. A trade-off between the number of antennas, the fixed physical space and EE was found. It is evident that high EE can be obtained, but at the cost of reducing the number of antennas or increasing the physical space for the antennas to be deployed. The results provide adequate insights into how future massive MIMO BSs can be set-up within constrained physical spaces.

However, when millimeter wave frequencies are considered, due to the smaller wavelength, the constraint on physical space is relaxed significantly and a much larger number of antennas can be incorporated within very small physical spaces. Hence, in order to fully realize the potential of massive MIMO systems, it is mandatory to shift the communication paradigm from micro wave to mmWave frequencies. Furthermore, interest in mmWave bands has recently gained significant attention due to the fact that microwave bandwidth is almost expended. However, in a mmWave network, blockages often attenuate the desired signal and may lead to the loss of transmitted information. This can be dealt with the use of relays, which was discussed in details in Chapter 5. New nodes that form a set of relays were derived using the generalized Matérn Hard Core Point Process (MHCPP). These active nodes are the ones that can withstand the blockage effects in the network to transfer information with less outage probability. Relay aided transmission was seen to improve the SNR by around 5dB for a specific coverage probability. It is quite evident from our analysis that the use of relays can prevent the attenuation of the desired signal by negating the effects of blockages, which in turn also increases the coverage probability and transmission capacity of mmWave networks.

Furthermore, in Chapter 6 we study the performance analysis of a multi-user MIMO mmWave network with multiple BSs, where the BSs are equipped with massive MIMO antenna arrays. In particular, we considered a realistic propagation scenario of the downlink of such a system with spatially distributed BSs equipped a with large 3D circular antenna array serving single-antenna users within a fixed coverage area of a densely built up urban environment. The performance of this system was analyzed based on important metrics, namely coverage probability, average rate and area spectral efficiency with respect to varying number of antennas at the BS, the intensity of the BSs and users and blockage densities within the coverage area.

Finally, in Chapter 7, to improve the spectrum efficiency even further, we studied the robust MSE-based transceiver design problem for a FD MIMO cognitive cellular system.The system under consideration suffered from self-interference and co-channel interference (CCI) under the limited dynamic range (DR) at the transmitters and receivers, and norm-bounded channel uncertainties. Since a globally optimal solution is difficult to obtain due to the non-convex nature of the problems, an alternating iterative algorithm that iterates between transmit and receiving beamforming matrices while keeping the other fixed was proposed. It was shown that the sum-rate achieved by FD system is higher than that of half duplex (HD) system under reasonable self-interference cancellation and/or CCI attenuation values.

Overall, we can conclude that these three technologies can indeed be the ones to fulfil the requirements of 5G, and will definitely shape the way we communicate in the near and far future. At this point, we note that in this thesis we have presented a fundamental analysis based on various assumptions in order to gain first-hand design insights. However, by lifting the constraints on the assumptions, it is possible to extend the current work to several other complicated scenarios, which will be considered for future work. A few possible extensions of the current work for each of massive MIMO, mmWave and FD are discussed in the section below.

## 8.2 Extensions

### 8.2.1 Massive MIMO

The deterministic sum rate derived in Chapter 3 and the EE optimal parameter values derived in Chapter 4 were based on the assumption of perfect channel state information (CSI) and a single cell scenario. Further, perfect interference mitigation scheme

for a given cell/BS was considered in Chapter 3. These assumptions enabled us to gain a first-hand design insight for massive MIMO systems. Extensions to imperfect CSI and multi-cell scenarios will be considered in future works. Below, we give some preliminaries on imperfect CSI and multi-cell scenario with respect to the considered system models.

#### 8.2.1.1 Imperfect CSI

In particular, CSI acquisition by the BS can be done through the use of uplink pilots, where a coherence interval of the channel is used for uplink training. Let us consider the use of orthogonal pilot squence of length $K\tau^{UL}$ and the power used by the $k$th user to transmit the uplink pilot be $\bar{p}\sigma^2/\beta_k$. The parameters and notations used here are in conjunction with Chapter 4. Now, using MMSE channel estimation [58] we have the estimated channel as

$$\hat{\mathbf{w}}_k \sim \mathcal{CN}\left(\mathbf{0}, \frac{\beta_k}{1+\frac{1}{\bar{p}K\tau^{UL}}}\mathbf{I}\right), \tag{8.1}$$

where the estimation error of the covariance matrix is given as $\beta_k\left(1-\frac{1}{1+\frac{1}{\bar{p}K\tau^{UL}}}\right)\mathbf{I}$. Now, treating the channel estimates as true channels and applying approximate zero forcing (ZF) in the uplink and downlink while also considering the estimation errors as noise, the achievable rate for the $k$th UE can be given as [58]

$$\tilde{R} = \log_2\left(1+\frac{\tilde{p}_k^{UL}}{||\mathbf{v}_k||^2\left(\sigma^2+\left(1-\frac{1}{1+\frac{1}{\bar{p}K\tau^{UL}}}\right)K\bar{p}\sigma^2\right)}\right). \tag{8.2}$$

If $\tilde{p}_k^{UL} = \frac{\bar{p}\sigma^2(M-K)||\mathbf{v}_k||^2}{1+\frac{1}{\rho K\tau^{UL}}}$, then the total average rate of the system is given as

$$\tilde{R} = \log_2\left(1+\frac{\bar{p}(M-K)}{1+\frac{1}{\tau^{UL}}+\frac{1}{\bar{p}K\tau^{UL}}}\right). \tag{8.3}$$

This rate can be obtained using the power consumed by the power amplifiers in a similar way as is given in (4.62), with $\bar{p}$ being the optimization parameter similar to Proposition 4.5. However, optimizing $\bar{p}$ to obtain an optimum EE is not straight forward due to the fact that unlike in the perfect CSI case, in (8.3) $\bar{p}$ appears in both the numerator and denominator. Consequently, the analytical difficulties of the imperfect

CSI case when mutual coupling effects are considered at the BS will be considered in future works.

#### 8.2.1.2 Multi-cell scenario

When multiple cells are considered, it becomes necessary to reuse the pilot sequences in the neighbouring cells, which results in pilot contamination [7]. It is important to investigate its effects on the resultant EE in massive MIMO systems. For example, assuming that there are $J$ cells in the network, let the location of the $k$th user in the $j$th cell be denoted by $\mathbf{x}_{jk}$ and the average channel attenuation due to path loss and shadowing between a user location $\mathbf{x} \in \mathbb{R}^2$ and the $j$th BS be represented by $\mathcal{F}_j(\mathbf{x})$. If a symmetric scenario is considered, where the parameters in all the cells including the number of BS antennas, user distributions and propagation conditions, etc., are the same, then the average channel attenuation $\mathbb{E}\{\mathcal{F}_j(\mathbf{x}_{jk})\}$ is independent of the index $j$ of the cell. Accordingly, let the uplink power for the $k$th UE in the cell $j$ given as

$$\tilde{p}_{jk}^{UL} = \frac{\bar{p}\sigma^2(M-K)||\mathbf{v}_{jk}||^2}{1 + P_{\mathrm{PC}} + \frac{1}{\rho K \tau^{UL}}}, \tag{8.4}$$

where $P_{\mathrm{PC}}$ is the power loss due to pilot contamination and $\mathbf{v}_{jk}$ is the receive filter. Now, applying approximate ZF and averaging over all channel realizations, we have [58]

$$\mathbb{E}\{||\mathbf{v}_{jk}||^2\} = \frac{1 + P_{\mathrm{PC}} + \frac{1}{\rho K \tau^{UL}}}{\beta_{jk}(M-K)}, . \tag{8.5}$$

Hence, $\tilde{p}_{jk}^{UL-\mathrm{pilot}} = \frac{\sigma^2 \bar{p}}{\beta_{jk}}$ is the power that needs be used for pilot transmission. Further, the BS in cell $j$ may not be aware of the positions of UEs in other cells, which might be using the same pilots. Accordingly, the average interference from adjacent cells due to using the same pilots needs to be calculated, which is another extension for future work along with calculation of the EE optimal parameters for the multi-cell scenario.

### 8.2.2 Millimeter wave

#### 8.2.2.1 Hybrid beamforming

In Chapter 6, it was considered that the BSs are equipped with fully-digital baseband processing. This approach however requires that a radio frequency (RF) chain be

associated with each antenna. This may become unfeasible when massive MIMO is considered. On the contrary, fully analog solutions require only a single RF chain for the whole antenna array. However, such techniques have zero capability of digital processing, which motivates the use of hybrid beamforming that promises to strike a balance between these two techniques. In the hybrid structure, the number of RF chains can vary from 1 (fully analog beamforming) to the total number of antennas (fully digital beamforming). Two architectures, namely a fully-connected architecture, where each RF chain has phase shifters connected to all antennas in the array and an array of sub-arrays architecture, where the entire array is divided into sub-arrays and all antennas in a sub- array are connected via phase shifters to exactly one RF chain have been proposed in literature [165, 166, 167]. While the beamforming gain is higher in the former, the power consumption and hardware complexity of precoder/combiner for a fixed number of antennas is lower in the latter. Accordingly, precoding and combining with hybrid beamforming can be implemented in Chapter 5 and 6 to develop a tractable model for coverage and rate in multi-user mmWave networks.

#### 8.2.2.2 Hybrid mmWave-microwave communication

Unlike microwave, mmWave provides a vast amount of unused spectrum. However, as discussed in Chapter 5 and 6, mmWave has its own limitations as well. Hence, to meet the quality of service (QoS) requirements of the network, it is imperative to harvest the benefits offered by both worlds. In order to take advantage of the vast spectrum while circumventing the shortcomings of mmWave bands, hybrid communication involving both microwave and mmWave BS can be considered, where mmWave communication is employed when blockage effects on the desired signal to interference plus noise ratio (SINR) is minimum, and switches to microwave otherwise. Accordingly, we give some qualitative comments on microWave and mmWave tiers' association probabilities.

Let us consider the downlink transmission in a hybrid cellular network comprising of both mmWave and microwave networks. Also, let the mmWave BSs be modeled as a two dimensional homogeneous poisson point process (PPP) $\Phi_m$ with density $\lambda_m$, while the microwave BSs follow another homogeneous PPP $\Phi_\mu$ with density $\lambda_\mu$. All the processes are independent of each other. Assuming the typical user equipment (UE) to be located at the origin, a simple offloading technique may be adopted wherein the typical UE is offloaded to the microwave network if the capacity achieved on the mmWave network drops below a certain threshold. Similar offloading strategies were analyzed in [18] and stated to be reasonable for mmWave based networks. Also assuming that the

typical UE is associated with the best BS, which provides the UE with the strongest signal, it is reasonable to consider an identical bias factor $B_\mu$ or $B_m$ as was considered in [168, 169], which is always positive. When $B = 1$, no biasing is considered and the association goes back to a traditional cell association based on maximum received power or nearest node. Leveraging the analysis from [168], and considering that the UE is connected to the best BS in terms of long term averaged biased received power, the UE association is generally conditioned on the least path loss distribution. So, it is important to characterize such distributions in mmWave networks under the effect of blockages. As mentioned earlier in Chapter 6, any link, i.e., the distance between the UE and BS in a mmWave network depends on the blockage probability model. Therefore, the least path loss distribution in a mmWave network is not the same as for the case of a microwave network.

Consider a point process, where the points represent the path loss between the UE and randomly placed BSs in a mmWave network. Let $\bar{\Phi}_m = \left\{\xi_l \triangleq \frac{x_l^{\alpha_m}}{P_m G_l B_m}\right\}$ be a homogeneous PPP of intensity $\lambda_m$, with $G_l$ being the antenna array gain function and $P_m$ the transmitted signal power. Here, the link distance $x$ is a random variable, and its LOS state occurs with the probability of $e^{-\beta x}$. By using Mapping theorem [43, Theorem 2.34], the density function of this one dimensional PPP under the effect of blockages can be given as[1]

$$\Lambda([0,r]) = \int_0^{(rP_mG_lB_m)^{\frac{1}{\alpha_L}}} 2\pi\lambda_m x e^{-\beta x}\mathrm{d}x + \int_0^{(rP_mG_lB_m)^{\frac{1}{\alpha_N}}} 2\pi\lambda_m x(1-e^{-\beta x})\mathrm{d}x. \tag{8.6}$$

Using the void probability of a PPP and with the help of (8.6), the least path loss distribution in a mmWave network can be given as

$$\begin{aligned} & F_{\xi_l}^m(r) \\ = \; & \exp\Bigg(-\pi\lambda_m(rP_mG_lB_m)^{\frac{1}{\alpha_N}} - \tfrac{2\pi\lambda_m}{\beta^2}(1-e^{-\beta(rP_mG_lB_m)^{\frac{1}{\alpha_L}}}(1+\beta(rP_mG_lB_m)^{\frac{1}{\alpha_L}})) \\ + \; & \tfrac{2\pi\lambda_m}{\beta^2}(1-e^{-\beta(rP_mG_lB_m)^{\frac{1}{\alpha_N}}}(1+\beta(rP_mG_lB_m)^{\frac{1}{\alpha_N}}))\Bigg). \end{aligned} \tag{8.7}$$

Now, let $p_\mu$ be the association probability of a typical user connected to a microwave network, i.e., the probability that all mmWave BSs have maximum path loss when the

[1]The notations of variables used here are the same as used in Chapter 6.

user is connected to the nearest microwave BS. If $r_\mu$ is the nearest microwave BS node, then $p_\mu$ can be represented as

$$\begin{aligned} p_\mu &= \mathbb{E}_{r_\mu}\left[\mathrm{P}\left[P_\mu B_\mu r_\mu^{-\alpha_\mu} > P_m G_l B_m r_m^{-\alpha_m}\right]\right], \\ &= \int_0^\infty \mathrm{P}\left(\frac{r_m^{\alpha_m}}{P_m G_l B_m} > \frac{r_\mu^{\alpha_\mu}}{P_\mu B_\mu}\right) f_{r_\mu}(r)\mathrm{d}r, \end{aligned} \tag{8.8}$$

where $\mathrm{P}\left(\frac{r_m^{\alpha_m}}{P_m G_l B_m} > \frac{r_\mu^{\alpha_\mu}}{P_\mu B_\mu}\right)$ can be obtained by taking the CCDF of equation (8.7) and $f_{r_\mu}(r)$ is given as

$$f_{r_\mu}(r_\mu) = 2\pi\lambda_\mu r_\mu \exp(-\lambda\pi r_\mu^2). \tag{8.9}$$

Hence, the association probability that a typical UE is connected to the microwave network can be given as [170]

$$p_\mu = 2\pi\lambda_\mu \int_0^\infty r \exp\left(-\Lambda_m\left(\left(\frac{\bar{P}_m}{\bar{P}_\mu}\right)^{\frac{1}{\alpha_m}} r^{\frac{\alpha_\mu}{\alpha_m}}\right)\right) e^{-\pi\lambda_\mu r^2}\mathrm{d}r, \tag{8.10}$$

where $\bar{P}_m = P_m G_l B_m$, $\bar{P}_\mu = P_\mu B_\mu$ and

$$\begin{aligned} &\Lambda_m\left(\tfrac{\bar{P}_m}{\bar{P}_\mu}^{\frac{1}{\alpha_m}} r^{\frac{\alpha_\mu}{\alpha_m}}\right) \\ =\ & \pi\lambda_m\left(\frac{\bar{P}_m}{\bar{P}_\mu}\right)^{\frac{1}{\alpha_N}} r^{\frac{\alpha_\mu}{\alpha_N}} - \frac{2\pi\lambda_m}{\beta^2}\left(1 - e^{-\beta\left(\frac{\bar{P}_m}{\bar{P}_\mu}\right)^{\frac{1}{\alpha_N}} r^{\frac{\alpha_\mu}{\alpha_N}}}\left(1 + \beta\left(\frac{\bar{P}_m}{\bar{P}_\mu}\right)^{\frac{1}{\alpha_N}} r^{\frac{\alpha_\mu}{\alpha_N}}\right)\right) \\ +\ & \frac{2\pi\lambda_m}{\beta^2}\left(1 - e^{-\beta\left(\frac{\bar{P}_m}{\bar{P}_\mu}\right)^{\frac{1}{\alpha_L}} r^{\frac{\alpha_\mu}{\alpha_L}}}\left(1 + \beta\left(\frac{\bar{P}_m}{\bar{P}_\mu}\right)^{\frac{1}{\alpha_L}} r^{\frac{\alpha_\mu}{\alpha_L}}\right)\right). \end{aligned}$$

The association probability for the mmWave network $p_m$ can be obtained similarly. With the association probabilities of the respective tiers of networks established, other important problems such as resource scheduling, power allocations, etc., and performance metrics such as outage probability, transmission capacity, area spectral efficiency, etc., of the hybrid network can now be evaluated.

### 8.2.3 Full duplex

#### 8.2.3.1 Per-antenna power constraint

In Chapter 7, the considered power constraint at the BS was for the BS as a whole However, in a physical implementation of a multi-antenna node, each antenna has its own power amplifier in its analog front-end, and is limited individually by the linearity of the power amplifier. Thus, a power constraint imposed on a per-antenna basis is more realistic. Assuming that the maximum transmit power of the $m$-th antenna at BS and the $n$-th antenna at the $i$-th UL user are set to $P_0^m$ and $P_i^n$, respectively. Then, we have the following transmit power constraints

$$\left\| \left( \mathbf{I}_{d_i^{UL}} \otimes \mathbf{v}_i^n \right) \mathrm{vec}\left( \mathbf{V}_i \right) \right\|_2^2 \leq P_i^n, \ i \in \mathcal{S}^{UL}, \tag{8.11}$$

$$\left\| \left[ \left( \mathbf{I}_{d_i^{DL}} \otimes \mathbf{v}^m \right) \mathrm{vec}\left( \mathbf{V}_i \right) \right]_{i \in \mathcal{S}^{DL}} \right\|_2^2 \leq P_0^m, \tag{8.12}$$

where the vectors $\mathbf{v}_i^n = [\mathbf{0}_{1\times n-1}, \ 1, \ \mathbf{0}_{1\times M_i - n}]$ and $\mathbf{v}^m = [\mathbf{0}_{1\times m-1}, \ 1, \ \mathbf{0}_{1\times M_0 - m}]$. Replacing (7.37) and (7.38) with (8.11) and (8.12), respectively, the proposed algorithms are still applicable for the resulting optimization problem and will be be studied in future work.

#### 8.2.3.2 Uncertainty in the noise covariance

We assumed in the proposed algorithms in Chapter 7 that the noise covariance matrices $\mathbf{R}_0$ and $\mathbf{R}_j^{DL}$ are known perfectly. However, since the noise covariance is obtained by antenna calibration measurements, in practical systems it is only known approximately. Hence, it is also important to design robust transceivers under channel and noise covariance uncertainties. To that end, we assume the model in [171], which characterizes the noise using only the square root of the covariance matrix, i.e., $\mathbf{R}_0^{1/2} = \tilde{\mathbf{R}}_0^{1/2} + \mathbf{\Delta}_{n_0}$ and $\left(\mathbf{R}_j^{DL}\right)^{1/2} = \left(\tilde{\mathbf{R}}_j^{DL}\right)^{1/2} + \mathbf{\Delta}_{n_j^{DL}}$, where $\tilde{\mathbf{R}}_0^{1/2}$ and $\tilde{\mathbf{R}}_j^{DL}$ are known while the covariance uncertainties are also bounded in their Frobenius norm, i.e., $\left\|\mathbf{\Delta}_{n_0}\right\|_F \leq \delta_{n_0}$ and $\left\|\mathbf{\Delta}_{n_j^{DL}}\right\|_F \leq \delta_{n_j^{DL}}$. With this model, the noise term $\left\|\mathrm{vec}\left(\mathbf{U}_i\right)\right\|_2^2$ in (7.99) is replaced with $\left\|\mathrm{vec}\left(\mathbf{U}_i^H \mathbf{R}_i^{1/2}\right)\right\|_2^2$, and the MSE at the $i$-th user is written as

$$\mathrm{tr}\{\mathbf{MSE}_i\} \triangleq a_i + \left\|\mathrm{vec}\left(\mathbf{U}_i^H \mathbf{R}_i^{1/2}\right)\right\|_2^2, \tag{8.13}$$

where $a_i$ includes all the terms in (7.99) except $\|\text{vec}\,(\mathbf{U}_i)\|_2^2$, and $\mathbf{R}_i$ is equal to $\mathbf{R}_0$ if $i$ is an UL user and $\mathbf{R}_i^{DL}$ otherwise.

The noise term in (8.13) is handled by introducing a slack variable $\omega_i$, i.e.,

$$\left\|\text{vec}\left(\mathbf{U}_i^H\tilde{\mathbf{R}}_i^{1/2}\right)+\left(\mathbf{I}_{d_i}\otimes\mathbf{U}_i^H\right)\text{vec}\left(\boldsymbol{\Delta}_{n_i}\right)\right\|_2\leq\omega_i, \tag{8.14}$$

where $\boldsymbol{\Delta}_{n_i}$ is equal to $\boldsymbol{\Delta}_{n_0}$ if $i$ is an UL user and $\boldsymbol{\Delta}_{n_i^{DL}}$ otherwise. Lemma 7.1 can be used in (8.14) to obtain an equivalent LMI that covers the noise term of the $i$-th user.

Consider the MSE constraint $\text{tr}\left\{\mathbf{MSE}_i\right\}\leq\tau_i$ in (7.31). By introducing slack variables $\nu_i$, from (8.13) it can be written as $\text{tr}\left\{\mathbf{MSE}_i\right\}=\nu_i^2+\omega_i^2\leq\tau_i$, where $\sqrt{a_i}\leq\nu_i$. Since these MSE constraints and the noise uncertainty constraint in (8.14) can be expressed in SDP forms, the proposed algorithms will be used in future to study the noise covariance uncertainty.

#### 8.2.3.3 Full duplex in massive MIMO communication

In Chapter 7, baseband processing techniques using sophisticated transmit and receive filters were used to cancel the self interference. However, the advent of massive MIMO systems has opened up possibilities to suppress the self interference to the desired 110dB by simply leveraging the excess antennas used in a large MIMO antenna array. To this end, simple precoders/detectors may be used at the BS to cancel the self interference [32, 33]. Accordingly, the precoder used in (7.1) for downlink can be modified to send the transmitted signal as

$$\mathbf{x}_0=\sum_{j=1}^{J}(\mathbf{V}_j^{DL})_{\text{mod}}(\mathbf{s}_j^{DL})_{\text{mod}},\;\;(\mathbf{s}_j^{DL})_{\text{mod}}=\begin{bmatrix}\mathbf{s}_j^{DL}\\\mathbf{0}_{N_0\times1}\end{bmatrix}, \tag{8.15}$$

where $\mathbf{0}_{N_0\times1}$ is the $N_0\times1$ all-zeros vector transmitted to the receiving antennas of the BS to suppress the self interference. The precoder can be a conventional precoder used for massive MIMO [13, 15] as $\mathbf{H}^H(\mathbf{H}\mathbf{H}^H)^{-1}$. However, in order to suppress the self interference, the conventional ZF precorder may be modified to send zeros to the BS receive antennas only as

$$(\mathbf{V}_j^{DL})_{\text{mod}}=\mathbf{H}_{\text{mod}}^H(\mathbf{H}_{\text{mod}}\mathbf{H}_{\text{mod}}^H)^{-1}, \tag{8.16}$$

where

$$\mathbf{H}_{\text{mod}} = \begin{bmatrix} \mathbf{H}_j^{DL} \\ \mathbf{H}_0 \end{bmatrix}. \tag{8.17}$$

By applying blockwise matrix inversion, the precoder in (8.16) is equivalent to defining the precoder used in (7.1) as

$$\mathbf{V}_j^{DL} = \left((\mathbf{H}_j^{DL})^H - \mathbf{H}_0^H(\mathbf{H}_0\mathbf{H}_0^H)^{-1}\mathbf{H}_0(\mathbf{H}_j^{DL})^H\right)\left(\mathbf{H}_j^{DL}(\mathbf{H}_j^{DL})^H - \mathbf{H}_j^{DL}\mathbf{H}_0^H(\mathbf{H}_0\mathbf{H}_0^H)^{-1}\mathbf{H}_0(\mathbf{H}_j^{DL})^H\right)^{-1} \tag{8.18}$$

The downlink MSE/sum-rate can now be calculated using this modified precoder. For asymptotically large number of antennas, the sum rate can then be approximated using tools such as law of large numbers or extreme value theory. Furthermore, with the calculation of the deterministic sum-rate, another open problem to calculate the optimal ratio between the number of transmit and receive antennas at the BS so as to maximize both the downlink and uplink sum-rate arises, which will also be studied in future works.

# List of publications

1. S. Biswas, C. Masouros and T. Ratnarajah, "Performance Analysis of Large Multiuser MIMO Systems With Space-Constrained 2-D Antenna Arrays," *IEEE Transactions on Wireless Communications*, vol. 15, no. 5, pp. 3492-3505, May 2016.

2. S. Biswas, S. Vuppala, J. Xue and T. Ratnarajah, "On the Performance of Relay Aided Millimeter Wave Networks," *IEEE Journal of Selected Topics in Signal Processing (Special Issue on mmWave)*, vol. 10, no. 3, pp. 576-588, April 2016.

3. S Biswas, J Xue, F Khan, T Ratnarajah, "Performance Analysis of Correlated Massive MIMO Systems with Spatially Distributed Users," in press *IEEE Systems Journal*, 2016.

4. A. C. Cirik, S. Biswas, S. Vuppala, and T. Ratnarajah, "Robust transceiver design for full-duplex multi-user MIMO systems," *IEEE Wireless Communications Letters*, vol. 5, no. 3, pp. 172-175, May 2016.

5. S. Biswas, S. Vuppala and T. Ratnarajah, "On the Performance of mmWave Networks aided by Wirelessly Powered Relays," *IEEE Journal of Selected Topics in Signal Processing (Special Issue on Exploiting Interference towards Energy Efficient and Secure Wireless Communications)*, vol. 10, no 8, pp 1522-1537, Dec. 2016.

6. A. C. Cirik, S. Biswas, S. Vuppala and T. Ratnarajah, "Beamforming design for full-duplex MIMO interference channels-QoS and energy efficiency considerations," *IEEE Transactions on Communications*, vol 64, no 11, pp. 4635-4651, Nov. 2016.

7. A. C. Cirik, S. Biswas, and T. Ratnarajah, "Robust transceiver design in full-duplex MIMO cognitive radios," under revision, *IEEE Transactions on Vehicular Technology*, June 2016.

8. S. Vuppala, S. Biswas, T. Ratnarajah "An Analysis on Secure Communication in Millimeter/Micro-Wave Hybrid Networks," *IEEE Transactions on Communications*, vol. 64, no. 8, pp. 3507-3519, Aug. 2016.

9. S. Biswas, S. Vuppala and T. Ratnarajah, "An Analysis on mmWave Systems Equipped with Large 3D Antenna Arrays," under revision in *IEEE Journal*, 2016.

10. A. C. Cirik, S. Biswas, S. Vuppala, and T. Ratnarajah, "Energy efficient beamforming design for full-duplex MIMO interference channels," in proc *IEEE International Conference on Communications (ICC)*, Paris, France, May 21-25, 2017.

11. S. Biswas, C. Masouros and T. Ratnarajah, "On the Energy Efficiency of Massive MIMO with Space-Constrained 2D Antenna Arrays", In Proc. *IEEE International Conference on Communications (ICC)*, Kuala Lumpur, Malaysia, May 23-27, 2016.

12. S. Biswas, S. Vuppala, J. Xue, and T. Ratnarajah, "An Analysis on Relay Assisted Millimeter Wave Networks," in proc, *IEEE International Conference on Communications (ICC)*, Kuala Lumpur, Malaysia, May 23-27, 2016.

13. A. C. Cirik, S. Biswas, O. Taghizadeh, A. Liu, and T. Ratnarajah, "Robust transceiver design in full-duplex MIMO cognitive radios," in proc, *IEEE International Conference on Communications (ICC)*, Kuala Lumpur, Malaysia, May 23-27, 2016.

14. S. Vuppala, S. Biswas, J. Xue, and T. Ratnarajah, "On the Security Region of Best Source Indices in Random Wireless Networks," in proc, *IEEE International Conference on Communications (ICC)*, Kuala Lumpur, Malaysia, May 23-27, 2016.

15. A. C. Cirik, J. Xue, S. Biswas, T. Ratnarajah and M. Sellathurai, "Transceiver design of optimum wirelessly powered full-duplex MIMO interference channel," In Proc *IEEE 17th International Workshop on Signal Processing Advances in Wireless Communications (SPAWC)*, Edinburgh, UK, July 3-6, 2016.

16. S. Vuppala, S. Biswas, T. Ratnarajah, "Analysis of secure communication in millimetre wave networks: are blockages beneficial?," *IEEE International Conference on Acoustics, Speech and Signal Processing (ICASSP)*, Shanghai, China, March 20-25, 2016.

17. S. Biswas, J. Xue, F. Khan and T. Ratnarajah, "On the Capacity of Correlated Massive MIMO Systems using Stochastic Geometry," in Proc. *IEEE International Symposium on Information Theory (ISIT)*, Hong Kong, June 14-19, 2015.

18. S. Biswas, C. Masouros and T. Ratnarajah, "On the effect of antenna correlation and coupling on energy-efficiency of massive MIMO systems," in proc, *IEEE Personal, Indoor, and Mobile Radio Communication (PIMRC)*, Washington D.C., USA, Sep 02-5, 2014.

# Bibliography


[1] "Ericsson mobility report: June 2016," Available at https://www.ericsson.com/res/docs/2016/ericsson-mobility-report-2016.pdf.

[2] "Cisco visual networking index: Cisco visual networking index: Global mobile data traffic forecast update, 2015-2020," Available at http://www.cisco.com/en/US/solutions/collateral/ns341/ns525/ns537/ns705/ns827/white_paper_c11-520862.pdf.

[3] Qualcomm, "The evolution of mobile technologies," Tech. Rep., 2014.

[4] J. G. Andrews, S. Buzzi, W. Choi, S. V. Hanly, A. Lozano, A. C. K. Soong, and J. C. Zhang, "What will 5g be?" *IEEE Journal on Selected Areas in Communications*, vol. 32, no. 6, pp. 1065–1082, June 2014.

[5] F. Boccardi, R. W. Heath, A. Lozano, T. L. Marzetta, and P. Popovski, "Five disruptive technology directions for 5g," *IEEE Communications Magazine*, vol. 52, no. 2, pp. 74–80, February 2014.

[6] H. Tullberg, P. Popovski, Z. Li, M. A. Uusitalo, A. Hoglund, O. Bulakci, M. Fallgren, and J. F. Monserrat, "The metis 5g system concept: Meeting the 5g requirements," *IEEE Communications Magazine*, vol. 54, no. 12, pp. 132–139, December 2016.

[7] T. L. Marzetta, "Noncooperative cellular wireless with unlimited numbers of base station antennas," *IEEE Transactions on Wireless Communications*, vol. 9, no. 11, pp. 3590–3600, November 2010.

[8] D. N. C. Tse and P. Viswanath, *Fundamentals of Wireless Communications*. Cambridge University Press, 2005.

[9] A. Goldsmith, S. A. Jafar, N. Jindal, and S. Vishwanath, "Capacity limits of MIMO channels," *IEEE Journal on Selected Areas in Communications*, vol. 21, no. 5, pp. 684–702, June 2003.

[10] Q. H. Spencer, C. B. Peel, A. L. Swindlehurst, and M. Haardt, "An introduction to the multi-user MIMO downlink," *IEEE Communications Magazine*, vol. 42, no. 10, pp. 60–67, Oct 2004.

[11] "Further advancements for E-UTRA; LTE-Advanced feasibility studies in RAN WG4," *3GPP technical specifications group radio access network*, March 2010.

[12] Rhodes and Schwarz, "WLAN 802.11n: From SISO to MIMO," *3GPP technical specifications group radio access network*, March 2010.

[13] H. Q. Ngo, E. G. Larsson, and T. L. Marzetta, "Energy and spectral efficiency of very large multiuser MIMO systems," *IEEE Transactions on Communications*, vol. 61, no. 4, pp. 1436–1449, April 2013.

[14] Q. Ngo, E. Larsson, and T. Marzetta, "Energy and spectral efficiency of very large multiuser MIMO systems," *IEEE Transactions on Communications*, vol. 61, no. 4, pp. 1436–1449, Apr. 2013.

[15] F. Rusek, D. Persson, B. K. Lau, E. G. Larsson, T. L. Marzetta, O. Edfors, and F. Tufvesson, "Scaling up MIMO: Opportunities and challenges with very large arrays," *IEEE Signal Processing Magazine*, vol. 30, no. 1, pp. 40–60, Jan 2013.

[16] A. Ghosh, T. N. Thomas, M. C. Cudak, R. Ratasuk, P. Moorut, F. W. Vook, T. S. Rappaport, G. R. MacCartney, S. Shun, and S. Nie, "Millimeter-wave enhanced local area systems: A high data-rate approach for future wireless networks," *IEEE Journal on Selected Areas in Communications*, vol. 32, no. 6, pp. 1153–1163, June 2014.

[17] A. Thornburg, T. Bai, and R. W. Heath, "Performance analysis of mmWave ad hoc networks," can be found at http://arxiv.org/pdf/1412.0765v1.pdf, 2014.

[18] S. Singh, M. N. Kulkarni, A. Ghosh, and J. G. Andrews, "Tractable model for rate in self-backhauled millimeter wave cellular networks," *IEEE Journal on Selected Areas in Communications*, vol. 33, no. 1, pp. 2196–2211, Jan. 2015.

[19] M. Akdeniz, Y. Liu, S. Rangan, and E. Erkip, "Millimeter wave picocellular system evaluation for urban deployments," in *Proc. IEEE Global Telecommunications Conference (Globecom'13)*, Dec. 2013, pp. 105–110.

[20] M. R. Akdeniz, Y. Liu, M. K. Samimi, S. Sun, S. Rangan, T. S. Rappaport, and E. Erkip, "Millimeter wave channel modeling and cellular capacity evaluation," *IEEE Journal on Selected Areas in Communications*, vol. 32, no. 6, pp. 1164–1179, June 2014.

[21] S. Rajagopal, S. Abu-Surra, and M. Malmrichegini, "Channel feasibility for outdoor non-line-of-sight mmWave mobile communication," in *Proc. IEEE Vehicular Technology Conference (VTC'12 Fall)*, 2012, pp. 1–6.

[22] G. R. MacCartney and T. S. Rappaport, "73GHz millimeter wave propagation measurements for outdoor urban mobile and backhaul communications in New York city," in *Proc. IEEE International Conference on Communications*, Sydney, Austrlia, June 2014, pp. 2429–2433.

[23] S. Nie, G. R. MacCartney, S. Shun, and T. S. Rappaport, "72 GHz millimeter wave indoor measurements for wireless and backhaul communications," in *Proc. IEEE International Symposium on Personal, Indoor and Mobile Radio Communications (PIMRC'13)*, Sept. 2013, pp. 2429–2433.

[24] M. Jain, J. I. Choi, T. Kim, D. Bharadia, S. Seth, K. Srinivasan, P. Levis, S. Katti, and P. Sinha, "Practical, real-time, full duplex wireless," in *Proceedings of the Annual International Conference on Mobile Computing and Networking*. New York, NY, USA: ACM, 2011, pp. 301–312. [Online]. Available: http://doi.acm.org/10.1145/2030613.2030647

[25] Y. Hua, Y. Ma, A. Gholian, Y. Li, A. C. Cirik, and P. Liang, "Radio self-interference cancellation by transmit beamforming, all-analog cancellation and blind digital tuning," *Signal Processing*, vol. 108, pp. 322 – 340, 2015. [Online]. Available: http://www.sciencedirect.com/science/article/pii/S0165168414004484

[26] A. Sahai, G. Patel, C. Dick, and A. Sabharwal, "On the impact of phase noise on active cancelation in wireless full-duplex," *IEEE Transactions on Vehicular Technology*, vol. 62, no. 9, pp. 4494–4510, Nov 2013.

[27] T. M. Kim, H. J. Yang, and A. J. Paulraj, "Distributed sum-rate optimization for full-duplex MIMO system under limited dynamic range," *IEEE Signal Processing Letters*, vol. 20, no. 6, pp. 555–558, June 2013.

[28] A. C. Cirik, "On duality of MIMO relays and performance limits of full-duplex MIMO radios," Ph.D. dissertation, University of California, Riverside, 2014.

[29] A. C. Cirik, R. Wang, Y. Hua, and M. Latva-aho, "Weighted sum-rate maximization for full-duplex MIMO interference channels," *IEEE Transactions on Communications*, vol. 63, no. 3, pp. 801–815, March 2015.

[30] D. Nguyen, L. N. Tran, P. Pirinen, and M. Latva-aho, "On the spectral efficiency of full-duplex small cell wireless systems," *IEEE Transactions on Wireless Communications*, vol. 13, no. 9, pp. 4896–4910, Sept 2014.

[31] S. Li, R. D. Murch, and V. K. N. Lau, "Linear transceiver design for full-duplex multi-user MIMO system," in *IEEE International Conference on Communications (ICC'14)*, June 2014, pp. 4921–4926.

[32] X. Xia, Y. Xu, K. Xu, D. Zhang, and W. Ma, "Full-duplex massive MIMO AF relaying with semiblind gain control," *IEEE Transactions on Vehicular Technology*, vol. 65, no. 7, pp. 5797–5804, July 2016.

[33] H. Shen, W. Xu, and C. Zhao, "Transceiver optimization for full-duplex massive MIMO AF relaying with direct link," *IEEE Access*, vol. PP, no. 99, pp. 1–1, 2016.

[34] A. Scaglione, P. Stoica, S. Barbarossa, G. B. Giannakis, and H. Sampath, "Optimal designs for space-time linear precoders and decoders," *IEEE Transactions on Signal Processing*, vol. 50, no. 5, pp. 1051–1064, May 2002.

[35] S. M. Kay, *Fundamentals of Statistical Signal Processing: Estimation Theory*. Englewood Cliffs, New Jersey: Prentice Hall Signal Processing Series, 1993, vol. I.

[36] W. W. Hager, "Updating the inverse of a matrix," *SIAM Review*, vol. 31, no. 2, pp. 221–239, 1989. [Online]. Available: http://dx.doi.org/10.1137/1031049

[37] D. Palomar, J. Cioffi, and M. Lagunas, "Joint tx-rx beamforming design for multicarrier mimo channels: a unified framework for convex optimization," *IEEE Trans. Signal Processing*, vol. 51, no. 9, pp. 2381 – 2401, Sept 2003.

[38] R. Couillet, M. Debbah, and J. Silverstein, "A deterministic equivalent for the analysis of correlated MIMO multiple access channels," *IEEE Transactions on Information Theory*, vol. 57, no. 6, pp. 3493–3514, Jun. 2011.

[39] J. Zhang, C.-K. Wen, S. Jin, X. Gao, and K.-K. Wong, "On capacity of large-scale MIMO multiple access channels with distributed sets of correlated antennas," *IEEE Journal on Selected Areas in Communications*, vol. 31, no. 2, pp. 133–148, Feb. 2013.

[40] J. Silverstein and Z. Bai, "On the empirical distribution of eigenvalues of a class of large dimensional random matrices," *Journal of Multivariate Analysis*, vol. 54, no. 2, pp. 175 – 192, 1995. [Online]. Available: http://www.sciencedirect.com/science/article/pii/S0047259X85710512

[41] J. N. Walid Hachem, Philippe Loubaton, "Deterministic equivalents for certain functionals of large random matrices," *The Annals of Applied Probability*, vol. 17, no. 3, pp. 875–930, 2007. [Online]. Available: http://www.jstor.org/stable/25442865

[42] A. Bose, S. Ganguly, and A. Sen, "Limiting spectral distribution of XX' matrices," *Annales de Institut Henri Poincarè - Probabilitiès et Statistiques*, vol. 46, no. 3, pp. 677–707, 2010.

[43] M. Haenggi, *Stochastic Geometry for Wireless Networks*. Cambridge University Press, 2012.

[44] M. Haenggi, J. G. Andrews, F. Baccelli, O. Dousse, and M. Franceschetti, "Stochastic geometry and random graphs for the analysis and design of wireless networks," *IEEE Journal on Selected Areas in Communications*, vol. 27, no. 7, pp. 1029–1046, September 2009.

[45] M. Haenggi and R. K. Ganti, "Interference in large wireless networks," *Foundations and Trends in Networking*, vol. 3, no. 2, pp. 127–248, Feb. 2009. [Online]. Available: http://dx.doi.org/10.1561/1300000015

[46] S. Cui, A. J. Goldsmith, and A. Bahai, "Energy-efficiency of mimo and cooperative mimo techniques in sensor networks," *IEEE Journal on Selected Areas in Communications*, vol. 22, no. 6, pp. 1089–1098, Aug 2004.

[47] S. Tombaz, A. Vastberg, and J. Zander, "Energy- and cost-efficient ultra-high-capacity wireless access," *IEEE Trans. on Wireless Communications*, vol. 18, no. 5, pp. 18–24, Oct 2011.

[48] D. Ha, K. Lee, and J. Kang, "Energy efficiency analysis with circuit power consumption in massive MIMO systems," *IEEE International Symposium on Personal, Indoor, and Mobile Radio Communications (PIMRC'13)*, pp. 938–942, Sept 2013.

[49] G. Miao, "Energy-efficient uplink multi-user mimo," *IEEE Transactions on Wireless Communications*, vol. 12, no. 5, pp. 2302–2313, May 2013.

[50] A. L. Moustakas, S. H. Simon, and A. M. Sengupta, "MIMO capacity through correlated channels in the presence of correlated interferers and noise: a (not so) large N analysis," *IEEE Transactions on Information Theory*, vol. 49, no. 10, pp. 2545–2561, Oct. 2003.

[51] J. Hoydis, S. ten Brink, and M. Debbah, "Massive MIMO in the UL/DL of cellular networks: How many antennas do we need?" *IEEE Journal on Selected Areas in Communications*, vol. 31, no. 2, pp. 160–171, Feb. 2013.

[52] M. Haenggi, "On distances in uniformly random networks," *IEEE Transactions on Information Theory*, vol. 51, no. 10, pp. 3584–3586, Oct. 2005.

[53] I. S. Gradshteyn and I. M. Ryzhik, *Table of Integrals, Series, and Products*, 6th ed. Academic Press, Jul. 2000.

[54] E. V. A. Schönhage, A.F.W. Grotefeld, *Fast Algorithms–A Multitape Turing Machine Implementation.* BI Wissenschafts-Verlag, Mannheim, 1994.

[55] P. B. B. Jonathan M. Borwein, *A Study in Analytic Number Theory and Computational Complexity.* John Wiley, 1998.

[56] Y. Chen, S. Zhang, S. Xu, and G. Y. Li, "Fundamental trade-offs on green wireless networks," *IEEE Communications Magazine*, vol. 49, no. 6, pp. 30–37, June 2011.

[57] E. Bjornson, L. Sanguinetti, J. Hoydis, and M. Debbah, "Designing multi-user MIMO for energy efficiency: When is massive MIMO the answer?" *IEEE Wireless Communications and Networking Conference (WCNC)*, pp. 242–247, April 2014.

[58] E. Bjrnson, L. Sanguinetti, J. Hoydis, and M. Debbah, "Optimal design of energy-efficient multi-user MIMO systems: Is massive MIMO the answer?" *IEEE Transactions on Wireless Communications*, vol. 14, no. 6, pp. 3059–3075, June 2015.

[59] W. Rudin, *Principles of Mathematical Analysis*, 3rd ed. New York: McGraw-Hill, 1976.

[60] H. He, J. Xue, T. Ratnarajah, F. A. Khan, and C. B. Papadias, "Modeling and analysis of cloud radio access networks using matern hard-core point processes," *IEEE Transactions on Wireless Communications*, vol. 15, no. 6, pp. 4074–4087, June 2016.

[61] G. Taricco and E. Riegler, "On the ergodic capacity of correlated Rician fading MIMO channels with interference," *IEEE Trans. Inf. Theory*, vol. 57, no. 7, pp. 4123–4137, July 2011.

[62] J. Hoydis, K. Hosseini, S. T. Brink, and M. Debbah, "Making smart use of excess antennas: Massive MIMO, small cells, and tdd," *Bell Labs Technical Journal*, vol. 18, no. 2, pp. 5–21, Sept 2013.

[63] C. Masouros, M. Sellathurai, and T. Ratnarajah, "Large-scale MIMO transmitters in fixed physical spaces: The effect of transmit correlation and mutual coupling," *IEEE Transactions on Communications*, vol. 61, no. 7, pp. 2794–2804, July 2013.

[64] C. A. Balanis. John Wiley and Sons, vol. 3rd edition.

[65] I. Gupta and A. Ksienski, "Effect of mutual coupling on the performance of adaptive arrays," *IEEE Transactions on Antennas and Propagation*, vol. 31, no. 5, pp. 785–791, Sep 1983.

[66] K. S. Y .Qiaowei, C. Qiang, "Performance of adaptive array antenna with arbitrary geometry in the presence of mutual coupling," *IEEE Transactions on Antennas and Propagation*, vol. 54, no. 7, pp. 1991–1996, July 2006.

[67] X. Artiga, B. Devillers, and J. Perruisseau-Carrier, "Mutual coupling effects in multi-user massive mimo base stations," in *IEEE International Symposium on Antennas and Propagation*, July 2012, pp. 1–2.

[68] B. Clerckx, C. Craeye, D. Vanhoenacker-Janvier, and C. Oestges, "Impact of antenna coupling on 2x2 MIMO communications," *IEEE Transactions on Vehicular Technology*, vol. 56, no. 3, pp. 1009–1018, May 2007.

[69] Z. Li, Z. Du, M. Takahashi, K. Saito, and K. Ito, "Reducing mutual coupling of MIMO antennas with parasitic elements for mobile terminals," *IEEE Transactions on Antennas and Propagation*, vol. 60, no. 2, pp. 473–481, Feb 2012.

[70] D. F. Kelley and W. L. Stutzman, "Array antenna pattern modeling methods that include mutual coupling effects," *IEEE Transactions on Antennas and Propagation*, vol. 41, no. 12, pp. 1625–1632, Dec 1993.

[71] T. Svantesson, "The effects of mutual coupling using a linear array of thin dipoles of finite length," in *IEEE Signal Processing Workshop on Statistical Signal and Array Processing (Cat. No.98TH8381)*, Sep 1998, pp. 232–235.

[72] A. Fehske, G. Fettweis, J. Malmodin, and G. Biczok, "The global footprint of mobile communications: The ecological and economic perspective," *IEEE Communications Magazine*, vol. 49, no. 8, pp. 55–62, August 2011.

[73] T. Ratnarajah and R. Vaillancourt, "Quadratic forms on complex random matrices and multiple-antenna systems," *IEEE Transactions on Information Theory*, vol. 51, no. 8, pp. 2976–2984, Aug 2005.

[74] D. Ying, F. W. Vook, T. A. Thomas, D. J. Love, and A. Ghosh, "Kronecker product correlation model and limited feedback codebook design in a 3D channel model," in *IEEE International Conference on Communications (ICC'14)*, June 2014, pp. 5865–5870.

[75] S. U. Pillai, T. Suel, and S. Cha, "The Perron-Frobenius theorem: some of its applications," *IEEE Signal Processing Magazine*, vol. 22, no. 2, pp. 62–75, March 2005.

[76] D. K. Nagar and A. K. Gupta, "Expectations of functions of complex wishart matrix," *Acta Applicandae Mathematicae*, vol. 113, no. 3, pp. 265–288, 2011. [Online]. Available: http://dx.doi.org/10.1007/s10440-010-9599-x

[77] R. V. R. Kumar and J. Gurugubelli, "How green the LTE technology can be?" in *International Conference on Wireless Communication, Vehicular Technology, Information Theory and Aerospace Electronic Systems Technology (Wireless VITAE'11)*, Feb 2011, pp. 1–5.

[78] E. Wolfstetter, *Topics in Microeconomics: Industrial Organization, Auctions and Incentives*. Cambridge University Press, 1999.

[79] A. C. Cirik, R. Wang, Y. Rong, and Y. Hua, "MSE-based transceiver designs for full-duplex MIMO cognitive radios," *IEEE Transactions on Communications*, vol. 63, no. 6, pp. 2056–2070, June 2015.

[80] S. Huberman and T. Le-Ngoc, "MIMO full-duplex precoding: A joint beamforming and self-interference cancellation structure," *IEEE Transactions on Wireless Communications*, vol. 14, no. 4, pp. 2205–2217, April 2015.

[81] S. Boyd and L. Vandenberghe, *Convex Optimization*. Cambridge University Press, 2004.

[82] S. Akoum, E. O. Ayach, and R. W. Heath, "Coverage and capacity in mmWave cellular systems," in *Proc. IEEE Asilomar Conference on Signals, Systems and Computers*, 2012, pp. 688–692.

[83] G. R. MacCartney, J. Zhang, S. Nie, and T. S. Rappaport, "Path loss models for 5G millimeter wave propagation channles in urban microcells," in *Proc. IEEE Globecom*, Dec. 2013, pp. 1–6.

[84] J. N. Laneman, D. N. C. Tse, and G. W. Wornell, "Cooperative diversity in wireless networks: Efficient protocols and outage behavior," *IEEE Transactions on Information Theory*, vol. 50, no. 12, pp. 3062–3080, 2004.

[85] M. Renzo, F. Graziosi, and F. Santucci, "A comprehensive framework for performance analysis of dual-hop cooperative wireless systems with fixed-gain relays over generalized fading channels," *IEEE Transactions on Wireless Communications*, vol. 8, no. 10, pp. 5060–5074, Oct. 2009.

[86] A. Behnad, A. M. Rabiei, and N. C. Beaulieu, "Performance analysis of opportunistic relaying in a Poisson field of amplify-and-forward relays," *IEEE Transactions on Communications*, vol. 61, no. 1, pp. 97–107, Jan. 2013.

[87] S. W. Peters, A. Y. Panah, K. T. Truong, and R. W. Heath, "Relay architectures for 3GPP LTE-advanced," *EURASIP Journal on Wireless Communications and Networking*, p. 14pages, Jul. 2009.

[88] W. Lu and M. D. Renzo, "Performance analysis of relay aided cellular networks by using stochastic geometry," in *Proc. IEEE International Workshop on Computer Aided Modeling and Design of Communication Links and Networks*, Athens, Greece, Dec. 2014.

[89] Z. Lin, Y. Gao, X. Zhang, and D. Yang, "Stochastic geometry analysis of achievable transmission capacity for relay-assisted device-to-device networks," in *Proc. IEEE International Conference on Communications - Mobile and Wireless Networking Symposium*, Sydney, Austrlia, June 2014.

[90] Z. Lin, X. Peng, F. Chin, and W. Feng, "Outage performance of relaying with directional antennas in the presence of co-channel interferences at relays," *IEEE Wireless Communicatin Letters*, vol. 1, no. 4, pp. 288 – 291, Aug. 2012.

[91] T. Bai, R. Vaze, and R. W. Heath, "Analysis of blockage effects on urban cellular networks," *IEEE Transactions on Wireless Communications*, vol. 13, no. 9, pp. 5070–5083, June 2014.

[92] L. Fenton, "The sum of Log-Normal probability distributions in scatter transmission systems," *IRE Trans. Communication. Systems*, vol. 8, no. 1, pp. 57–67, Mar. 1960.

[93] T. Bai and R. W. Heath, "Coverage and rate analysis for millimeter-wave cellular networks," *IEEE Transactions on Wireless Communications*, vol. 14, no. 2, pp. 1100–1114, Feb. 2015.

[94] F. Baccelli and B. Blaszczyszyn, *Stochastic Geometry and Wireless Networks*. NOW Publishers, 2009.

[95] A. Thornburg, T. Bai, and R. W. Heath, "Performance analysis of outdoor mmwave ad hoc networks," *IEEE Transactions on Signal Processing*, vol. 64, no. 15, pp. 4065–4079, Aug. 2016.

[96] M. D. Renzo and W. Lu, "End-to-end error probability and diversity analysis of AF-based dual-hop cooperative relaying in a Poisson field of interferers at the destination," *IEEE Transactions on Wireless Communications*, vol. 4, no. 1, pp. 15 – 32, Jan. 2015.

[97] H. ElSawy and E. Hossain, "A modified hard core point process for analysis of random CSMA wireless networks in general fading environments," *IEEE Transactions on Communications*, vol. 61, no. 4, pp. 1520 – 1534, April 2013.

[98] A.Guo and M. Haenggi, "Spatial stochastic models and metrics for the structure of base stations in cellular networks," *IEEE Transactions on Wireless Communications*, vol. 12, no. 11, pp. 5800 – 5812, Nov. 2013.

[99] H. Q. Nguyen, F. Baccelli, and D. Kofman, "A stochastic geometry analysis of dense IEEE 802.11 networks," in *IEEE International International Conference on Computer Communications*, 2007, p. 11991207.

[100] A. Hasan and J. G. Andrews, "The guard zone in wireless ad hoc networks," *IEEE Transactions on Wireless Communications*, vol. 4, no. 3, pp. 897–906, March 2007.

[101] M. Haenggi, "Mean interference in hard-core wireless networks," *IEEE Communications Letters*, vol. 15, no. 8, pp. 792–794, Aug. 2011.

[102] M. O. Hasna and M. S. Alouini, "Harmonic mean and end-to-end performance of transmission systems with relays," *IEEE Transactions on Communications*, vol. 52, no. 1, pp. 30–135, 2004.

[103] H. A. David and H. N. Nagaraja, *Order Statistics*. Wiley, 2003.

[104] E. Castillo, *Extreme value theory in engineering*. Academic Press, 1988.

[105] J. Xue, T. Ratnarajah, M. Sellathurai, and Z. Ding, "Performance analysis for multi-way relaying in rician fading channels," *IEEE Transactions on Communications*, vol. 63, no. 11, pp. 4050–4062, Nov. 2015.

[106] E. J. Gumbel, *Statistics of Extremes*. Columbia University Press, 1957.

[107] *Mathematical Methods of Statistics*. Princeton University Press, 1946.

[108] S. Biswas, J. Xue, F. A. Khan, and T. Ratnarajah, "Performance analysis of correlated massive MIMO systems with spatially distributed users," *IEEE Systems Journal*, vol. PP, no. 99, pp. 1–12, 2016.

[109] S. K. Yong and J. S. Thompson, "Three-dimensional spatial fading correlation models for compact MIMO receivers," *IEEE Transactions on Wireless Communications*, vol. 4, no. 6, pp. 2856–w869, Nov. 2005.

[110] A. Forenza, D. J. Love, and R. W. Heath, "Simplified spatial correlation models for clustered MIMO channels with different array configurations," *IEEE Transactions on Vehicular Technology*, vol. 56, no. 4, pp. 1924–1934, Jul. 2007.

[111] J. Salz and J. Winters, "Effect of fading correlation on adaptive arrays in digital mobile radio," *IEEE Transactions on Vehicular Technology*, vol. 43, no. 4, pp. 1049–1057, Nov. 1994.

[112] W. J. L. Queiroz, F. Madeiro, W. T. A. Lopes, and M. S. Alencar, "Spatial correlation for DoA characterization using Von mises, Cosine, and Gaussian distributions," *International Journal of Antennas and Propagation*, vol. 2011, Jul. 2011.

[113] "Study on elevation beamforming/full-dimension (FD) MIMO for LTE," 3GPP Technical Reports TR36.897, Tech. Rep.

[114] "E-UTRA and UTRA; radio frequency (RF) requirement background for active antenna system (AAS) base station (BS)," 3GPP Technical Reports TR36.847, Tech. Rep.

[115] M. Shafi, M. Zhang, A. Moustakas, P. Smith, A. Molisch, F. Tufvesson, and S. Simon, "Polarized MIMO channels in 3-D: Models, measurements and mutual information," *IEEE Jornal on Selected Areas in Communications*, vol. 24, no. 3, pp. 514–527, Mar. 2006.

[116] M. D. Qurrat Ul Ain Nadeem, A. Kammoun and M. S. Alouini, "A generalized spatial correlation model for 3D MIMO channels based on the fourier coefficients of power spectrums," *IEEE Transactions on Signal Processing*, vol. 63, no. 14, pp. 3671–3686, Jul. 2015.

[117] ——, "Spatial correlation characterization of a uniform circular array in 3D MIMO systems," in *Proc. IEEE International Workshop on Signal Processing Advances in Wireless Communications (SPAWC'16)*, Edinburgh, UK, Jul. 2016.

[118] I. Krasikov, "Uniform bounds for bessel functions," *Journal of Applied Analysis*, vol. 12, no. 1, pp. 83–91, 2006.

[119] M. Franceschetti, J. Bruck, and L. J. Schulman, "A random walk model of wave propagation," *IEEE Transactions on Antennas and Propagation*, vol. 52, no. 5, pp. 1304–1317, May 2004.

[120] J. G. Andrews, F. Baccelli, and R. K. Ganti, "A tractable approach to coverage and rate in cellular networks," *IEEE Transactions on Communications*, vol. 59, no. 11, pp. 3122–3134, Nov. 2011.

[121] H. S. Dhillon, R. K. Ganti, F. Baccelli, and J. G. Andrews, "Modeling and analysis of k-tier downlink heterogeneous cellular networks," *IEEE Selected Areas in Communications*, vol. 30, no. 3, pp. 550 – 560, Apr. 2012.

[122] K. A. Hamdi, "A useful lemma for capacity analysis of fading inteference channels," *IEEE Transactions on Communications*, vol. 58, no. 2, pp. 411–416, Feb. 2010.

[123] M. D. Renzo, A. Guidotti, and G. E. Corazza, "Average rate of downlink heterogeneous cellular networks over generalized fading channels: A stochastic geometry approach," *IEEE Transactions on Wireless Communications*, vol. 61, no. 7, pp. 3050 – 3071, July 2013.

[124] P. Ioannides and C. A. Balanis, "Uniform circular arrays for smart antennas," *IEEE Antennas and Propagation Magazine*, vol. 47, no. 4, pp. 192–206, Aug 2005.

[125] M. N. Kulkarni, A. Ghosh, and J. G. Andrews, "A comparison of MIMO techniques in downlink millimeter wave cellular networks with hybrid beamforming," *IEEE Transactions on Communications*, vol. 64, no. 5, pp. 1952–1967, May 2016.

[126] J. G. Andrews, R. K. Ganti, M. Haenggi, N. Jindal, and S. Weber, "A primer on spatial modeling and analysis in wireless networks," *IEEE Communications Magazine*, vol. 48, no. 11, pp. 156–163, Nov. 2010.

[127] M. S. Alouini and A. J. Goldsmith, "Area spectral efficiency of cellular mobile radio systems," *IEEE Transactions on Vehicular Technology*, vol. 48, no. 4, pp. 1047–1066, Jul 1999.

[128] A. Ghosh, T. Thomas, M. Cudak, R. Ratasuk, P. Moorut, F. Vook, T. Rappaport, G. Maccartney, S. Sun, and S. Nie, "Millimeter-wave enhanced local area systems: A high-data-rate approach for future wireless networks," *IEEE Journal on Selected Areas in Communications*, vol. 32, no. 6, pp. 1152–1163, June 2014.

[129] *Regularized Hypergeometric Function.* Mathworld: A wolfram, 2010.

[130] W. Lee, S. R. Lee, H. B. Kong, S. Lee, and I. Lee, "Downlink vertical beamforming designs for active antenna systems," *IEEE Transactions on Communications*, vol. 62, no. 6, pp. 1897–1907, June 2014.

[131] S. Haykin, "Cognitive radio: brain-empowered wireless communications," *IEEE Journal on Selected Areas in Communications*, vol. 23, no. 2, pp. 201–220, Feb 2005.

[132] W. Afifi and M. Krunz, "Exploiting self-interference suppression for improved spectrum awareness/efficiency in cognitive radio systems," in *Proc. IEEE INFOCOM*, April 2013, pp. 1258–1266.

[133] W. Cheng, X. Zhang, and H. Zhang, "Imperfect full duplex spectrum sensing in cognitive radio networks," in *Proc. of ACM Workshop on Cognitive Radio Networks*, ser. CoRoNet '11. New York, NY, USA: ACM, 2011, pp. 1–6. [Online]. Available: http://doi.acm.org/10.1145/2030678.2030680

[134] L. Zhang, Y. C. Liang, Y. Xin, and H. V. Poor, "Robust cognitive beamforming with partial channel state information," *IEEE Transactions on Wireless Communications*, vol. 8, no. 8, pp. 4143–4153, August 2009.

[135] Y. Zhang, E. DallAnese, and G. B. Giannakis, "Distributed optimal beamformers for cognitive radios robust to channel uncertainties," *IEEE Transactions on Signal Processing*, vol. 60, no. 12, pp. 6495–6508, Dec 2012.

[136] G. Zheng, S. Ma, K. k. Wong, and T. S. Ng, "Robust beamforming in cognitive radio," *IEEE Transactions on Wireless Communications*, vol. 9, no. 2, pp. 570–576, February 2010.

[137] A. Mutapcic and S. Boyd, "Cutting-set methods for robust convex optimization with pessimizing oracles," *Optimization Methods Software*, vol. 24, no. 3, pp. 381–406, Jun. 2009. [Online]. Available: http://dx.doi.org/10.1080/10556780802712889

[138] A. Mutapcic, S. J. Kim, and S. Boyd, "A tractable method for robust downlink beamforming in wireless communications," in *Conference Record of the Forty-First Asilomar Conference on Signals, Systems and Computers*, Nov 2007, pp. 1224–1228.

[139] B. P. Day, A. R. Margetts, D. W. Bliss, and P. Schniter, "Full-duplex bidirectional mimo: Achievable rates under limited dynamic range," *IEEE Transactions on Signal Processing*, vol. 60, no. 7, pp. 3702–3713, July 2012.

[140] W. Li, J. Lilleberg, and K. Rikkinen, "On rate region analysis of half- and full-duplex OFDM communication links," *IEEE Journal on Selected Areas in Communications*, vol. 32, no. 9, pp. 1688–1698, Sept 2014.

[141] H. Suzuki, T. V. A. Tran, I. B. Collings, G. Daniels, and M. Hedley, "Transmitter noise effect on the performance of a MIMO-OFDM hardware implementation achieving improved coverage," *IEEE Journal on Selected Areas in Communications*, vol. 26, no. 6, pp. 867–876, August 2008.

[142] W. Namgoong, "Modeling and analysis of nonlinearities and mismatches in ac-coupled direct-conversion receiver," *IEEE Transactions on Wireless Communications*, vol. 4, no. 1, pp. 163–173, Jan 2005.

[143] G. Scutari, D. P. Palomar, and S. Barbarossa, "Cognitive MIMO radio," *IEEE Signal Processing Magazine*, vol. 25, no. 6, pp. 46–59, November 2008.

[144] J. Wang, G. Scutari, and D. P. Palomar, "Robust MIMO cognitive radio via Game theory," *IEEE Transactions on Signal Processing*, vol. 59, no. 3, pp. 1183–1201, March 2011.

[145] S. J. Kim and G. B. Giannakis, "Optimal resource allocation for MIMO ad hoc cognitive radio networks," *IEEE Transactions on Information Theory*, vol. 57, no. 5, pp. 3117–3131, May 2011.

[146] D. Bharadia and S. Katti, "Full duplex mimo radios," in *Proceedings of the 11th USENIX Conference on Networked Systems Design and Implementation*, ser. NSDI'14. Berkeley, CA, USA: USENIX Association, 2014, pp. 359–372. [Online]. Available: http://dl.acm.org/citation.cfmid=2616448.2616482

[147] D. P. Bertsekas, *Nonlinear Programming*. Belmont, MA: Athena Scientific, 1999, vol. 2nd edition.

[148] A. Ben-Tal and A. Nemirovski, *Lectures on Modern Convex Optimization: Analysis, Algorithms, Engineering Applications*. Philadelphia, PA: SIAM, 2001, vol. 2nd edition.

[149] M. B. Shenouda and T. N. Davidson, "On the design of linear transceivers for multiuser systems with channel uncertainty," *IEEE Journal on Selected Areas in Communications*, vol. 26, no. 6, pp. 1015–1024, August 2008.

[150] E. A. Gharavol and E. G. Larsson, "The sign-definiteness lemma and its applications to robust transceiver optimization for multiuser MIMO systems," *IEEE Transactions on Signal Processing*, vol. 61, no. 2, pp. 238–252, Jan 2013.

[151] H. Shen, B. Li, M. Tao, and X. Wang, "MSE-based transceiver designs for the MIMO interference channel," *IEEE Transactions on Wireless Communications*, vol. 9, no. 11, pp. 3480–3489, November 2010.

[152] K. T. Phan, S. A. Vorobyov, N. D. Sidiropoulos, and C. Tellambura, "Spectrum sharing in wireless networks via qos-aware secondary multicast beamforming," *IEEE Transactions on Signal Processing*, vol. 57, no. 6, pp. 2323–2335, June 2009.

[153] Q. Zhao, S. Geirhofer, L. Tong, and B. M. Sadler, "Opportunistic spectrum access via periodic channel sensing," *IEEE Transactions on Signal Processing*, vol. 56, no. 2, pp. 785–796, Feb 2008.

[154] F. Gao, R. Zhang, Y. C. Liang, and X. Wang, "Multi-antenna cognitive radio systems: Environmental learning and channel training," in *2009 IEEE International Conference on Acoustics, Speech and Signal Processing*, April 2009, pp. 2329–2332.

[155] E. A. Gharavol, Y. C. Liang, and K. Mouthaan, "Robust downlink beamforming in multiuser MISO cognitive radio networks with imperfect channel-state information," *IEEE Transactions on Vehicular Technology*, vol. 59, no. 6, pp. 2852–2860, July 2010.

[156] T. W. Ban, W. Choi, B. C. Jung, and D. K. Sung, "Multi-user diversity in a spectrum sharing system," *IEEE Transactions on Wireless Communications*, vol. 8, no. 1, pp. 102–106, Jan 2009.

[157] A. Ghasemi and E. S. Sousa, "Fundamental limits of spectrum-sharing in fading environments," *IEEE Transactions on Wireless Communications*, vol. 6, no. 2, pp. 649–658, Feb 2007.

[158] J. M. Peha, "Approaches to spectrum sharing," *IEEE Communications Magazine*, vol. 43, no. 2, pp. 10–12, Feb 2005.

[159] D. I. Kim, L. B. Le, and E. Hossain, "Joint rate and power allocation for cognitive radios in dynamic spectrum access environment," *IEEE Transactions on Wireless Communications*, vol. 7, no. 12, pp. 5517–5527, December 2008.

[160] P. Ubaidulla and A. Chockalingam, "Relay precoder optimization in MIMO-relay networks with imperfect CSI," *IEEE Transactions on Signal Processing*, vol. 59, no. 11, pp. 5473–5484, Nov 2011.

[161] "Further enhancements to LTE time division duplex (TDD) for downlink-uplink (DL-UL) interference management and traffic adaptation (release 11)," *TR* 36.828*, 3GPP*, 2012.

[162] S. Goyal, P. Liu, S. Panwar, R. A. DiFazio, R. Yang, J. Li, and E. Bala, "Improving small cell capacity with common-carrier full duplex radios," in *2014 IEEE International Conference on Communications (ICC)*, June 2014, pp. 4987–4993.

[163] M. Duarte, C. Dick, and A. Sabharwal, "Experiment-driven characterization of full-duplex wireless systems," *IEEE Transactions on Wireless Communications*, vol. 11, no. 12, pp. 4296–4307, December 2012.

[164] Y. C. Eldar, A. Ben-Tal, and A. Nemirovski, "Robust mean-squared error estimation in the presence of model uncertainties," *IEEE Transactions on Signal Processing*, vol. 53, no. 1, pp. 168–181, Jan 2005.

[165] A. Alkhateeb, G. Leus, and R. W. Heath, "Limited feedback hybrid precoding for multi-user millimeter wave systems," *IEEE Transactions on Wireless Communications*, vol. 14, no. 11, pp. 6481–6494, Nov 2015.

[166] X. Gao, L. Dai, S. Han, C. L. I, and R. W. Heath, "Energy-efficient hybrid analog and digital precoding for mmwave MIMO systems with large antenna arrays," *IEEE Journal on Selected Areas in Communications*, vol. 34, no. 4, pp. 998–1009, April 2016.

[167] O. E. Ayach, S. Rajagopal, S. Abu-Surra, Z. Pi, and R. W. Heath, "Spatially sparse precoding in millimeter wave MIMO systems," *IEEE Transactions on Wireless Communications*, vol. 13, no. 3, pp. 1499–1513, March 2014.

[168] H.-S. Jo, Y. J. Sang, P. Xia, and J. G. Andrews, "Heterogeneous cellular networks with flexible cell association: A comprehensive downlink SINR analysis," *IEEE Transactions on Wireless Communications*, vol. 11, no. 10, pp. 3484–3495, Oct. 2012.

[169] S. Singh, H. S. Dhillon, and J. G. Andrews, "Offloading in heterogeneous networks: Modeling, analysis, and design insights," *IEEE Transactions on Wireless Communications*, vol. 12, no. 5, pp. 2484–2497, May 2013.

[170] S. Vuppala, S. Biswas, and T. Ratnarajah, "An analysis on secure communication in millimeter/micro-wave hybrid networks," *IEEE Transactions on Communications*, vol. 64, no. 8, pp. 3507–3519, Aug 2016.

[171] Y. Guo and B. C. Levy, "Robust MSE equalizer design for MIMO communication systems in the presence of model uncertainties," *IEEE Transactions on Signal Processing*, vol. 54, no. 5, pp. 1840–1852, May 2006.